

Aus der der Klinik für Neurologie, Abteilung für Experimentelle Neurologie
der Medizinischen Fakultät Charité – Universitätsmedizin Berlin

DISSERTATION

The role of CD4+ T cells in chronic immune responses and cognitive
decline following experimental stroke

Die Rolle von CD4+ T-Zellen bei der chronischen Immunantwort und
Entstehung von Demenz nach experimentellem Schlaganfall

zur Erlangung des akademischen Grades
Medical Doctor - Doctor of Philosophy (MD/PhD)

vorgelegt der Medizinischen Fakultät
Charité – Universitätsmedizin Berlin

von

Luis Weitbrecht

aus Heidenheim an der Brenz

Datum der Promotion: 23. März 2024

Inhaltsverzeichnis

Abstract	1
Zusammenfassung	3
List of Abbreviations	6
1.Introduction	5
1.1. Hypothesis	6
2.Materials and Methods	7
2.1. Animals and Housing	7
2.2. Experimental Stroke Model (MCAo)	7
2.3. Stroke Volumetry – Magnetic Resonance Imaging (MRI)	7
2.4. Bronchoscopy-Guided Application of S. Pneumoniae	7
2.5. Microbiological Investigation	7
2.6. Drug Administration	8
2.6.1. CD4 Depletion	8
2.6.2. Tamoxifen	8
2.6.3. Antibiotics	8
2.6.4. Glycolic Acid	8
2.7. Immunofluorescence Staining – Stereological Quantification	8
2.8. Leukocyte Retrieval and Flow Cytometry	9
2.9. mRNA Expression Analysis – Quantitative Reverse Transcription Polymerase Chain Reaction (qRT-PCR)	10
2.10. Cognitive Assessment	11
2.11. Motor Assessment	11
2.11.1. Pole Test	11
2.11.2. Gait Analysis – CatWalk	12
2.11.3. Corner Test	12
2.12. Statistical Analysis	12
2.13. Study Approval	12

2.14. Use of Published Data	12
3. Results Publication 1: “CD4+ T Cells Promote Delayed B Cell Responses in the Ischemic Brain After Experimental Stroke”	14
3.1. CNS Autoreactivity Exacerbates Infarct Volumes and Lymphocyte Infiltration in 2D2 Mice After Stroke Compared to Wild-Type Mice	14
3.2. Delayed CD4 Depletion Inhibits CD4 ⁺ T Cell Infiltration into the Ischemic Brain at Day 14 After Stroke	15
3.3. CNS-Resident Microglia and Infiltrating Myeloid Cells After CD4 Depletion	18
3.3.1. Microglia and Infiltrating Myeloid Cells Can Be Distinguished by Flow Cytometry Using CD45 and CD11b Expression	18
3.3.2. CD4 Depletion Mitigates Microglial Loss and Reduces Myeloid Cell Infiltration into the Brain After Severe Infarction	19
3.4. Expression of Lymphocyte-Attracting and ELS-Inducing Cytokines in the Ischemic Brain	22
3.5. CD4 Depletion Reduces B Cell Infiltration into the Ischemic Brain at Day 14 After Stroke	23
3.6. CD4 ⁺ T and B Cells Infiltrate the Ischemic Brain Once the CD4 ⁺ T Cell Population Recovers in the Periphery	25
3.7. Temporary Inhibition of CD4 ⁺ T and B Cell Infiltration to the Brain Alleviates Cognitive Decline Without Influencing Infarct Volumes or Mortality	27
4. Results Publication 2: “Impact of Key Nicotinic AChR Subunits on Post-Stroke Pneumococcal Pneumonia”	29
4.1. Increased Susceptibility to Aspiration-Induced Pneumonia After Stroke is not Altered by Genetic Deficiency of Nicotinic Acetylcholine Receptors	29
5. Results Publication 3: “A Primeval Mechanism of Tolerance to Desiccation Based on Glycolic Acid Saves Neurons in Mammals from Ischemia by Reducing Intracellular Calcium-Mediated Excitotoxicity”	30
5.1. Glycolic Acid Improves Functional Outcomes After Experimental Stroke	30
6. Discussion	35
References	43
7. Affidavit	52

7.1. Statutory Declaration	52
7.2. Declaration of Contribution to the Publications	53
8.Publications	55
8.1. Publication 1	55
8.1.1. Excerpt From the ISI Journal Summary List	55
8.1.2. Print Copy	57
8.2. Publication 2	71
8.2.1. Excerpt From the ISI Journal Summary List	71
8.2.2. Print Copy	75
8.3. Publication 3	91
8.3.1. Excerpt From the ISI Journal Summary List	91
8.3.2. Print Copy	92
9.Curriculum Vitae	111
10.List of Publications	111
Acknowledgements	114

List of Tables

Table 1: Primary Antibodies for Immunofluorescence Staining	9
Table 2: Primary Antibodies for Flow Cytometry	10
Table 3: Primers for qRT-PCR.....	11

List of Figures

Figure 1: Flow Cytometry Gating Strategy	13
Figure 2: 2D2 Mice Show Enhanced Immune Responses After MCAo	15
Figure 3: Leukocyte Infiltration into the Brain Increases with Infarct Volumes	16
Figure 4: Experimental Set-Up and CD4 Depletion Efficacy	17
Figure 5: CD45 Expression is Sufficient to Distinguish Infiltrating Myeloid Cells (IMC) and Microglia by Flow Cytometry 14 Days After MCAo	19
Figure 6: CD4 Depletion Reduces Microglial Loss and Myeloid Cell Infiltration at Day 14 After MCAo.....	21
Figure 7: Lymphocyte-Attracting Cytokines Are Upregulated in the Ischemic Brain After Stroke	22
Figure 8: CD4 Depletion Inhibits B Cell Infiltration into the Ischemic Brain at Day 14 After MCAo	24
Figure 9: Lymphocytes Infiltrate the Ischemic Brain After the CD4 ⁺ Population Recovers in the Periphery	26
Figure 10: Long-Term Functional Outcome After Stroke and CD4 Depletion.....	28
Figure 11: The Susceptibility to Aspiration-Induced Pneumococcal Pneumonia After Experimental Stroke Is Not Altered in nAChR Knockout (KO) Mice	29
Figure 12: Impact of <i>S. Pneumoniae</i> Infection on the Pulmonary Immune Cell Repertoire in WT and nAChR KO Mice.....	30
Figure 13: Glycolic Acid Improves Histological and Functional Outcomes After MCAo	32
Figure 14: Glycolic Acid Does Not Improve the Performance on CatWalk or Pole Test	34
Figure 15: Differential B Cell Functions in the CNS After Stroke.....	37

List of Abbreviations

APC	Antigen presenting cell
CCL19	C-C motif ligand 19
CD	Cluster of differentiation
CFU	Colony forming units
CNS	Central nervous system
CreERT2	Cre recombinase (Cre) estrogen ligand-binding domain (ERT2) fusion protein
CSF	Cerebrospinal fluid
CXCL13	C-X-C motif ligand 13
CXCR5	C-X-C motif receptor 5
Cx3Cr1	CX3C chemokine receptor 1
DAPI	4',6-diamidino-2-phenylindole
ELS	Ectopic lymphoid structures
FSC	Forward scatter
GA	Glycolic acid
IMC	Infiltrating myeloid cell
Ig	Immunoglobulin
i.p.	Intraperitoneal
KO	Knock-out
LI	Laterality index
Ltb	Lymphotoxin beta
MBP	Myelin basic protein
MCA	Middle cerebral artery
MCAo	Middle cerebral artery occlusion
MHC-II	Major histocompatibility complex class II
MOG	Myelin oligodendrocyte glycoprotein
MRI	Magnetic resonance imaging
MS	Multiple sclerosis

NGS	Normal goat serum
nAChR	Nicotinic acetylcholine receptor
PBS	Phosphate buffered saline
PFA	Paraformaldehyde
PSCI	Post-stroke cognitive impairment
qRT-PCR	Quantitative reverse transcription polymerase chain reaction
SAP	Stroke-associated pneumonia
SD	Standard deviation
SEM	Standard error of the mean
SIDS	Stroke-induced immunodepression syndrome
SSC	Sideward scatter
s.c.	Subcutaneous
TCR	T cell receptor
Treg	Regulatory T cell
WT	Wild type
YFP	Yellow fluorescent protein
2D2	Myelin oligodendrocyte glycoprotein T cell receptor transgenic mice

Abstract

Stroke is a leading cause of morbidity and mortality in developed countries. Treatment options are limited to pharmacological thrombolysis and mechanical thrombectomy despite extensive efforts to develop new treatment strategies for acute stroke and aftercare. Ongoing research aims to reduce lethal stroke complications such as pneumonia, to rescue brain tissue from ischemic damage with neuroprotective substances, and importantly, to improve long-term outcomes in stroke patients by modulating chronic immune responses in the brain. The disruption of cerebral perfusion leads to an activation of the innate immune system and enables an infiltration of adaptive immune cells into the ischemic brain tissue. Delayed accumulation of B lymphocytes in ectopic lymphoid structures (ELS) within the infarct area has been associated with post-stroke cognitive decline, as displayed in vascular dementia. Therefore, we aimed to investigate the effect of late CD4⁺ T cell depletion on B cell responses in the brain and the long-term functional outcome after stroke. Repeated injections of monoclonal CD4-antibody at day three to nine after 60min middle cerebral artery occlusion (MCAo) in 2D2 mice (strain carrying transgenic T cell receptors reactive to myelin oligodendrocyte glycoprotein) successfully prevented initial infiltration of CD4⁺ T cells to the ischemic area. B cell numbers and ELS formation were reduced in CD4-depleted mice when compared to an isotype-treated control group at 14 days after stroke. Once the peripheral CD4⁺ T cell population had recovered, CD4⁺ T and B lymphocytes infiltrated the ischemic brain and formed ELS with evidence for local B cell differentiation and antibody production. Even though we found no difference regarding lymphocyte numbers and ELS phenotype between treatment groups at late time-points, CD4 depletion had a beneficial effect on cognitive functions after stroke. Taken together, these main findings indicate a pivotal role for CD4⁺ T cells in delayed autoreactive B cell responses after stroke and their contribution to cognitive decline. In a second publication we investigated the mechanisms of stroke-induced immunodepression syndrome (SIDS). Stroke leads to suppression of the immune system via the autonomic nerve system and especially cholinergic signaling, which promotes stroke-associated pneumonia (SAP). CNS-reactive immune responses can be exacerbated by systemic infections on the one hand and decreased by SIDS on the other. In an aspiration model with *Streptococcus pneumoniae*, a typical Gram-positive pathogen of SAP, we found reduced bacterial clearance in the lung with an altered pulmonary immune cell repertoire in animals with stroke when compared to controls. In this aspiration model, using different knockout models for nicotinic acetylcholine receptors, we did not find evidence for functional involvement of cholinergic mechanisms in mediating SIDS, as observed in a spontaneous SAP model with predominantly Gram-negative bacteria. In a third paper, we demonstrated a protective effect of glycolic acid on neuronal metabolism. Glycolic acid resulted in better performance in various behavioral tests in mice when administered during reperfusion after stroke. If this protective effect is confirmed in further studies,

intra-arterial application would also be feasible in humans in the acute phase of stroke, during mechanical recanalization by thrombectomy. Overall, this dissertation provides further evidence for dysregulation of the immune system in the chronic phase after stroke. Here, an exaggerated immune response of autoreactive lymphocytes in the brain seems to contribute to the development of cognitive deficits, whereas peripheral immunosuppression by the autonomic nervous system promotes severe infections. In addition to direct neuroprotective approaches, these pathomechanisms offer new targets for immunomodulatory therapeutic strategies. However, the sometimes opposing immune mechanisms in the CNS and peripheral organs such as the lungs need to be considered.

Zusammenfassung

Der ischämische Schlaganfall gehört zu den häufigsten Ursachen für Tod und lebenslange Behinderung. In der Akutphase wird der Krankheitsverlauf durch den Untergang von Nervengewebe und systemische Infektionen bestimmt, während in der Folgezeit autoreaktive Immunprozesse im Hirn mutmaßlich zur Entstehung von Demenz beitragen. Zerebrale Ischämie führt durch Aktivierung des angeborenen und später des erworbenen Immunsystems zu einer lokalen Entzündungsreaktion. Dabei bilden CD4⁺ T-Zellen und B-Zellen ektope lymphfollikelähnliche Strukturen (ELS) im Hirn, was mit der Entstehung von verzögert auftretenden kognitiven Defiziten als Form der vaskulären Demenz in Verbindung gebracht wurde. Die vorliegende Arbeit beleuchtet verschiedene Aspekte der Pathophysiologie des Schlaganfalls anhand eines Mausmodells. Schwerpunktmäßig wurde die Rolle von CD4⁺ T-Zellen bei autoreaktiven B-Zellantworten nach Schlaganfall untersucht. Hierfür induzierten wir einen ischämischen Schlaganfall in 2D2-Mäusen und injizierten einen Anti-CD4-Antikörper. So wurden die peripheren CD4⁺ T-Zellen depletiert und deren anfängliche Infiltration in das ischämische Gewebe verhindert. Das Ausmaß der B-Zellinfiltration und ELS-Bildung im Hirn waren zwei Wochen nach Schlaganfall im Vergleich mit Kontrolltieren signifikant reduziert. Jedoch begann die Infiltration von CD4⁺ T- und B-Lymphozyten ins ischämische Hirn erneut, sobald sich die periphere CD4⁺ T-Zellpopulation erholt hatte. Sieben bis zehn Wochen nach Schlaganfall entstanden ELS mit Anzeichen von lokaler B-Zelldifferenzierung und Antikörperproduktion. Obwohl zu diesen Zeitpunkten kein Unterschied in der Lymphozytenzahl und dem Organisationsgrad der ELS zwischen den Behandlungsgruppen festzustellen war, hatte die CD4-Depletion positive Auswirkungen auf die kognitive Funktion. Insgesamt sprechen diese Ergebnisse für eine Schlüsselrolle von CD4⁺ T Zellen bei der autoreaktiven Immunantwort nach Schlaganfall und ihrer Beteiligung an den verzögert auftretenden kognitiven Defiziten nach Schlaganfall. In der zweiten Arbeit untersuchten wir Mechanismen des Schlaganfall-induzierten Immundepressionssyndroms (SIDS). Schlaganfall führt über autonome und insbesondere auch cholinerge Signale zu einer Suppression des Immunsystems, wodurch Schlaganfall-assoziierte Pneumonien (SAP) begünstigt werden. Autoreaktive Immunantworten können durch systemische Infektionen einerseits verstärkt und andererseits durch die Immundepression vermindert werden. In einem Aspirationsmodell mit *Streptococcus pneumoniae*, einem typischen Gram-positiven Erreger der SAP, konnten wir bei Tieren mit Schlaganfall eine reduzierte bakterielle Clearance bei verändertem pulmonalem Immunzellrepertoire im Vergleich zu Kontrolltieren ohne Schlaganfall nachweisen. In diesem Aspirationsmodell konnten wir mit Hilfe verschiedener Knockout-Modelle nikotinerger Acetylcholinrezeptoren keinen Hinweis für die funktionelle Beteiligung cholinergischer Mechanismen in der Vermittlung von SIDS feststellen, wie dies bei einem spontanen SAP-Modell mit überwiegend Gram-negativen Bakterien beobachtet wurde. In der

dritten Arbeit konnten wir eine protektive Wirkung von Glykolsäure für den neuronalen Metabolismus nachweisen. Glykolsäure führte in Mäusen zu besseren Leistungen in verschiedenen Verhaltenstests, wenn sie während der Reperfusion nach Schlaganfall verabreicht wurde. Sollte der protektive Effekt sich in weiteren Studien bestätigen, wäre auch beim Menschen eine intraarterielle Anwendung in der Akutphase des Schlaganfalls, während der mechanischen Rekanalisation mittels Thrombektomie, möglich. Insgesamt liefert diese Doktorarbeit weitere Belege für eine Dysregulation des Immunsystems während der chronischen Phase nach Schlaganfall. Hierbei scheint eine überschießende Immunreaktion von autoreaktiven Lymphozyten im Hirn zur Entstehung von kognitiven Defiziten beizutragen, während die periphere Immunsuppression durch das vegetative Nervensystem schwere Infektionen begünstigt. Neben direkten neuroprotektiven Ansätzen liefern diese Pathomechanismen neue Targets für immunmodulatorische Therapiestrategien, wobei die teils gegenläufigen Immunmechanismen im ZNS und peripheren Organen wie der Lunge berücksichtigt werden müssen.

1. Introduction

Ischemic stroke is among the leading causes of mortality and disability worldwide (Johnson et al., 2019). Acute neurological and physical dysfunction caused by ischemic brain damage are followed by dementia or post-stroke cognitive impairment (PSCI) in up to 50 percent of stroke survivors (Pendlebury et al., 2019). The risk for developing post-stroke dementia increases over the course of time, indicating that the underlying pathomechanism may be a chronic process (Pendlebury & Rothwell, 2009).

To this date, the treatment options for acute stroke are limited to thrombolysis by intravenous administration of recombinant tissue plasminogen activator and percutaneous endovascular interventions for local thrombolysis or thrombectomy (Roaldsen et al., 2021). Due to an increasing risk of intracerebral bleeding over time, these therapies can only be administered within few hours after stroke onset (Hacke et al., 2008; Jovin et al., 2015). However, improvements in acute stroke care have enabled an increasing number of patients for treatment within the required time frame (Stroke Unit Trialists, 2013). Consequently, the number of patients suffering from long term disability after stroke, such as PSCI, has increased with the number of stroke survivors (Johnson et al., 2019). Subsequent treatment is limited to secondary stroke prevention as numerous attempts to implement preclinical findings into clinical practice have failed, highlighting the need for a better understanding of the processes that determine stroke patients' long-term outcome (Endres et al., 2008).

Only recently it was discovered that B cell responses facilitate cognitive decline in an experimental stroke model, suggesting a role for the adaptive immune system in the pathogenesis of PSCI (Doyle et al., 2015). According to the current understanding innate-like lymphocytes infiltrate the ischemic brain early after stroke onset with a peak for both T and B cells at day three (Gelderblom et al., 2009). This early response is deemed independent from central nervous system (CNS) antigens (Kleinschnitz et al., 2010). After a temporary decrease in brain-residing lymphocytes, a second wave of T and B cell infiltration to the ischemic tissue was observed around day 14 after stroke (Doyle et al., 2015; Stubbe et al., 2013). Such delayed adaptive immune responses may be initiated once CNS antigens are released from damaged brain cells and drained to peripheral lymphoid tissue to be presented to lymphocytes by antigen presenting cells (APC) (Kono & Rock, 2008; Planas et al., 2012; van Zwam et al., 2009).

After priming in the periphery, lymphocytes infiltrate the ischemic brain in an antigen-specific manner where they form ectopic lymphoid structures (ELS) (Doyle et al., 2015; Miró-Mur et al., 2020). This process may be supported by resident microglia and infiltrating myeloid cells (IMC), which shift to a detrimental phenotype during the chronic phase of stroke and produce cytokines to create a proinflammatory environment (Hu et al., 2012; Jin et al., 2010). Findings from cancer, autoimmune diseases and other states of chronic inflammation indicate that ELS execute similar

functions as lymphoid follicles, including B cell differentiation, antibody production and hypermutation, thereby facilitating chronic on-site immune responses (Corsiero et al., 2016). Multiple studies demonstrated that autoantibodies directed against CNS-specific proteins, such as myelin oligodendrocyte glycoprotein (MOG) and myelin basic protein (MBP), can be found in stroke patients and are associated with cognitive decline (Becker et al., 2011; Becker et al., 2016; Pruss et al., 2012).

This thesis highlights the role of CD4⁺ T cells during chronic immune responses in the brain after experimental stroke and for post-stroke cognitive decline. However, we provide additional data providing insights into other determinants of stroke patients' functional outcome. For instance, acute cerebral ischemia induces a state of peripheral immunodepression predisposing patients to severe pulmonary infections that account for a threefold increase of stroke mortality (Katzan et al., 2003). This stroke-induced immunodepression syndrome (SIDS) is mediated by an activation of the sympathetic and the parasympathetic nervous system (Engel et al., 2015; Prass et al., 2003). Using various knockout models, we investigated the role of nicotinic acetylcholine receptor (nAChR) subtypes for the pulmonary bacterial clearance and local immune cell composition after stroke.

Additionally, we investigated the neuroprotective properties of glycolic acid (GA) during cerebral reperfusion after experimental stroke. GA was previously characterized as a metabolite that protects *Caenorhabditis elegans* dauer larva during desiccation, a process which is characterized by a sudden withdrawal and subsequent supply of oxygen and nutrients comparable to the occlusion/reperfusion mechanism during stroke (Erkut et al., 2016). Here, we used multiple behavioral tests to assess the sensorimotor functions of mice after stroke with or without GA treatment.

1.1. Hypothesis

We hypothesized that adaptive immune responses in the ischemic brain contribute to PSCI and therefore serve as a potential therapeutic target to improve stroke patients' long-term outcome. As formation of lymphoid tissue and general B cell functions vastly rely on chemokines secreted or induced by CD4⁺ T helper cells and cell-cell-interaction (Corsiero et al., 2016; Cupedo & Mebius, 2003), we also hypothesized that the treatment with an antibody depleting CD4⁺ T cells would mitigate B cell infiltration, ELS formation and alleviate cognitive decline after stroke.

Therefore, we induced an ischemic stroke by middle cerebral artery occlusion (MCAo) in male and female mice and subsequently characterized the kinetics of immune cell infiltration and ELS formation in the brain. After administering a CD4⁺ T cell depleting antibody or an isotype control, we measured ELS formation by flow cytometry, histology and qRT-PCR while cognitive functions were assessed by behavioral testing.

2. Materials and Methods

The materials and methods listed below have previously been published and are described in detail elsewhere (Chovsepian et al., 2022; Jagdmann et al., 2020; Weitbrecht et al., 2021). A brief outline is provided for each method.

2.1. Animals and Housing

Experiments were conducted with male and female 2D2 mice (Bettelli et al., 2003) and C57BL/6J (WT) mice between the ages of 10 to 14 weeks when entering the study. Male 8-week-old Cx3Cr1^{CreERT2}-YFP transgenic mice were used for validating CD45 to distinguish microglia from IMC. Male α 2 nAChR knock-out (KO) α 5 nAChR KO, α 7 nAChR KO, α 9/10 nAChR KO mice and corresponding WT littermates aged between 12-20 weeks were used for infection experiments.

2.2. Experimental Stroke Model (MCAo)

Ischemic stroke was modeled by 60-minute middle cerebral artery (MCA) occlusion (MCAo). MCA perfusion was disrupted by introducing a monofilament into the common carotid artery towards the origin of the MCA, where it was left for 60 minutes. Thereafter, the filament was withdrawn to reestablish perfusion. A sham-operation where the filament was immediately withdrawn after exposition to the MCA was performed in control animals. The success of MCAo was verified immediately with the modified Bederson score (Bederson et al., 1986) and at day one with T2-weighted magnetic resonance imaging.

2.3. Stroke Volumetry – Magnetic Resonance Imaging (MRI)

Infarct volumes were quantified by T2-weighted MRI as previously described (Hetze et al., 2012). Infarct volumes were calculated and expressed as percentage of the edema corrected ipsilateral hemisphere volume (Gerriets et al., 2004). For aspiration-induced pneumonia experiments stroke volumes were determined by hematoxylin staining.

2.4. Bronchoscopy-Guided Application of *S. Pneumoniae*

Streptococcus pneumoniae (*S. pneumoniae*) was diluted in PBS to 2000 colony forming units (CFU)/50 μ L. Under anesthesia with midazolam (5.0mg/kg BW) and medetomidin (0.5mg/kg BW) the bronchoscope was advanced along the trachea to the bifurcation where 50 μ L pneumococcal suspension were administered. Subsequently, mice recovered under flumazenil (0.5mg/kg BW) and atipamezol (5mg/kg BW) to antagonize the anesthesia.

2.5. Microbiological Investigation

Bronchoalveolar lavage (BAL) was performed as described elsewhere (Sun et al., 2017). BAL fluid and homogenized lung tissue were serially diluted and incubated on Columbia-Agar plates at 37 °C for 18h. Bacterial colonies were counted to calculate the CFUs per ml tissue/liquid.

2.6. Drug Administration

2.6.1. CD4 Depletion

200µg of CD4 depletion antibody (anti-mouse CD4, clone GK1.5) or isotype control antibody were injected intraperitoneally (i.p.) at day 3, 5, 7 and 9 after MCAo to eliminate peripheral CD4⁺ T cells in MCAo and sham animals.

2.6.2. Tamoxifen

4mg Tamoxifen was injected four weeks prior to MCAo surgery in 8-week-old Cx3Cr1^{CreERT2}-YFP transgenic mice to induce YFP expression in Cx3Cr1-positive cells. Due to the high turnover of peripheral myeloid cells, YFP was expressed in microglia and brain-resident macrophages but not IMC when the tissue was analyzed by flow cytometry at day 14 after stroke (Goldmann et al., 2016).

2.6.3. Antibiotics

For aspiration-induced pneumonia experiments, spontaneous pneumonia was prevented by i.p. injections of marbofloxacin (5mg/kg body weight) at the day of MCAo and the day before.

2.6.4. Glycolic Acid

100 µl of glycolic acid (GA) or 0.9% NaCl (vehicle) solution were injected i.p. immediately after MCAo or sham operation and on the following 3 days. GA powder was diluted in pure water to a concentration of 15.6 mg/ml (60 mg/ kg BW).

2.7. Immunofluorescence Staining – Stereological Quantification

Mouse brains were snap frozen and cut into 30µm slices on a sliding microtome. Antibodies were diluted in 1% normal goat serum and 0.3% Tween20 in PBS. Sections were incubated with primary antibodies (Tab. 1) at 4°C overnight. Slices were washed and incubated with secondary antibodies for 2 hours at room temperature on a shaker. DAPI was used to stain nuclei. Fluorescent images were taken using a confocal microscope. Stereological cell quantification was performed using LEICA LAF software, where CD4⁺ and B220⁺ cells were counted in 9 frames (173µm × 173µm) per hemisphere. One slice around the bregma including lesions in both striatum and cortex was chosen to represent each animal.

Table 1*Primary Antibodies for Immunofluorescence Staining*

Antigen	Conjugate	Dilution	Clone	Type	Source
B220	Alexa488	1:200	RA3-6B2	Monoclonal	BioLegend
CD3		1:200	500A2	Monoclonal	BD Bioscience
CD4		1:200	RM-4-5	Monoclonal	BD Bioscience
Laminin 1+2		1:400	Ab7463	Polyclonal	Abcam
CD138		1:200	281-2	Monoclonal	BD Bioscience
IgM	Alexa594	1:200	A21044	Polyclonal	Life Technologies
IgG	Oregon Green 488	1:200	O6280	Polyclonal	Life Technologies

2.8. Leukocyte Retrieval and Flow Cytometry

Mice were transcardially perfused with PBS after deep anesthesia. Cerebrums were separated from the cerebellum and kept on ice in medium with penicillin, streptomycin, and 2 mM L-alanyl-L-glutamine. Hemispheres were pressed through a 70µm cell strainer separately to obtain single cell suspensions. After centrifugation, cell pellets were resuspended in 35% Percoll. The 35% Percoll solution was carefully layered on top of 70% Percoll and centrifuged at room temperature for 30 minutes at 1159g to obtain mononuclear cells at the 35%/70% interface.

Peripheral blood was collected by submandibular puncture or from the vena cava in deeply anesthetized mice. Obtained blood samples were treated with erythrocyte lysis reagent. Leukocytes collected from brain or blood were incubated with primary, fluorochrome-conjugated antibodies (Tab. 2) that were diluted in PBS, 0.5% bovine serum albumin and 2mM ethylenediaminetetraacetic acid for 20 minutes at 4°C in the dark according to the manufacturers' instructions. Pacific orange was used to discriminate living from dead cells in blood samples. Cells were analyzed using LSRII SORP and FACSCanto II flow cytometers with FlowJo v10.0 software. Gating strategies are provided in Figure 1 and 5A.

Table 2*Primary Antibodies for Flow Cytometry*

Brain Leukocytes				
Antigen	Conjugate	Clone	Type	Source
CD11b	ECD	M1/70	Monoclonal	eBioscience
CD138	BV605	281-2	Monoclonal	BD Biosciences
CD19	BV785	6D5	Monoclonal	BioLegend
CD25	BV711	PC61	Monoclonal	BD Biosciences
CD3e	Pacific Blue	17A2	Monoclonal	BioLegend
CD44	PE-Cy7	IM7	Monoclonal	eBioscience
CD45	Alexa700	30-F11	Monoclonal	BioLegend
CD8	PE-Cy5	53-6.7	Monoclonal	BioLegend
GL7	Alexa488	GL7	Monoclonal	eBioscience
IgD	BV510	11-26c.2a	Monoclonal	BD Biosciences
TCR V β 11	PE	RR3-15	Monoclonal	BioLegend
Blood Leukocytes				
CD11b	PE-Cy7	M1/70	Monoclonal	eBioscience
CD19	PerCp-Cy5.5	1D3	Monoclonal	FisherScientific
CD3	PE	17A2	Monoclonal	BioLegend
CD4	FITC	RM4-5	Monoclonal	BD Bioscience
CD8	Alexa647	53-6.7	Monoclonal	BioLegend
Ly6C	BV421	HK1.4	Monoclonal	BioLegend
Ly6G	APC-Cy7	1A8	Monoclonal	BioLegend

2.9. mRNA Expression Analysis – Quantitative Reverse Transcription Polymerase Chain Reaction (qRT-PCR)

Phenol-chloroform extraction was used to isolate the RNA from both hemispheres separately. DNaseI was employed according to the manufacturer's instructions to digest genomic DNA. Extracted mRNA was reverse-transcribed to cDNA using the M-MLV reverse transcriptase. The cDNA was then quantified using a LightCycler 480. Target gene expression was normalized to *Reep5* as housekeeping gene. The relative expression of the target gene in ipsilateral hemispheres was expressed as a ratio of ipsilateral to contralateral hemisphere expression. Primers are specified in Table 3.

Table 3*Primers for qRT-PCR*

Gene	Forward sequence	Reverse sequence
<i>Ccxcr5</i>	CCCCTAACCCTGGACATGGGCTC	AGTGTGCCGGTGCCTCTCCA
<i>Cxcl13</i>	TACGCCCCCTGGGAATGGCT	AGTGGCTTCAGGCAGCTCTTCT
<i>Cxcl12</i>	TGGACGCCAAGGTCGTCGCC	GAACCGGCAGGGGCATCGGT
<i>Ccl19</i>	CTGCTGGTTCTCTGGACCTTC	GCGGAAGGCTTTACGATGT
<i>Ltb</i>	ACCTCATAGGCGCTTGGATG	CGACGTGGCAGTAGAGGTAA
<i>Pax5</i>	CCGACTCCTCGGACCATCAGGACA	GGCCTGACACCTTGATGGGCA
<i>Cst7</i>	AGTCCCATGTCAGCAAAGCC	ATATAGAGTCCGCTTCAAGGCAG
<i>Csf1</i>	CTCTAGCCGAGGCCATGTG	GCTCCTCCACTTCCACTTGT
<i>Ctsd</i>	ACATAGCCTGCTGGGTCCAC	CCTGAGCCGTAGTGGATGTC
<i>ApoE</i>	CTGAGAAGGGAAGATGGGGTTC	GGCTAGGCATCCTGTCAGCAA
<i>Lpl</i>	CTCCAGAGTTTGACCGCCTT	TTCCCGTTACCGTCCATCCA
<i>Ctsl</i>	GTGGACTGTTCTCACGCTCA	ACAAGATCCGTCCTTCGCTT
<i>P2ry13</i>	TCGTGGGTTGAGCTAGTAACTG	TCCCGAGCATCAGCTTTGTT
<i>Hexb</i>	CATCGACCACAGTCCCAATTC	CCAAAAACATAGTTGTAATATCGCC
<i>Cx3Cr1</i>	GTGAGACTGGGTGAGTACTG	GTGGACATGGTGAGGTCCTGAG
<i>Tmem119</i>	CACCCAGAGCTGGTTCCATAGC	GGTCTCTCCGGTGTGGGACT

Note. Adapted from (Weitbrecht et al., 2021).

2.10. Cognitive Assessment

The Y-maze test was used to examine the cognitive function and spatial working memory of mice after stroke and CD4 depletion as previously described (Itoh et al., 1993). The number of arm entries in 8-minut-sessions served as an indicator for exploration behavior and memory. Behavioral tests were performed at baseline (day -1), 2 weeks and 7 weeks after MCAo.

2.11. Motor Assessment

After stroke, mice show impaired motor functions and a preference towards the nonaffected limb (Balkaya et al., 2012). For the glycolic acid experiments, various functional tests were performed to assess such deficits.

2.11.1. Pole Test

Animals were placed on top of a vertical pole facing upwards. The time from the start of a full 180° turn (time to turn) and latency to reach the ground (time to descend) was measured. 3 successful

trials per mouse were taken. Trials in which mice took longer than 5 s to turn or longer than 20 s to descend were excluded. Pausing was also an exclusion criterion.

2.11.2. Gait Analysis – CatWalk

Quantitative gait analysis using the semi-automated CatWalk (Noldus Information Technology) system was used to assess deficits of motor function at day 10 after MCAo. The animals' footprints on a transparent, fluorescently illuminated platform were recorded by a camera from underneath. Mice were trained to walk across the platform on 3 consecutive days before MCAo. Each mouse was observed until 3 successful trials were recorded (speed variation <60%, no pausing). Analysis was performed with CatWalk XT 10.5 Software, which visualizes the footprints and calculates statistics regarding their dimensions and the time and distance ratios between footfalls.

2.11.3. Corner Test

At day 12 after MCAO, mice were placed in a cardboard box where two opposing corners were set at a 30° angle. Mice were motivated to move into the corner by a small opening in the wall. As a response to the whiskers touching the walls of the corner, the animals rear and turn to either side with a preference for the healthy side after stroke. Mice were observed during 10-minute sessions and the turns in each direction were counted. The laterality index (LI) was calculated as described: $LI = (TL - TD) / (TD + TL)$ (Balkaya et al., 2013). TL: turn left (stroke-affected side); TD: turn right (nonaffected side).

2.12. Statistical Analysis

Data are presented as scattered dot plots with mean \pm standard deviation (SD) or box plots (25-75 percentile) with whiskers (5-95 percentile), if not stated otherwise in the figure legend. Tests were two-sided and a p-value <0.05 was considered statistically significant. Normal distribution was verified with the Kolmogorow-Smirnov test. Where data was not normally distributed, a log-transformation was performed before analysis.

2.13. Study Approval

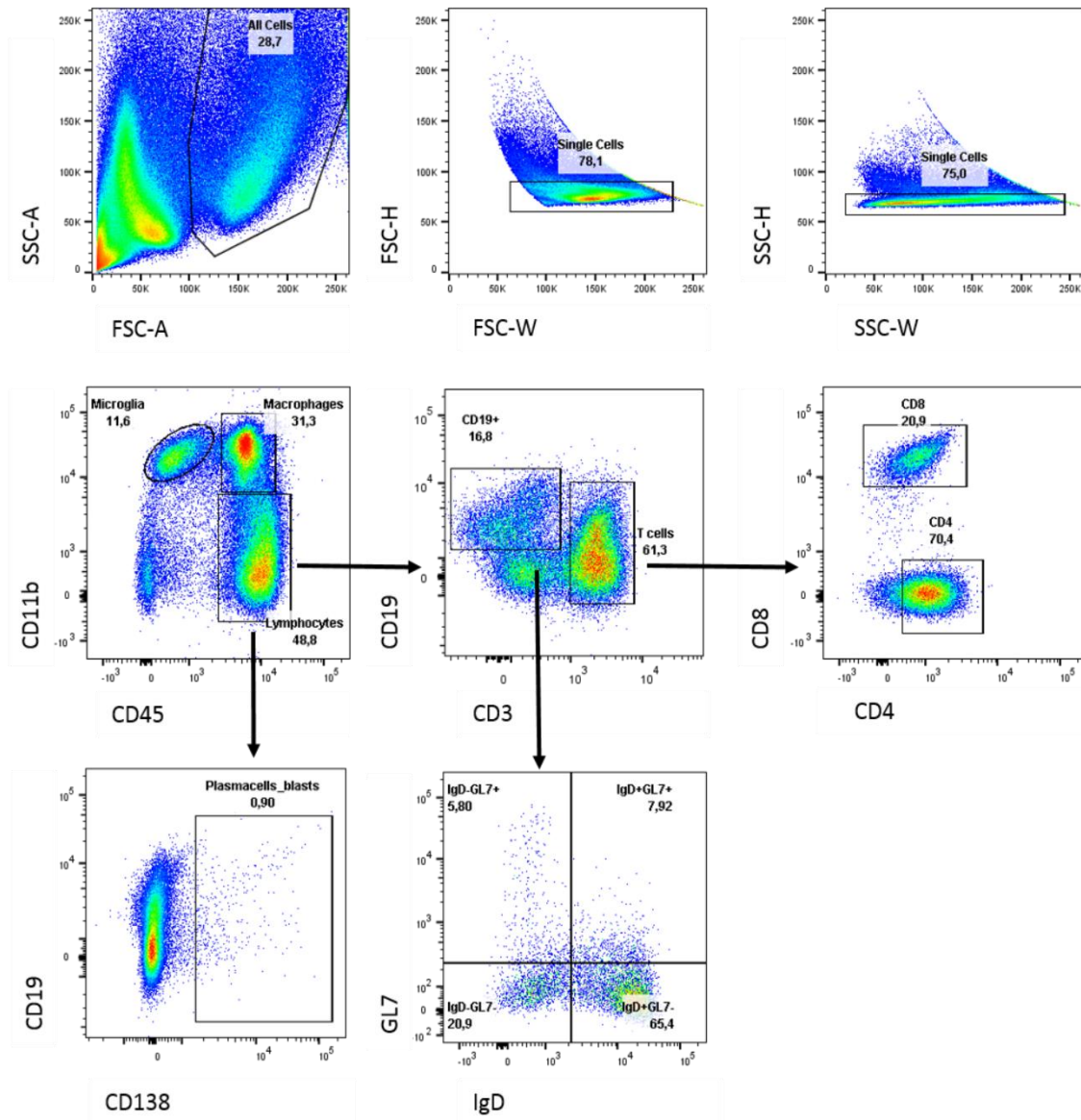
All animal experiments were conducted in accordance with the ARRIVE guidelines (Kilkenny et al., 2010), Directive 2010/63/EU of the European Parliament and German national laws and approved by local authority (Landesamt für Gesundheit und Soziales, Berlin, Germany).

2.14. Use of Published Data

The data, tables, and figures presented in this thesis have in part been published as indicated. All included publications are licensed under a Creative Common License (CC-BY) and permission to reprint figures, data and text are therefore granted by the publisher.

Figure 1

Flow Cytometry Gating Strategy



Note. “Isolated leukocytes were gated based on forward (FSC) and sideward (SSC) scatter to determine single cells. CD45 was used to separate CD11b⁺ myeloid cells into microglia (CD11b^{hi}CD45^{lo}) and infiltrating myeloid cells (CD11b^{hi}CD45^{hi}). Lymphocytes were defined as CD45⁺CD11b⁻ and gated into CD138⁺ plasmablasts / plasma cells [...] CD3⁺ T cells and CD19⁺ cells of B cell lineage. CD3⁺ T cells were discriminated into CD4⁺ T helper cells and CD8⁺ cytotoxic T cells. CD19⁺ cells were further discriminated to define IgD⁻GL7⁺ [germinal center- like] B cells.” Reprinted (Weitbrecht et al., 2021).

3. Results Publication 1: “CD4⁺ T Cells Promote Delayed B Cell Responses in the Ischemic Brain After Experimental Stroke”

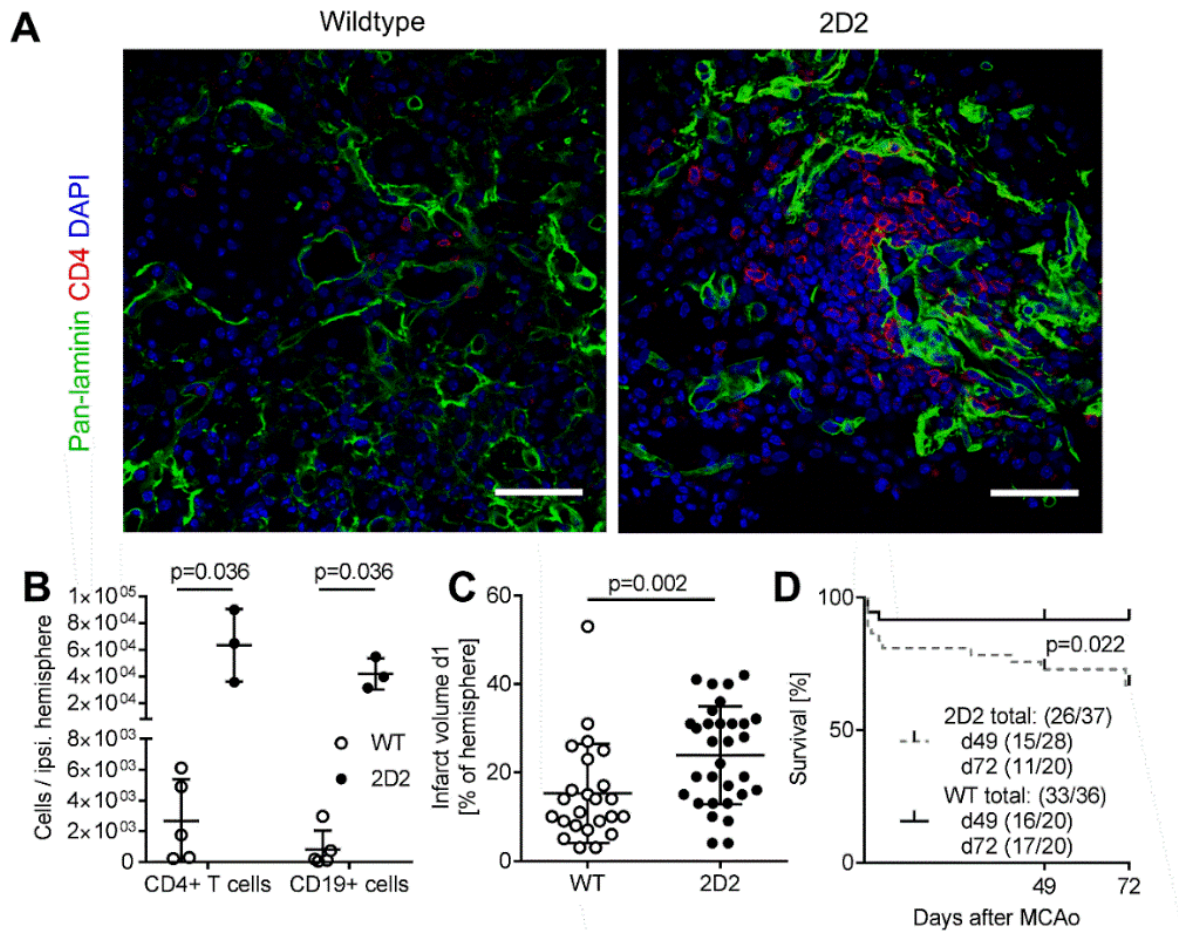
The results (except section 3.4) have previously been published as indicated. Selected results of two separate publications are enclosed in section 4-5.

3.1. CNS Autoreactivity Exacerbates Infarct Volumes and Lymphocyte Infiltration in 2D2 Mice After Stroke Compared to Wild-Type Mice

Previous studies suggest that CNS antigen-specific lymphocytes infiltrate the brain following experimental stroke and exacerbate stroke outcome (Jin et al., 2018; Ren et al., 2012; Römer et al., 2015). Therefore, we investigated lymphocyte infiltration to the brain, infarct volumes at day 14 and survival following 60min MCAo in WT mice and 2D2 mice, a transgenic strain with more than 80% of peripheral CD4⁺ T cells expressing T cell receptors (TCRs) directed against the CNS-specific antigen MOG. Immunofluorescence staining of selected brain slices and flow cytometry indicated that CD4⁺ T cell and B cell infiltration into the ischemic brain was more pronounced in the ipsilateral hemisphere of 2D2 mice compared to WT animals (Fig. 2A-B). Lymphocytes did not infiltrate the contralateral hemisphere of MCAo mice or the brains of sham-operated control mice (data not shown). Larger infarct volumes at day 14 after MCAo (Fig. 2C) and lower long-term survival (Fig. 2D) compared to WT mice are additional indicators for an exacerbated immune response in 2D2 mice, which makes them a useful model organism when investigating the role of CD4⁺ T cell-dependent CNS antigen-specific immune cell responses after experimental stroke.

Figure 2

2D2 Mice Show Enhanced Immune Responses After MCAo



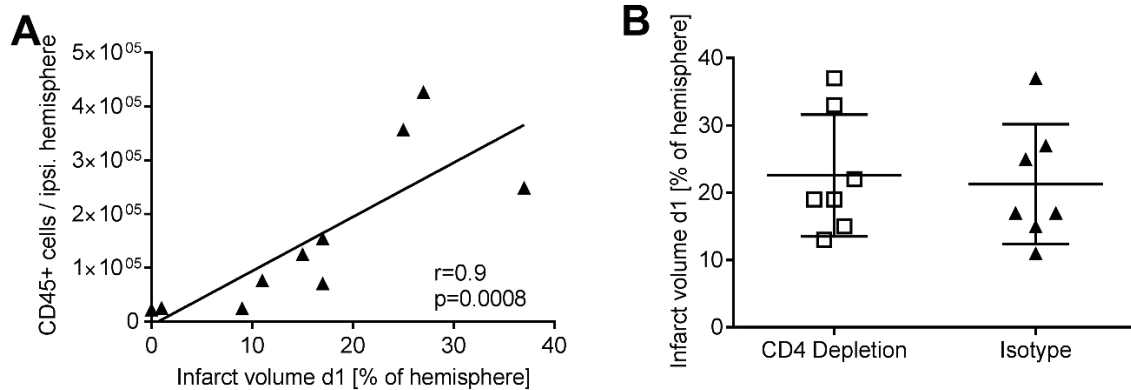
Note. “**A**) Representative immunostaining of CD4⁺ T cells that infiltrate the ischemic brain through the vascular basement membrane (laminin) in 2D2 mice and WT mice 14 days after MCAo. Scale bar = 50 μ m. **B**) Flow cytometry quantification of CD4⁺ T cells and CD19⁺ [B] cells in ipsilateral hemispheres of 2D2 and WT mice 14 days after MCAo (Mann-Whitney U Test). **C**) Infarct volumes measured by T2-weighted MRI on day 1 after MCAo in 2D2 and WT mice. **D**) Long-term survival after 60min MCAo in 2D2 and WT mice (Log-Rank (Mantel-Cox) Test).” Mice were sacrificed after 49 days or 72 days. Sample size is displayed as surviving/total mice used in the study. Reprinted (Weitbrecht et al., 2021).

3.2. Delayed CD4 Depletion Inhibits CD4⁺ T Cell Infiltration into the Ischemic Brain at Day 14 After Stroke

We observed immune cell infiltration into the CNS at day 14, 49 and 72 by histology, flow cytometry and qRT-PCR after administering a monoclonal anti-CD4 antibody or an immunoglobulin (Ig) G control antibody. We had previously observed that leukocyte infiltration into the ischemic brain correlates with infarct sizes (Fig. 3A). Infarct volumes at day 1 were therefore used to allocate the animals into equal groups for subsequent antibody treatment (Fig. 3B).

Figure 3

Leukocyte Infiltration into the Brain Increases with Infarct Volumes

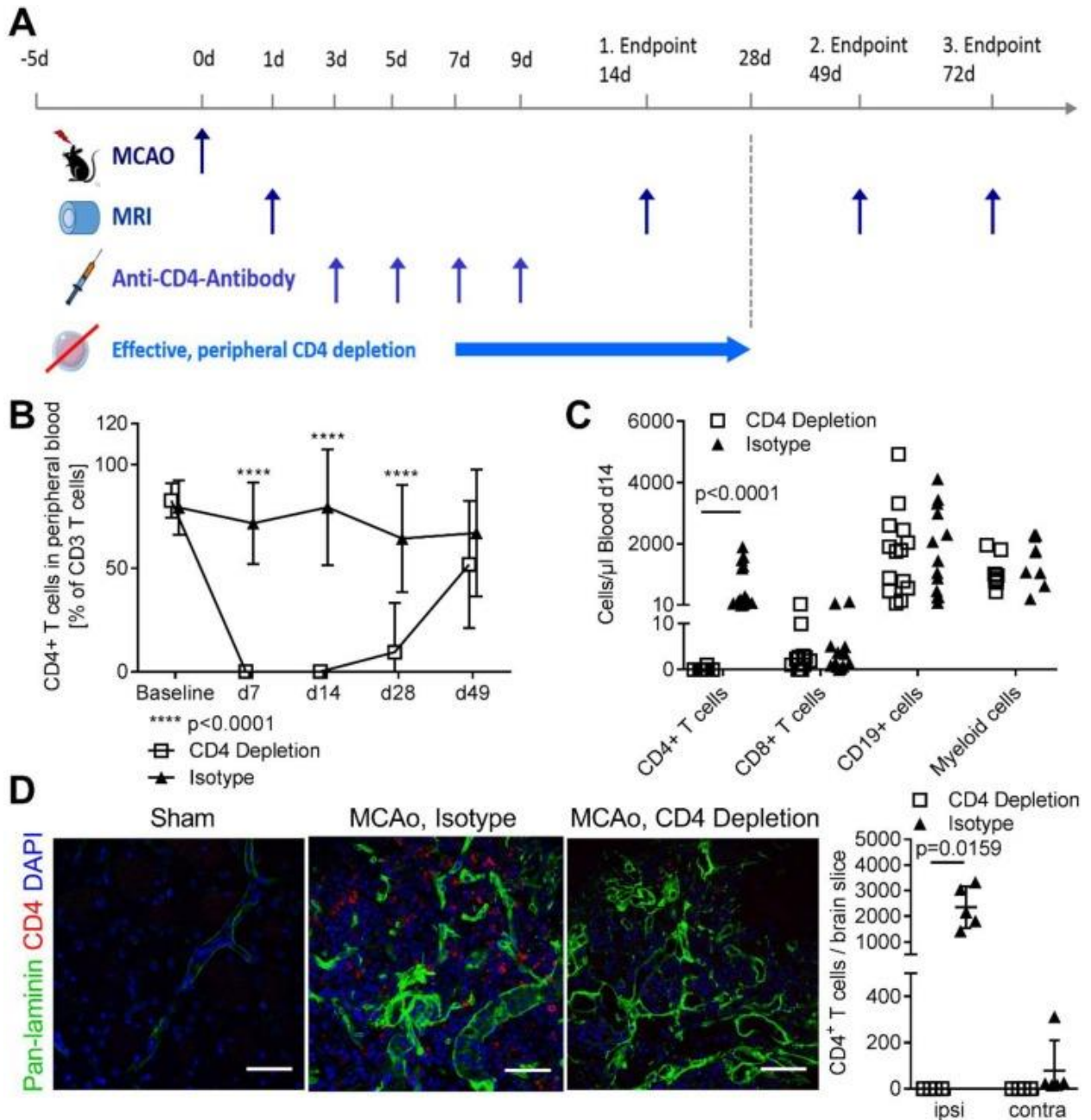


Note. “**A**) Infiltration of CD45⁺ leukocytes correlated with infarct volumes at day 1 ($r = 0.826$; $p = 0.016$; Spearman correlation) in isotype-treated mice [...]. **B**) Mice were assigned to equal treatment groups according to their initial infarct volumes.” Adapted from (Weitbrecht et al., 2021).

By depleting circulating CD4⁺ T cells with repeated anti-CD4 antibody injections at day 3, 5, 7 and 9 after MCAo, we focused our observations on delayed but not immediate or early immune responses after stroke onset (Fig. 4A). Following this protocol, we eliminated CD4⁺ T cells from the peripheral blood between day 7 and day 28 after stroke in CD4-depleted animals (Fig. 4B), while numbers of CD8⁺ T cells, CD19⁺ B cells and myeloid cells were not affected (Fig. 4C). Accordingly, at day 14 after MCAo CD4⁺ T cell infiltration into the brain was completely prevented by CD4 depletion, whereas isotype-treated control animals showed a diffuse infiltration pattern into the ischemic tissue in immunofluorescence staining (Fig. 4D).

Figure 4

Experimental Set-Up and CD4 Depletion Efficacy



Note. “**A**) Stroke was induced by 60 min MCAo and verified by MRI. Anti-CD4 antibody or IgG-isotype control was injected i.p. at day 3, 5, 7 and 9 after MCAo. Leukocyte infiltration was investigated at day 14, 49 [and] 72 after stroke by histology, flow cytometry and qRT-PCR. Additional MRI analysis on day 14 and 48 was performed to assess infarct maturation after CD4 depletion. **B**) Flow cytometry quantification of CD4⁺ T cells in blood samples of CD4-depleted and isotype-treated mice at baseline, day 7, 14, 28 and 49 after MCAo (2way ANOVA and Sidak’s multiple comparison) [...]. **C**) Flow cytometry quantification of circulating CD4⁺ T cells, CD8⁺ T cells, CD19⁺ [B] cells [...] and CD11b⁺ myeloid cells [...] at day 14 after MCAo (Mann-Whitney U-Test). **D**) Representative immunostaining for CD4⁺ T cells in ipsilateral hemispheres of sham-operated mice, isotype-treated MCAo mice and CD4-depleted MCAo mice 14 days after stroke onset with stereological quantification for CD4-depleted [...] and isotype-treated [...] mice (Mann-Whitney U-Test). Scale bar = 50μm.” Reprinted (Weitbrecht et al., 2021).

3.3. CNS-Resident Microglia and Infiltrating Myeloid Cells After CD4 Depletion

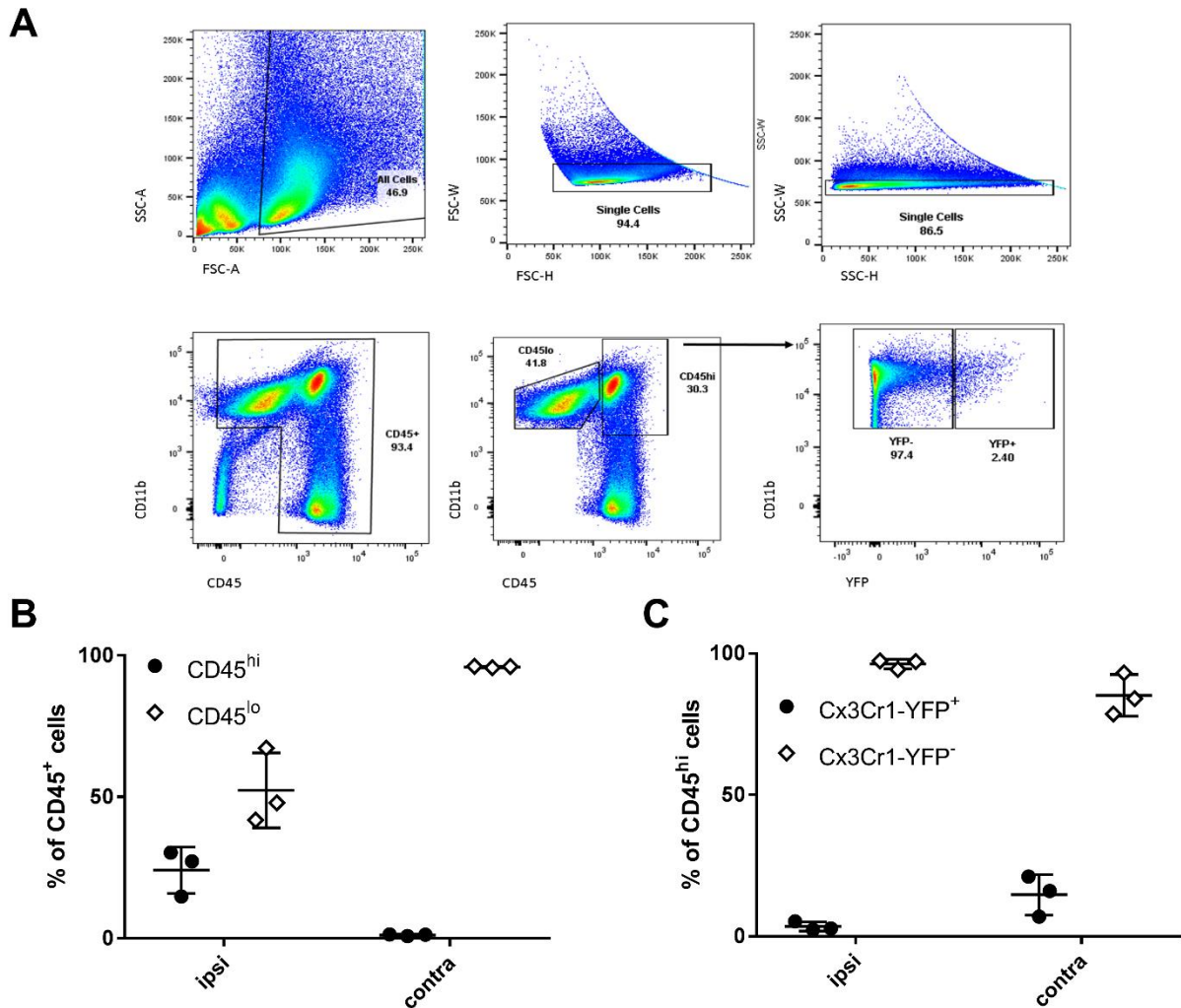
To investigate whether CD4 depletion influenced myeloid cell numbers in the delayed phase after stroke, we aimed to quantify resident microglia and IMC 14 days after MCAo by flow cytometry. Resting microglia express low levels of CD45 and can therefore be distinguished from IMC. However, there are no well-established markers to differentiate microglia from IMC in an activated state.

3.3.1. *Microglia and Infiltrating Myeloid Cells Can Be Distinguished by Flow Cytometry Using CD45 and CD11b Expression*

To validate CD45 as a marker to differentiate microglia from IMC after stroke, we administered Tamoxifen in 8-week-old Cx3Cr1^{CreERT2}-YFP transgenic mice to induce YFP expression in all Cx3Cr1-positive myeloid cells. Due to the high turnover of circulating monocytes, YFP was only expressed in the long-lived microglia and perivascular macrophages when we performed MCAo 4 weeks later (Goldmann et al., 2016). Using CD45 expression levels measured by flow cytometry, we discriminated CD11b⁺ myeloid cells into CD45^{hi} IMC and CD45^{lo} microglia and perivascular macrophages at day 14 after stroke (Fig. 5A). Around 25% of CD45⁺ cells in the ipsilateral hemisphere showed high CD45 expression, whereas all CD45⁺ cells in the contralateral hemisphere were CD45^{lo} (Fig. 5B). Nearly all CD45^{hi} cells were YFP⁻ and had therefore infiltrated from the periphery (Fig. 5C), which verifies that IMC and microglia can be distinguished by CD45 expression.

Figure 5

CD45 Expression is Sufficient to Distinguish Infiltrating Myeloid Cells (IMC) and Microglia by Flow Cytometry 14 Days After MCAo



Note. “8-week-old Cx3Cr1^{CreERT2}-YFP transgenic mice received 2 s.c. injections of 4mg Tamoxifen each to induce YFP expression in Cx3Cr1-positive cells. Stroke was induced 4 weeks after tamoxifen injections and brain tissue was analyzed by flow cytometry at day 14 after stroke. Due to the high turnover of peripheral myeloid cells, YFP was expressed in microglia and brain-resident macrophages but not IMC at this time [...]. **A**) Isolated leukocytes were gated based on [...] FSC and [...] SSC to determine single cells. CD45⁺ cells were discriminated into CD45^{hi} and CD45^{lo} populations. CD45^{hi} cells were further discriminated into YFP⁺ and YFP⁻. **B**) Quantification of CD45^{hi} and CD45^{lo} cells in ipsilateral and contralateral hemispheres. Data expressed as percent of CD45⁺ cells. **C**) Less than 5% of CD45^{hi} cells are YFP⁺ in the ipsilateral hemispheres at day 14 after MCAo indicating that CD45 gating is sufficient to distinguish microglia and brain-resident macrophages from IMC by flow cytometry.” Reprinted (Weitbrecht et al., 2021).

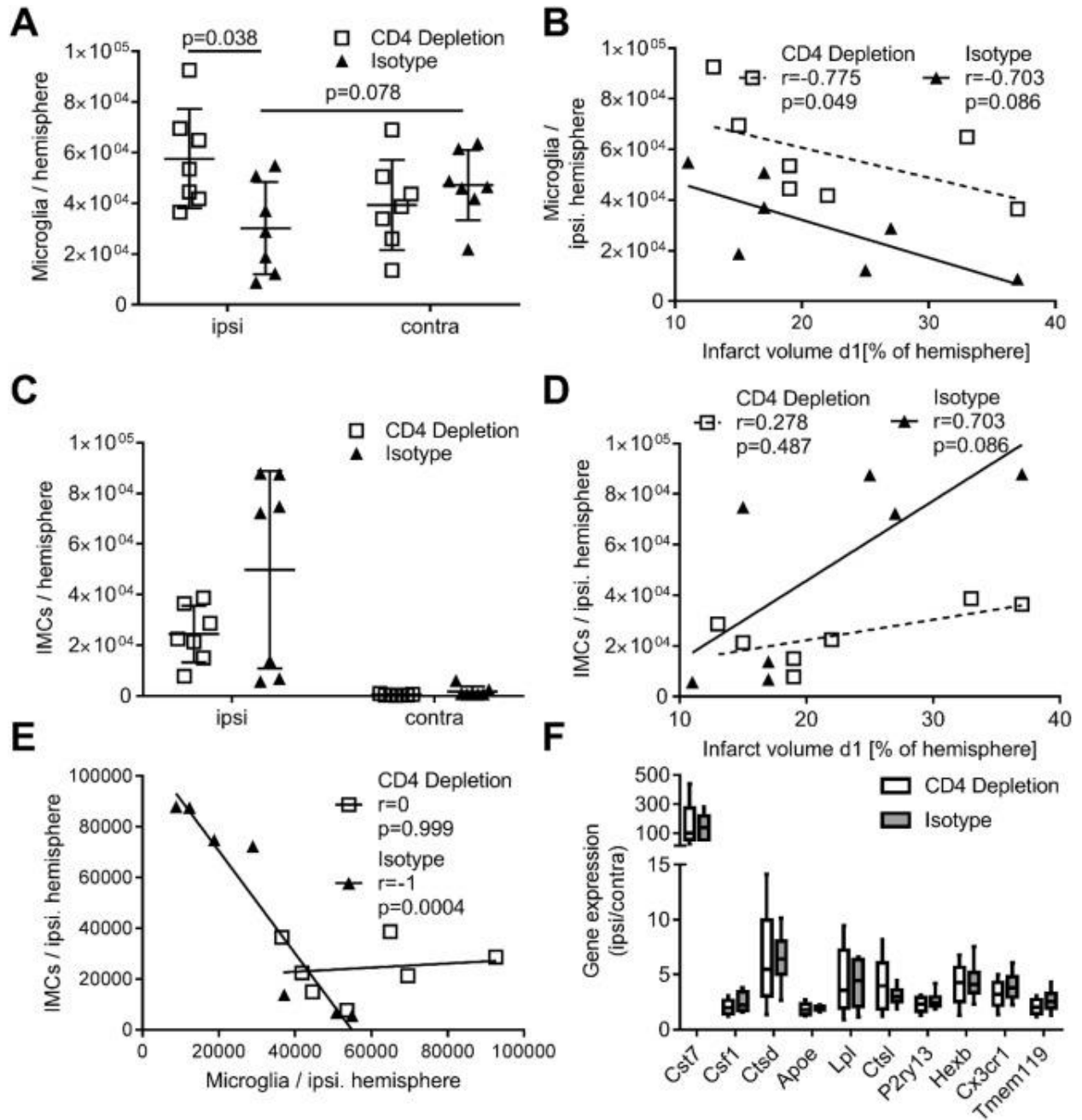
3.3.2. CD4 Depletion Mitigates Microglial Loss and Reduces Myeloid Cell Infiltration into the Brain After Severe Infarction

We used flow cytometry to investigate CNS myeloid cell populations as described above (see 3.3.1) and to determine whether CD4 depletion influenced numbers of IMC and resident microglia

in the delayed phase after stroke. At day 14 after MCAo, we observed a loss of microglia in the ipsilateral compared to the contralateral hemisphere of isotype-treated mice that was not statistically significant. This trend was completely abrogated by CD4 depletion. In fact, microglia numbers were significantly higher in the ipsilateral hemisphere of CD4-depleted mice compared to isotype-treated mice (Fig. 6A). Microglia numbers in the ipsilateral hemisphere of both treatment groups depended on infarct volumes and decreased with increasing lesion size. However, the correlation did not reach statistical significance in isotype-treated animals (Fig. 6B). Infiltration of myeloid cells from the periphery to the CNS was only observed in the ipsilateral hemisphere and was highly elevated only in a subgroup of isotype-treated animals (Fig. 6C). A correlation analysis indicated that these animals had suffered from large infarcts, suggesting that excessive myeloid cell infiltration may depend on infarct volumes. However, this interdependence did not reach statistical significance (Fig. 6D). In contrast, we observed only moderate IMC numbers in CD4-depleted mice, even in animals with large infarcts (Fig. 6D). Further correlation analysis indicated a relationship between IMC and microglia numbers in isotype-treated animals, where infiltration of myeloid cells into the ipsilateral hemisphere increased with decreasing microglia numbers, but not in CD4-depleted animals (Fig. 6E).

Figure 6

CD4 Depletion Reduces Microglial Loss and Myeloid Cell Infiltration at Day 14 After MCAo



“Note. **A-E**) Flow cytometry quantification of microglia and IMC [...]. **A**) Quantification of $CD45^{lo}CD11b^{+}$ microglia in ipsilateral and contralateral hemispheres of CD4-depleted and isotype-treated mice (Wilcoxon test). **B**) Correlation of microglia numbers in the ipsilateral hemisphere with infarct volume on day 1 in CD4-depleted and isotype-treated mice (Spearman correlation). **C**) Quantification of $CD45^{hi}CD11b^{+}$ IMC in ipsilateral hemispheres of CD4-depleted and isotype-treated mice (Wilcoxon test). **D**) Correlation of IMC numbers in the ipsilateral hemisphere with infarct volume on day 1 in CD4-depleted and isotype-treated mice (Spearman correlation). **E**) Correlation of microglia numbers with IMC numbers in the ipsilateral hemisphere CD4-depleted [...] and isotype-treated [...] mice (Spearman correlation). **F**) qRT-PCR analysis of microglial markers for activation (*Cst7*, *Csf1*, *Ctsd*, *ApoE*, *Lpl*, *Ctsl*) and homeostasis (*P2ry13*, *Hexb*, *Cx3cr1*, *Tmem119*). Data is presented as ratio of gene expression in ipsilateral to

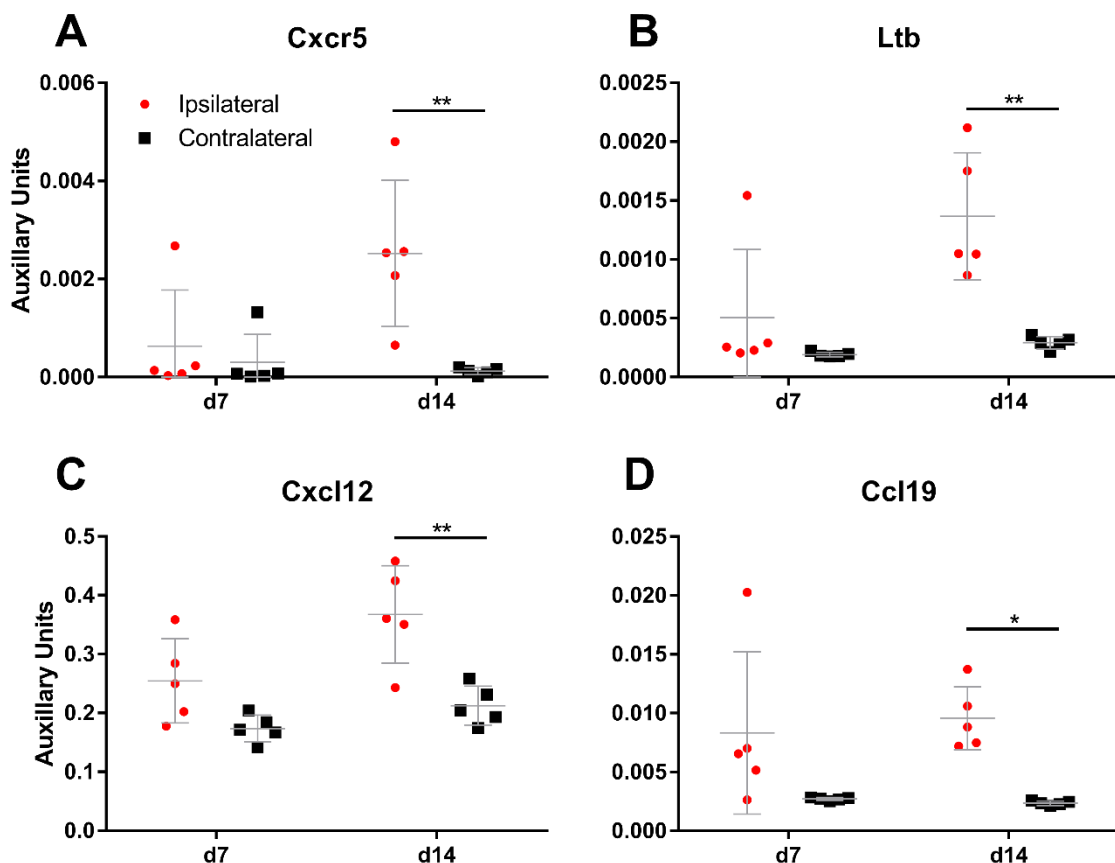
contralateral hemisphere of CD4-depleted [...] and isotype-treated [...] animals. Box plots with mean and whiskers (5–95%)” Reprinted (Weitbrecht et al., 2021).

3.4. Expression of Lymphocyte-Attracting and ELS-Inducing Cytokines in the Ischemic Brain

The expression of mRNA coding for the lymphocyte-attracting chemokines C-X-C motif ligand 12 (CXCL12) and (C-C motif) ligand 19 (CCL19) was significantly upregulated in the ipsilateral compared to the contralateral hemisphere 14 days after MCAo. Likewise, we observed elevated expression of the lymphoid follicle-inducing cytokine Lymphotoxin-beta (LTb) and CXC receptor 5 (CXCR5) (Fig. 7 A-D).

Figure 7

Lymphocyte-Attracting Cytokines Are Upregulated in the Ischemic Brain After Stroke



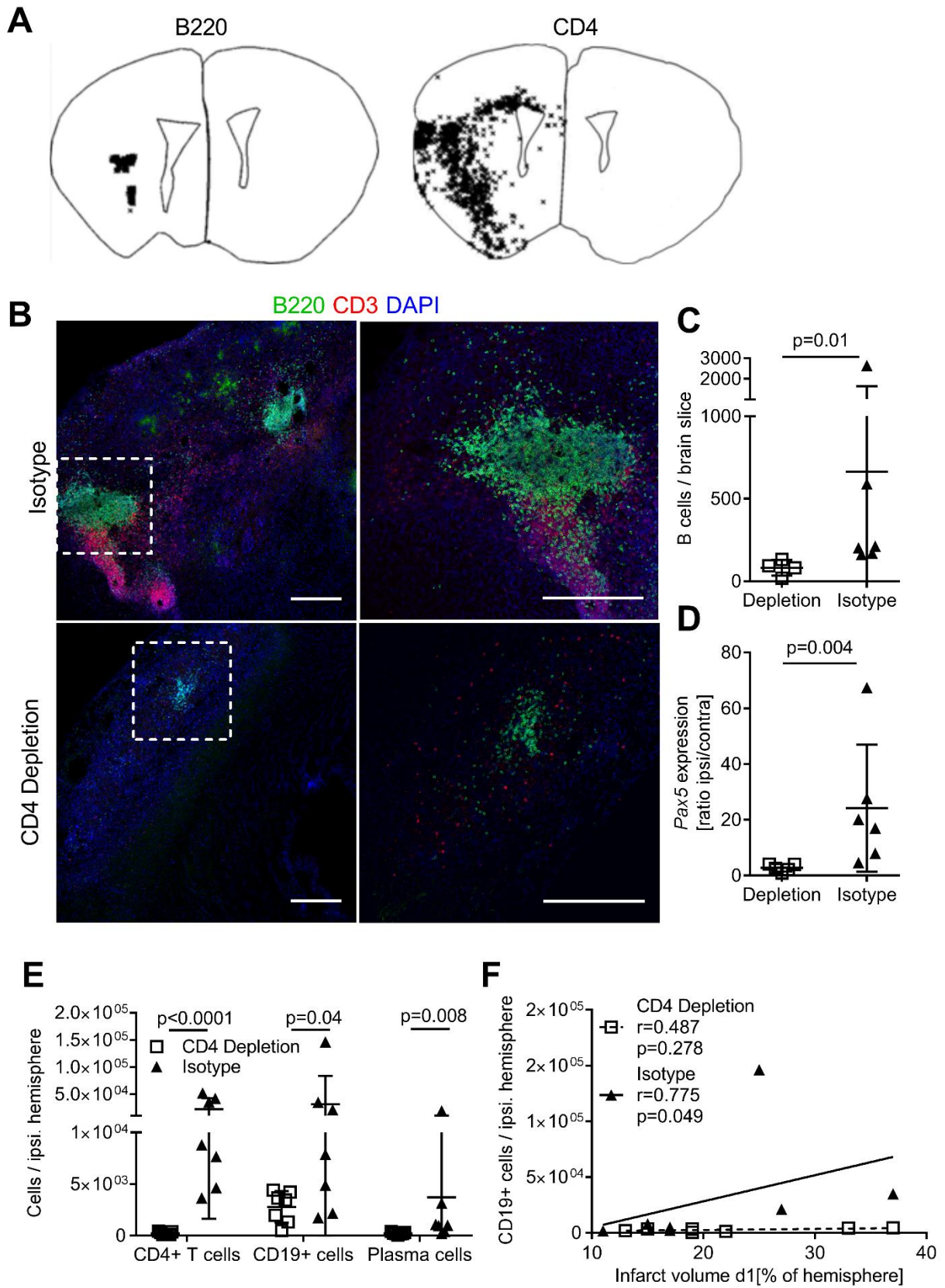
Note. qRT-PCR analysis at day 7 and 14 after MCAo in 2D2 mice reveals an upregulation of CXCR5 which enables B cells and Tfh to enter lymphoid tissue, the ELS-inducing cytokine LTb and the lymphocyte-attracting cytokines CXCL12 and CCL19 in the ipsilateral compared to the contralateral hemisphere. Two-way ANOVA; *p<0.05; **p<0.01; ***p<0.001.

3.5. CD4 Depletion Reduces B Cell Infiltration into the Ischemic Brain at Day 14 After Stroke

Immunohistological staining of CNS tissue at 14 days after MCAo revealed that infiltrating B cells accumulated in the ischemic area while CD4⁺ T cells showed diffuse infiltration of the surrounding area (Fig. 8A). The composition of resulting lymphocyte clusters resembled that of lymphoid follicles as described for ELS (Fig. 8B). In comparison with isotype-treated mice (Fig. 8B, top panels), B cell infiltration and ELS formation was strongly reduced in CD4-depleted animals (Fig. 8B, bottom panels). We confirmed this finding by stereological quantification (Fig. 8C) and by qRT-PCR measurement of the B cell marker Pax5 in tissue homogenates (Fig. 8D). In addition to the significant reduction of CD4⁺T cells and CD19⁺ B cells, we also found a decrease in plasma cell numbers in the ischemic brain of CD4-depleted animals using flow cytometry (Fig. 8E). A correlation of CD19⁺ B cell infiltration with infarct volumes was completely abrogated by CD4 depletion as well (Fig. 8F).

Figure 8

CD4 Depletion Inhibits B Cell Infiltration into the Ischemic Brain at Day 14 After MCAo



Note. “**A)** Representative images indicating distribution of B220⁺ B cells and CD4⁺ T cells in the ipsilateral hemisphere at day 14 after MCAo. **B)** Immunostaining of infarct area in CD4-depleted and isotype-treated mice (left panels) and B cell follicles in detail (right panels). Scale bar = 250µm. **C)** Stereological quantification of B220⁺ B cells after CD4 depletion [...] or isotype treatment [...] (Mann-Whitney U Test). **D)** qRT-PCR analysis of the B cell marker Pax5, displayed as ratio of gene expression in ipsilateral to contralateral hemisphere in CD4-depleted [...] and isotype-treated [...] animals (Mann-Whitney U Test). **E)** Flow cytometry quantification of CD4⁺ T cells, CD19⁺ B cells and CD138⁺ [plasma cells] in CD4-depleted and isotype-treated animals. Cell numbers are presented as mean with SD. Data was log-transformed prior to statistical analysis to attain normal distribution. Data was analyzed with Kolmogorov-Smirnov test for normality followed by unpaired t-test. **F)** Flow cytometry: Correlation of CD19⁺ B cell numbers in the ipsilateral hemisphere with infarct volumes at day 1 in CD4-depleted and isotype-treated mice (Spearman correlation).” Reprinted (Weitbrecht et al., 2021).

3.6. CD4⁺ T and B Cells Infiltrate the Ischemic Brain Once the CD4⁺ T Cell Population Recovers in the Periphery

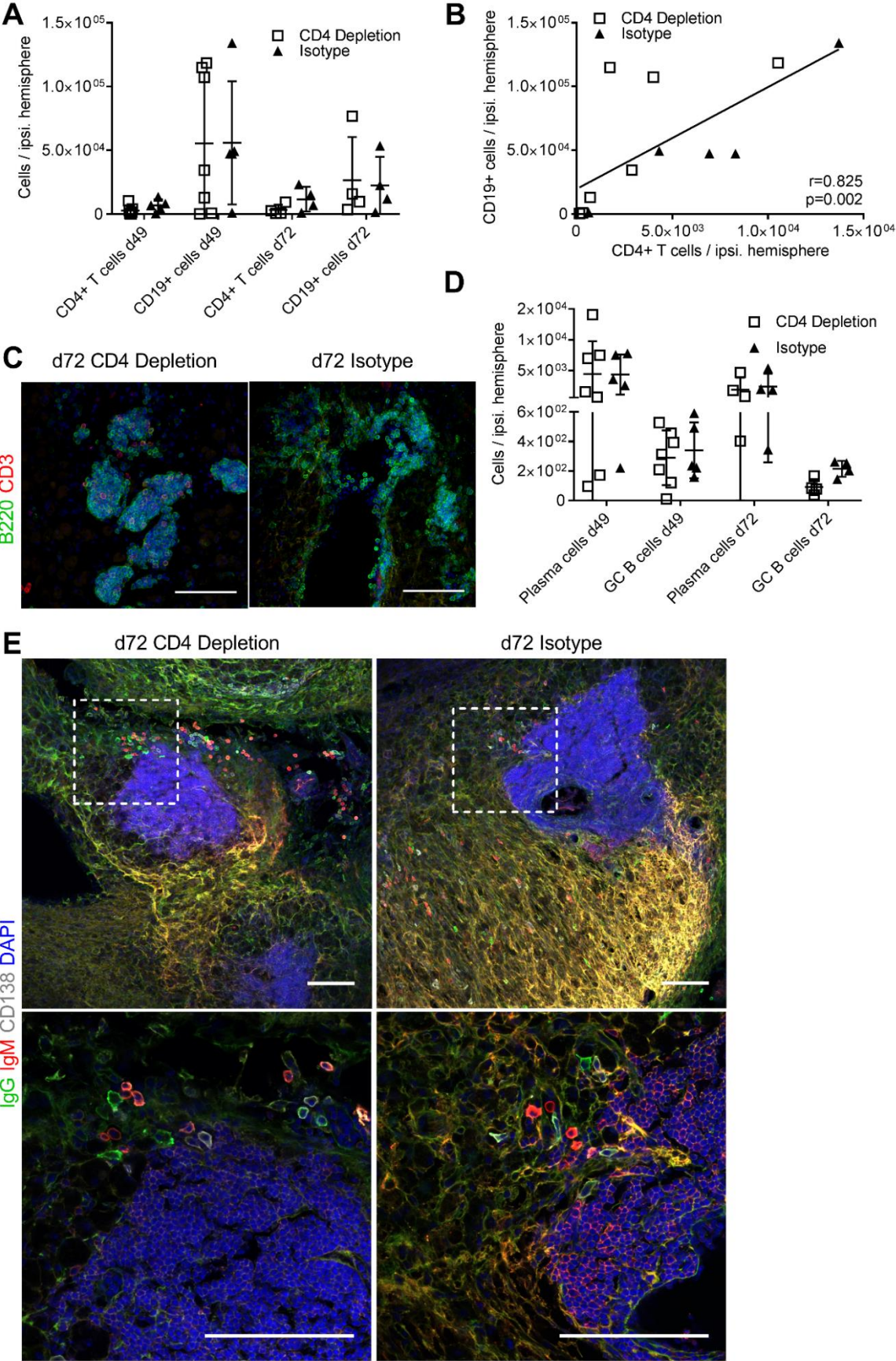
Treatment with anti-CD4 antibody between day 3 and 9 after MCAo reduced B cell infiltration into the brain and ELS formation at day 14 after stroke. However, circulating CD4⁺ T cells started recovering at day 28 after stroke in CD4-depleted mice. Therefore, we wondered whether the inhibitory effect of anti-CD4 antibody on B cell infiltration to the brain would also persist at later time-points when the peripheral CD4⁺ T cell population had recovered.

At day 49 and 72 after stroke we found high numbers of B cells within the ischemic brain of isotype-treated mice and animals where CD4⁺ T cells had recovered after previous CD4 depletion (Fig. 9A). In line with our hypothesis that CD4⁺ T cells facilitate B cell infiltration, we observed equal numbers of CD4⁺ T cells in both treatment groups (Fig. 9A) correlating with B cell infiltration at 49 days (Fig. 9B). Moreover, we found large, highly organized ELS at day 49 and 72 in both groups regardless of previous treatment. This may indicate that an adaptive immune response develops within the damaged brain tissue in response to the ischemic cell death (Fig. 9C). Further evidence for this hypothesis is provided by the presence of antibody-producing plasma cells and GL7⁺IgD⁻ germinal center-like B cells that differentiate from naïve B cells within lymphoid tissue upon exposure to their cognate antigen (Fig. 9D). CD138⁺ plasma cells expressed either IgM or IgG and were found in proximity to ELS (Fig. 9E). Diffuse IgM and IgG staining may represent autoreactive, locally produced antibodies binding to the surrounding tissue.

Overall, these data indicate that infiltration of B lymphocytes into the ischemic brain is not limited to the early phase after stroke but depends on the presence of peripheral CD4⁺ T cells and that brain-infiltrating B cells may differentiate within ELS, inducing an adaptive immune response on-site.

Figure 9

Lymphocytes Infiltrate the Ischemic Brain After the CD4⁺ Population Recovers in the Periphery



Note. “**A)** Flow cytometry quantification of CD4⁺ T cells and CD19⁺ B cells in the ipsilateral hemisphere of CD4-depleted and isotype-treated mice at day 49 (CD4 depletion: n = 7; isotype: n = 5) and day 72 (n = 4 per group) after MCAo. At this time, the CD4⁺ T cell population had recovered in the periphery of depleted animals. **B)** Correlation of CD19⁺ B cell numbers with CD4⁺ T cells in the ipsilateral hemisphere at day 49 after MCAo. Mice from both treatment groups are analyzed collectively in one correlation (n = 12) (Spearman correlation). **C)** Representative images of B cell follicles in ischemic brains of CD4-depleted and isotype-treated mice at day 72. Scale bar = 100 μm. **D)** CD138⁺ [plasma cells] and GL7⁺IgD⁻ [germinal center-like] B cells were detected by flow cytometry in both treatment groups at day 49 and 72 after MCAo. **E)** Representative images of IgG⁺ and IgM⁺ plasma cells in proximity to cell-rich ELS in CD4-depleted and isotype-treated mice at day 72 after MCAo. Top panels display ELS with surrounding plasma cells at 20x magnification. Bottom panels display 63x magnification of indicated areas. Scale bar = 100 μm.” Reprinted (Weitbrecht et al., 2021).

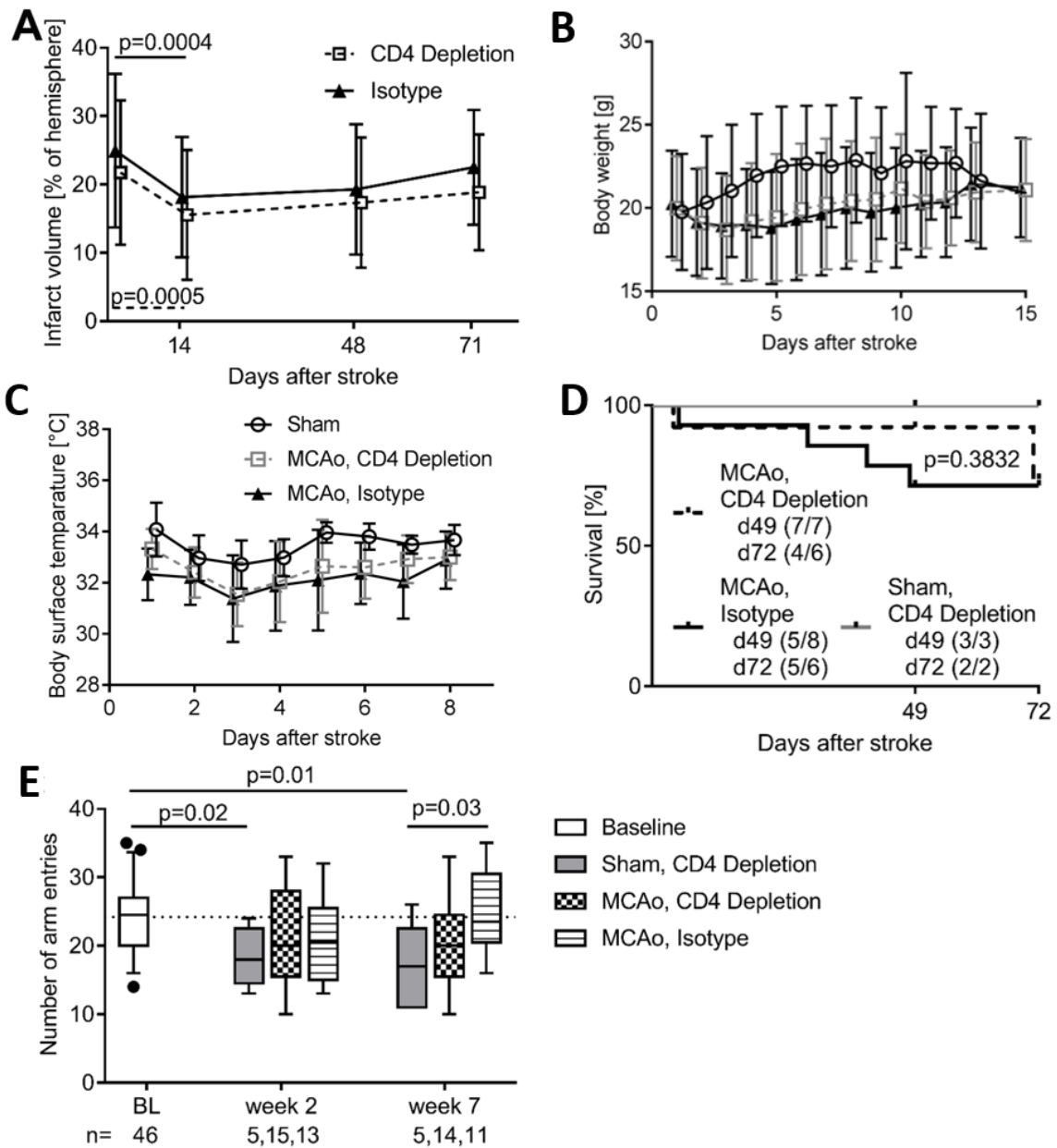
3.7. Temporary Inhibition of CD4⁺ T and B Cell Infiltration to the Brain Alleviates Cognitive Decline Without Influencing Infarct Volumes or Mortality

To assess long-term neurological outcome, mice underwent repeated MRI brain scans for up to 10 weeks after stroke. Here we observed a significant reduction of infarct volumes from day 1 to day 14 in both CD4-depleted and isotype-treated mice and a similar infarct maturation in both treatment groups beyond this time-point (Fig. 10A). In addition, no significant differences in survival or weight loss and body temperature, two parameters of the animals' overall well-being, were observed between groups (Fig. 10B-D).

A previous study suggested that infiltrating B cells and CNS antigen-specific autoantibody responses lead to cognitive impairment after stroke (Doyle et al., 2015). Therefore, we investigated whether CD4 depletion and the subsequent reduction in brain B cell infiltration would alleviate cognitive decline after stroke by subjecting all mice to behavioral testing in a Y-maze prior to the MCAo (baseline), as well as 2 weeks and 7 weeks after MCAo. Using the number of arm entries to assess learning and memory abilities, we observed that after 2 weeks all groups had decreased entries when compared to baseline, but only sham-operated and MCAo mice which received CD depletion displayed a further decrease in arm entries after 7 weeks. In contrast, isotype-treated control mice had almost as many arm entries after 7 weeks as they did at baseline (Fig. 10E) indicating differences in cognitive function between CD4-depleted and isotype-treated animals over the course of time after stroke.

Figure 10

Long-Term Functional Outcome After Stroke and CD4 Depletion



Note. A) “Long-term infarct maturation was assessed by T2-weighted infarct volumetry in CD4-depleted and isotype-treated mice at day 1 ($n = 15$ per group), 14 ($n = 13-14$), 48 ($n = 11-12$) and 71 ($n = 4-7$) after MCAo.” **B)** “CD4 depletion did not influence weight loss (sham: $n = 11$; CD4 depletion: $n = 28$; isotype: $n = 24$) or **C)** hypothermia (sham: $n = 8$; CD4 depletion: $n = 26$; isotype: $n = 21$) after MCAo.” **D)** “Long-term survival after 60min MCAo in CD4-depleted and isotype-treated animals from 2 separate experiments (Log-rank Mantel-Cox Test). Mice were sacrificed after 49 days or 72 days. Sample size is displayed as surviving/total mice used in the study. **E)** The number of spontaneous Y-maze arm entries was used to test learning and memory abilities, where decreased arm entries after repeated testing was interpreted as a learning effect due to functional memory (paired and unpaired t-test).” Adapted from (Weitbrecht et al., 2021).

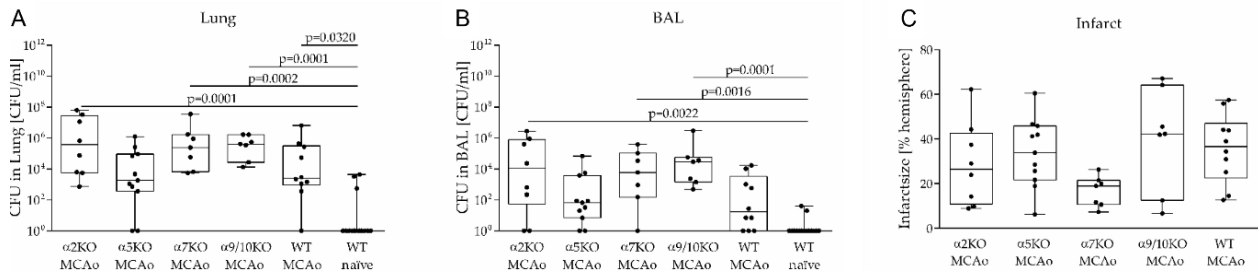
4. Results Publication 2: “Impact of Key Nicotinic AChR Subunits on Post-Stroke Pneumococcal Pneumonia”

4.1. Increased Susceptibility to Aspiration-Induced Pneumonia After Stroke is not Altered by Genetic Deficiency of Nicotinic Acetylcholine Receptors

Our group has previously demonstrated that cholinergic signaling via the parasympathetic nervous system mediated peripheral immunosuppression and therefore contributed to post-stroke pneumonia (Engel et al., 2015). We used aspiration-induced pneumonia, where *S. pneumoniae* was applied one day after MCAo surgery to the tracheal bifurcation in various nAChR deficient mouse strains and WT mice, to model stroke-associated pneumonia. The WT naïve control animals were infected with *S. pneumoniae* but were not subjected to MCAo. We obtained bacterial cultures from homogenized lung tissue and bronchoalveolar lavage (BAL) at day one after infection. We observed an elevated bacterial burden across all nAChR KO strains and WT mice, whereas bacterial clearance was preserved in control animals without infarcts (Fig. 11A-B). Histological staining revealed comparable infarct sizes between various nAChR KO strains and WT mice (Fig. 11C).

Figure 11

The Susceptibility to Aspiration-Induced Pneumococcal Pneumonia After Experimental Stroke Is Not Altered in nAChR Knockout (KO) Mice



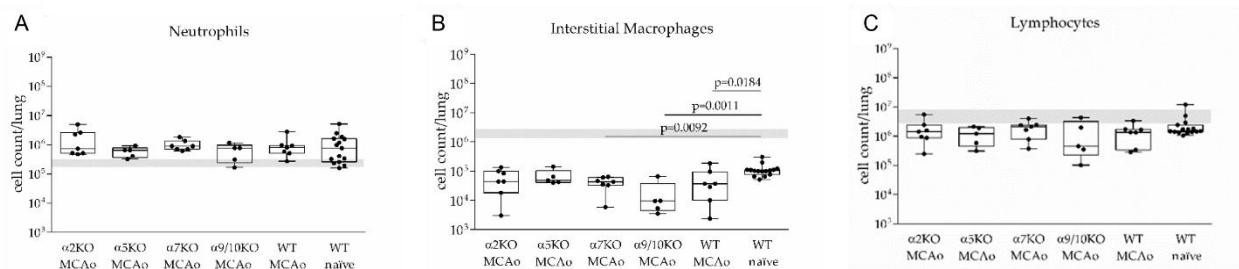
Note. “**A–C**) Untreated WT mice (naïve) or WT and nAChR KO mice subjected to MCAo surgery were infected with *S. pneumoniae* three days after MCAo.” Microbiological analysis of lung tissue and bronchoalveolar lavage (BAL) at day one after infection showed no effect on bacterial burden in mice deficient of α2, α5, α7 and α9/10 nAChRs. **C**) Histological staining indicated that nAChR deficiency did not impact infarct size four days after MCAo. Data from 6 independent experiments are shown (n = 7–15 per group) as box plots compared to WT naïve mice as a reference group for bacterial analysis and compared to WT MCAo mice as the reference group for infarct analysis using the Kruskal–Wallis test followed by Dunn’s test for multiple comparisons. Adapted (Jagdmann et al., 2020).

We then performed flow cytometry of homogenized lung tissue at day one after infection to determine whether impaired bacterial clearance after stroke correlated with changes in the pulmonary immune cell composition. Here we found a reduction in interstitial macrophages in α7

and $\alpha 9/10$ nAChRs KO mice and WT mice when compared to WT mice without stroke (Fig. 12B), while neutrophil and lymphocyte numbers were similar across all groups (Fig. 12A, C).

Figure 12

Impact of *S. Pneumoniae* Infection on the Pulmonary Immune Cell Repertoire in WT and nAChR KO Mice



Note. Immune cells were isolated from lung tissue and quantified by flow cytometry one day after infection with *S. pneumoniae*, **B**) where WT MCAo mice and MCAo mice deficient of $\alpha 7$ and $\alpha 9/10$ nAChRs showed a significant reduction in interstitial macrophages when compared to WT mice without MCAo surgery. **A, C**) The number of pulmonary neutrophils and lymphocytes did not differ between MCAo mice and naïve WT mice. The grey area represents numbers of leukocyte subsets in healthy mice (median with IQR). Data from 6 independent experiments are shown ($n = 5-15$ per group) as box plots compared to naïve WT mice as a reference group using the Kruskal–Wallis test followed by Dunn’s test for multiple comparison. Gating: Neutrophils ($CD45^+/CD11b^{hi}/Gr1^{hi}$); interstitial macrophages ($CD45^+/Gr1^-/SiglecF^-/CD11b^{hi}/F480^+$); lymphocytes (B cells: $CD45^+/CD11b^-/CD19^+$; T cells: $CD45^+/CD11b^-/CD3^+$; NK cells: $CD45^+/NK1.1^+/CD3^-$; NKT cells: $CD45^+/NK1.1^+/CD3^+$). Adapted (Jagdmann et al., 2020).

5. Results Publication 3: “A Primeval Mechanism of Tolerance to Desiccation Based on Glycolic Acid Saves Neurons in Mammals from Ischemia by Reducing Intracellular Calcium-Mediated Excitotoxicity”

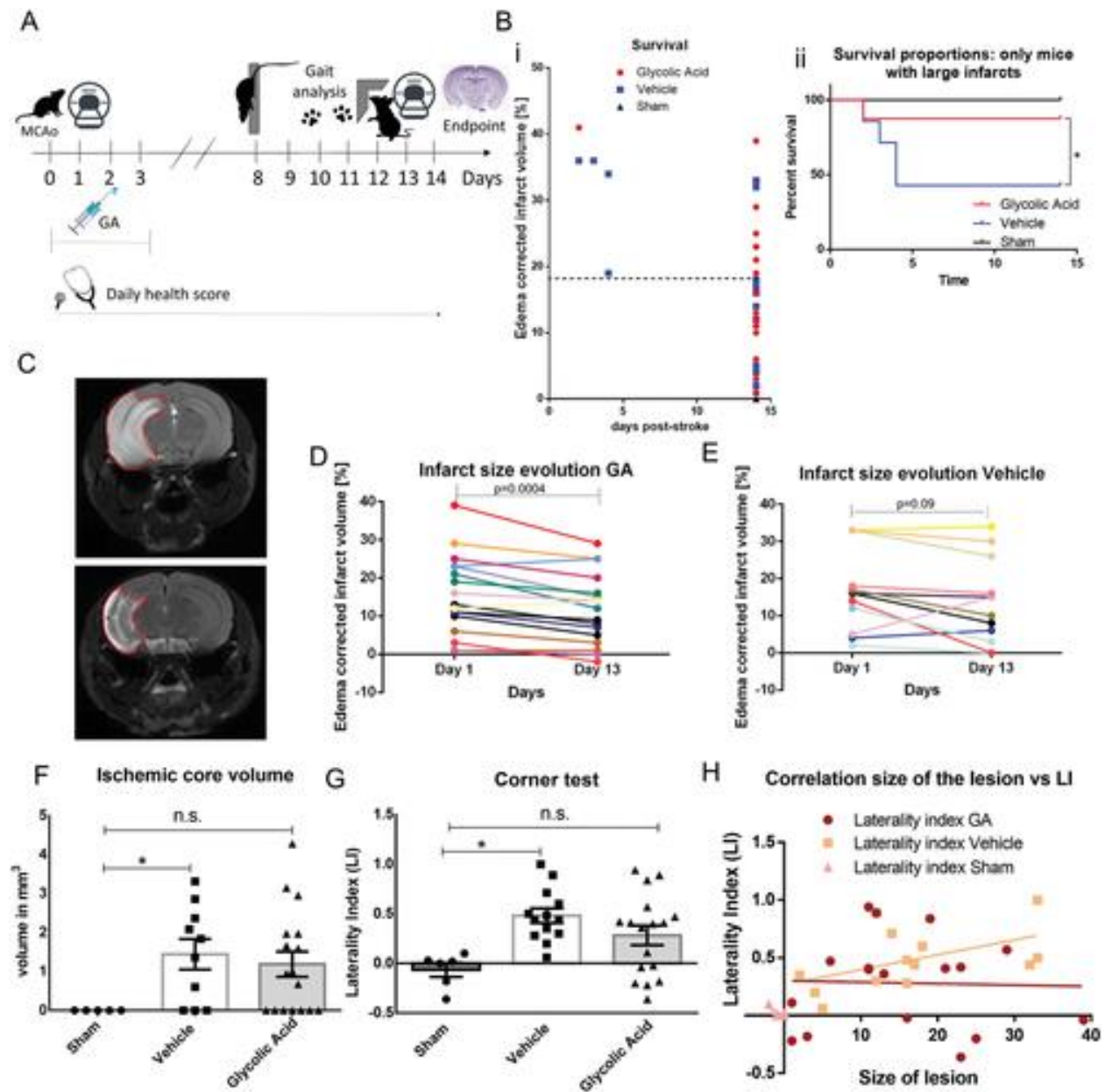
5.1. Glycolic Acid Improves Functional Outcomes After Experimental Stroke

Additionally, we investigated the neuroprotective properties of glycolic acid (GA) after stroke. Mice were subjected to MCAo or sham surgery and received GA injections i.p. immediately after stroke and on the following 3 days. Overall well-being of the animals, infarct progression and functional outcome were assessed by daily scoring, repeated MRI and behavioral testing until reaching the primary endpoint at day 14 after stroke (Fig. 13A). Survival did not differ between GA-treated and vehicle-treated control mice (Chovsepian et al., 2022). However, we observed that death only occurred in a subgroup of animals with large infarct volumes ($>18\%$ of ipsilateral hemisphere) (Fig. 13B-i). Within this subgroup mortality was significantly lower in GA-treated mice compared to control animals (Fig. 13B-ii). MRI infarct volumetry at day 1 after MCAo showed no difference in infarct lesions between GA-treated and vehicle-treated mice (data not shown) (Chovsepian et

al., 2022). An additional MRI at day 14 indicated that infarct lesions had decreased significantly after GA but not after vehicle treatment (Fig. 13C-E). Sensorimotor functions after stroke were analyzed with the corner test. Here, the laterality index (LI) of vehicle-treated animals was significantly higher compared to sham animals indicating a preference towards the non-affected side. In contrast, a similar LI in GA-treated animals and sham mice suggested that GA treatment alleviated stroke-induced sensorimotor dysfunction (Fig. 13G). We performed a gait analysis using the CatWalk system to further assess the effect of glycolic acid on motor functions after stroke. A camera recording each footprint on a transparent platform from underneath allowed for an analysis of various gait parameters, none of which showed any differences between GA-treated and control animals however (Fig, 14A-F). Likewise, both GA-treated and vehicle-treated animals performed similarly in the pole test (Fig. 14 G-H).

Figure 13

Glycolic Acid Improves Histological and Functional Outcomes After MCAo

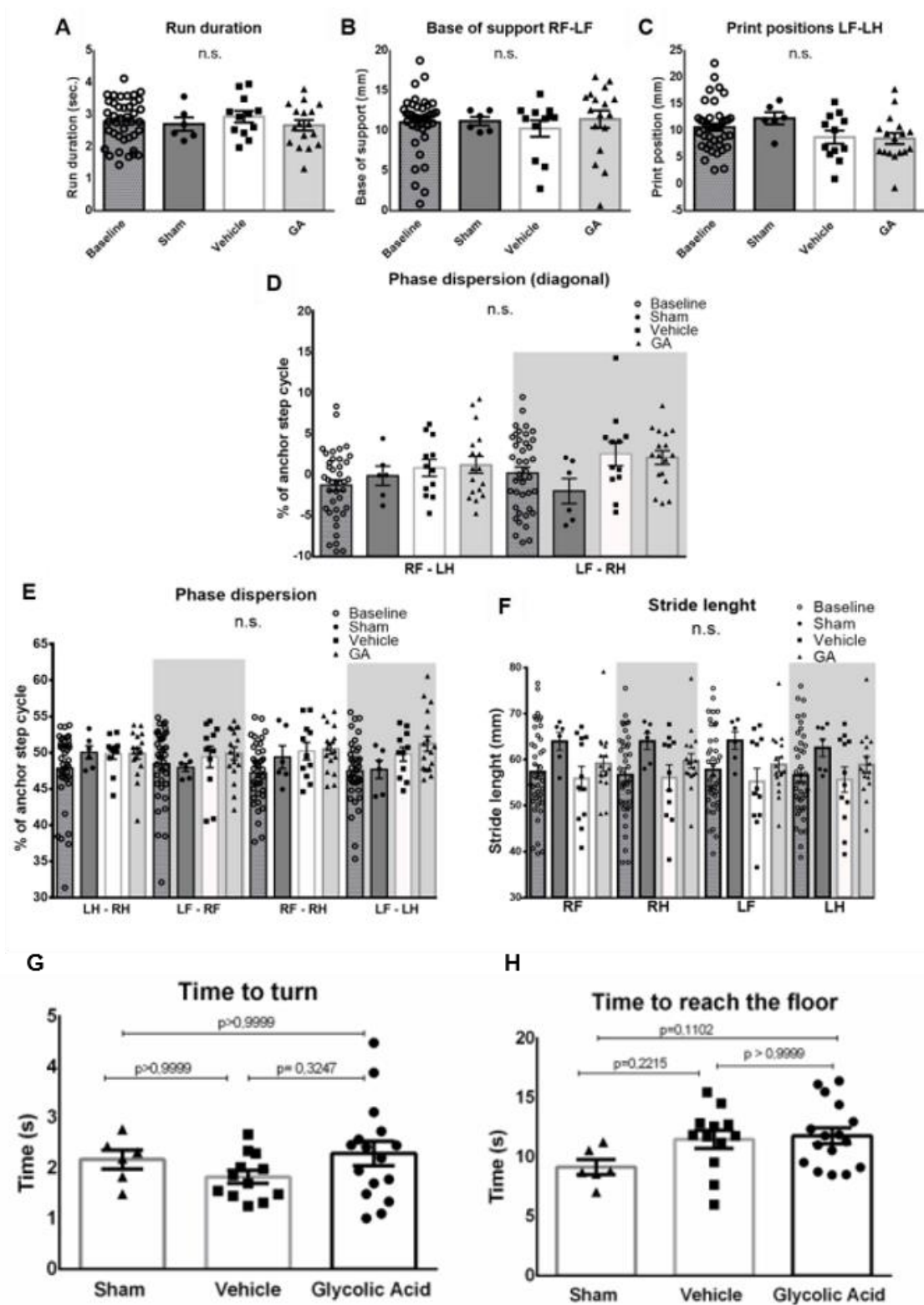


Note. Caption Figure 13 (previous page) A) Experimental design. Day 0: MCAo or sham operation. Day 0-3: Glycolic acid (GA) treatment. Day 1: Infarct volumetry by MRI. Day 8: Pole test. Day 10: Gait analysis. Day 12: Corner test. Day 13: MRI. Day 14: Primary endpoint. **B)** Only animals with infarcts larger than 18% of hemispheric volume reached humane endpoints and were sacrificed before reaching the primary endpoint at day 14 **(i)**. Early survival after stroke in mice with large infarcts (>18%) was improved after GA treatment (33% of vehicle-treated mice vs. 58.8% of GA-treated mice (Mantel–Cox survival test: Chi square = 6.215, $p = 0.0447$) **(ii)**. **C)** Representative MRI images: Infarct maturation after GA treatment at day 1 (top) and day 13 (bottom) after MCAo. **D-E)** Infarct volumes decreased significantly from day 1 to day 13 in GA-treated mice (paired t-test, $p = 0.0004$, $n = 17$), whereas no difference was detected in vehicle treated animals (paired t-test, $p = 0.091$, $n = 10$). **F)** Stereological quantification of ischemic core volumes (sham vs. vehicle: $p = 0.0243$; sham vs. GA: $p = 0.0638$, unpaired t-test; $n_{GA} = 17$, $n_{veh} = 10$, and $n_{sham} = 5$). **G)** The corner test was used to assess sensorimotor functions after stroke. Impaired animals show a preference for the non-affected limb when turning in the corner (high laterality index – LI). When compared to sham animals, the LI was significantly increased in vehicle-treated mice ($p = 0.0064$) but not GA-treated animals ($p = 0.1042$; one-way ANOVA followed by Bonferroni’s multiple comparisons test; $n_{GA} = 17$, $n_{veh} = 13$, $n_{sham} = 6$). **H)** The functional outcome after MCAO (LI index) was not correlated with the infarct size in either treatment group (GA-treated mice: Pearson’s $r = -0.03202$, $p = 0.9$; vehicle-treated mice: Pearson’s $r = 0.5086$, $p = 0.07$; $n_{GA} = 17$, $n_{veh} = 13$, and $n_{sham} = 6$). Data are presented as mean \pm SEM. Adapted (Chovsepian et al., 2022).

Note. Caption Figure 14 (following page) A-F) Gait analysis using the Catwalk system revealed no significant differences in the tested parameters between baseline, sham animals and GA or vehicle treatment regarding **A)** run duration **B)** base of support (distance between right and left forelimb), **C)** print position (distance between the two limbs of the same side), **D)** diagonal phase dispersion (contact of the target paw in relation to step cycle of the anchor paw), **E)** non-diagonal phase dispersion (all other comparisons) and **F)** stride length (distance between two successive steps with the same paw). **G-H)** No significant changes in motor function after MCAo were detected between sham mice and vehicle or GA treatment by the pole test regarding **G)** time until mice turn downward and **H)** time until mice touch the floor. One-way ANOVA, followed by Tukey’s multiple comparison’s test; Data displayed as mean \pm SEM; $n_{baseline}=36$ (CatWalk only), $n_{GA}=17$, $n_{veh}=13$, $n_{sham}=6$. Adapted (Chovsepian et al., 2022).

Figure 14

Glycolic Acid Does Not Improve the Performance on CatWalk or Pole Test



6. Discussion

This thesis depicts various aspects that determine the functional outcome after experimental stroke. The main publication characterizes CD4⁺ T cells as key players that facilitate infiltration of autoreactive B cells to the brain which contribute to long-term cognitive decline after experimental stroke. Other papers that I contributed to demonstrate that an altered pulmonary immune cell repertoire after stroke may increase susceptibility to pneumonia independently of single nAChR-subtype signaling and characterized glycolic acid as a novel neuroprotective substance that had beneficial effects on infarct remodeling and sensorimotor functions when administered during reperfusion.

Early immune responses in the brain following stroke have been studied extensively while the role of adaptive responses in the chronic phase are only poorly understood. A previous study demonstrated that delayed B cell infiltration to the CNS and ELS formation contribute to cognitive decline following stroke (Doyle et al., 2015). The main finding of our study is that this process largely depends on CD4⁺ T cell-dependent mechanisms and therefore supports our primary hypothesis. Additionally, we provide evidence that lymphocyte infiltration following stroke is a protracted process lasting more than 28 days in mice. The observation of reduced B cell infiltration, ELS formation within the brain and improved cognitive function in mice that underwent CD4 depletion sets the ground for new therapeutic targets in stroke (Weitbrecht et al., 2021).

The involvement of CD4⁺ T cells in early stroke pathology has been extensively investigated in various animal models in the past. Yet, the picture emerging from these studies is far from clear as divergent and even contradictory findings have been reported for certain T cell subsets. For instance, different kinetics of T cell infiltration have been reported (Gelderblom et al., 2009; Vindegaard et al., 2017). Overall, early T cell infiltration seems to increase infarct volumes by exacerbating neuroinflammation (Brait et al., 2010; Hurn et al., 2007; Kleinschnitz et al., 2010; Yilmaz et al., 2006), while regulatory T cells (Treg) may be harmful early after stroke and acquire protective functions later on (Liesz et al., 2015; Shi et al., 2021).

It remains a controversial discussion whether T cells infiltrate the ischemic brain in a CNS antigen-dependent manner. It has been argued that T cells may fulfill their detrimental function even when they were deprived of antigen recognition and co-stimulatory pathways by genetic modification (Kleinschnitz et al., 2010). On the other hand it was shown that inhibiting CNS-reactive T cell responses in mice by treating them with a recombinant T cell receptor ligand made up of partial major histocompatibility complex class II (MHC-II) molecules and CNS-specific myelin peptides inhibited immune cell infiltration and reduced infarct volumes (Subramanian et al., 2009). In addition, multiple studies have demonstrated that stroke outcomes can be altered by exposing the immune system to CNS-specific antigens before stroke, thereby inducing either immunologic tolerance or autoimmunity (Becker et al., 1997; Frenkel et al., 2003; Ren et al., 2012). Our study

provides additional evidence that CNS antigen-dependent lymphocyte infiltration exacerbates stroke outcomes as 2D2 mice with a pre-existing CNS autoreactive T cell repertoire showed a significant increase in lymphocyte infiltration, infarct volumes and mortality when compared to WT mice (Weitbrecht et al., 2021).

Under physiological conditions, lymphocytes have restricted access to the CNS due to the blood-brain barrier (Wilson et al., 2010). However, after stroke, multiple pathways may enable CNS antigen to reach peripheral lymphatic tissue and to be presented to lymphocytes by APCs. Inflammatory cytokines and the ischemic damage disrupt the blood-brain-barrier, allowing soluble antigens and APCs carrying phagocytosed antigen to enter the blood stream (Hochmeister et al., 2008). Additionally, CNS antigen may be transported to cervical lymph nodes along the recently discovered glymphatic system and meningeal lymphatic vessels (Eide et al., 2018; Louveau et al., 2015). Accordingly, an analysis of post-mortem lymphatic tissue of stroke patients showed T cells in proximity to APCs carrying phagocytosed CNS antigen (Planas et al., 2012). Therefore, it seems likely that delayed CNS antigen-specific lymphocyte infiltration, which peaks around week 7 in several studies including ours, involves priming in cervical lymph nodes (Miró-Mur et al., 2020; Weitbrecht et al., 2021; Zbesko et al., 2021).

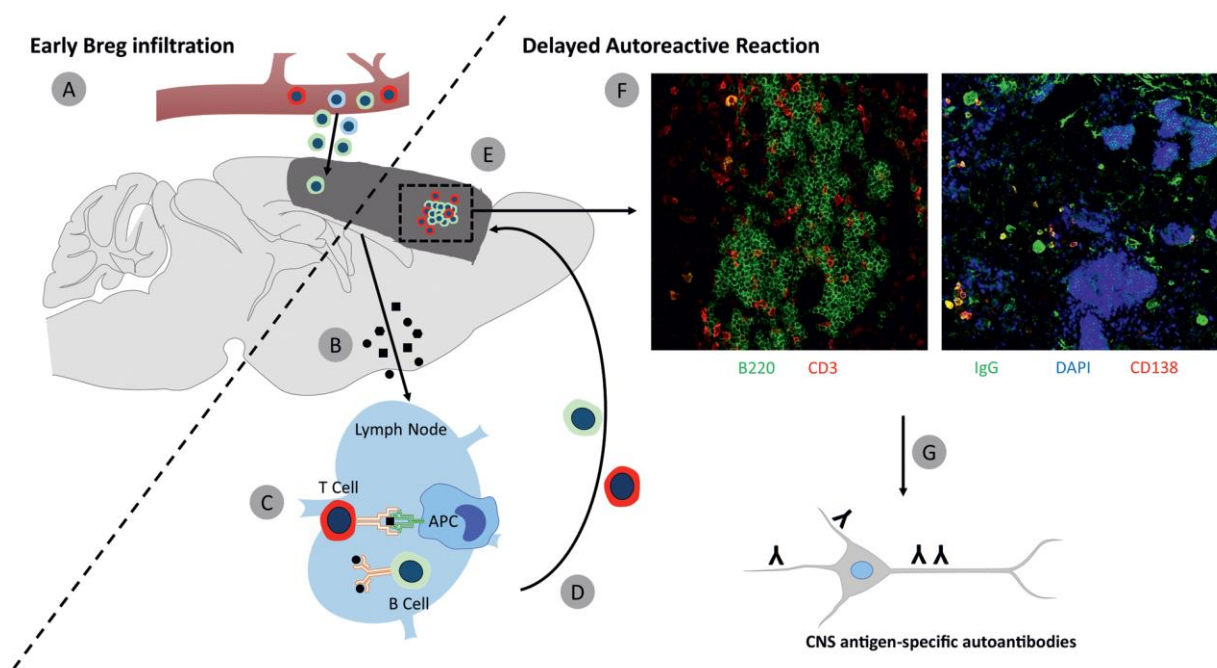
Upon entering the brain, lymphocytes form ELS consisting of B cells and T cells surrounded by microglia, dendritic-like cells, and stromal cells (Doyle et al., 2015; Weitbrecht et al., 2021). We have demonstrated that lymphocyte-attracting cytokines are upregulated in the ischemic brain of 2D2 mice (unpublished, Fig. 7), indicating that the underlying mechanisms of ELS induction may be similar to those reported in other systemic states of inflammation and autoimmunity (Corsiero et al., 2016). Differences in the local immune cell and stromal cell composition between the brain and peripheral organs, however, limit the possibility to draw conclusions on post-stroke ELS induction from other diseases. For example, it remains to be determined which cells produce ELS-inducing cytokines in the ischemic brain, while this is well characterized for systemic autoimmunity (Corsiero et al., 2016).

Nevertheless, ELS formation has also been reported in CNS pathologies such as multiple sclerosis (MS) and the mouse model for MS – experimental autoimmune encephalitis (EAE) (Mitsdoerffer & Peters, 2016). Here, ELS are found in the perivascular spaces and meninges (Lucchinetti et al., 2011; Prineas, 1979; Serafini et al., 2004). Even though the mechanisms leading to ELS induction in MS are largely unknown (Negron et al., 2020), extensive research in this field may provide some insights in ELS functions during stroke pathology. As previously reported for MS and EAE (Lehmann-Horn et al., 2016; Serafini et al., 2004), our study provides first evidence that ELS in the ischemic brain host germinal centers where B cells undergo clonal expansion, IgG hypermutation and differentiate to antibody-producing plasma cells (Weitbrecht et al., 2021). Concordantly, oligoclonal bands and CNS-reactive autoantibodies were observed in

the cerebrospinal fluid (CSF) of MS and stroke patients repeatedly (Pruss et al., 2012; Reiber et al., 1998; Tsementzis et al., 1986). The efficacy of B cell depleting antibodies in the treatment of cognitive decline in a stroke model and relapsing-remitting MS suggests a fundamental role for B cells in both diseases (Doyle et al., 2015; Gelfand et al., 2017). For instance, it was found that the presence of antibodies directed against myelin in stroke patients is associated with cognitive decline (Becker et al., 2016) and that they contribute to demyelination in MS by complement-dependent mechanisms (Liu et al., 2017). Additionally, B cells may exert functions beyond antibody production after stroke as they do in MS such as proinflammatory cytokine production and antigen presentation (Li et al., 2018). Contrary to their detrimental function during late immune responses, B cells also show beneficial properties in early neuroinflammation and regeneration following stroke which we discussed recently in our review “Friend or foe? – B cells in stroke” (Fig. 15) (Berchtold&Weitbrecht et al., 2019).

Figure 15

Differential B Cell Functions in the CNS After Stroke



Note. A) Early after stroke, different immune cell subsets, such as T cells (red), B cells (green), and myeloid cells (blue) infiltrate into the ischemic brain region. Amongst them, IL-10 producing regulatory B cells exert a beneficial role by inhibiting the inflammatory process. **B)** Due to the tissue damage, brain-specific antigens are released and drained towards the cervical lymph nodes. **C)** In the lymph node, the antigens can be presented to T cells by APCs or directly recognized by autoreactive B cell clones. **D-E)** The activated autoreactive B and T cells then infiltrate in a delayed manner into the ischemic brain region and start forming ELS.

F) Histological analysis of the mouse stroke brain 7 weeks after surgery. Left picture: Large B cell clusters (B220⁺, green) have formed in the infarct core and are surrounded by T cells (CD3⁺, red). Right picture: The B cells in the clusters express IgG (green) and surrounding the cluster IgG-producing plasma cells (CD138 and IgG double-positive, red/green respectively) can be observed. **G)** The antibodies produced in the local immune reaction in the ischemic brain can bind to neuronal antigens and cause delayed cognitive decline.” Reprinted (Berchtold&Weitbrecht et al., 2019).

Using an anti-CD4 antibody we demonstrated that CD4⁺ T cells are essential in B cell infiltration and ELS formation in the delayed phase after stroke (Weitbrecht et al., 2021). Even though the underlying mechanisms remain unknown at this point, a recent study in MS patients suggests that CXCL13 and its corresponding receptor CXCR5, both expressed by CD4⁺ T cells, play a crucial role for B cell recruitment to the CNS and formation of ELS, similarly to our findings in experimental stroke (Harrer et al., 2021; Weitbrecht et al., 2021). During states of inflammation and autoimmunity, infiltrating antigen-specific CD4⁺ T cells may acquire functions of specialized follicular T helper cells, which are normally found in secondary lymphoid tissue (Vu Van et al., 2016). By producing the B cell attracting chemokine CXCL13 and by cell-cell-interaction they facilitate B cell infiltration and orchestrate the ELS formation within inflamed tissues (Manzo et al., 2008; Vu Van et al., 2016). Other studies have demonstrated that IL-17, which is mainly secreted by CD4⁺ T helper 17 cells, induces production of CXCL12 and CXCL13 in stromal cells and infiltrating monocytes (Carlsen et al., 2004; Fleige et al., 2014). Interestingly, our results suggest that CD4 depletion inhibits monocyte infiltration particularly in mice with large infarcts (Weitbrecht et al., 2021). Therefore, various pathways may explain the reduced infiltration of B cells after CD4 depletion which have not been determined in our study.

Several limitations need to be addressed in the context of this study. As described above, it is known that various CD4⁺ T cell subsets may exert functions over the course of post-stroke neuroinflammation which are contradictory in part (Cramer et al., 2019). Unspecific depletion of all CD4⁺ T cell subsets after stroke may therefore lead to distorted results. Importantly, CD4-negative T cells, which were not addressed by our depletion protocol, also contribute to stroke pathology. For instance, it was shown that $\gamma\delta$ -T cells exacerbate outcomes after stroke and secrete IL-17, which may induce the production of lymphocyte-attracting cytokines (Shichita et al., 2012). Likewise, protective and detrimental functions have been shown for cytotoxic CD8⁺ T cells during chronic stroke pathology (Selvaraj et al., 2021; Xie et al., 2019). Intravenous infusions with a mixture of immunoglobulins from healthy donors represent a key treatment strategy in various autoinflammatory and autoimmune diseases. The mechanism of action for this therapy is not fully understood. However, it is assumed that the donor IgGs eliminate circulating autoantibodies by directly binding to them, by upregulation of inhibitory Fc receptors, by stimulation of the complement system or by reducing T cell-mediated microglial activation (Bayry

et al., 2003; Janke & Yong, 2006; Samuelsson et al., 2001). Therefore, administering anti-CD4 antibody or isotype-control may have immunomodulatory effects that are unrelated to CD4⁺ T cell reduction even if this effect has not been investigated for monoclonal antibodies. In our study we used 2D2 mice which foster an increased potential for CNS-reactive lymphocyte responses due to their genetically modified TCR recognizing MOG (Bettelli et al., 2003). As a consequence, our study may have yielded results that do not necessarily represent the WT phenotype in which lower levels of neuroinflammation are expected. In addition, it is known that stroke susceptibility and the extend of ischemic damage varies between mouse strains due to differences in cerebrovascular anatomy, cytokine expression and glutamate-induced excitotoxicity (Barone et al., 1993; Lambertsen et al., 2002; Schauwecker & Steward, 1997). Therefore, we need to reproduce our observation of reduced B cell infiltration after CD4 depletion in WT mice and eventually in human stroke patients.

We hypothesized that CNS-specific antibodies that are produced locally by infiltrated B cells following differentiation within ELS, lead to PSCI in stroke patients based on the finding that B cell depletion in experimental stroke alleviates cognitive decline (Doyle et al., 2015). Similarly we observed that CD4 depletion had beneficial effects on long-term cognitive functions in mice even if the reduction in B cell infiltration to the brain was only transient (Weitbrecht et al., 2021). A permanent CD4 depletion protocol may have yielded more pronounced effects, which needs to be addressed in future experiments. In addition, we are in the process of establishing more sensitive behavioral test as detecting cognitive dysfunction in mice has proven difficult in the past (Rosell et al., 2013). All taken together, clinical studies indicate a correlation between CNS-reactive antibodies and cognitive decline, which preclinical studies suggest can be treated by immunomodulatory therapy (Becker et al., 2016; Doyle et al., 2015).

Nevertheless, stroke outcomes are also determined by acute complications such as stroke-associated pneumonia (SAP) (Rocco et al., 2012). Dysphagia and subsequent aspiration of gram-negative pharyngeal bacteria facilitate the induction of SAP which triples stroke mortality (Katzan et al., 2003; Westendorp et al., 2011). Interestingly, stroke patients who suffered from pneumonia were more likely to develop autoreactive Th1 responses to CNS antigens such as MBP and glial fibrillary acidic protein. Moreover, it was shown that a CNS-reactive Th1 repertoire was associated with a poor long-term outcome according to the modified Rankin Scale (Becker et al., 2011).. Therefore, states of systemic inflammation including SAP during stroke seem to aggravate CNS inflammation and cognitive decline following stroke (Elkind, Boehme, et al., 2020; Tsai et al., 2019) indicating that preventing SAP may also reduce stroke patients' risk of dementia.

Our research group had previously discovered in a mouse model that an overactivation of the sympathetic nervous system caused stroke-induced immunodepression syndrome (SIDS), a long-known phenomenon that contributes to post-stroke infection susceptibility (Prass et al.,

2003). Immune responses are further suppressed by parasympathetic signaling and binding of acetylcholine to its receptor $\alpha 7nAChR$ expressed on alveolar epithelial cells and tissue resident macrophages of the lung (Engel et al., 2015; Lafargue et al., 2012). Vagotomy and the genetic knock-out of $\alpha 7nAChR$ reduced the pulmonary bacterial burden of Gram-negative pathogens in a model of spontaneous pneumonia after stroke (Engel et al., 2015). However, in an aspiration model of pneumonia with the Gram-positive pathogen *S. pneumoniae* these receptors were not involved (Jagdmann et al., 2020). This contradictory finding might be due to differences in immune responses to gram-negative bacteria as observed in spontaneous SAP and the gram-positive *S. pneumoniae* which were used in our study (Kumar, 2020). However, susceptibility to SAP may also depend on other factors such as housing conditions, microbiome and the individual mouse strains used in the experiments (Schulte-Herbruggen et al., 2006; Stanley et al., 2016). Prophylactic antibiotic treatment had shown promising results in experimental stroke (Meisel et al., 2004) but did not improve the functional outcome in clinical trials despite preventing SAP (Westendorp et al., 2015), emphasizing the lack of therapeutic strategies in post-stroke care. In theory, SAP susceptibility could be reduced by blocking excessive sympathetic and parasympathetic signaling, thereby inhibiting SIDS (Engel et al., 2015; Meisel & Meisel, 2011; Prass et al., 2003). However, it was propagated that peripheral immunosuppression may dampen CNS autoreactivity induced by stroke (Vogelgesang & Dressel, 2011). In fact, blocking SIDS with Propranolol and Mifepristone reduced early post-stroke pneumonia but increased CNS antigen specific T cell responses in 2D2 mice at a later time (Romer et al., 2015). Therefore, caution is advised when considering immunomodulatory therapy after stroke as neuroinflammation could be exacerbated by treating SIDS and *vice versa* (Meisel & Meisel, 2011).

Upon cerebral ischemia danger associated molecular patterns (DAMPs) and reactive oxygen species are released from the damaged tissue which activates resident microglia and attracts innate immune cells from the periphery. Various cytokines are produced on-site to attract further immune cells and create an inflammatory environment exacerbating local tissue damage and attracting further immune cells from the innate and adaptive immune system (Chamorro et al., 2012; Iadecola & Anrather, 2011). The concept of neuroprotection aims at reducing neuronal cell death and the consecutive outpour of DAMPs caused by acute ischemia therefore interrupting this vicious cycle from the beginning (Chamorro et al., 2016; Endres et al., 2022). Other targets of neuroprotective approaches are excitotoxicity and oxidative and nitrosative stress (Chamorro et al., 2016)

Our recent research yields promising results for glycolic acid as a neuroprotective substance in stroke therapy. When injected into the left common carotid artery during reperfusion in mice that underwent global cerebral ischemia, glycolic acid significantly increased neuronal survival in the ipsilateral hippocampus compared to the contralateral side. When administered i.p. from day 0 to

day 3 after MCAo, glycolic acid enhanced infarct shrinkage over time in comparison to vehicle-treated animals. In addition, mice that received glycolic acid performed better in behavioral tests (Chovsepian et al., 2022). Finally, we used a novel endovascular stroke model in swine to improve the resemblance of experimental stroke to the events during acute stroke in human patients (Golubczyk et al., 2020). Here, an intraarterial (i.a.) catheter was used to inject thrombin and thereby induce cerebral ischemia which lasted for 2 hours. Subsequently, reperfusion was initiated by i.a. thrombolysis with alteplase and a bolus of glycolic acid or NaCl was administered using the same catheter immediately afterwards. While the initial infarct volumes before reperfusion did not differ between treatment groups, infarct lesions were significantly smaller in swine treated with glycolic acid at later time-points as observed in MCAo mice. Our observation that glycolic acid inhibits Ca^{2+} influx into neuronal cells and thereby reduces glutamate-dependent excitotoxicity in an *in vitro* model of oxygen and glucose deprivation may explain the neuroprotective effects in our experiments (Chovsepian et al., 2022).

Even if this preclinical study showed promising results for glycolic acid in stroke treatment, countless equally promising neuroprotective substances have failed to show benefits in randomized controlled trials (RCT). Since the 1980s countless phase 2 and 3 studies have attempted to implement neuroprotective substances into clinical practice, all of which have failed (Chamorro et al., 2016). Various problems in stroke research have been identified since then, among them flawed design of preclinical and clinical studies, differences in experimental stroke and stroke in humans, and publication bias (Chamorro et al., 2016; Endres et al., 2008; Mergenthaler & Meisel, 2012). Lately, the scientific community has made increasing efforts to overcome this translational roadblock, for instance by introducing reporting-guidelines in animal research (i.e., ARRIVE guideline) or by promoting publication of negative results. In fact, some substances are tested in preclinical multicentered RCTs for animals, before entering a clinical trial stage. Nevertheless, this does not guarantee success as demonstrated recently for Natalizumab, which failed to improve stroke patients' outcome in an RCT after showing beneficial effects in multiple preclinical studies and a preclinical (Elkind, Veltkamp, et al., 2020; Llovera et al., 2015). Nevertheless, there is an urgent need for new therapeutics, as current treatment options are limited to thrombolysis and endovascular thrombectomy (Roaldsen et al., 2021).

Altogether, our research suggests a critical role for infiltrating immune cells in the pathogenesis of dementia after stroke, which can be targeted by immunomodulatory therapy. To establish more specific therapeutic targets, the underlying cell-cell-interactions, cytokine signaling, and pathogenic properties of CNS-reactive autoantibodies need to be investigated in detail. Systemic immunodepression syndrome may represent an endogenous mechanism ameliorating neuroinflammation after stroke but increases the risk for fatal infections which in turn exacerbate

CNS-reactive immune responses. These complex interactions need to be considered for the development of new therapeutic approaches.

References

- Balkaya, M., Krober, J., Gertz, K., Peruzzaro, S., & Endres, M. (2013). Characterization of long-term functional outcome in a murine model of mild brain ischemia [Research Support, Non-U.S. Gov't]. *Journal of neuroscience methods*, 213(2), 179-187. <https://doi.org/10.1016/j.jneumeth.2012.12.021>
- Balkaya, M., Kröber, J. M., Rex, A., & Endres, M. (2012). Assessing Post-Stroke Behavior in Mouse Models of Focal Ischemia. *Journal of Cerebral Blood Flow & Metabolism*, 33(3), 330-338. <https://doi.org/10.1038/jcbfm.2012.185>
- Barone, F. C., Knudsen, D. J., Nelson, A. H., Feuerstein, G. Z., & Willette, R. N. (1993). Mouse strain differences in susceptibility to cerebral ischemia are related to cerebral vascular anatomy. *J Cereb Blood Flow Metab*, 13(4), 683-692. http://www.ncbi.nlm.nih.gov/entrez/query.fcgi?cmd=Retrieve&db=PubMed&dopt=Citation&list_uids=8314921
- Bayry, J., Thirion, M., Misra, N., Thorenoor, N., Delignat, S., Lacroix-Desmazes, S., Bellon, B., Kaveri, S., & Kazatchkine, M. D. (2003). Mechanisms of action of intravenous immunoglobulin in autoimmune and inflammatory diseases. *Neurological Sciences*, 24(4), s217-s221. <https://doi.org/10.1007/s10072-003-0081-7>
- Becker, K. J., Kalil, A. J., Tanzi, P., Zierath, D. K., Savos, A. V., Gee, J. M., Hadwin, J., Carter, K. T., Shibata, D., & Cain, K. C. (2011). Autoimmune responses to the brain after stroke are associated with worse outcome [Research Support, N.I.H., Extramural]. *Stroke; a journal of cerebral circulation*, 42(10), 2763-2769. <https://doi.org/10.1161/STROKEAHA.111.619593>
- Becker, K. J., McCarron, R. M., Ruetzler, C., Laban, O., Sternberg, E., Flanders, K. C., & Hallenbeck, J. M. (1997). Immunologic tolerance to myelin basic protein decreases stroke size after transient focal cerebral ischemia. *Proc Natl Acad Sci U S A*, 94(20), 10873-10878. http://www.ncbi.nlm.nih.gov/entrez/query.fcgi?cmd=Retrieve&db=PubMed&dopt=Citation&list_uids=9380727
- Becker, K. J., Tanzi, P., Zierath, D., & Buckwalter, M. S. (2016). Antibodies to myelin basic protein are associated with cognitive decline after stroke. *J Neuroimmunol*, 295-296, 9-11. <https://doi.org/10.1016/j.jneuroim.2016.04.001>
- Bederson, J. B., Pitts, L. H., Tsuji, M., Nishimura, M. C., Davis, R. L., & Bartkowski, H. (1986). Rat middle cerebral artery occlusion: evaluation of the model and development of a neurologic examination. *Stroke*, 17(3), 472-476. http://www.ncbi.nlm.nih.gov/entrez/query.fcgi?cmd=Retrieve&db=PubMed&dopt=Citation&list_uids=3715945
- Berchtold & Weisbrecht, Meisel, C., & Meisel, A. (2019). Friend or foe? – B cells in stroke. *Neuroforum*, 25(3), 173-183. <https://doi.org/https://doi.org/10.1515/nf-2018-0031>
- Bettelli, E., Pagany, M., Weiner, H. L., Linington, C., Sobel, R. A., & Kuchroo, V. K. (2003). Myelin oligodendrocyte glycoprotein-specific T cell receptor transgenic mice develop spontaneous autoimmune optic neuritis. *J Exp Med*, 197, 1073-1081. <https://doi.org/10.1084/jem.20021603>
- Brait, V. H., Jackman, K. A., Walduck, A. K., Selemidis, S., Diep, H., Mast, A. E., Guida, E., Broughton, B. R. S., Drummond, G. R., & Sobey, C. G. (2010). Mechanisms contributing to cerebral infarct size after stroke: gender, reperfusion, T lymphocytes, and Nox2-derived superoxide. *J Cereb Blood Flow Metab*, 30(7), 1306-1317. <https://doi.org/10.1038/jcbfm.2010.14>
- Carlsen, H. S., Baekkevold, E. S., Morton, H. C., Haraldsen, G., & Brandtzaeg, P. (2004). Monocyte-like and mature macrophages produce CXCL13 (B-cell-attracting chemokine 1) in inflammatory lesions with lymphoid neogenesis. *Blood*, 104. <https://doi.org/10.1182/blood-2004-02-0701>

- Chamorro, Á., Dirnagl, U., Urra, X., & Planas, A. M. (2016). Neuroprotection in acute stroke: targeting excitotoxicity, oxidative and nitrosative stress, and inflammation. *The Lancet Neurology*, 15(8), 869-881. [https://doi.org/https://doi.org/10.1016/S1474-4422\(16\)00114-9](https://doi.org/https://doi.org/10.1016/S1474-4422(16)00114-9)
- Chamorro, A., Meisel, A., Planas, A. M., Urra, X., van de Beek, D., & Veltkamp, R. (2012). The immunology of acute stroke [Research Support, Non-U.S. Gov't Review]. *Nature reviews. Neurology*, 8(7), 401-410. <https://doi.org/10.1038/nrneurol.2012.98>
- Chovsepian, A., Berchtold, D., Winek, K., Mamrak, U., Ramírez Álvarez, I., Dening, Y., Golubczyk, D., Weitbrecht, L., Dames, C., Aillery, M., Fernandez-Sanz, C., Gajewski, Z., Dieterich, M., Janowski, M., Falkai, P., Walczak, P., Plesnila, N., Meisel, A., & Pan-Montojo, F. (2022). A Primeval Mechanism of Tolerance to Desiccation Based on Glycolic Acid Saves Neurons in Mammals from Ischemia by Reducing Intracellular Calcium-Mediated Excitotoxicity [\[https://doi.org/10.1002/advs.202103265\]](https://doi.org/10.1002/advs.202103265). *Advanced Science*, 9(4), 2103265.
- Corsiero, E., Nerviani, A., Bombardieri, M., & Pitzalis, C. (2016). Ectopic Lymphoid Structures: Powerhouse of Autoimmunity [Mini Review]. *Frontiers in Immunology*, 7(430). <https://doi.org/10.3389/fimmu.2016.00430>
- Cramer, J. V., Benakis, C., & Liesz, A. (2019). T cells in the post-ischemic brain: Troopers or paramedics? *J Neuroimmunol*, 326, 33-37. <https://doi.org/https://doi.org/10.1016/j.jneuroim.2018.11.006>
- Cupedo, T., & Mebius, R. E. (2003). Role of chemokines in the development of secondary and tertiary lymphoid tissues. *Seminars in Immunology*, 15(5), 243-248. <https://doi.org/https://doi.org/10.1016/j.smim.2003.08.002>
- Doyle, K. P., Quach, L. N., Sole, M., Axtell, R. C., Nguyen, T. V., Soler-Llavina, G. J., Jurado, S., Han, J., Steinman, L., Longo, F. M., Schneider, J. A., Malenka, R. C., & Buckwalter, M. S. (2015). B-lymphocyte-mediated delayed cognitive impairment following stroke. *J Neurosci*, 35(5), 2133-2145. <https://doi.org/10.1523/JNEUROSCI.4098-14.2015>
- Eide, P. K., Vatnehol, S. A. S., Emblem, K. E., & Ringstad, G. (2018). Magnetic resonance imaging provides evidence of glymphatic drainage from human brain to cervical lymph nodes. *Scientific Reports*, 8(1), 7194. <https://doi.org/10.1038/s41598-018-25666-4>
- Elkind, M. S. V., Boehme, A. K., Smith, C. J., Meisel, A., & Buckwalter, M. S. (2020). Infection as a Stroke Risk Factor and Determinant of Outcome After Stroke. *Stroke*, 51(10), 3156-3168. <https://doi.org/10.1161/STROKEAHA.120.030429>
- Elkind, M. S. V., Veltkamp, R., Montaner, J., Johnston, S. C., Singhal, A. B., Becker, K., Lansberg, M. G., Tang, W., Kasliwal, R., & Elkins, J. (2020). Natalizumab in acute ischemic stroke (ACTION II). *Neurology*, 95(8), e1091. <https://doi.org/10.1212/WNL.000000000010038>
- Endres, M., Engelhardt, B., Koistinaho, J., Lindvall, O., Meairs, S., Mohr, J. P., Planas, A., Rothwell, N., Schwaninger, M., Schwab, M. E., Vivien, D., Wieloch, T., & Dirnagl, U. (2008). Improving outcome after stroke: overcoming the translational roadblock. *Cerebrovasc Dis*, 25(3), 268-278. <https://doi.org/000118039> [pii]10.1159/000118039
- Endres, M., Moro, M. A., Nolte, C. H., Dames, C., Buckwalter, M. S., & Meisel, A. (2022). Immune Pathways in Etiology, Acute Phase, and Chronic Sequelae of Ischemic Stroke. *Circulation Research*, 130(8), 1167-1186. <https://doi.org/10.1161/CIRCRESAHA.121.319994>
- Engel, O., Akyuz, L., Da Costa Goncalves, A. C., Winek, K., Dames, C., Thielke, M., Herold, S., Böttcher, C., Priller, J., Volk, H. D., Dirnagl, U., Meisel, C., Meisel, A., Akyüz, L., Da Costa Goncalves, A. C., Winek, K., Dames, C., Thielke, M., Herold, S., Böttcher, C., Priller, J., Volk, H. D., Dirnagl, U., Meisel, C., & Meisel, A. (2015). Cholinergic Pathway Suppresses Pulmonary Innate Immunity Facilitating Pneumonia after Stroke. *Stroke*, 46, 3232-3240. <https://doi.org/10.1161/STROKEAHA.115.008989>

- Erkut, C., Gade, V. R., Laxman, S., & Kurzchalia, T. V. (2016). The glyoxylate shunt is essential for desiccation tolerance in *C. elegans* and budding yeast. *eLife*, 5, e13614. <https://doi.org/10.7554/eLife.13614>
- Fleige, H., Ravens, S., Moschovakis, G. L., Bölter, J., Willenzon, S., Sutter, G., Häussler, S., Kalinke, U., Prinz, I., & Förster, R. (2014). IL-17–induced CXCL12 recruits B cells and induces follicle formation in BALT in the absence of differentiated FDCs. *The Journal of Experimental Medicine*, 211(4), 643-651. <https://doi.org/10.1084/jem.20131737>
- Frenkel, D., Huang, Z., Maron, R., Koldzic, D. N., Hancock, W. W., Moskowitz, M. A., & Weiner, H. L. (2003). Nasal vaccination with myelin oligodendrocyte glycoprotein reduces stroke size by inducing IL-10-producing CD4+ T cells. *J Immunol*, 171(12), 6549-6555. http://www.ncbi.nlm.nih.gov/entrez/query.fcgi?cmd=Retrieve&db=PubMed&dopt=Citation&list_uids=14662856
- Gelderblom, M., Leyboldt, F., Steinbach, K., Behrens, D., Choe, C. U., Siler, D. A., Arumugam, T. V., Orthey, E., Gerloff, C., Tolosa, E., & Magnus, T. (2009). Temporal and spatial dynamics of cerebral immune cell accumulation in stroke [Research Support, Non-U.S. Gov't]. *Stroke; a journal of cerebral circulation*, 40(5), 1849-1857. <https://doi.org/10.1161/STROKEAHA.108.534503>
- Gelfand, J. M., Cree, B. A. C., & Hauser, S. L. (2017). Ocrelizumab and Other CD20(+) B-Cell-Depleting Therapies in Multiple Sclerosis. *Neurotherapeutics*, 14(4), 835-841. <https://doi.org/10.1007/s13311-017-0557-4>
- Gerriets, T., Stolz, E., Walberer, M., Müller, C., Kluge, A., Bachmann, A., Fisher, M., Kaps, M., & Bachmann, G. (2004). Noninvasive Quantification of Brain Edema and the Space-Occupying Effect in Rat Stroke Models Using Magnetic Resonance Imaging. *Stroke*, 35(2), 566-571. <https://doi.org/10.1161/01.STR.0000113692.38574.57>
- Goldmann, T., Wieghofer, P., Jordao, M. J., Prutek, F., Hagemeyer, N., Frenzel, K., Amann, L., Staszewski, O., Kierdorf, K., Krueger, M., Locatelli, G., Hochgerner, H., Zeiser, R., Epelman, S., Geissmann, F., Priller, J., Rossi, F. M., Bechmann, I., Kerschensteiner, M., Linnarsson, S., Jung, S., & Prinz, M. (2016). Origin, fate and dynamics of macrophages at central nervous system interfaces. *Nat Immunol*, 17(7), 797-805. <https://doi.org/10.1038/ni.3423>
- Golubczyk, D., Kalkowski, L., Kwiatkowska, J., Zawadzki, M., Holak, P., Glodek, J., Milewska, K., Pomianowski, A., Janowski, M., Adamiak, Z., Walczak, P., & Malysz-Cymborska, I. (2020). Endovascular model of ischemic stroke in swine guided by real-time MRI. *Scientific Reports*, 10(1), 17318. <https://doi.org/10.1038/s41598-020-74411-3>
- Hacke, W., Kaste, M., Bluhmki, E., Brozman, M., Dávalos, A., Guidetti, D., Larrue, V., Lees, K. R., Medeghri, Z., Machnig, T., Schneider, D., von Kummer, R., Wahlgren, N., & Toni, D. (2008). Thrombolysis with Alteplase 3 to 4.5 Hours after Acute Ischemic Stroke. *New England Journal of Medicine*, 359(13), 1317-1329. <https://doi.org/10.1056/NEJMoa0804656>
- Harrer, C., Otto, F., Pilz, G., Haschke-Becher, E., Trinkka, E., Hitzl, W., Wipfler, P., & Harrer, A. (2021). The CXCL13/CXCR5-chemokine axis in neuroinflammation: evidence of CXCR5+CD4 T cell recruitment to CSF. *Fluids and Barriers of the CNS*, 18(1), 40. <https://doi.org/10.1186/s12987-021-00272-1>
- Hetze, S., Romer, C., Teufelhart, C., Meisel, A., Engel, O., Römer, C., Teufelhart, C., Meisel, A., & Engel, O. (2012). Gait analysis as a method for assessing neurological outcome in a mouse model of stroke. *Journal of Neuroscience Methods*, 206, 7-14. <https://doi.org/10.1016/j.jneumeth.2012.02.001>
- Hochmeister, S., Zeitelhofer, M., Bauer, J., Nicolussi, E.-M., Fischer, M.-T., Heinke, B., Selzer, E., Lassmann, H., & Bradl, M. (2008). After Injection into the Striatum, in Vitro-Differentiated Microglia- and Bone Marrow-Derived Dendritic Cells Can Leave the Central Nervous System via the Blood

Stream. *The American Journal of Pathology*, 173(6), 1669-1681.
<https://doi.org/https://doi.org/10.2353/ajpath.2008.080234>

- Hu, X., Li, P., Guo, Y., Wang, H., Leak, R. K., Chen, S., Gao, Y., & Chen, J. (2012). Microglia/Macrophage Polarization Dynamics Reveal Novel Mechanism of Injury Expansion After Focal Cerebral Ischemia. *Stroke*, 43(11), 3063-3070. <https://doi.org/doi:10.1161/STROKEAHA.112.659656>
- Hurn, P. D., Subramanian, S., Parker, S. M., Afentoulis, M. E., Kaler, L. J., Vandenbark, A. A., & Offner, H. (2007). T- and B-cell-deficient mice with experimental stroke have reduced lesion size and inflammation [Research Support, N.I.H., Extramural Research Support, U.S. Gov't, Non-P.H.S.]. *J Cereb Blood Flow Metab*, 27(11), 1798-1805. <https://doi.org/10.1038/sj.icbfm.9600482>
- Iadecola, C., & Anrather, J. (2011). The immunology of stroke: from mechanisms to translation. *Nat Med*, 17(7), 796-808. <https://doi.org/10.1038/nm.2399>
- Itoh, J., Ukai, M., & Kameyama, T. (1993). Dynorphin A-(1-13) potently prevents memory dysfunctions induced by transient cerebral ischemia in mice. *European Journal of Pharmacology*, 234(1), 9-15. [https://doi.org/https://doi.org/10.1016/0014-2999\(93\)90699-1](https://doi.org/https://doi.org/10.1016/0014-2999(93)90699-1)
- Jagdmann, S., Dames, C., Berchtold, D., Winek, K., Weitbrecht, L., Meisel, A., & Meisel, C. (2020). Impact of Key Nicotinic AChR Subunits on Post-Stroke Pneumococcal Pneumonia. *Vaccines*, 8(2). <https://doi.org/10.3390/vaccines8020253>
- Janke, A. D., & Yong, V. W. (2006). Impact of IVIg on the interaction between activated T cells and microglia. *Neurological Research*, 28(3), 270-274. <https://doi.org/10.1179/016164106X98143>
- Jin, R., Yang, G., & Li, G. (2010). Inflammatory mechanisms in ischemic stroke: role of inflammatory cells. *J Leukoc Biol*, 87(5), 779-789. <https://doi.org/jlb.1109766>
- Jin, W.-N., Gonzales, R., Feng, Y., Wood, K., Chai, Z., Dong, J.-F., La Cava, A., Shi, F.-D., & Liu, Q. (2018). Brain Ischemia Induces Diversified Neuroantigen-Specific T-Cell Responses That Exacerbate Brain Injury. *Stroke*, 49(6), 1471-1478. <https://doi.org/10.1161/STROKEAHA.118.020203>
- Johnson, C. O., Nguyen, M., Roth, G. A., Nichols, E., Alam, T., Abate, D., Abd-Allah, F., Abdelalim, A., Abraha, H. N., Abu-Rmeileh, N. M. E., Adebayo, O. M., Adeoye, A. M., Agarwal, G., Agrawal, S., Aichour, A. N., Aichour, I., Aichour, M. T. E., Alahdab, F., Ali, R., Alvis-Guzman, N., Anber, N. H., Anjomshoa, M., Arabloo, J., Arauz, A., Ärnlov, J., Arora, A., Awasthi, A., Banach, M., Barboza, M. A., Barker-Collo, S. L., Bärnighausen, T. W., Basu, S., Belachew, A. B., Belayneh, Y. M., Bennett, D. A., Bensenor, I. M., Bhattacharyya, K., Biadgo, B., Bijani, A., Bikbov, B., Bin Sayeed, M. S., Butt, Z. A., Cahuana-Hurtado, L., Carrero, J. J., Carvalho, F., Castañeda-Orjuela, C. A., Castro, F., Catalá-López, F., Chaiah, Y., Chiang, P. P.-C., Choi, J.-Y. J., Christensen, H., Chu, D.-T., Cortinovis, M., Damasceno, A. A. M., Dandona, L., Dandona, R., Daryani, A., Davletov, K., de Courten, B., De la Cruz-Góngora, V., Degefa, M. G., Dharmaratne, S. D., Diaz, D., Dubey, M., Duken, E. E., Edessa, D., Endres, M., Faraon, E. J. A., Farzadfar, F., Fernandes, E., Fischer, F., Flor, L. S., Ganji, M., Gebre, A. K., Gebremichael, T. G., Geta, B., Gezae, K. E., Gill, P. S., Gnedovskaya, E. V., Gómez-Dantés, H., Goulart, A. C., Grosso, G., Guo, Y., Gupta, R., Haj-Mirzaian, A., Haj-Mirzaian, A., Hamidi, S., Hankey, G. J., Hassen, H. Y., Hay, S. I., Hegazy, M. I., Heidari, B., Herial, N. A., Hosseini, M. A., Hostiuc, S., Irvani, S. S. N., Islam, S. M. S., Jahanmehr, N., Javanbakht, M., Jha, R. P., Jonas, J. B., Jozwiak, J. J., Jürisson, M., Kahsay, A., Kalani, R., Kalkonde, Y., Kamil, T. A., Kanchan, T., Karch, A., Karimi, N., Karimi-Sari, H., Kasaeian, A., Kassa, T. D., Kazemeini, H., Kefale, A. T., Khader, Y. S., Khalil, I. A., Khan, E. A., Khang, Y.-H., Khubchandani, J., Kim, D., Kim, Y. J., Kisa, A., Kivimäki, M., Koyanagi, A., Krishnamurthi, R. K., Kumar, G. A., Lafranconi, A., Lewington, S., Li, S., Lo, W. D., Lopez, A. D., Lorkowski, S., Lotufo, P. A., Mackay, M. T., Majdan, M., Majdzadeh, R., Majeed, A., Malekzadeh, R., Manafi, N., Mansournia, M. A., Mehndiratta, M. M., Mehta, V., Mengistu, G., Meretoja, A., Meretoja, T. J., Miazgowski, B., Miazgowski, T., Miller, T. R., Mirrahimov, E. M., Mohajer, B., Mohammad, Y., Mohammadoo-khorasani, M., Mohammed, S., Mohebi, F., Mokdad, A. H., Mokhayeri, Y., Moradi, G., Morawska, L., Moreno Velásquez, I., Mousavi, S. M., Muhammed, O. S. S., Muruet, W., Naderi,

- M., Naghavi, M., Naik, G., Nascimento, B. R., Negoi, R. I., Nguyen, C. T., Nguyen, L. H., Nirayo, Y. L., Norrving, B., Noubiap, J. J., Ofori-Asenso, R., Ogbo, F. A., Olagunju, A. T., Olagunju, T. O., Owolabi, M. O., Pandian, J. D., Patel, S., Perico, N., Piradov, M. A., Polinder, S., Postma, M. J., Poustchi, H., Prakash, V., Qorbani, M., Rafiei, A., Rahim, F., Rahimi, K., Rahimi-Movaghar, V., Rahman, M., Rahman, M. A., Reis, C., Remuzzi, G., Renzaho, A. M. N., Ricci, S., Roberts, N. L. S., Robinson, S. R., Roeber, L., Roshandel, G., Sabbagh, P., Safari, H., Safari, S., Safiri, S., Sahebkar, A., Salehi Zahabi, S., Samy, A. M., Santalucia, P., Santos, I. S., Santos, J. V., Santric Milicevic, M. M., Sartorius, B., Sawant, A. R., Schutte, A. E., Sepanlou, S. G., Shafieesabet, A., Shaikh, M. A., Shams-Beyranvand, M., Sheikh, A., Sheth, K. N., Shibuya, K., Shigematsu, M., Shin, M.-J., Shiue, I., Siabani, S., Sobaih, B. H., Sposato, L. A., Sutradhar, I., Sylaja, P. N., Szoeki, C. E. I., Te Ao, B. J., Temsah, M.-H., Temsah, O., Thrift, A. G., Tonelli, M., Topor-Madry, R., Tran, B. X., Tran, K. B., Truelsen, T. C., Tsadik, A. G., Ullah, I., Uthman, O. A., Vaduganathan, M., Valdez, P. R., Vasankari, T. J., Vasanthan, R., Venketasubramanian, N., Vosoughi, K., Vu, G. T., Waheed, Y., Weiderpass, E., Weldegewergs, K. G., Westerman, R., Wolfe, C. D. A., Wondafraash, D. Z., Xu, G., Yadollahpour, A., Yamada, T., Yatsuya, H., Yimer, E. M., Yonemoto, N., Yousefifard, M., Yu, C., Zaidi, Z., Zamani, M., Zarghi, A., Zhang, Y., Zodpey, S., Feigin, V. L., Vos, T., & Murray, C. J. L. (2019). Global, regional, and national burden of stroke, 1990–2016: a systematic analysis for the Global Burden of Disease Study 2016. *The Lancet Neurology*, *18*(5), 439-458. [https://doi.org/https://doi.org/10.1016/S1474-4422\(19\)30034-1](https://doi.org/https://doi.org/10.1016/S1474-4422(19)30034-1)
- Jovin, T. G., Chamorro, A., Cobo, E., de Miquel, M. A., Molina, C. A., Rovira, A., San Román, L., Serena, J., Abilleira, S., Ribó, M., Millán, M., Urra, X., Cardona, P., López-Cancio, E., Tomasello, A., Castaño, C., Blasco, J., Aja, L., Dorado, L., Quesada, H., Rubiera, M., Hernandez-Pérez, M., Goyal, M., Demchuk, A. M., von Kummer, R., Gallofré, M., & Dávalos, A. (2015). Thrombectomy within 8 Hours after Symptom Onset in Ischemic Stroke. *New England Journal of Medicine*, *372*(24), 2296-2306. <https://doi.org/10.1056/NEJMoa1503780>
- Katzan, I. L., Cebul, R. D., Husak, S. H., Dawson, N. V., & Baker, D. W. (2003). The effect of pneumonia on mortality among patients hospitalized for acute stroke. *Neurology*, *60*(4), 620-625. http://www.ncbi.nlm.nih.gov/entrez/query.fcgi?cmd=Retrieve&db=PubMed&dopt=Citation&list_uids=12601102
- Kilkenny, C., Browne, W. J., Cuthill, I. C., Emerson, M., & Altman, D. G. (2010). Improving bioscience research reporting: the ARRIVE guidelines for reporting animal research [Research Support, Non-U.S. Gov't]. *PLoS biology*, *8*(6), e1000412. <https://doi.org/10.1371/journal.pbio.1000412>
- Kleinschnitz, C., Schwab, N., Kraft, P., Hagedorn, I., Dreykluft, A., Schwarz, T., Austinat, M., Nieswandt, B., Wiendl, H., & Stoll, G. (2010). Early detrimental T-cell effects in experimental cerebral ischemia are neither related to adaptive immunity nor thrombus formation [Research Support, Non-U.S. Gov't]. *Blood*, *115*(18), 3835-3842. <https://doi.org/10.1182/blood-2009-10-249078>
- Kono, H., & Rock, K. L. (2008). How dying cells alert the immune system to danger. *Nature reviews. Immunology*, *8*(4), 279-289. <https://doi.org/10.1038/nri2215>
- Kumar, V. (2020). Pulmonary Innate Immune Response Determines the Outcome of Inflammation During Pneumonia and Sepsis-Associated Acute Lung Injury [Review]. *Frontiers in Immunology*, *11*(1722). <https://doi.org/10.3389/fimmu.2020.01722>
- Lafargue, M., Xu, L., Carles, M., Serve, E., Anjum, N., Iles, K. E., Xiong, X., Giffard, R., & Pittet, J. F. (2012). Stroke-induced activation of the alpha7 nicotinic receptor increases *Pseudomonas aeruginosa* lung injury [Research Support, N.I.H., Extramural]. *FASEB journal : official publication of the Federation of American Societies for Experimental Biology*, *26*(7), 2919-2929. <https://doi.org/10.1096/fj.11-197384>
- Lambertsen, K. L., Gregersen, R., & Finsen, B. (2002). Microglial—Macrophage Synthesis of Tumor Necrosis Factor after Focal Cerebral Ischemia in Mice is Strain Dependent. *Journal of Cerebral Blood Flow & Metabolism*, *22*(7), 785-797. <https://doi.org/10.1097/00004647-200207000-00004>

- Lehmann-Horn, K., Wang, S.-z., Sagan, S. A., Zamvil, S. S., & von Büdingen, H. C. (2016). B cell repertoire expansion occurs in meningeal ectopic lymphoid tissue. *JCI Insight*, 1(20). <https://doi.org/10.1172/jci.insight.87234>
- Li, R., Patterson, K. R., & Bar-Or, A. (2018). Reassessing B cell contributions in multiple sclerosis. *Nature Immunology*, 19(7), 696-707. <https://doi.org/10.1038/s41590-018-0135-x>
- Liesz, A., Hu, X., Kleinschnitz, C., & Offner, H. (2015). Functional role of regulatory lymphocytes in stroke: facts and controversies. *Stroke*, 46, 1422-1430. <https://doi.org/10.1161/STROKEAHA.114.008608>
- Liu, Y., Given, K. S., Harlow, D. E., Matschulat, A. M., Macklin, W. B., Bennett, J. L., & Owens, G. P. (2017). Myelin-specific multiple sclerosis antibodies cause complement-dependent oligodendrocyte loss and demyelination. *Acta neuropathologica communications*, 5(1), 25-25. <https://doi.org/10.1186/s40478-017-0428-6>
- Llovera, G., Hofmann, K., Roth, S., Salas-Pédomo, A., Ferrer-Ferrer, M., Perego, C., Zanier, E. R., Mamrak, U., Rex, A., Party, H., Agin, V., Fauchon, C., Orset, C., Haelewyn, B., De Simoni, M.-G., Dirnagl, U., Grittner, U., Planas, A. M., Plesnila, N., Vivien, D., & Liesz, A. (2015). Results of a preclinical randomized controlled multicenter trial (pRCT): Anti-CD49d treatment for acute brain ischemia. *Science Translational Medicine*, 7(299), 299ra121. <https://doi.org/10.1126/scitranslmed.aaa9853>
- Louveau, A., Smirnov, I., Keyes, T. J., Eccles, J. D., Rouhani, S. J., Peske, J. D., Derecki, N. C., Castle, D., Mandell, J. W., Lee, K. S., Harris, T. H., & Kipnis, J. (2015). Structural and functional features of central nervous system lymphatic vessels. *Nature*, 523(7560), 337-341. <https://doi.org/10.1038/nature14432>
- Lucchinetti, C. F., Popescu, B. F. G., Bunyan, R. F., Moll, N. M., Roemer, S. F., Lassmann, H., Brück, W., Parisi, J. E., Scheithauer, B. W., Giannini, C., Weigand, S. D., Mandrekar, J., & Ransohoff, R. M. (2011). Inflammatory Cortical Demyelination in Early Multiple Sclerosis. *New England Journal of Medicine*, 365(23), 2188-2197. <https://doi.org/10.1056/NEJMoa1100648>
- Manzo, A., Vitolo, B., Humby, F., Caporali, R., Jarrossay, D., Dell'Accio, F., Ciardelli, L., Ugucioni, M., Montecucco, C., & Pitzalis, C. (2008). Mature antigen-experienced T helper cells synthesize and secrete the B cell chemoattractant CXCL13 in the inflammatory environment of the rheumatoid joint. *Arthritis & Rheumatism*, 58(11), 3377-3387. <https://doi.org/doi:10.1002/art.23966>
- Meisel, C., & Meisel, A. (2011). Suppressing immunosuppression after stroke. *The New England journal of medicine*, 365(22), 2134-2136. <https://doi.org/10.1056/NEJMci1112454>
- Meisel, C., Prass, K., Braun, J., Victorov, I., Wolf, T., Megow, D., Halle, E., Volk, H. D., Dirnagl, U., & Meisel, A. (2004). Preventive antibacterial treatment improves the general medical and neurological outcome in a mouse model of stroke. *Stroke*, 35(1), 2-6. <https://doi.org/10.1161/01.STR.0000109041.89959.4C>
- Mergenthaler, P., & Meisel, A. (2012). Do stroke models model stroke? *Disease models & mechanisms*, 5(6), 718-725. <https://doi.org/10.1242/dmm.010033>
- Miró-Mur, F., Urra, X., Ruiz-Jaén, F., Pedragosa, J., Chamorro, Á., & Planas, A. M. (2020). Antigen-Dependent T Cell Response to Neural Peptides After Human Ischemic Stroke [Original Research]. *Frontiers in Cellular Neuroscience*, 14(206). <https://doi.org/10.3389/fncel.2020.00206>
- Mitsdoerffer, M., & Peters, A. (2016). Tertiary Lymphoid Organs in Central Nervous System Autoimmunity. *Frontiers in Immunology*, 7, 451-451. <https://doi.org/10.3389/fimmu.2016.00451>
- Negron, A., Stüve, O., & Forsthuber, T. G. (2020). Ectopic Lymphoid Follicles in Multiple Sclerosis: Centers for Disease Control? [Review]. *Frontiers in Neurology*, 11(1580). <https://doi.org/10.3389/fneur.2020.607766>

- Pendlebury, S. T., & Rothwell, P. M. (2009). Prevalence, incidence, and factors associated with pre-stroke and post-stroke dementia: a systematic review and meta-analysis. *The Lancet Neurology*, 8(11), 1006-1018. [https://doi.org/https://doi.org/10.1016/S1474-4422\(09\)70236-4](https://doi.org/https://doi.org/10.1016/S1474-4422(09)70236-4)
- Pendlebury, S. T., Rothwell, P. M., & Oxford Vascular, S. (2019). Incidence and prevalence of dementia associated with transient ischaemic attack and stroke: analysis of the population-based Oxford Vascular Study. *Lancet Neurol*, 18(3), 248-258. [https://doi.org/10.1016/S1474-4422\(18\)30442-3](https://doi.org/10.1016/S1474-4422(18)30442-3)
- Planas, A. M., Gomez-Choco, M., Urra, X., Gorina, R., Caballero, M., & Chamorro, A. (2012). Brain-derived antigens in lymphoid tissue of patients with acute stroke. *J Immunol*, 188(5), 2156-2163. <https://doi.org/10.4049/jimmunol.1102289>
- Prass, K., Meisel, C., Hoflich, C., Braun, J., Halle, E., Wolf, T., Ruscher, K., Victorov, I. V., Priller, J., Dirnagl, U., Volk, H. D., & Meisel, A. (2003). Stroke-induced immunodeficiency promotes spontaneous bacterial infections and is mediated by sympathetic activation reversal by poststroke T helper cell type 1-like immunostimulation. *J Exp Med*, 198(5), 725-736. <https://doi.org/10.1084/jem.20021098>
- Prineas, J. W. (1979). Multiple sclerosis: presence of lymphatic capillaries and lymphoid tissue in the brain and spinal cord. *Science*, 203(4385), 1123. <https://doi.org/10.1126/science.424741>
- Pruss, H., Iggena, D., Baldinger, T., Prinz, V., Meisel, A., Endres, M., Dirnagl, U., & Schwab, J. M. (2012). Evidence of intrathecal immunoglobulin synthesis in stroke: a cohort study. *Arch Neurol*, 69(6), 714-717. <https://doi.org/10.1001/archneurol.2011.3252>
- Reiber, H., Ungefehr, S., & Jacobi, C. (1998). The intrathecal, polyspecific and oligoclonal immune response in multiple sclerosis. *Multiple Sclerosis Journal*, 4(3), 111-117. <https://doi.org/10.1177/135245859800400304>
- Ren, X., Akiyoshi, K., Grafe, M. R., Vandenbark, A. A., Hurn, P. D., Herson, P. S., & Offner, H. (2012). Myelin specific cells infiltrate MCAO lesions and exacerbate stroke severity. *Metabolic brain disease*, 27(1), 7-15. <https://doi.org/10.1007/s11011-011-9267-5>
- Roaldsen, M. B., Jusufovic, M., Berge, E., & Lindekleiv, H. (2021). Endovascular thrombectomy and intra-arterial interventions for acute ischaemic stroke. *Cochrane Database of Systematic Reviews*(6). <https://doi.org/10.1002/14651858.CD007574.pub3>
- Rocco, A., Fam, G., Sykora, M., Diedler, J., Nagel, S., & Ringelb, P. (2012). Poststroke infections are an independent risk factor for poor functional outcome after three-months in thrombolysed stroke patients. *International journal of stroke : official journal of the International Stroke Society*. <https://doi.org/10.1111/j.1747-4949.2012.00822.x>
- Romer, C., Engel, O., Winek, K., Hochmeister, S., Zhang, T., Royl, G., Klehmet, J., Dirnagl, U., Meisel, C., & Meisel, A. (2015). Blocking stroke-induced immunodeficiency increases CNS antigen-specific autoreactivity but does not worsen functional outcome after experimental stroke. *J Neurosci*, 35(20), 7777-7794. <https://doi.org/10.1523/JNEUROSCI.1532-14.2015>
- Römer, C., Engel, O., Winek, K., Hochmeister, S., Zhang, T., Royl, G., Klehmet, J., Dirnagl, U., Meisel, C., Meisel, A., Romer, C., Engel, O., Winek, K., Hochmeister, S., Zhang, T., Royl, G., Klehmet, J., Dirnagl, U., Meisel, C., & Meisel, A. (2015). Blocking stroke-induced immunodeficiency increases CNS antigen-specific autoreactivity but does not worsen functional outcome after experimental stroke. *The Journal of neuroscience : the official journal of the Society for Neuroscience*, 35, 7777-7794. <https://doi.org/10.1523/JNEUROSCI.1532-14.2015>
- Rosell, A., Agin, V., Rahman, M., Morancho, A., Ali, C., Koistinaho, J., Wang, X., Vivien, D., Schwaninger, M., & Montaner, J. (2013). Distal Occlusion of the Middle Cerebral Artery in Mice: Are We Ready to Assess Long-Term Functional Outcome? *Translational Stroke Research*, 4(3), 297-307. <https://doi.org/10.1007/s12975-012-0234-1>

- Samuelsson, A., Towers Terri, L., & Ravetch Jeffrey, V. (2001). Anti-inflammatory Activity of IVIG Mediated Through the Inhibitory Fc Receptor. *Science*, 291(5503), 484-486. <https://doi.org/10.1126/science.291.5503.484>
- Schauwecker, P. E., & Steward, O. (1997). Genetic determinants of susceptibility to excitotoxic cell death: Implications for gene targeting approaches. *Proceedings of the National Academy of Sciences*, 94(8), 4103. <https://doi.org/10.1073/pnas.94.8.4103>
- Schulte-Herbruggen, O., Klehmet, J., Quarcoo, D., Meisel, C., & Meisel, A. (2006). Mouse strains differ in their susceptibility to poststroke infections. *Neuroimmunomodulation*, 13(1), 13-18. <https://doi.org/NIM2006013001013>
- Selvaraj, U. M., Ujas, T. A., Kong, X., Kumar, A., Plautz, E. J., Zhang, S., Xing, C., Sudduth, T. L., Wilcock, D. M., Turchan-Cholewo, J., Goldberg, M. P., & Stowe, A. M. (2021). Delayed diapedesis of CD8 T cells contributes to long-term pathology after ischemic stroke in male mice. *Brain Behav Immun*, 95, 502-513. <https://doi.org/https://doi.org/10.1016/j.bbi.2021.05.001>
- Serafini, B., Rosicarelli, B., Magliozzi, R., Stigliano, E., & Aloisi, F. (2004). Detection of Ectopic B-cell Follicles with Germinal Centers in the Meninges of Patients with Secondary Progressive Multiple Sclerosis. *Brain Pathology*, 14(2), 164-174. <https://doi.org/10.1111/j.1750-3639.2004.tb00049.x>
- Shi, L., Sun, Z., Su, W., Xu, F., Xie, D., Zhang, Q., Dai, X., Iyer, K., Hitchens, T. K., Foley, L. M., Li, S., Stolz, D. B., Chen, K., Ding, Y., Thomson, A. W., Leak, R. K., Chen, J., & Hu, X. (2021). Treg cell-derived osteopontin promotes microglia-mediated white matter repair after ischemic stroke. *Immunity*, 54(7), 1527-1542.e1528. <https://doi.org/https://doi.org/10.1016/j.immuni.2021.04.022>
- Shichita, T., Ago, T., Kamouchi, M., Kitazono, T., Yoshimura, A., & Ooboshi, H. (2012). Novel therapeutic strategies targeting innate immune responses and early inflammation after stroke [Research Support, Non-U.S. Gov't Review]. *Journal of neurochemistry*, 123 Suppl 2, 29-38. <https://doi.org/10.1111/j.1471-4159.2012.07941.x>
- Stanley, D., Mason, L. J., Mackin, K. E., Srikhanta, Y. N., Lyras, D., Prakash, M. D., Nurgali, K., Venegas, A., Hill, M. D., Moore, R. J., & Wong, C. H. (2016). Translocation and dissemination of commensal bacteria in post-stroke infection. *Nat Med*. <https://doi.org/10.1038/nm.4194>
- Stroke Unit Trialists, C. (2013). Organised inpatient (stroke unit) care for stroke. *Cochrane Database of Systematic Reviews*(9). <https://doi.org/10.1002/14651858.CD000197.pub3>
- Stubbe, T., Ebner, F., Richter, D., Engel, O., Klehmet, J., Roysl, G., Meisel, A., Nitsch, R., Meisel, C., & Brandt, C. (2013). Regulatory T cells accumulate and proliferate in the ischemic hemisphere for up to 30 days after MCAO [Research Support, Non-U.S. Gov't]. *J Cereb Blood Flow Metab*, 33(1), 37-47. <https://doi.org/10.1038/jcbfm.2012.128>
- Subramanian, S., Zhang, B., Kosaka, Y., Burrows, G. G., Grafe, M. R., Vandenbark, A. A., Hurn, P. D., & Offner, H. (2009). Recombinant T Cell Receptor Ligand Treats Experimental Stroke. *Stroke*, 40(7), 2539-2545. <https://doi.org/10.1161/STROKEAHA.108.543991>
- Sun, F., Xiao, G., & Qu, Z. (2017). Murine Bronchoalveolar Lavage. *Bio-protocol*, 7(10), e2287. <https://doi.org/10.21769/BioProtoc.2287>
- Tsai, A. S., Berry, K., Beneyto, M. M., Gaudilliere, D., Ganio, E. A., Culos, A., Ghaemi, M. S., Choisy, B., Djebali, K., Einhaus, J. F., Bertrand, B., Tanada, A., Stanley, N., Fallahzadeh, R., Baca, Q., Quach, L. N., Osborn, E., Drag, L., Lansberg, M. G., Angst, M. S., Gaudilliere, B., Buckwalter, M. S., & Aghaeepour, N. (2019). A year-long immune profile of the systemic response in acute stroke survivors. *Brain*, 142(4), 978-991. <https://doi.org/10.1093/brain/awz022>

- Tsementzis, S. A., Chao, S. W., Hitchcock, E. R., Gill, J. S., & Beevers, D. G. (1986). Oligoclonal immunoglobulin G in acute subarachnoid hemorrhage and stroke. *Neurology*, *36*(3), 395. <https://doi.org/10.1212/WNL.36.3.395>
- van Zwam, M., Huizinga, R., Melief, M. J., Wierenga-Wolf, A. F., van Meurs, M., Voerman, J. S., Biber, K. P., Boddeke, H. W., Hopken, U. E., Meisel, C., Meisel, A., Bechmann, I., Hintzen, R. Q., t Hart, B. A., Amor, S., Laman, J. D., & Boven, L. A. (2009). Brain antigens in functionally distinct antigen-presenting cell populations in cervical lymph nodes in MS and EAE. *J Mol Med*, *87*(3), 273-286. <https://doi.org/10.1007/s00109-008-0421-4>
- Vindegaard, N., Muñoz-Briones, C., El Ali, H. H., Kristensen, L. K., Rasmussen, R. S., Johansen, F. F., & Hasseldam, H. (2017). T-cells and macrophages peak weeks after experimental stroke: Spatial and temporal characteristics. *Neuropathology*, *37*(5), 407-414. <https://doi.org/doi:10.1111/neup.12387>
- Vogelgesang, A., & Dressel, A. (2011). Immunological consequences of ischemic stroke: immunosuppression and autoimmunity. *J Neuroimmunol*, *231*(1-2), 105-110. [https://doi.org/S0165-5728\(10\)00443-1](https://doi.org/S0165-5728(10)00443-1) [pii]
- Vu Van, D., Beier, K. C., Pietzke, L.-J., Al Baz, M. S., Feist, R. K., Gurka, S., Hamelmann, E., Kroczeck, R. A., & Hutloff, A. (2016). Local T/B cooperation in inflamed tissues is supported by T follicular helper-like cells. *Nature Communications*, *7*(1), 10875. <https://doi.org/10.1038/ncomms10875>
- Weitbrecht, L., Berchtold, D., Zhang, T., Jagdmann, S., Dames, C., Winek, K., Meisel, C., & Meisel, A. (2021). CD4+ T cells promote delayed B cell responses in the ischemic brain after experimental stroke. *Brain Behav Immun*, *91*, 601-614. <https://doi.org/https://doi.org/10.1016/j.bbi.2020.09.029>
- Westendorp, W. F., Nederkoorn, P. J., Vermeij, J. D., Dijkgraaf, M. G., & van de Beek, D. (2011). Post-stroke infection: a systematic review and meta-analysis [Meta-Analysis Research Support, Non-U.S. Gov't Review]. *BMC neurology*, *11*, 110. <https://doi.org/10.1186/1471-2377-11-110>
- Westendorp, W. F., Vermeij, J. D., Zock, E., Hooijenga, I. J., Kruijt, N. D., Bosboom, H. J., Kwa, V. I., Weisfelt, M., Remmers, M. J., Ten Houten, R., Schreuder, A. H., Vermeer, S. E., van Dijk, E. J., Dippel, D. W., Dijkgraaf, M. G., Spanjaard, L., Vermeulen, M., van der Poll, T., Prins, J. M., Vermeij, F. H., Roos, Y. B., Kleyweg, R. P., Kerkhoff, H., Brouwer, M. C., Zwinderman, A. H., van de Beek, D., Nederkoorn, P. J., & for the, P. i. (2015). The Preventive Antibiotics in Stroke Study (PASS): a pragmatic randomised open-label masked endpoint clinical trial. *Lancet*. [https://doi.org/10.1016/S0140-6736\(14\)62456-9](https://doi.org/10.1016/S0140-6736(14)62456-9)
- Wilson, E. H., Weninger, W., & Hunter, C. A. (2010). Trafficking of immune cells in the central nervous system. *The Journal of Clinical Investigation*, *120*(5), 1368-1379. <https://doi.org/10.1172/JCI41911>
- Xie, L., Li, W., Hersh, J., Liu, R., & Yang, S.-H. (2019). Experimental ischemic stroke induces long-term T cell activation in the brain. *J Cereb Blood Flow Metab*, *39*(11), 2268-2276. <https://doi.org/10.1177/0271678X18792372>
- Yilmaz, G., Arumugam, T. V., Stokes, K. Y., & Granger, D. N. (2006). Role of T lymphocytes and interferon-gamma in ischemic stroke [Research Support, N.I.H., Extramural]. *Circulation*, *113*(17), 2105-2112. <https://doi.org/10.1161/CIRCULATIONAHA.105.593046>
- Zbesko, J. C., Frye, J. B., Becktel, D. A., Gerardo, D. K., Stokes, J., Calderon, K., Nguyen, T.-V. V., Bhattacharya, D., & Doyle, K. P. (2021). IgA natural antibodies are produced following T-cell independent B-cell activation following stroke. *Brain Behav Immun*, *91*, 578-586. <https://doi.org/https://doi.org/10.1016/j.bbi.2020.09.014>

7. Affidavit

7.1. Statutory Declaration

"I, Luis Weitbrecht, by personally signing this document in lieu of an oath, hereby affirm that I prepared the submitted dissertation on the topic "The role of CD4⁺ T cells in chronic immune responses and cognitive decline following experimental stroke" (German: "Die Rolle von CD4⁺ T-Zellen bei der chronischen Immunantwort und Entstehung von Demenz nach experimentellem Schlaganfall"), independently and without the support of third parties, and that I used no other sources and aids than those stated.

All parts which are based on the publications or presentations of other authors, either in letter or in spirit, are specified as such in accordance with the citing guidelines. The sections on methodology (in particular regarding practical work, laboratory regulations, statistical processing) and results (in particular regarding figures, charts and tables) are exclusively my responsibility.

Furthermore, I declare that I have correctly marked all of the data, the analyses, and the conclusions generated from data obtained in collaboration with other persons, and that I have correctly marked my own contribution and the contributions of other persons (cf. declaration of contribution). I have correctly marked all texts or parts of texts that were generated in collaboration with other persons.

My contributions to any publications to this dissertation correspond to those stated in the below joint declaration made together with the supervisor. All publications created within the scope of the dissertation comply with the guidelines of the ICMJE (International Committee of Medical Journal Editors; www.icmje.org) on authorship. In addition, I declare that I shall comply with the regulations of Charité – Universitätsmedizin Berlin on ensuring good scientific practice.

I declare that I have not yet submitted this dissertation in identical or similar form to another Faculty.

The significance of this statutory declaration and the consequences of a false statutory declaration under criminal law (Sections 156, 161 of the German Criminal Code) are known to me."

Date

Signature

7.2. Declaration of Contribution to the Publications

Luis Weitbrecht contributed the following to the below listed publications:

Publication 1:

Luis Weitbrecht & Daniel Berchtold, Tian Zhang, Sandra Jagdmann, Claudia Dames, Katarzyna Winek, Christian Meisel & Andreas Meisel; “CD4⁺ T cells promote delayed B cell responses in the ischemic brain after experimental stroke”; Brain, Behavior, and Immunity; 2021 Jan; Epub 2020 Sep 28

Conception and Study Design:

Andreas Meisel (AM), Christian Meisel (CM) and Katarzyna Winek (KW) formulated the main hypothesis and study design based on preliminary data by Tian Zhang (TZ), Claudia Dames (CD) and KW. Single experiments were designed and planned by Daniel Berchtold (DB) and Luis Weitbrecht (LW).

Methods and Experiments:

LW contributed to the following procedures: MCAo and sham surgery, supportive care after stroke, temperature and weight monitoring, neurological and general health scoring, antibody injections, MRI infarct volumetry (Fig 2C, 7A), immunohistological staining (Fig. 5B, 6C, E), microscopy (Fig 5B, 6C), behavioral testing (Fig. 7C), blood sampling and tissue sampling for flow cytometry and qPCR (Fig. 3C, 4, 5E, F, 6A, B, D). Tissue samples for flow cytometry were prepared by LW and DB, flow cytometry analysis was performed by DB, flow cytometry experiments were designed by CD and DB. Tissue samples for qPCR were prepared by LW and DB. The analysis was performed by Daniel Berchtold and a technical assistant.

Statistical Analysis and Interpretation:

All data was statistically analyzed by LW, except for the data presented in Fig. 2B (TZ) and the supplementary Fig. 7 which is only included in the dissertation but not the publication (DB). Results were interpreted by LW under guidance of AM and CM.

Figures and Paper Manuscript:

All figures were created by LW except for figure 2A and 3D (TZ). All parts of the manuscript were

drafted and finalized by LW after revision by AM, CM, KW and DB. The peer-reviewers' suggestions and questions during the publication process were answered by LW in collaboration with AM and CM.

Publication 2:

Sandra Jagdmann, Claudia Dames, Daniel Berchtold, Katarzyna Winek, **Luis Weitbrecht**, Andreas Meisel, and Christian Meisel. "Impact of Key Nicotinic Achr Subunits on Post-Stroke Pneumococcal Pneumonia." *Vaccines* 8, no. 2 (2020).

LW contributed to the following procedures: MCAo and sham surgery, supportive care after stroke, temperature and weight monitoring, neurological and general health scoring, tissue harvesting for further analysis.

Publication 3:

Alexandra Chovsepian, Daniel Berchtold, Katarzyna Winek, Uta Mamrak, Inés Ramirez Álvarez, Yanina Dening, Dominika Golubczyk, **Luis Weitbrecht**, Claudia Dames, Marine Aillery, Celia Fernandez-Sanz, Zdzislaw Gajewski, Marianne Dieterich, Mirosław Janowski, Peter Falkai, Piotr Walczak, Nikolaus Plesnila, Andreas Meisel, and Francisco Pan-Montojo. "A Primeval Mechanism of Tolerance to Desiccation Based on Glycolic Acid Saves Neurons from Ischemia in Mammals by Reducing Intracellular Calcium-Mediated Excitotoxicity." *Advanced Science* (2022): 9, 2103265.

LW contributed to the following procedures: MCAo and sham surgery, supportive care after stroke, temperature and weight monitoring, neurological and general health scoring, glycolic acid injections. The MRI data presented in Fig. 13C-E were gathered by LW and analyzed by LW and Alexandra Chovsepian (AC) after an introduction by LW. All behavioral experiments were performed by LW (Fig. 13 G-H, Fig. 14 A-H) and data was analyzed by LW or AC after an introduction by LW.

Signature, date and stamp of first supervising university professor / lecturer

Signature of doctoral candidate

8. Publications

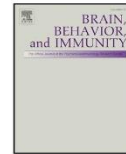
8.1. Publication 1

8.1.1. Excerpt From the ISI Journal Summary List

Journal Data Filtered By: **Selected JCR Year: 2018** Selected Editions: SCIE,SSCI
 Selected Categories: **"NEUROSCIENCES"** Selected Category Scheme: WoS
Gesamtanzahl: 267 Journale

Rank	Full Journal Title	Total Cites	Journal Impact Factor	Eigenfactor Score
1	NATURE REVIEWS NEUROSCIENCE	43,107	33.162	0.068480
2	NATURE NEUROSCIENCE	63,390	21.126	0.164700
3	ACTA NEUROPATHOLOGICA	20,206	18.174	0.041660
4	BEHAVIORAL AND BRAIN SCIENCES	9,377	17.194	0.010240
5	TRENDS IN COGNITIVE SCIENCES	27,095	16.173	0.040040
6	JOURNAL OF PINEAL RESEARCH	10,695	15.221	0.010560
7	NEURON	95,348	14.403	0.218680
8	TRENDS IN NEUROSCIENCES	20,163	12.314	0.024480
9	Annual Review of Neuroscience	14,042	12.043	0.015020
10	MOLECULAR PSYCHIATRY	20,353	11.973	0.049290
11	BRAIN	52,970	11.814	0.074030
12	BIOLOGICAL PSYCHIATRY	43,122	11.501	0.053320
13	PROGRESS IN NEUROBIOLOGY	12,929	10.658	0.013230
14	Nature Human Behaviour	1,230	10.575	0.006550
15	SLEEP MEDICINE REVIEWS	6,920	10.517	0.010920
16	ANNALS OF NEUROLOGY	37,336	9.496	0.048630
17	Molecular Neurodegeneration	4,248	8.274	0.011350
18	NEUROSCIENCE AND BIOBEHAVIORAL REVIEWS	26,724	8.002	0.051580
19	FRONTIERS IN NEUROENDOCRINOLOGY	4,196	7.852	0.005490
20	Neurology-Neuroimmunology & Neuroinflammation	1,996	7.353	0.008220
21	NEUROPSYCHOPHARMACOLOGY	25,672	7.160	0.039090

Rank	Full Journal Title	Total Cites	Journal Impact Factor	Eigenfactor Score
22	Brain Stimulation	5,457	6.919	0.014470
23	NEUROPATHOLOGY AND APPLIED NEUROBIOLOGY	3,876	6.878	0.006420
24	NEUROENDOCRINOLOGY	5,046	6.804	0.005690
25	NEUROSCIENTIST	4,986	6.791	0.008520
26	BRAIN BEHAVIOR AND IMMUNITY	14,533	6.170	0.025700
27	BRAIN PATHOLOGY	5,263	6.155	0.007880
28	Alzheimers Research & Therapy	3,160	6.142	0.010700
29	JOURNAL OF NEUROSCIENCE	175,046	6.074	0.233460
30	JOURNAL OF CEREBRAL BLOOD FLOW AND METABOLISM	19,766	6.040	0.028050
31	PAIN	38,312	6.029	0.039070
32	CURRENT OPINION IN NEUROBIOLOGY	15,090	6.014	0.033650
33	Acta Neuropathologica Communications	3,063	5.883	0.014190
34	Translational Stroke Research	1,955	5.847	0.004330
35	GLIA	14,003	5.829	0.018760
36	NEUROIMAGE	99,720	5.812	0.132720
37	NEURAL NETWORKS	13,063	5.785	0.016060
38	NEUROPSYCHOLOGY REVIEW	2,971	5.739	0.003940
39	Molecular Autism	2,107	5.712	0.008000
40	Journal of Neuroinflammation	11,767	5.700	0.023240
41	Multiple Sclerosis Journal	11,501	5.649	0.022750
42	Annual Review of Vision Science	458	5.622	0.003300
43	Neurotherapeutics	4,475	5.552	0.009060
44	Translational Neurodegeneration	810	5.534	0.002420



Full-length Article

CD4⁺ T cells promote delayed B cell responses in the ischemic brain after experimental strokeLuis Weitbrecht^{a,1}, Daniel Berchtold^{a,1}, Tian Zhang^a, Sandra Jagdmann^b, Claudia Dames^b, Katarzyna Winek^a, Christian Meisel^{b,2}, Andreas Meisel^{a,c,d,e,*,2}^a Charité – Universitätsmedizin, corporate member of Freie Universität Berlin, Humboldt-Universität zu Berlin, and Berlin Institute of Health, Department of Experimental Neurology, Germany^b Charité – Universitätsmedizin, corporate member of Freie Universität Berlin, Humboldt-Universität zu Berlin, and Berlin Institute of Health, Institute for Medical Immunology, Germany^c Charité – Universitätsmedizin, corporate member of Freie Universität Berlin, Humboldt-Universität zu Berlin, and Berlin Institute of Health, Center for Stroke Research Berlin, Germany^d Charité – Universitätsmedizin, corporate member of Freie Universität Berlin, Humboldt-Universität zu Berlin, and Berlin Institute of Health, Neurocore Cluster of Excellence, Germany^e Charité – Universitätsmedizin, corporate member of Freie Universität Berlin, Humboldt-Universität zu Berlin, and Berlin Institute of Health, Department of Neurology, Germany

ARTICLE INFO

Keywords:

Stroke
CD4-positive T-lymphocytes
B-lymphocytes
Chronic inflammation
Tertiary lymphoid tissue
Cognitive impairment

ABSTRACT

CD4⁺ T lymphocytes are key mediators of tissue damage after ischemic stroke. However, their infiltration kinetics and interactions with other immune cells in the delayed phase of ischemia remain elusive. We hypothesized that CD4⁺ T cells facilitate delayed autoreactive B cell responses in the brain, which have been previously linked to post-stroke cognitive impairment (PSCI). Therefore, we treated myelin oligodendrocyte glycoprotein T cell receptor transgenic 2D2 mice of both sexes with anti-CD4 antibody following 60-minute middle cerebral artery occlusion and assessed lymphocyte infiltration for up to 72 days. Anti-CD4-treatment eliminated CD4⁺ T cells from the circulation and ischemic brain for 28 days and inhibited B cell infiltration into the brain, particularly in animals with large infarcts. Absence of CD4⁺ T cells did not influence infarct maturation or survival. Once the CD4⁺ population recovered in the periphery, both CD4⁺ T and B lymphocytes entered the infarct site forming follicle-like structures. Additionally, we provide further evidence for PSCI that could be attenuated by CD4 depletion. Our findings demonstrate that CD4⁺ T cells are essential in delayed B cell infiltration into the ischemic brain after stroke. Importantly, lymphocyte infiltration after stroke is a long-lasting process. As CD4 depletion improved cognitive functions in an experimental set-up, these findings set the stage to elaborate more specific immune modulating therapies in treating PSCI.

1. Introduction

Ischemic stroke is a leading cause of mortality and long-term disability worldwide (Feigin et al., 2014). Improvements in stroke management have increased survival in developed countries, which in turn led to an increased prevalence of post-stroke cognitive impairment (PSCI) (Mijajlović et al., 2017). Acute ischemic brain damage and neuronal loss contribute to cognitive decline after stroke. However, the patients' risk of developing cognitive deficits remains elevated and even increases for many years when compared to individuals without stroke

history (Pendlebury and Rothwell, 2009). A recent seminal study links PSCI to autoreactive B lymphocyte responses in the brain (Doyle et al., 2015).

In experimental stroke, T and B lymphocytes infiltrate into the CNS in a delayed manner and can be detected for up to 12 weeks (Doyle et al., 2015). This pathway may involve priming in cervical lymph nodes or palatine tonsils and therefore be antigen-specific, as antigen-presenting cells (APCs) co-localize with CNS antigen in these lymphoid organs after experimental and human stroke (Planas et al., 2012; van Zwam et al., 2009).

* Corresponding author at: Charité - Universitätsmedizin Berlin, Department of Experimental Neurology, Charitéplatz 1, 10117 Berlin, Germany.

E-mail address: Andreas.Meisel@charite.de (A. Meisel).¹ Both authors contributed equally and share the first authorship.² Both authors contributed equally and share the last authorship.<https://doi.org/10.1016/j.bbi.2020.09.029>

Received 19 April 2020; Received in revised form 13 August 2020; Accepted 24 September 2020

0889-1591/© 2020 The Authors. Published by Elsevier Inc. This is an open access article under the CC BY license (<http://creativecommons.org/licenses/by/4.0/>).

Myelin oligodendrocyte glycoprotein (MOG) T-cell receptor (TCR) transgenic (2D2) mice where more than 80% of peripheral CD4⁺ T cells express TCRs recognizing MOG have been used to investigate mechanisms of autoreactive immune responses in models of CNS disorders including stroke. These mice have been used to unravel how stroke-induced immunodepression (SIDS) increases autoreactive CNS antigen-specific T-cell responses in the ischemic brain, a finding which has been demonstrated to be predictive for wild type mice too (Römer et al., 2015). CD4⁺ T cells from 2D2 mice proliferate and expand in the infarcted brain upon activation by local APCs. When transferred from stroke-experienced 2D2 mice to lymphocyte-deficient mice, CNS antigen-specific CD4⁺ T cells exacerbated ischemic brain injury and increased neurological deficits when another stroke was induced in the recipients (Jin et al., 2018). Given the interdependence of T and B lymphocyte responses, these antigen-specific T cells may boost B cell autoreactivity after stroke and justify the use of 2D2 mice in investigating antigen-specific lymphocyte infiltration.

Once in the brain, T and B cells aggregate in clusters surrounded by myeloid cells (Doyle et al., 2015). These so-called ectopic lymphoid structures (ELS) have also been observed in chronic tissue inflammation such as in various autoimmune diseases (Corsiero et al., 2012). ELS host formation of germinal centers (GCs), facilitate B cell differentiation and production of antibodies to disease-specific antigens that worsen the outcome (Corsiero et al., 2016). Similar processes might occur after CNS injury as CNS antigen-specific autoantibodies have been described in stroke and were associated with cognitive decline (Becker et al., 2016a). However, little is known about the mechanisms underlying ELS formation in the brain.

In the present study, we aimed to investigate the role of CD4⁺ T cells in B cell infiltration and ELS formation by depleting peripheral CD4⁺ T cells after experimental stroke.

2. Methods

The data that support the findings of this study are available from the corresponding author on reasonable request.

2.1. Animals and study approval

2D2 mice (Bettelli et al., 2003) (strain name: C57BL/6 Tg (Tcr α 2D2, Tcr β 2D2) 1Kuch/J; stock number 006912; The Jackson Laboratory; RRID: IMSR_JAX:006912) and C57BL/6J (WT) mice (Janvier Labs, Le Genest-Saint-Isle, France) were used in the study. Mice of both sexes were 10–14 weeks old when entering the study. Mice were housed in the Charité animal facility with a 12 h light/dark cycle (lights on from 6:00 until 18:00) and enriched environment. Mice had ad libitum access to food and water. All animal experiments were conducted in accordance with the ARRIVE guidelines, European Community Council Directives 86/609/EEC and German national laws and approved by local authority (Landesamt für Gesundheit und Soziales, Berlin, Germany).

2.2. Experimental stroke

60 min middle cerebral artery occlusion (MCAo) was performed according to the standard operating procedures of the laboratory (Engel et al., 2011). In brief, anesthesia was induced with 2.5% isoflurane (Forene, Abbott, Wiesbaden Germany) in 1:2 mixtures of O₂/N₂O and maintained at 1.0%–1.5% isoflurane. A silicon rubber-coated monofilament with a diameter of 0.19 ± 0.01 mm (Doccol, MA, USA) was introduced into the common carotid artery, advanced along the internal carotid artery towards the origin of the MCA, and left there for 60 min. For reperfusion, the inserted filament was withdrawn and the internal carotid artery was ligated permanently under anesthesia. The filament was withdrawn immediately after exposition to the MCA in sham-operated controls. Body temperature was maintained with a heating pad.

A drop of 1% Bupivacaine gel was applied to the wound for pain relief. Success of MCAo was verified using the modified Bederson score (Bederson et al., 1986) and MRI infarct volumetry on day 1. Allocation of animals to different operators and sham or MCAo group was randomized. After surgery, animals were allowed to recover in a heated cage before returning to home cages. Following exclusion criteria were applied: Unsuccessful stroke confirmed by MRI assessment, death at the day of operation or death prior to the first antibody injection in depletion experiments.

2.3. T2-weighted magnetic resonance imaging (MRI)

For quantification of ischemic lesion, animals were subjected to T2-weighted MRI as previously described (Hetzte et al., 2012). Images were acquired using a 7 T rodent scanner (Pharmascan 70/16, Bruker BioSpin, Ettlingen, Germany) with the Bruker software Paravision 5.1. Acquired images were analyzed semi-automatically with Analyze 10.0 Software (AnalyzeDirect, Inc.; Lenexa, KS, USA). Infarct volumes were expressed as percentage of infarct lesion of edema corrected ipsilateral hemisphere (Gerriets et al., 2004).

2.4. Drug administration

Mice in CD4 depletion and sham group received intraperitoneal injections of 200 µg CD4 depleting antibody (anti-mouse CD4, clone GK1.5, diluted in sterile phosphate-buffered saline (PBS) at 1 mg/ml) at day 3, 5, 7 and 9 after MCAo. The control group received an isotype control antibody (rat IgG2b isotype control, clone LTF-2) according to the same injection scheme. Randomization of mice to treatment groups was stratified by infarct volumes on day one and has been performed by a group member who did not participate in experiments. Investigators were blinded to treatment groups during data analysis.

2.5. Immunofluorescence staining

PBS-perfused brains were fixed, snap-frozen, cut into 30 µm thick slices on a sliding microtome (LEICA, Wetzlar, Germany) and stored as free-floating sections. Brain tissue was blocked against unspecific binding with 10% normal goat serum (NGS, BIOZOL, Eching, Germany) and 0.3% Tween 20 (Sigma-Aldrich, St. Louis, MO, USA) in PBS. Primary and secondary antibodies were diluted in 1% NGS and 0.3% Tween 20 in PBS. Sections were incubated with primary antibodies at 4 °C overnight. Primary antibodies were against B220 (Alexa488 conjugated, 1:200, clone RA3-6B2, BioLegend, San Diego, CA, USA), CD3 (1:200, clone 500A2, BD Bioscience), CD4 (1:200, clone RM-4-5, BD Bioscience), Laminin 1+2 (1:400, polyclonal, ab7463, Abcam, Cambridge, UK), CD138 (1:200, clone 281-2, BD Bioscience), IgM (coupled with Alexa594, polyclonal, A21044, Life Technologies), IgG (coupled with Oregon Green488, polyclonal, O6380, Life Technologies). After washing with PBS, sections were incubated at room temperature (RT) with secondary antibodies for 2 h on a shaker. Nuclei were counterstained with DAPI (2 µg/ml, Honeywell Fluka, Seelze, Germany). Sections were mounted onto SuperFrost Ultra Plus® slides (R. Langenbrinck, Emmendingen, Germany) with Shandon Immount (Thermo Scientific, Waltham, MA, USA). The specificity of primary stainings was confirmed by doing control stainings with only secondary antibody. Fluorescent pictures were taken with a confocal microscope (Leica TCS SPE). For representative images maximal projections of 20 µm Z stack scanning with 10 steps were created or single planes of Z stack were chosen. Quantification of infiltrating CD4⁺ T cells and B cells in 2D2 mice was performed by counting 9 frames (173 µm × 173 µm) per hemisphere using LEICA LAF software. 1 slice around bregma including lesions in both striatum and cortex was chosen to represent each animal.

2.6. Isolation of leukocytes from brain and blood

Mice were deeply anesthetized with an intraperitoneal injection of ketamine 10% (150 mg/kg, CP-Pharma, Burgdorf, Germany) and Xylazine (15 mg/kg, Xylavet, CP-Pharma) diluted with 0.9% NaCl and transcardially perfused with PBS. Whole brains without cerebellum were dissected and kept in RPMI 1640 medium (Biochrom, Berlin, Germany) on ice, supplemented with 10% FCS (Biochrom), 50U/ml penicillin, 50 µg/ml streptomycin (Biochrom), 2 mM L-alanyl-L-glutamine (Biochrom). Hemispheres were separated and a single cell suspension was prepared by pressing the tissue through a 70 µm cell strainer (Corning Science, Mexico S.A. de C.V.) into RPMI 1640 medium. After 10 min centrifugation at 250g, the cell pellet was resuspended in 35% Percoll (GE Healthcare, Buckinghamshire, UK). The 35% Percoll solution was carefully layered on top of 4 ml 70% stock isotonic Percoll and centrifuged at RT for 30 min at 1159g without acceleration and break. Mononuclear cells were collected from the 35%/70% interface. The peripheral blood for was collected either by submandibular bleeding from living animals (baseline and any intermediate time points) or from vena cava in deeply anesthetized mice (for endpoint). Blood was collected in lithium heparin coated tubes (Sarstedt AG, Nümbrecht, Germany). 50 µl of blood were subjected to erythrocyte lysis (BD Pharm Lyse, BD Biosciences, San Jose, CA, USA).

2.7. Flow cytometry

Blood or brain leukocytes were stained with primary, fluorochrome-conjugated antibodies diluted in PBS + 0.5% BSA + 2 mM EDTA for 20 min at 4 °C in the dark. The following fluorescent anti-mouse monoclonal antibodies were used for brain leukocytes: CD11b (ECD, clone M1/70), CD138 (BV605, clone 281-2), CD19 (BV785, clone 6D5), CD25 (BV711, clone PC61), CD3e (Pacific Blue, clone 17A2), CD4 (APC-eF780, clone RM4-5), CD44 (PE-Cy7, clone IM7), CD45 (Alexa700, clone 30-F11), CD8 (PE-Cy5, clone 53-6.7), GL7 (Alexa488, clone GL7), IgD (BV510, clone 11-26c.2a), TCR Vβ11 (PE, clone RR3-15). The following fluorescent anti-mouse monoclonal antibodies were used for blood leukocytes: CD11b (PE-Cy7, clone M1/70), CD19 (PerCp-Cy5.5, clone 1D3), CD3 (PE, clone 17A2), CD4 (FITC, clone RM4-5), CD8 (Alexa647, clone 53-6.7), Ly6C (BV421, clone HK1.4), Ly6G (APC-Cy7, clone 1A8). Pacific Orange staining was used for discrimination between living and dead cells acquired from blood samples only. Leukocytes were phenotyped using LSRII SORP and FACSCanto II flow cytometers (BD, Franklin Lakes, NJ, USA) and FlowJo (BD) vers.10.0 software. Gating strategies are provided in Fig. 1.

2.8. mRNA expression analysis in brain by qRT-PCR

Total RNA was isolated from ipsilateral and contralateral hemispheres separately by phenol-chloroform extraction, digested with DNaseI (RQ1 RNase-free DNase, Promega Corporation, Madison, WI, USA) to remove genomic DNA and reverse-transcribed to cDNA using the M-MLV reverse transcriptase (Promega) with random hexamers (Roche, Basel, Switzerland) according to the protocol provided by the manufacturer. The cDNA was then quantified using a LightCycler 480 (Roche) and the LightCycler FastStart DNA Master SYBR Green I Kit (Roche) according to the manufacturer's guidelines. Target gene expression was normalized to *Reep5* as housekeeping gene. The relative expression of the target gene in ipsilateral hemispheres was expressed as a ratio of ipsilateral to contralateral hemisphere expression. Primers are specified in Table 1.

2.9. Y-maze

Spatial working memory performance of mice was assessed by the Y-maze test (Maurice et al., 1994). This test is based on the natural tendency of mice to explore novel environments more than familiar

ones. Spontaneous exploration behavior in 8 min session was recorded at baseline (day -1) at day -1 and 2 weeks and 7 weeks after MCAo. Arm entries were quantified to determine cognitive functions where a decline in arm entries at subsequent time-points was interpreted as functional memory. The Y-maze consisted of three wooden, black-painted arms positioned at 120° to each other (arm dimensions: 40 cm long, 10.5 cm high and 3 cm wide). The test was performed in a testing room with diffused dim light (35 lux).

2.10. Statistical analysis

Data are presented as scattered dot plot with mean ± standard deviation or box plot (25–75 percentile) with whiskers (5–95 percentile) using Prism 7.0 software (GraphPad, San Diego, CA, USA). Where data were not normally distributed, Mann-Whitney *U* test was performed for comparison of 2 groups and paired data were analyzed using the Wilcoxon test. Where applicable, data were log-transformed to attain normal distribution. Normal distribution was verified by Kolmogorow-Smirnov test. The effectiveness of CD4 depletion in the peripheral blood was analyzed by 2-way ANOVA and Sidak's multiple comparison. Comparison between 2 groups was made with paired or unpaired *T*-test. Correlation was analyzed by Spearman *r*. Survival curves were analyzed with the log-rank (Mantel-Cox) test. Power analysis was performed using G*Power software (Faul et al., 2007) where an effect size of 0.5 with $\alpha = 0.05$ and $1 - \beta = 0.8$ was determined based on previous comparable experiments. Statistical analysis was performed using Prism 7.0 software (GraphPad, San Diego, CA, USA), where tests were two-sided and $p < 0.05$ was considered statistically significant.

3. Results

3.1. 2D2 mice suffer from greater infarcts and increased lymphocyte infiltration compared to wild-type mice

To focus on CNS antigen-specific lymphocyte infiltration, we used myelin oligodendrocyte glycoprotein (MOG) T cell receptor (TCR) transgenic (2D2) mice, which are prone to autoreactive immune responses due to their enriched CNS antigen-specific T cell repertoire (Bettelli et al., 2003). Lymphocyte CNS infiltration and outcome at day 14 after MCAo were compared between 2D2 and C57Bl6 (WT) mice. Immunofluorescence staining of selected brain slices and flow cytometry analysis of leukocytes isolated from homogenized brain tissue revealed about 20-fold increased CNS infiltration of CD4⁺ T cells and B cells into the ipsilateral hemisphere of 2D2 mice compared to WT animals (Fig. 2A-B). No lymphocyte infiltration was observed in the contralateral hemispheres of MCAo mice or in brains of sham-operated control mice (data not shown). Additionally, 2D2 mice showed larger infarct volumes (Fig. 2C) and higher mortality compared to WT mice (Fig. 2D). These findings indicate that 2D2 mice serve as a useful model to investigate CD4⁺ T cell-dependent CNS antigen-specific immune cell responses after experimental stroke.

3.2. Anti-CD4 treatment eliminates peripheral CD4⁺ T cells and prevents their early infiltration into the ischemic brain

In order to investigate the role of CD4⁺ T cells in delayed but not immediate early immune responses after stroke, we depleted circulating CD4⁺ T cells by repeated injections of monoclonal anti-CD4 antibody once every other day between day three and day nine after stroke onset (Fig. 3A). Leukocyte infiltration into the ischemic brain strongly depends on infarct size (Supplementary Fig. 1A). Therefore, mice were assigned to treatment groups by their infarct volume on day 1 after surgery (Supplementary Fig. 1B). Seven days after MCAo, CD4⁺ T cells were eliminated from the periphery and did not recover until day 28 (Fig. 3B). Numbers of blood CD8⁺ T cells, CD19⁺ cells and myeloid

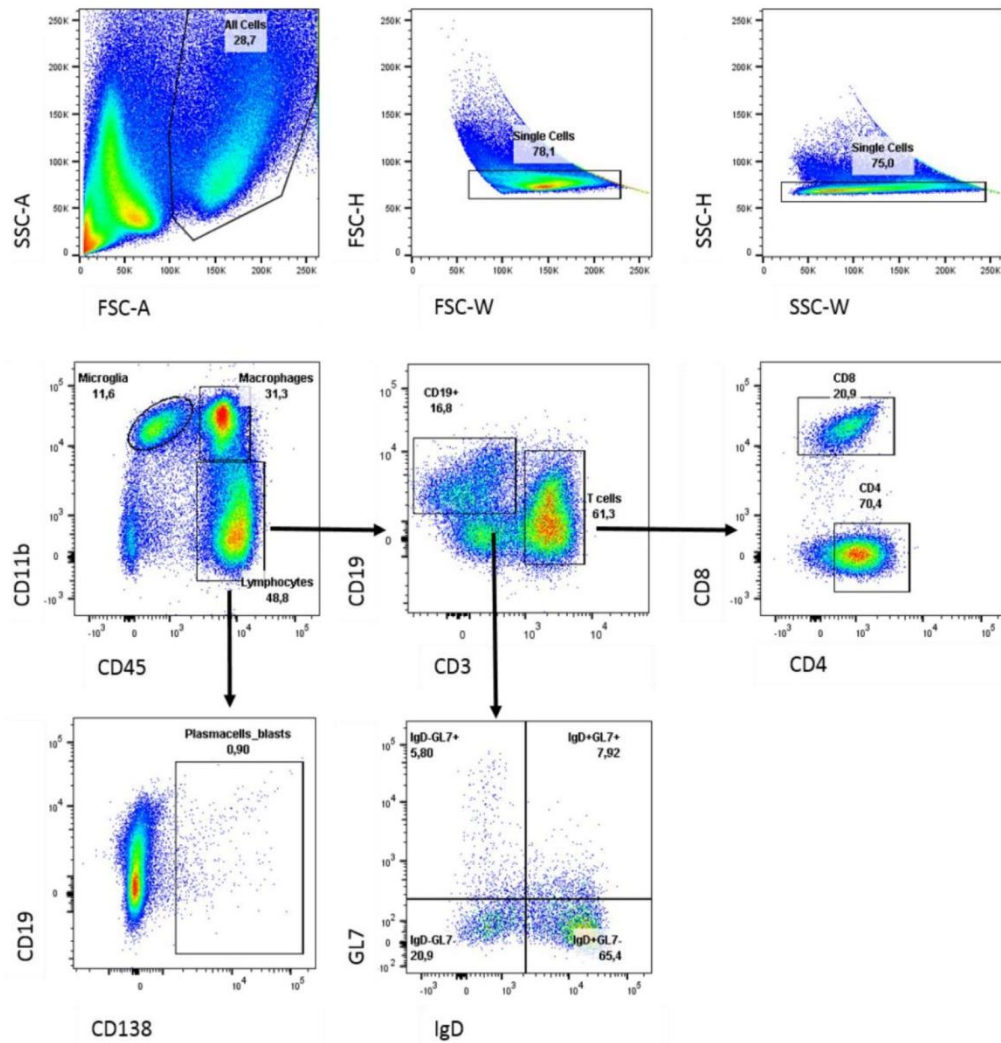


Fig. 1. Flow cytometry gating strategy. Isolated leukocytes were gated based on forward (FSC) and sideward (SSC) scatter to determine single cells. CD45 was used to separate CD11b⁺ myeloid cells into microglia (CD11b^{hi}CD45^{lo}) and infiltrating myeloid cells (IMC) (CD11b^{hi}CD45^{hi}). Lymphocytes were defined as CD45⁺CD11b⁻ and gated into CD138⁺ plasmablasts/plasma cells (PC), CD3⁺ T cells and CD19⁺ cells of B cell lineage. CD3⁺ T cells were discriminated into CD4⁺ T-helper cells and CD8⁺ cytotoxic T cells. CD19⁺ cells were further discriminated to define IgD⁺GL7⁺ GC-like B cells.

cells were not affected by peripheral CD4 depletion (Fig. 3C), while infiltration of CD4⁺ T cells into the ischemic brain at day 14 after MCAo was effectively prevented in anti-CD4 antibody-treated compared to isotype-treated control mice (Fig. 3D).

3.3. Anti-CD4 treatment reduces microglial loss and myeloid cell infiltration 14 days after MCAo

To test whether CD4 depletion influenced myeloid cells in the delayed phase of cerebral ischemia, we quantified resident microglia and infiltrating myeloid cells (IMC) by flow cytometry 14 days after MCAo in 2D2 mice. Microglia and IMC can be distinguished by high CD45

expression in IMC and low CD45 expression in microglia. It was shown previously that microglia upregulate CD45 upon activation (Stein et al., 2007). However, when inducing MCAo in a transgenic microglia reporter mouse, we found that CD45 expression levels are sufficient to distinguish microglia and IMC by flow cytometry 14 days after stroke (Supplementary Fig. 2). The trend towards microglial loss in the ipsilateral compared to the contralateral hemisphere in isotype-treated mice was prevented by CD4 depletion as microglia numbers were significantly higher in the ipsilateral hemisphere of CD4-depleted mice compared to isotype-treated mice (Fig. 4A). Microglia numbers in the ipsilateral hemisphere were lower with increasing lesion size in both treatment groups, without reaching statistical significance in isotype-

Table 1
qRT-PCR primers.

Gene	F:	R:
<i>Pax5</i>	CGGACTCTCTGGACCATCAGGACA	GGGCTGACACCTTGATGGGCA
<i>Cst7</i>	AGTCCATGTTCAGCAAAGCC	ATATAGAGTCCGCTTCAAGGCAG
<i>Csf1</i>	CTCTAGCCGAGGCCATGTG	GCTCTCCACTTCCACTTGT
<i>Ctsd</i>	ACATAGCCTGCTGGGTCCAC	CCTGAGCCGTAGTGGATGTC
<i>Apoe</i>	CTGAGAAGGGAAGATGGGGTTC	GGCTAGGCATCTGTGACGAA
<i>Lpl</i>	CTCCAGAGTTTGACCCGCTT	TTCCTGTTACCGTCCATCCA
<i>Ctsl</i>	GTGGACTGTTCTACGCTCA	ACAAGATCCGCTCTCGCTT
<i>P2ry13</i>	TCGTGGGTTGAGCTAGTAAC TG	TCCGAGCATCAGCTTGT
<i>Hexb</i>	CATCGACCAGATCCCAATTC	CCAAAACATAGTTGTAATATCGCC
<i>Cx3cr1</i>	GTGAGACTGGGTGAGTGACTG	GTGGACATGGTGAAGTCTGAG
<i>Tmem119</i>	CACCCAGAGCTGGTCCATAGC	GGTCTCTCCGGTGTG GGA CT

treated mice (Fig. 4B). However, there was considerable myeloid cell infiltration in a subpopulation of isotype-treated mice (Fig. 4C). IMC numbers positively correlated with infarct lesion size in isotype-treated animals without reaching statistical significance. In contrast, no correlation between infarct size and myeloid cell infiltration was observed in CD4-depleted mice, and even in animals with large infarcts only low numbers of IMC were found (Fig. 4D). Infiltration of myeloid cells into the ipsilateral hemisphere increased with decreasing microglia numbers in isotype-treated mice, but not in CD4-depleted animals (Fig. 4E).

Expression of specific markers for microglial activation (*Cst7*, *Csf1*, *Ctsd*, *Apoe*, *Lpl*, *Ctsl*) as well as microglial homeostasis (*P2ry13*, *Hexb*, *Cx3cr1*, *Tmem119*) were upregulated in the ischemic hemisphere compared to the contralateral hemisphere in both treatment groups equally (Fig. 4F).

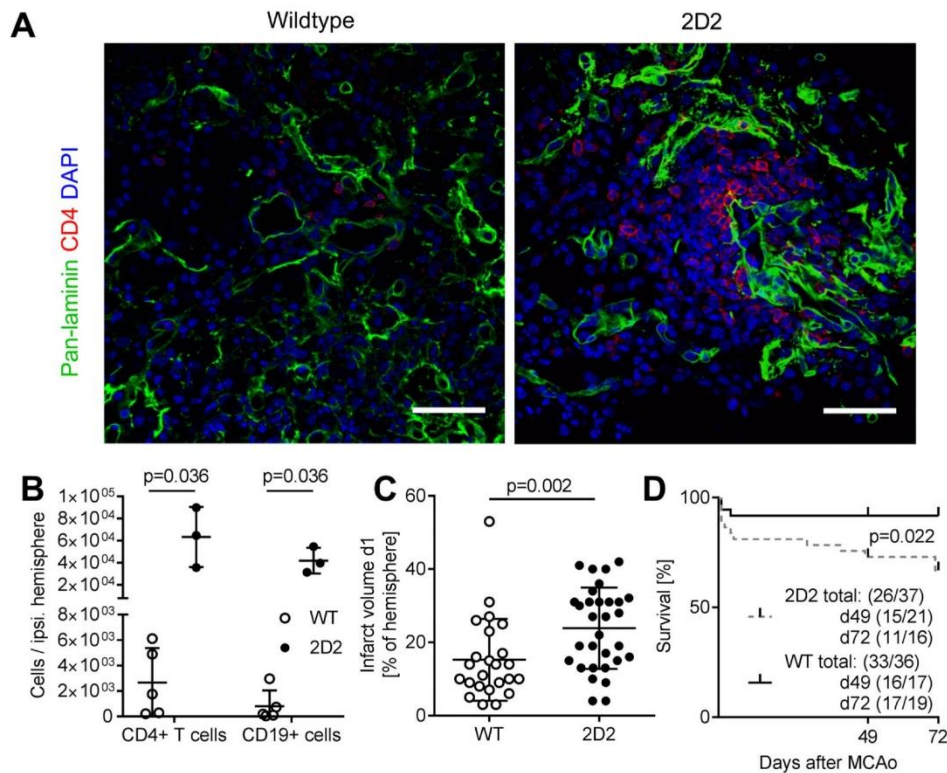


Fig. 2. Enhanced immune responses in 2D2 mice after MCAO. A) Representative immunostaining of CD4⁺ T cells that infiltrate the ischemic brain through the vascular basement membrane (laminin) in 2D2 mice and WT mice 14 days after MCAO. Scale bar = 50 μ m. B) Flow cytometry quantification of CD4⁺ T cells and CD19⁺ cells in ipsilateral hemispheres of 2D2 (n = 3) and WT (n = 5) mice 14 days after MCAO (Mann-Whitney U Test). C) Infarct volumes measured by T2-weighted MRI on day 1 after MCAO in 2D2 (n = 31) and WT (n = 24) mice. D) Long-term survival after 60 min MCAO in 2D2 and WT mice (Log-Rank (Mantel-Cox) Test). Mice were sacrificed after 49 days (surviving/total mice used in the study: WT n = 16/17; 2D2 n = 15/21) or 72 days (WT n = 17/19; 2D2 n = 11/16).

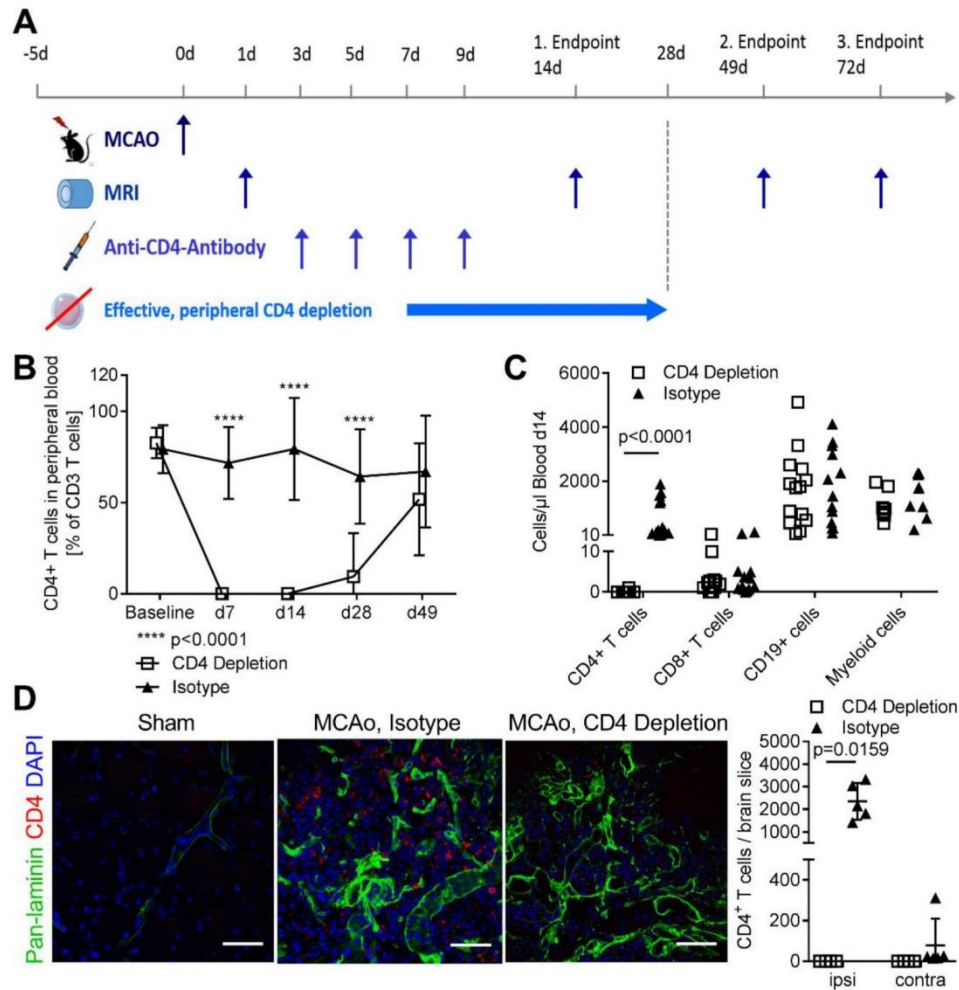


Fig. 3. Experimental set-up and CD4 depletion efficacy. A) Stroke was induced by 60 min MCAo and verified by MRI. Anti-CD4-antibody or IgG-isotype control was injected intraperitoneally at day 3, 5, 7 and 9 after MCAo. Leukocyte infiltration was investigated at day 14, 49, 72 after stroke by histology, flow cytometry and qRT-PCR. Additional MRI analysis on day 14 and 48 was performed to assess infarct maturation after CD4 depletion. B) Flow cytometry quantification of CD4 T cells in blood samples of CD4-depleted and isotype-treated mice at baseline, day 7, 14, 28 and 49 after MCAo (2way ANOVA and Sidak's multiple comparison). CD4 depletion: n(baseline) = 12, n(d7) = 7, n(d14) = 14, n(d28) = 9, n(d49) = 14; Isotype: n(baseline) = 8, n(d7) = 4, n(d14) = 14, n(d28) = 9, n(d49) = 11. C) Flow cytometry quantification of circulating CD4⁺ T cells, CD8⁺ T cells, CD19⁺ cells (n = 14 per group) and CD11b⁺ myeloid cells (n = 9 per group) at day 14 after MCAo (Mann-Whitney U-Test). D) Representative immunostaining for CD4⁺ T cells in ipsilateral hemispheres of sham-operated mice, isotype-treated MCAo mice and CD4-depleted MCAo mice 14 days after stroke onset with stereological quantification for CD4-depleted (n = 4) and isotype-treated (n = 5) mice (Mann-Whitney U-Test). Scale bar = 50 μm.

3.4. Anti-CD4 treatment reduces brain infiltration of B cells 14 days after MCAo

Infiltrating B cells were not randomly distributed across the affected hemisphere at 14 days after MCAo but clustered in few areas of the infarct core reminiscent of ELS, while CD4 T cells scattered more widely in the surrounding area (Fig. 5A). ELS formation was observed in both isotype-treated and CD4-depleted mice, but B cell infiltration was strongly reduced after CD4 depletion at 14 days after MCAo (Fig. 5B-C). We confirmed these findings by measurement of the B cell marker *Pax5*

in the ipsilateral hemisphere using qRT-PCR (Fig. 5D). Flow cytometry analysis also showed a significant reduction in CD19⁺ B cells and CD138⁺ plasmablasts/plasma cells (PC) after CD4 depletion compared to isotype-treatment (Fig. 5E). Only in isotype-treated but not CD4-depleted mice, infiltration of CD19⁺ cells into the brain positively correlated with infarct volumes measured on day 1 (Fig. 5F).

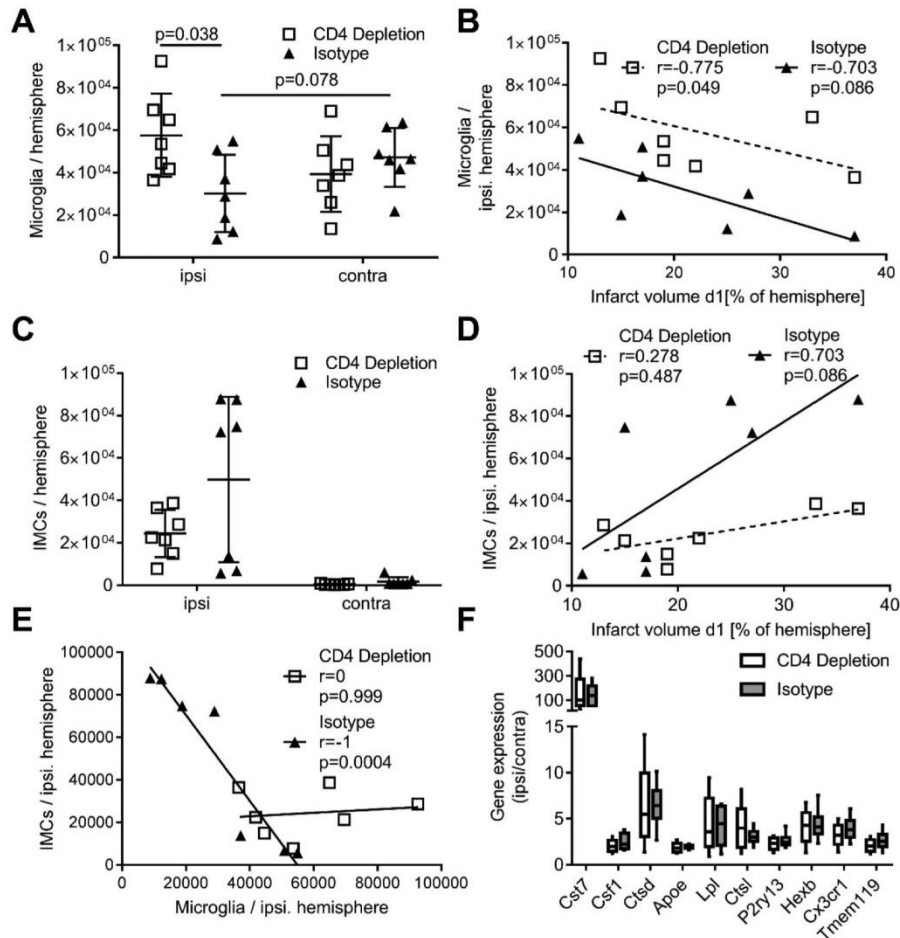
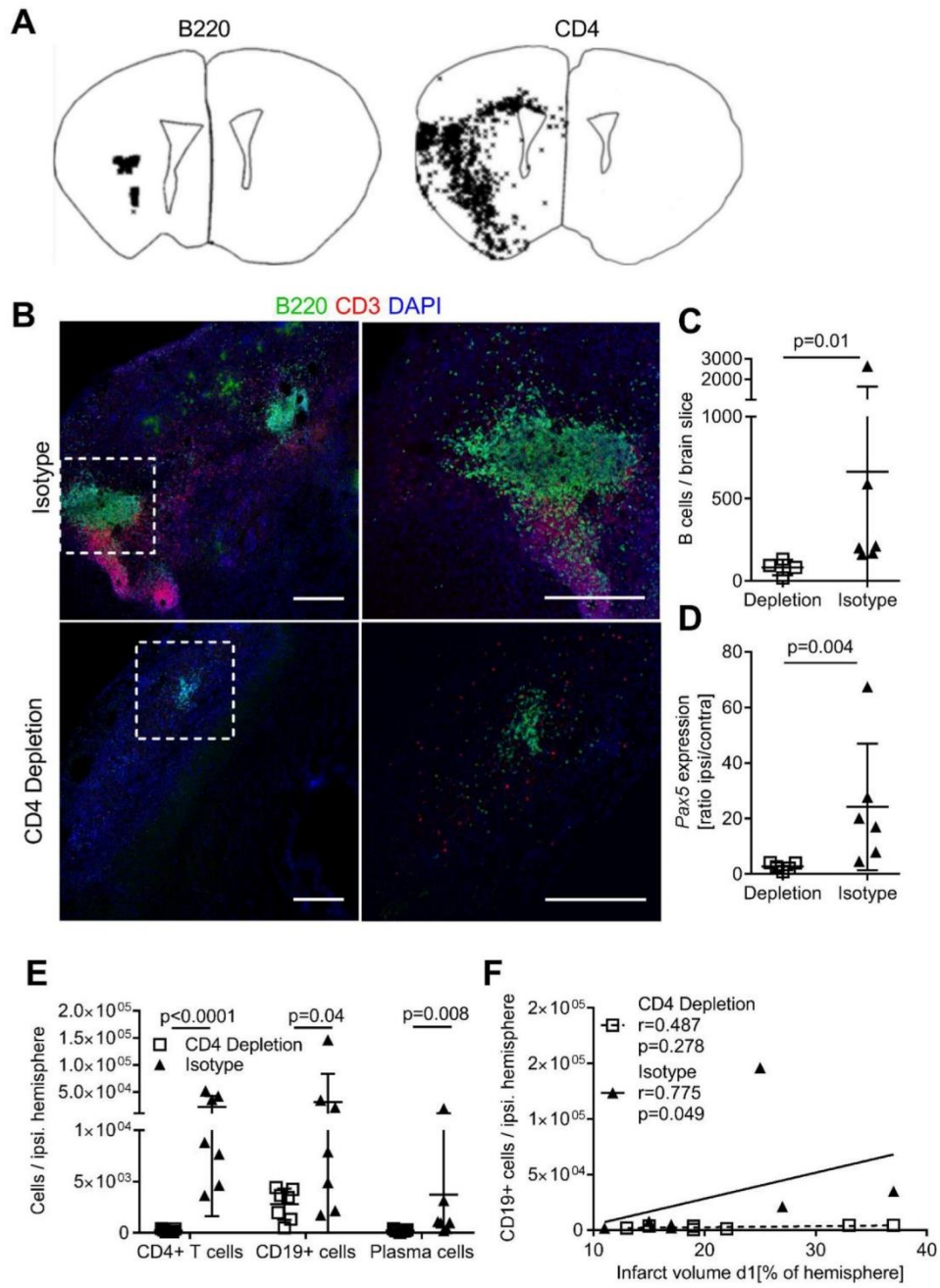


Fig. 4. CD4 depletion reduces microglial loss and myeloid cell infiltration at day 14 after MCAo. A-E) Flow cytometry quantification of microglia and infiltrating myeloid cells (IMC) ($n = 7$ per group). A) Quantification of CD45^{lo}CD11b⁺ microglia in ipsilateral and contralateral hemispheres of CD4-depleted and isotype-treated mice (Wilcoxon test). B) Correlation of microglia numbers in the ipsilateral hemisphere with infarct volume on day 1 in CD4-depleted and isotype-treated mice (Spearman correlation). C) Quantification of CD45^{hi}CD11b⁺ IMC in ipsilateral hemispheres of CD4-depleted and isotype-treated mice (Wilcoxon test). D) Correlation of IMC numbers in the ipsilateral hemisphere with infarct volume on day 1 in CD4-depleted and isotype-treated mice (Spearman correlation). E) Correlation of microglia numbers with IMC numbers in the ipsilateral hemisphere of CD4-depleted and isotype-treated mice (Spearman correlation). F) qRT-PCR analysis of microglial markers for activation (*Cst7*, *Csf1*, *Ctsd*, *ApoE*, *Lpl*, *Ctsl*) and homeostasis (*P2ry13*, *Hexb*, *Cx3cr1*, *Tmem119*). Data is presented as ratio of gene expression in ipsilateral to contralateral hemisphere of CD4-depleted ($n = 5$) and isotype-treated ($n = 6$) animals. Box plots with mean and whiskers (5–95%).

3.5. CD4⁺ T and B cells infiltrate the ischemic brain as soon as peripheral CD4⁺ T cell population recovers

Since peripheral CD4⁺ T cell recovery in CD4-depleted animals started about 28 days after MCAo and administration of CD4-depleting antibody between day 3 and 9 almost completely prevented ELS formation at day 14, we next wondered whether the delayed CD4 depletion had a long-lasting inhibitory effect on lymphocyte infiltration into the brain. In line with our hypothesis that T cells facilitate B cell infiltration, at day 49 and 72 after MCAo in both isotype- and anti-CD4-treated mice, we found high numbers of B cells within the ischemic hemisphere. In addition, we observed equal numbers of CD4⁺ T cells in both treatment groups (Fig. 6A) and a strong correlation with B cell infiltration after 49 days (Fig. 6B). Interestingly, lymphoid follicles

were spacious and highly organized in both treatment groups at day 49 and 72, which may indicate an active adaptive immune response within the ischemic brain even more than 4 weeks after stroke onset (Fig. 6C). In fact, flow cytometry analysis of brain B cell subsets at day 49 and 72 demonstrated the presence of antibody-producing PC and GC-like B cells that express a distinct cell surface marker composition (GL7⁺IgD⁻) upon antigen-recognition indicating local B cell differentiation within ELS (Fig. 6D). This finding is supported by an immunostaining depicting IgM⁺ and IgG⁺ PC in proximity to ELS in both CD4-depleted and isotype-treated mice at day 72 after stroke (Fig. 6E). Representative images display unspecific staining in green (IgG) or red (IgM), which may be due to autoreactive antibodies produced by the respective PC subset binding to surrounding tissue.



(caption on next page)

Fig. 5. CD4 depletion inhibits B cell infiltration into the ischemic brain at day 14 after MCAo. A) Representative images indicating distribution of B220⁺ B cells and CD4⁺ T cells in the ipsilateral hemisphere at day 14 after MCAo. B) Immunostaining of infarct area in CD4-depleted and isotype-treated mice (left panels) and B cell follicles in detail (right panels). Scale bar = 250 μ m. C) Stereological quantification of B220⁺ B cells after CD4 depletion (n = 4) or isotype treatment (n = 6) (Mann-Whitney U Test). D) qRT-PCR analysis of the B cell marker *Pax5*, displayed as ratio of gene expression in ipsilateral to contralateral hemisphere in CD4-depleted (n = 5) and isotype-treated (n = 6) animals (Mann-Whitney U Test). E) Flow cytometry quantification of CD4⁺ T cells, CD19⁺ cells and CD138⁺ PC in CD4-depleted and isotype-treated animals. Cell numbers are presented as mean with SD. Data were log-transformed prior to statistical analysis to attain normal distribution. Data were analyzed with Kolmogorow-Smirnov test for normality followed by unpaired t-test. n = 7 per group. F) Flow cytometry: Correlation of CD19⁺ cell numbers in the ipsilateral hemisphere with infarct volume on day 1 in CD4-depleted and isotype-treated mice (Spearman correlation). n = 7 per group.

3.6. Anti-CD4 treatment has no effect on infarct maturation or long-term survival after ischemic stroke but alleviates cognitive decline

To assess effects of anti-CD4 treatment on long-term outcome we determined infarct maturation by MRI over 10 weeks after stroke onset. Both treatment groups showed a significant decrease in infarct sizes from day 1 to day 14 after stroke and further infarct maturation was similar (Fig. 7A). In addition, we observed no differences in survival (Fig. 7B), weight loss, or body temperature (Supplementary Fig. 1C-D) between CD4-depleted and isotype-treated mice. As a previous study reported a link between infiltrating B cells and CNS antigen-specific autoantibody responses to cognitive impairment after stroke (Doyle et al., 2015), we next investigated whether CD4 depletion and the resulting reduction of brain B cell infiltration would alleviate cognitive decline after stroke. Using the number of arm entries in the Y-maze test to assess learning and memory abilities, we observed that sham-operated mice had progressively decreasing entries 2 weeks and 7 weeks after stroke when compared to baseline. While after 2 weeks all groups behaved similarly, after 7 weeks arm entries rose back to baseline level in isotype-treated mice with a significant difference to sham-operated mice. CD4-depleted mice had arm entry numbers in between sham-operated and isotype-treated animals at week 7 suggesting potential differences in cognitive function between CD4-depleted and isotype-treated animals in the long-term course after stroke (Fig. 7C). However, the effect was not statistically different between both groups at this time-point.

4. Discussion

Delayed infiltration of B cells into the ischemic brain has been linked to PSCI recently (Doyle et al., 2015). Using antibody-based CD4⁺ T cell depletion after MCAo in 2D2 mice, we demonstrated that B cell infiltration into the ischemic brain and their differentiation within lymphoid follicle-like structures depends on the presence of CD4⁺ T cells. Importantly, lymphocyte infiltration into the brain is a process lasting for at least 72 days after stroke onset. Finally, we provide further experimental evidence for a crucial role of lymphocytes in PSCI, which can be targeted by CD4⁺ T cell depletion.

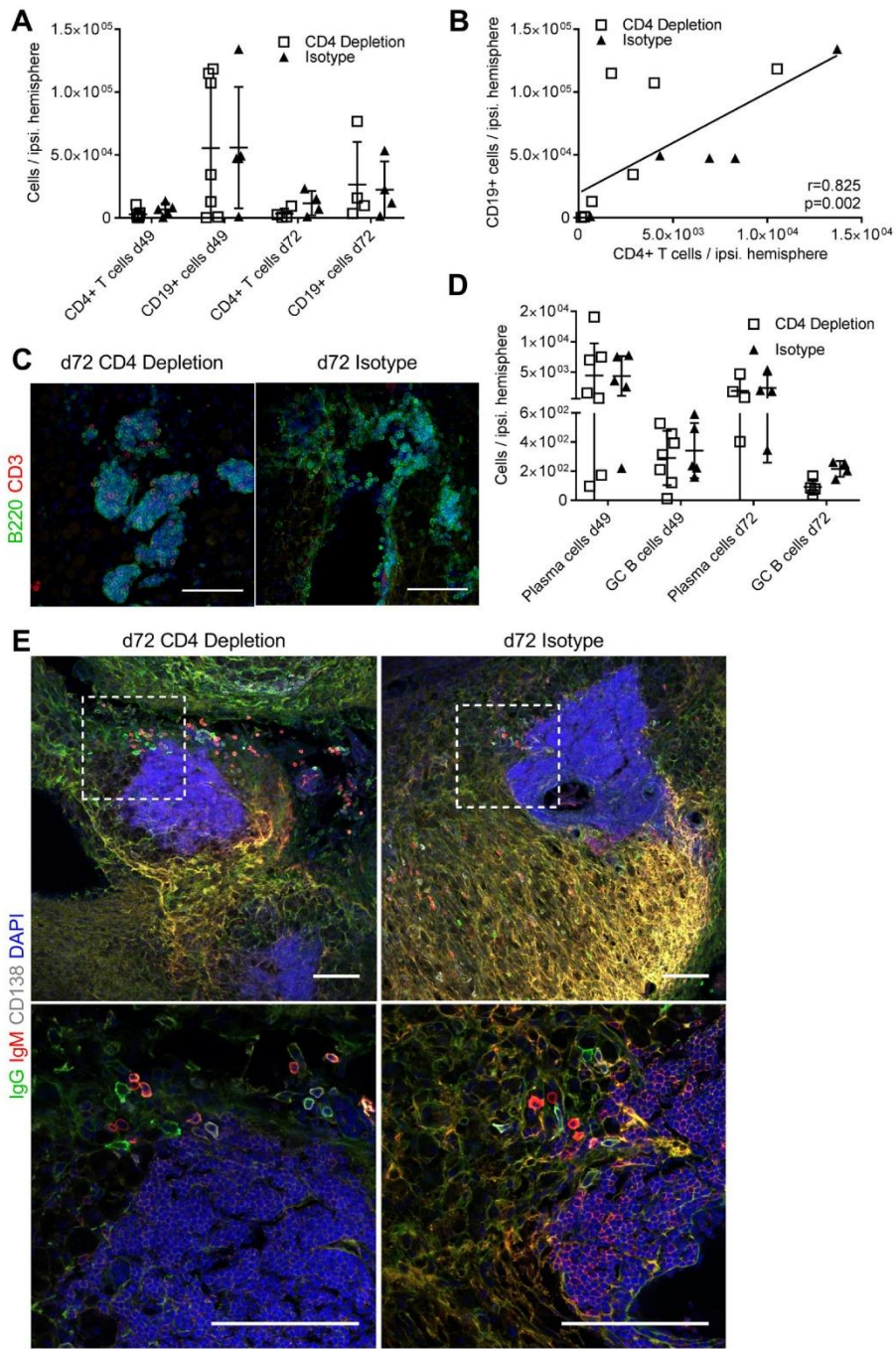
According to current understanding, early ischemic injury is mediated primarily by myeloid immune cells and innate-like lymphocytes and therefore independent of antigen-specificity (Benakis et al., 2014; Kleinschnitz et al., 2010). However, modulation of the adaptive immunity by inducing CNS-specific tolerance or autoimmunity greatly influences stroke severity. It was shown that adoptive transfer of T cells reactive to the CNS-antigen MOG exacerbates early infarct lesions and stroke outcomes (Ren et al., 2012), whereas induction of immunologic tolerance to MOG prior to experimental stroke reduces the infarct size (Frenkel et al., 2003). Here, we demonstrate that 2D2 mice, in which more than 80% of peripheral CD4⁺ T cells express functional T cell receptors recognizing MOG, suffer from significantly larger infarcts already 1 day after MCAo when compared to WT. These results corroborate that antigen-specific immune responses by pre-existing memory T cells may boost lesions following cerebral ischemia. However, additional factors such as cerebrovascular anatomy, susceptibility to excitotoxicity and varying cytokine expression are mouse strain-specific and may contribute to the observed difference in infarct volumes

(Knauss et al., 2020; Barone et al., 1993; Lamberts et al., 2002; Schauwecker and Steward, 1997). Greater infarct volumes in 2D2 mice were associated with higher mortality compared to WT mice, whereas no differences in infarct maturation or mortality were observed between CD4-depleted and isotype-treated mice. Therefore, we propose that survival and infarct volumes are determined by early rather than late CNS-specific immune responses.

We had previously characterized stroke induced-immunodepression (SIDS), a mechanism mediated by activation of the sympathetic nervous system (SNS) predisposing stroke patients to severe infection (Harms et al., 2008; Prass et al., 2003). It was shown that post-stroke infections favored by SIDS further exacerbate CNS-specific autoreactivity and impede recovery after human and experimental stroke (Becker et al., 2011, 2016; Hoffmann et al., 2017). Importantly, MBP-specific immune responses worsened stroke patients' outcome independently of infarct severity or age (Becker et al., 2011). Inhibiting the sympathetic nervous system by administration of propranolol prevented SIDS and post-stroke infections in WT and 2D2 mice similarly (Prass et al., 2003; Römer et al., 2015). In contrast, inhibition of SIDS resulted in enhanced CNS-specific T cell responses after stroke in 2D2 mice (Römer et al., 2015). Stroke-induced immunodepression may therefore promote contrary effects after stroke, protecting stroke patients from autoreactive responses to CNS antigens directly after acute injury while predisposing them to infections which in turn may exacerbate CNS autoreactivity.

Infiltration of activated lymphocytes following stroke has been recognized as a potential therapeutic target. In experimental stroke, combined deficiency of T and B cells as well as selective depletion of CD4⁺ or CD8⁺ T cells reduce lesion volumes (Hurn et al., 2007; Liesz et al., 2011). Depletion of regulatory CD4⁺ T cells (Treg) results in beneficial, deleterious or even no effects, depending on the stroke model and the time point investigated (Liesz et al., 2015; Stubbe et al., 2013). A multicenter preclinical trial demonstrated that antibody treatment directed against CD49d, an integrin- α subunit involved in leukocyte extravasation, reduced infarct volumes and leukocyte infiltration into the ischemic brain tissue after permanent but not transient MCAo (Llovera et al., 2015). Recent phase II clinical trials investigating anti-CD49d-treatment in human stroke patients failed in improving post-stroke long-term outcome (Elkins et al., 2017; Simats et al., 2016), which might be due to different timing of treatment.

Permanent CD4 T cell deficiency and early depletion after stroke onset have reduced infarct volumes consistently in experimental stroke models (Hurn et al., 2007; Kleinschnitz et al., 2013; Liesz et al., 2011). This is most likely due to early detrimental T cell effects within the ischemic brain following stroke (Gu et al., 2012; Kleinschnitz et al., 2010). On the other hand, peripheral T cells play a crucial role in protecting from post-stroke infections (Prass et al., 2003). Our experiments aimed at investigating delayed B cell infiltration and ELS formation. Considering our previous data on a delayed T cell infiltration into the ischemic brain (Stubbe et al., 2013) and in order to avoid interference with the early T cell effects, we established a depletion protocol eliminating CD4⁺ T cells between day 7 and 28. Using this setup we focused our investigation on delayed lymphocyte infiltration and autoreactivity without interfering with immediate or early immune responses. The observation of a "chronic" lymphocyte infiltration as late as day 49 and 72 after stroke was an unexpected finding of our study. This very important finding needs to be addressed in further



(caption on next page)

Fig. 6. Lymphocytes infiltrate the ischemic brain after the CD4⁺ population recovers in the periphery. A) Flow cytometry quantification of CD4⁺ T cells and CD19⁺ cells in the ipsilateral hemisphere of CD4-depleted and isotype-treated mice at day 49 (CD4 depletion: n = 7; isotype: n = 5) and day 72 (n = 4 per group) after MCAo. At this time-point, the CD4⁺ T cell population had recovered in the periphery of depleted animals. B) Correlation of CD19⁺ cell numbers with CD4⁺ T cells in the ipsilateral hemisphere at day 49 after MCAo. Mice from both treatment groups are analyzed collectively in one correlation (n = 12) (Spearman correlation). C) Representative images of B cell follicles in ischemic brains of CD4-depleted and isotype-treated mice at day 72. Scale bar = 100 μ m. D) CD138⁺ PC and GL7⁺ IgD⁻ GC B cells were detected by flow cytometry in both treatment groups at day 49 and 72 after MCAo. E) Representative images of IgG⁺ and IgM⁺ PC in proximity to cell-rich ELS in CD4-depleted and isotype-treated mice at day 72 after MCAo. Top panels display ELS with surrounding PC at 20x magnification. Bottom panels display 63x magnification of indicated areas. Scale bar = 100 μ m.

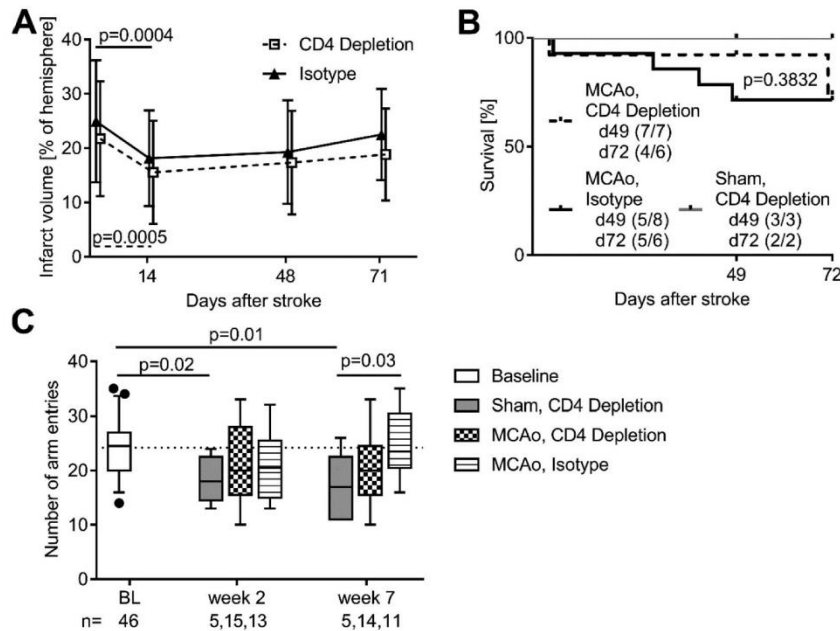


Fig. 7. CD4-depletion attenuates cognitive decline after MCAo. A) Long-term infarct maturation was assessed by T2-weighted infarct volumetry in CD4-depleted and isotype-treated mice at day 1 (n = 15 per group), 14 (n = 13–14), 48 (n = 11–12) and 71 (n = 4–7) after MCAo. B) Long-term survival after 60 min MCAo in CD4-depleted and isotype-treated animals from two separate experiments (Log-rank Mantel-Cox Test). Mice were sacrificed after 49 days or 72 days. Sample size is displayed as surviving/total mice used in the study. C) The number of spontaneous Y-maze arm entries was used to test learning and memory abilities, where decreased arm entries after repeated testing was interpreted as a learning effect due to functional memory (paired and unpaired t-test).

longitudinal experiments.

Additional effects of the anti-CD4 treatment that are unrelated to CD4⁺ T cell reduction may influence leukocyte infiltration after stroke, for instance by altering the blood brain barrier. However, the observation that B cells infiltrate the ischemic brain at late time-points, once the CD4⁺ population recovers in the periphery, indicates that infiltration of CD4⁺ T cells and B cells are directly linked. It was recently found that interferon- γ (IFN γ) promotes transendothelial lymphocyte migration in the CNS by upregulation of endothelial adhesion molecules (Sonar et al., 2017). We had previously observed enhanced IFN γ production upon ex-vivo antigen stimulation in MOG-specific CD4⁺ T cells, suggesting that CD4 depletion may have further neuro-protective effects by preventing leukocyte transmigration across the blood brain barrier (Römer et al., 2015).

In accordance with very recently published data (Harris et al., 2020), delayed elimination of CD4⁺ T cells had no effect on long-term survival or infarct maturation in our experiments. Therefore, CD4⁺ T cells' effect on infarct size seems limited to the acute phase of stroke. CD4⁺ T cell subsets such as T-helper (Th)17, follicular Th (TFH) and Treg exert distinct and partly opposing functions after stroke (Cramer et al., 2019). Global CD4⁺ T cell depletion approaches may therefore produce distorted results neglecting subset specific effects. For instance,

previous findings indicate upregulation of regulatory cytokines such as IL-10 and TGF- β in MOG-specific Tregs isolated from the infarcted brain upon ex-vivo MOG stimulation. However, Tregs only made up less than 1% of peripheral CD4⁺ T cells in 2D2 mice before and after MCAo probably limiting their effect in stroke pathology (Römer et al., 2015). In addition, CD4⁻ T cell populations such as IL-17-producing $\gamma\delta$ T cells may also contribute to ischemic brain injury in a delayed manner and cannot be targeted by CD4 depletion (Shichita et al., 2009). In order to account for subset specific T cell functions in B cell infiltration after stroke, further experiments with more specific depletion or adoptive cell transfer approaches are required.

Delayed B lymphocyte accumulation in ELS in the ischemic brain after experimental stroke was recently linked to PSCI that could be prevented by genetic B cell deficiency or antibody-mediated B cell depletion (Doyle et al., 2015). Here, we demonstrate that CD4⁺ T cells are essential in B cell infiltration after stroke. The underlying molecular signals are currently unknown. However, the mechanisms may be similar to other states of chronic inflammation where ELS formation has been described. In autoimmunity, TFH cells have been shown to promote ELS functions including B cell expansion, differentiation, class switch and production of disease specific autoantibodies that worsen patients' outcomes (Corsiero et al., 2016; Crotty, 2014). A number of

cytokines and chemokines have been shown to promote B cell infiltration and ELS formation during chronic inflammation, including IL-17, lymphotoxin- $\alpha_1\beta_2$ and various members of the CCL and CXCL family (Aloisi and Pujol-Borrell, 2006). CD4⁺ T cell subsets participate in lymphoid neogenesis during chronic inflammation either directly by secreting cytokines such as IL-17 or indirectly by promoting the expression of lymphoid chemokines in myeloid and stromal cells (Al-Kufaidy et al., 2017; Carlsen et al., 2004; Corsiero et al., 2012; Fleige et al., 2014). In addition, we had previously described that CNS-infiltrating MOG-specific T cells produce IFN- γ following stroke (Klehm et al., 2016; Römer et al., 2015). Exposure to IFN- γ induces the expression of adhesion molecules in brain endothelial cells which enable transendothelial lymphocyte migration (Sonar et al., 2017).

The unique cellular composition of the CNS makes comparison between ELS formation in stroke and other autoimmune diseases difficult. Nevertheless, ELS formation in the meninges has been observed in multiple sclerosis (MS) (Serafini et al., 2004). As B cell depleting therapy is highly effective in relapsing-remitting MS, B cells and ELS are suspected to play a fundamental role in the pathogenesis of this disease as well (Naismith et al., 2010).

Here, we demonstrate that CD4⁺ T cells are essential for B cell infiltration and formation of ELS in the ischemic brain. As previously reported in WT mice (Doyle et al., 2015), we found that B cells aggregated in the ischemic tissue, forming dense clusters with surrounding T cells in 2D2 mice. However, B cell infiltration and ELS formation was earlier and more pronounced in 2D2 mice. Stroke complications such as hemorrhagic transformation (HT) could possibly aggravate lymphocyte infiltration. However, we have not observed HT in the present study suggesting that B and T cell infiltration occurs independently of HT. In fact, our findings in isotype-treated mice suggest that the magnitude of B cell infiltration depends on lesion size. Although CD4⁺ T cell depletion reduces B cell brain-infiltration to a large extent it did not prevent ELS formation entirely. This finding and further data discussed by Zbesko et al. in this issue indicate that additional CD4⁺ T cell independent mechanisms are involved in B cell infiltration (Zbesko et al., 2020).

Additionally, we found that CD4 depletion attenuates microglial loss in the ipsilateral hemisphere 14 days after MCAo independently of infarct size. Recruitment of IMC to the ischemic hemisphere was highly variable in isotype-treated mice, but myeloid cell infiltration in CD4-depleted mice was consistently low. IMC could facilitate ELS induction as monocyte-derived macrophages drive lymphoid neogenesis during autoimmunity by CXCL13 production (Carlsen et al., 2004). In experimental stroke, myeloid cell infiltration was considered to be limited to the acute and subacute phase of stroke. However, a second peak of T cells and macrophages in the CNS after experimental stroke was described recently, raising the possibility of interaction between T cells and macrophages contributing to ELS formation (Vindegaard et al., 2017).

Consistent with previous reports, we observed post-ischemic microglial loss (Otxoa-de-Amezaga et al., 2018) and infiltration of myeloid cells, mainly monocytes/macrophages. Mechanisms linked directly to cerebral hypoxia account for the majority of microglial cell death during early stroke pathology (Eyo et al., 2013; Wang et al., 2017). However, at later time-points autoreactivity could contribute to this process, as immune responses directed against a number of CNS-specific antigens have been described after stroke (Ortega et al., 2015). Accordingly, compared to isotype-treated mice we observed higher numbers of microglia in the ipsilateral hemisphere in mice in which delayed CD4⁺ T cell responses were prevented by anti-CD4 treatment. This finding may suggest that prolonged autoreactive inflammatory CD4⁺ T cell responses could increase microglial loss after stroke. Despite the pronounced effect on myeloid cell numbers, CD4 depletion did not affect the expression of microglial homeostasis and activation markers after stroke. CD4⁺ T cell signals that could mediate microglia cell death are currently unknown and need further investigation.

We speculate that IMC compensate for post-ischemic microglial loss, especially in animals with large infarcts (Mildner et al., 2007). Indeed, we found that numbers of IMC increased with infarct volumes and decreased with the number of resident microglia. Both correlations were completely abrogated by CD4 depletion indicating an essential role for CD4⁺ T cells in delayed IMC recruitment after stroke. Considering the reduction of both, infiltrating B cells and myeloid cells by CD4 depletion, CD4⁺ T cells may either be involved in B cell and myeloid cell recruitment independently or promote myeloid cell infiltration, which in turn further facilitate B cell recruitment (Ortega et al., 2015).

Circulating CD4⁺ T cells were eliminated until day 28 after stroke but recovered after 49 days. Importantly, with the recovery of CD4⁺ T cells in the periphery, T as well as B lymphocyte infiltration into the brain started also in the depletion group, indicating that the cues for increased lymphocyte trafficking across the blood-brain barrier are present over a long period of time after ischemic brain injury.

Antibodies to neuronal antigens worsen stroke patients' functional outcome (Becker et al., 2016a). B cell expansion, hypermutation and differentiation to antibody-producing PC occur in the GCs of ELS (Corsiero et al., 2016). The presence of lymphocytes expressing GC B cell and PC markers in brains 49 and 72 days after MCAo suggests that these GC-specific processes leading to autoreactive CNS antigen-specific antibody production also occur in stroke. Conclusively, we observed IgG and IgM producing PC in proximity to ELS. The antigen specificity of these antibodies remains yet to be determined. Unspecific IgM and IgG staining in the infarcted tissue suggest reactivity to multiple target antigens however. We also observed CD138⁺IgM⁻IgG⁻ PC that could possibly produce IgA as described (Zbesko et al., 2020).

Production of CNS-specific antibodies may contribute to PSCI (Becker et al., 2016a), which could be prevented by antibody-based B cell depletion or primary B cell deficiency in an experimental setup (Doyle et al., 2015). Increased B cell numbers and IgG bound to brain tissue were also observed in post-mortem brain samples analyzed from stroke patients with dementia compared to those without dementia (Doyle et al., 2015). To our knowledge, ELS have not been reported in brain tissue after stroke in humans, yet. This may be due to the fact that ELS in experimental stroke can only be detected in the core area of ischemia. However, tissue samples from patients who have died after a stroke are usually not collected from these areas during autopsy for the brain banks. Interestingly, a recent study using B cell depletion suggests that B cells contribute to post-stroke recovery by promoting neurogenesis (Ortega et al., 2020). In our hands, anti-CD4 treatment reduced B cell infiltration only temporarily. Even though CD4⁺ T cells and B cells infiltrated the CNS also in the depletion group at later time points, our behavioral data suggest that CD4⁺ T cell depletion could improve long-term functional outcomes after stroke.

Altogether, our results indicate that B cell infiltration into the CNS after experimental stroke is facilitated by CD4⁺ T cell-mediated responses, which might include additional responses by microglia and infiltrating peripheral myeloid cells. Furthermore, we demonstrate that post-stroke lymphocyte infiltration is a long-lasting process that could serve as a target to prevent PSCI.

Acknowledgements

We thank Sabine Kolodziej and Claudia Muselmann-Genschow for excellent technical assistance. We would like to acknowledge the assistance of the BIH Cytometry Core and the Charité NeuroCure 7T Experimental MRI. We would like to thank Marco Prinz for kindly providing us with Cx3Cr1^{CreERT2}-YFP mice.

Sources of Funding

The German Research Foundation (TRR167, TRR84, TRR43), Einstein Foundation (A-2017-406) and Leducq Foundation (19CVD01)

supported this study.

Appendix A. Supplementary data

Supplementary data to this article can be found online at <https://doi.org/10.1016/j.bbi.2020.09.029>.

References

- Al-Kufaidy, R., Vazquez-Tello, A., BaHammam, A.S., Al-Muhsen, S., Hamid, Q., Halwani, R., 2017. IL-17 enhances the migration of B cells during asthma by inducing CXCL13 chemokine production in structural lung cells. *J. Allergy Clin. Immunol.* 139, 696–699.e695.
- Aloisi, F., Pujol-Borrell, R., 2006. Lymphoid neogenesis in chronic inflammatory diseases. *Nat. Rev. Immunol.* 6, 205–217.
- Barone, F.C., Knudsen, D.J., Nelson, A.H., Feuerstein, G.Z., Willette, R.N., 1993. Mouse strain differences in susceptibility to cerebral ischemia are related to cerebral vascular anatomy. *J. Cereb. Blood Flow Metab.* 13, 683–692.
- Becker, K.J., Kalil, A.J., Tanzi, P., Zierath, D.K., Savos, A.V., Gee, J.M., Hadwin, J., Carter, K.T., Shibata, D., Cain, K.C., 2011. Autoimmune responses to the brain after stroke are associated with worse outcome. *Stroke* 42, 2763–2769.
- Becker, K.J., Tanzi, P., Zierath, D., Buckwalter, M.S., 2016a. Antibodies to myelin basic protein are associated with cognitive decline after stroke. *J. Neuroimmunol.* 295–296, 9–11.
- Becker, K.J., Zierath, D., Kunze, A., Fecteau, L., Lee, B., Skerrett, S., 2016b. The contribution of antibiotics, pneumonia and the immune response to stroke outcome. *J. Neuroimmunol.* 295–296, 68–74.
- Bederson, J.B., Pitts, L.H., Tsuji, M., Nishimura, M.C., Davis, R.L., Bartkowski, H., 1986. Rat middle cerebral artery occlusion: evaluation of the model and development of a neurologic examination. *Stroke* 17, 472–476.
- Benakis, C., Garcia-Bonilla, L., Iadecola, C., Anrather, J., 2014. The role of microglia and myeloid immune cells in acute cerebral ischemia. *Front. Cell. Neurosci.* 8, 461.
- Bettelli, E., Pagany, M., Weiner, H.L., Linington, C., Sobel, R.A., Kuchroo, V.K., 2003. Myelin oligodendrocyte glycoprotein-specific T cell receptor transgenic mice develop spontaneous autoimmune optic neuritis. *J. Exp. Med.* 197, 1073–1081.
- Carlsen, H.S., Baekkevold, E.S., Morton, H.C., Haraldsen, G., Brandtzaeg, P., 2004. Monocyte-like and mature macrophages produce CXCL13 (B cell-attracting chemokine 1) in inflammatory lesions with lymphoid neogenesis. *Blood* 104, 3021–3027.
- Corsiero, E., Bombardieri, M., Manzo, A., Bugatti, S., Ugucioni, M., Pitzalis, C., 2012. Role of lymphoid chemokines in the development of functional ectopic lymphoid structures in rheumatic autoimmune diseases. *Immunol. Lett.* 145, 62–67.
- Corsiero, E., Nerviani, A., Bombardieri, M., Pitzalis, C., 2016. Ectopic lymphoid structures: powerhouse of autoimmunity. *Front. Immunol.* 7.
- Cramer, J.V., Benakis, C., Liesz, A., 2019. T cells in the post-ischemic brain: troopers or paramedics? *J. Neuroimmunol.* 326, 33–37.
- Crotty, S., 2014. T follicular helper cell differentiation, function, and roles in disease. *Immunity* 41, 529–542.
- Doyle, K.P., Quach, L.N., Sole, M., Axtell, R.C., Nguyen, T.V., Soler-Llavina, G.J., Jurado, S., Han, J., Steinman, L., Longo, F.M., Schneider, J.A., Malenka, R.C., Buckwalter, M.S., 2015. B-lymphocyte-mediated delayed cognitive impairment following stroke. *J. Neurosci.* 35, 2133–2145.
- Elkins, J., Velkamp, R., Montaner, J., Johnston, S.C., Singhal, A.B., Becker, K., Lansberg, M.G., Tang, W., Chang, L., Muralidharan, K., Gheuens, S., Mehta, L., Elkind, M.S.V., 2017. Safety and efficacy of natalizumab in patients with acute ischaemic stroke (ACTION): a randomised, placebo-controlled, double-blind phase 2 trial. *Lancet Neurol.* 16, 217–226.
- Engel, O., Kolodziej, S., Dirnagl, U., Prinz, V., 2011. Modeling stroke in mice - middle cerebral artery occlusion with the filament model. *J. Vis. Exp.*
- Eyo, U.B., Miner, S.A., Ahlers, K.E., Wu, L.-J., Dailey, M.E., 2013. P2X7 receptor activation regulates microglial cell death during oxygen-glucose deprivation. *Neuropharmacology* 73, 311–319.
- Faul, F., Erdfelder, E., Lang, A.G., Buchner, A., 2007. G*Power 3: a flexible statistical power analysis program for the social, behavioral, and biomedical sciences. *Behav. Res. Methods* 39, 175–191.
- Feigin, V.L., Forouzanfar, M.H., Krishnamurthi, R., Mensah, G.A., Connor, M., Bennett, D.A., Moran, A.E., Sacco, R.L., Anderson, L., Truelsen, T., O'Donnell, M., Venketasubramanian, N., Barker-Collo, S., Lawes, C.M., Wang, W., Shinohara, Y., Witt, E., Ezzati, M., Naghavi, M., Murray, C., Global Burden of Diseases, I, Risk Factors, S., the, G.B.D.S.E.G., 2014. Global and regional burden of stroke during 1990–2010: findings from the Global Burden of Disease Study 2010. *Lancet* 383, 245–254.
- Fleige, H., Ravens, S., Moschovakis, G.L., Bölter, J., Willenzon, S., Sutter, G., Häussler, S., Kalinke, U., Prinz, L., Förster, R., 2014. IL-17-induced CXCL12 recruits B cells and induces follicle formation in BALB/c in the absence of differentiated FDCs. *J. Exp. Med.* 211, 643–651.
- Frenkel, D., Huang, Z., Maron, R., Koldzic, D.N., Hancock, W.W., Moskowitz, M.A., Weiner, H.L., 2003. Nasal vaccination with myelin oligodendrocyte glycoprotein reduces stroke size by inducing IL-10-producing CD4+ T cells. *J. Immunol.* 171, 6549–6555.
- Gerriets, T., Stolz, E., Walberer, M., Müller, C., Kluge, A., Bachmann, A., Fisher, M., Kaps, M., Bachmann, G., 2004. Noninvasive quantification of brain edema and the space-occupying effect in rat stroke models using magnetic resonance imaging. *Stroke* 35, 566–571.
- Gu, L., Xiong, X., Zhang, H., Xu, B., Steinberg Gary, K., Zhao, H., 2012. Distinctive effects of T cell subsets in neuronal injury induced by cocultured splenocytes in vitro and by in vivo stroke in mice. *Stroke* 43, 1941–1946.
- Harms, H., Prass, K., Meisel, C., Klehmet, J., Rogge, W., Drenckhahn, C., Göhler, J., Bereswill, S., Göbel, U., Wernecke, K.D., Wolf, T., Arnold, G., Halle, E., Volk, H.-D., Dirnagl, U., Meisel, A., 2008. Preventive antibacterial therapy in acute ischemic stroke: a randomized controlled trial. *PLoS ONE* 3, e2158.
- Harris, N.M., Roy-O'Reilly, M., Ritzel, R.M., Holmes, A., Sansing, L.H., O'Keefe, L.M., McCullough, L.D., Chauhan, A., 2020. Depletion of CD4 T cells provides therapeutic benefits in aged mice after ischemic stroke. *Exp. Neurol.* 113202.
- Hetze, S., Romer, C., Teufelhart, C., Meisel, A., Engel, O., Römer, C., Teufelhart, C., Meisel, A., Engel, O., 2012. Gait analysis as a method for assessing neurological outcome in a mouse model of stroke. *J. Neurosci. Methods* 206, 7–14.
- Hoffmann, S., Harms, H., Ulm, L., Nabavi, D.G., Mackert, B.-M., Schmehl, I., Jungehulsing, G.J., Montaner, J., Bustamante, A., Hermans, M., Hamilton, F., Göhler, J., Malzahn, U., Malsch, C., Heuschmann, P.U., Meisel, C., Meisel, A., Investigators, P., 2017. Stroke-induced immunodepression and dysphagia independently predict stroke-associated pneumonia - The PREDICT study. *J. Cereb. Blood Flow Metab.* 37, 3671–3682.
- Hurn, P.D., Subramanian, S., Parker, S.M., Afentoulis, M.E., Kaler, L.J., Vandenberg, A.A., Offner, H., 2007. T- and B-cell-deficient mice with experimental stroke have reduced lesion size and inflammation. *J. Cereb. Blood Flow Metab.* 27, 1798–1805.
- Jin, W.-N., Gonzales, R., Feng, Y., Wood, K., Chai, Z., Dong, J.-F., La Cava, A., Shi, F.-D., Liu, Q., 2018. Brain ischemia induces diversified neuroantigen-specific T-cell responses that exacerbate brain injury. *Stroke* 49, 1471–1478.
- Klehmet, J., Hoffmann, S., Walter, G., Meisel, C., Meisel, A., 2016. Stroke induces specific alteration of T memory compartment controlling auto-reactive CNS antigen-specific T cell responses. *J. Neurol. Sci.* 368, 77–83.
- Kleinschnitz, C., Kraft, P., Dreykluft, A., Hagedorn, I., Göbel, K., Schuhmann, M.K., Langhauser, F., Helluy, X., Schwarz, T., Bittner, S., Mayer, C.T., Brede, M., Varallyay, C., Pham, M., Bendzus, M., Jakob, P., Magnus, T., Meuth, S.G., Iwakura, Y., Zerneck, A., Sparwasser, T., Nieswandt, B., Stoll, G., Wiendl, H., 2013. Regulatory T cells are strong promoters of acute ischemic stroke in mice by inducing dysfunction of the cerebral microvasculature. *Blood* 121, 679–691.
- Kleinschnitz, C., Schwab, N., Kraft, P., Hagedorn, I., Dreykluft, A., Schwarz, T., Austinat, M., Nieswandt, B., Wiendl, H., Stoll, G., 2010. Early detrimental T-cell effects in experimental cerebral ischemia are neither related to adaptive immunity nor thrombus formation. *Blood* 115, 3835–3842.
- Knauss, Samuel, Albrecht, Carolin, Dirnagl, Ulrich, Mueller, Susanne, Harms, Christoph, Hoffmann, Christian Johannes, Koch, Stefan Paul, Endres, Matthias, Boehm-Sturm, Philipp, et al., 2020. A semiquantitative non-invasive measurement of PcamA patency in C57Bl/6 mice explains variance in ischemic brain damage in filament MCAo. *Front. Neurosci.* <https://doi.org/10.3389/fnins.2020.576741>. In press.
- Lambertsen, K.L., Gregersen, R., Finsen, B., 2002. Microglial—macrophage synthesis of tumor necrosis factor after focal cerebral ischemia in mice is strain dependent. *J. Cereb. Blood Flow Metab.* 22, 785–797.
- Liesz, A., Hu, X., Kleinschnitz, C., Offner, H., 2015. Functional role of regulatory lymphocytes in stroke: facts and controversies. *Stroke* 46, 1422–1430.
- Liesz, A., Zhou, W., Mracsko, E., Karcher, S., Bauer, H., Schwarting, S., Sun, L., Bruder, D., Stegemann, S., Cerwenka, A., Sommer, C., Dalpke, A.H., Veltkamp, R., 2011. Inhibition of lymphocyte trafficking shields the brain against deleterious neuroinflammation after stroke. *Brain* 134, 704–720.
- Llovera, G., Hofmann, K., Roth, S., Salas-Perdomo, A., Ferrer-Ferrer, M., Perego, C., Zanier, E.R., Mamrak, U., Rex, A., Party, H., Agin, V., Fauchon, C., Orset, C., Haelewyn, B., De Simoni, M.G., Dirnagl, U., Grittner, U., Planas, A.M., Plesnila, N., Vivien, D., Liesz, A., 2015. Results of a preclinical randomized controlled multicenter trial (pRCT): anti-CD49d treatment for acute brain ischemia. *Sci. Transl. Med.* 7, 299ra121.
- Maurice, T., Hiramatsu, M., Itoh, J., Kameyama, T., Hasegawa, T., Nabeshima, T., 1994. Low dose of 1,3-di(2-tolyl)guanidine (DTG) attenuates MK-801-induced spatial working memory impairment in mice. *Psychopharmacology* 114, 520–522.
- Mijajlović, M.D., Pavlović, A., Brainin, M., Heiss, W.-D., Quinn, T.J., Ihle-Hansen, H.B., Hermann, D.M., Assayag, E.B., Richard, E., Thiel, A., Kliper, E., Shin, Y.-I., Kim, Y.-H., Choi, S., Jung, S., Lee, Y.-B., Sinanović, O., Levine, D.A., Schiesinger, I., Mead, G., Milošević, V., Leys, D., Hagberg, G., Ursin, M.H., Teuschl, Y., Prokopenko, S., Mozheyko, E., Bezdenezhnykh, A., Matz, K., Aleksić, V., Muresanu, D., Korczyn, A.D., Bornstein, N.M., 2017. Post-stroke dementia – a comprehensive review. *BMC Med.*
- Mildner, A., Schmidt, H., Nitsche, M., Merkler, D., Hanisch, U.K., Mack, M., Heikenwalder, M., Bruck, W., Priller, J., Prinz, M., 2007. Microglia in the adult brain arise from Ly-6ChiCCR2+ monocytes only under defined host conditions. *Nat. Neurosci.* 10, 1544–1553.
- Naimsmith, R.T., Piccio, L., Lyons, J.A., Lauber, J., Tutlam, N.T., Parks, B.J., Trinkaus, K., Song, S.K., Cross, A.H., 2010. Rituximab add-on therapy for breakthrough relapsing multiple sclerosis: a 52-week phase II trial. *Neurology* 74, 1860–1867.
- Ortega, S.B., Noorbhai, I., Poinssat, K., Kong, X., Anderson, A., Monson, N.L., Stowe, A.M., 2015. Stroke induces a rapid adaptive autoimmune response to novel neuronal antigens. *Discovery Med.* 19, 381–392.
- Ortega, S.B., Torres, V.O., Latchney, S.E., Whoolery, C.W., Noorbhai, I.Z., Poinssat, K., Selvaraj, U.M., Benson, M.A., Meeuwissen, A.J.M., Plautz, E.J., Kong, X., Ramirez, D.M., Ajay, A.D., Meeks, J.P., Goldberg, M.P., Monson, N.L., Eisch, A.J., Stowe, A.M., 2020. B cells migrate into remote brain areas and support neurogenesis and functional recovery after focal stroke in mice. *Proceedings of the National Academy of Sciences.* 201913292.
- Otxoa-de-Amezaga, A., Miró-Mur, F., Pedragosa, J., Gallizioli, M., Justicia, C., Gaja-Capdevila, N., Ruiz-Jaen, F., Salas-Perdomo, A., Bosch, A., Calvo, M., Márquez-Kisinosky, L., Denes, A., Gunzer, M., Planas, A.M., 2018. Microglial cell loss after

- ischemic stroke favors brain neutrophil accumulation. *Acta Neuropathol.*
- Pendlebury, S.T., Rothwell, P.M., 2009. Prevalence, incidence, and factors associated with pre-stroke and post-stroke dementia: a systematic review and meta-analysis. *Lancet Neurol.* 8, 1006–1018.
- Planas, A.M., Gomez-Choco, M., Urrea, X., Gorina, R., Caballero, M., Chamorro, A., 2012. Brain-derived antigens in lymphoid tissue of patients with acute stroke. *J. Immunol.* 188, 2156–2163.
- Prass, K., Meisel, C., Hoflich, C., Braun, J., Halle, E., Wolf, T., Ruscher, K., Victorov, I.V., Priller, J., Dirnagl, U., Volk, H.D., Meisel, A., 2003. Stroke-induced immunodeficiency promotes spontaneous bacterial infections and is mediated by sympathetic activation reversal by poststroke T helper cell type 1-like immunostimulation. *J. Exp. Med.* 198, 725–736.
- Ren, X., Aklyoshi, K., Graf, M.R., Vandenberg, A.A., Hurn, P.D., Herson, P.S., Offner, H., 2012. Myelin specific cells infiltrate MCAO lesions and exacerbate stroke severity. *Metab. Brain Dis.* 27, 7–15.
- Römer, C., Engel, O., Winek, K., Hochmeister, S., Zhang, T., Rojl, G., Klehmet, J., Dirnagl, U., Meisel, C., Meisel, A., Romer, C., Engel, O., Winek, K., Hochmeister, S., Zhang, T., Rojl, G., Klehmet, J., Dirnagl, U., Meisel, C., Meisel, A., 2015. Blocking stroke-induced immunodeficiency increases CNS antigen-specific autoreactivity but does not worsen functional outcome after experimental stroke. *J. Neurosci.* 35, 7777–7794.
- Schauwecker, P.E., Steward, O., 1997. Genetic determinants of susceptibility to excitotoxic cell death: implications for gene targeting approaches. *Proc. Natl. Acad. Sci.* 94, 4103.
- Serafini, B., Rosicarelli, B., Magliozzi, R., Stigliano, E., Aloisi, F., 2004. Detection of ectopic B-cell follicles with germinal centers in the meninges of patients with secondary progressive multiple sclerosis. *Brain Pathol.* 14, 164–174.
- Shichita, T., Sugiyama, Y., Ooboshi, H., Sugimori, H., Nakagawa, R., Takada, I., Iwaki, T., Okada, Y., Iida, M., Cua, D.J., Iwakura, Y., Yoshimura, A., 2009. Pivotal role of cerebral interleukin-17-producing gammadeltaT cells in the delayed phase of ischemic brain injury. *Nat. Med.* 15, 946–950.
- Simats, A., García-Berrocó, T., Montaner, J., 2016. Natalizumab: a new therapy for acute ischemic stroke? *Expert Rev. Neurother.* 16, 1013–1021.
- Sonar, S.A., Shaikh, S., Joshi, N., Atre, A.N., Lal, G., 2017. IFN- γ promotes transendothelial migration of CD4+ T cells across the blood-brain barrier. *Immunol. Cell Biol.* 95, 843–853.
- Stein, V.M., Baumgärtner, W., Schröder, S., Zurbriggen, A., Vandeveld, M., Tipold, A., 2007. Differential expression of CD45 on canine microglial cells. *J. Vet. Med. Ser. A* 54, 314–320.
- Stubbe, T., Ebner, F., Richter, D., Engel, O., Klehmet, J., Rojl, G., Meisel, A., Nitsch, R., Meisel, C., Brandt, C., 2013. Regulatory T cells accumulate and proliferate in the ischemic hemisphere for up to 30 days after MCAO. *J. Cereb. Blood Flow Metab.* 33, 37–47.
- van Zwam, M., Huizinga, R., Melief, M.J., Wierenga-Wolf, A.F., van Meurs, M., Voerman, J.S., Biber, K.P., Boddeke, H.W., Hopken, U.E., Meisel, C., Meisel, A., Bechmann, I., Hintzen, R.Q., Hart, B.A., Amor, S., Laman, J.D., Boven, L.A., 2009. Brain antigens in functionally distinct antigen-presenting cell populations in cervical lymph nodes in MS and EAE. *J. Mol. Med.* 87, 273–286.
- Vindgaard, N., Muñoz-Briones, C., El Ali, H.H., Kristensen, L.K., Rasmussen, R.S., Johansen, F.F., Hasseldam, H., 2017. T-cells and macrophages peak weeks after experimental stroke: spatial and temporal characteristics. *Neuropathology* 37, 407–414.
- Wang, X., Ma, J., Fu, Q., Zhu, L., Zhang, Z., Zhang, F., Lu, N., Chen, A., 2017. Role of hypoxia-inducible factor-1 α in autophagic cell death in microglial cells induced by hypoxia. *Mol. Med. Rep.* 15, 2097–2105.
- Zbesko, Jacob, Beischel Frye, Jennifer, Becktel, Danielle, Gerardo, Diana, Stokes, Jessica, Calderon, Kylie, Nguyen, Thuy-Vi, Bhattacharya, Deepa, Doyle, Kristian, et al., 2020. IgA natural antibodies are produced following T-cell independent B-cell activation following stroke. *Brain Behav. Immun.* <https://doi.org/10.1016/j.bbi.2020.09.014>. In this issue.

8.2. Publication 2

8.2.1. Excerpt From the ISI Journal Summary List

Journal Data Filtered By: **Selected JCR Year: 2020** Selected Editions: SCIE,SSCI
 Selected Categories: **"Immunology"** Selected Category Scheme: WoS
Gesamtanzahl: 162 Journale

Rank	Full Journal Title	Total Cites	Journal Impact Factor	Eigenfactor Score
1	NATURE REVIEWS IMMUNOLOGY	55,784	53.106	0.063920
2	IMMUNITY	70,517	31.745	0.122940
3	Annual Review of Immunology	20,292	28.527	0.017290
4	NATURE IMMUNOLOGY	54,588	25.606	0.080490
5	Science Immunology	5,232	17.727	0.022200
6	TRENDS IN IMMUNOLOGY	16,915	16.687	0.024570
7	JOURNAL OF EXPERIMENTAL MEDICINE	74,803	14.307	0.062280
8	Journal for ImmunoTherapy of Cancer	11,042	13.751	0.028830
9	ALLERGY	25,131	13.146	0.023300
10	IMMUNOLOGICAL REVIEWS	19,337	12.988	0.024380
11	Lancet HIV	5,368	12.767	0.022020
12	Cellular & Molecular Immunology	8,489	11.530	0.010550
13	Cancer Immunology Research	11,185	11.151	0.027290
14	SEMINARS IN IMMUNOLOGY	6,814	11.130	0.008220
15	JOURNAL OF ALLERGY AND CLINICAL IMMUNOLOGY	63,614	10.793	0.069980
16	AUTOIMMUNITY REVIEWS	13,493	9.754	0.014810
17	Seminars in Immunopathology	5,651	9.623	0.009960
18	CLINICAL INFECTIOUS DISEASES	89,276	9.079	0.113210
19	Journal of Allergy and Clinical Immunology-In Practice	9,255	8.861	0.019690
20	CLINICAL REVIEWS IN ALLERGY & IMMUNOLOGY	4,546	8.667	0.006270
21	Journal of Neuroinflammation	19,657	8.322	0.027070

Rank	Full Journal Title	Total Cites	Journal Impact Factor	Eigenfactor Score
22	JOURNAL OF CLINICAL IMMUNOLOGY	6,537	8.317	0.007110
23	OncolImmunology	14,987	8.110	0.030230
24	Frontiers in Immunology	84,852	7.561	0.182280
25	CURRENT OPINION IN IMMUNOLOGY	11,347	7.486	0.014270
26	IMMUNOLOGY	14,248	7.397	0.011160
27	Inflammation and Regeneration	743	7.354	0.001450
28	Journal of Innate Immunity	3,032	7.349	0.003370
29	npj Vaccines	1,342	7.344	0.003850
30	Mucosal Immunology	9,440	7.313	0.017940
31	BRAIN BEHAVIOR AND IMMUNITY	24,161	7.217	0.026930
32	Emerging Microbes & Infections	8,988	7.163	0.012560
33	JOURNAL OF AUTOIMMUNITY	10,437	7.094	0.012240
34	CANCER IMMUNOLOGY IMMUNOTHERAPY	11,382	6.968	0.012190
35	Journal of Inflammation Research	1,321	6.922	0.002130
36	EMERGING INFECTIOUS DISEASES	44,051	6.883	0.049780
37	Immunity & Ageing	1,468	6.400	0.001750
38	PEDIATRIC ALLERGY AND IMMUNOLOGY	5,778	6.377	0.005590
39	ANNALS OF ALLERGY ASTHMA & IMMUNOLOGY	10,809	6.347	0.011650
40	EXERCISE IMMUNOLOGY REVIEW	1,093	6.308	0.000710
41	Immune Network	1,629	6.303	0.002620
42	Clinical & Translational Immunology	1,574	6.161	0.003690
43	INFECTIOUS DISEASE CLINICS OF NORTH AMERICA	4,090	5.982	0.006870

Rank	Full Journal Title	Total Cites	Journal Impact Factor	Eigenfactor Score
44	Virulence	5,784	5.882	0.007420
45	ALLERGOLOGY INTERNATIONAL	3,122	5.836	0.004520
46	BIODRUGS	2,581	5.807	0.003770
47	Allergy Asthma & Immunology Research	2,345	5.764	0.003570
48	BIOLOGY OF BLOOD AND MARROW TRANSPLANTATION	17,149	5.742	0.026390
49	EUROPEAN JOURNAL OF IMMUNOLOGY	24,504	5.532	0.017040
50	BONE MARROW TRANSPLANTATION	16,801	5.483	0.015200
51	JOURNAL OF IMMUNOLOGY	146,980	5.422	0.087490
52	Journal of the International AIDS Society	6,474	5.396	0.017390
53	INTERNATIONAL REVIEWS OF IMMUNOLOGY	1,840	5.311	0.001570
54	Frontiers in Cellular and Infection Microbiology	13,426	5.293	0.024490
55	JOURNAL OF INFECTIOUS DISEASES	54,782	5.226	0.066740
56	Expert Review of Vaccines	5,376	5.217	0.008860
57	IMMUNOLOGY AND CELL BIOLOGY	5,812	5.126	0.006570
58	CLINICAL AND EXPERIMENTAL ALLERGY	12,339	5.018	0.009930
59	Journal of Inflammation-London	1,812	4.981	0.001710
60	JOURNAL OF LEUKOCYTE BIOLOGY	21,186	4.962	0.016370
61	TRANSPLANTATION	27,214	4.939	0.024800
62	INTERNATIONAL IMMUNOPHARMACOLOGY	20,562	4.932	0.019780
63	CELLULAR IMMUNOLOGY	6,746	4.868	0.007120
64	INTERNATIONAL IMMUNOLOGY	7,333	4.823	0.005160
65	Journal of Immunology Research	7,621	4.818	0.014510

Rank	Full Journal Title	Total Cites	Journal Impact Factor	Eigenfactor Score
66	CURRENT ALLERGY AND ASTHMA REPORTS	3,395	4.806	0.004480
67	MEDIATORS OF INFLAMMATION	16,551	4.711	0.020320
68	FISH & SHELLFISH IMMUNOLOGY	29,735	4.581	0.021130
69	INFLAMMATION RESEARCH	5,662	4.575	0.004000
70	HLA	1,447	4.513	0.001740
71	Expert Review of Clinical Immunology	3,774	4.473	0.005630
71	INFLAMMOPHARMACOLOGY	2,992	4.473	0.003040
73	JOURNAL OF IMMUNOTHERAPY	3,872	4.456	0.003070
74	Vaccines	3,381	4.422	0.005970
75	MOLECULAR IMMUNOLOGY	14,321	4.407	0.014030
76	JOURNAL OF MICROBIOLOGY IMMUNOLOGY AND INFECTION	4,936	4.399	0.005200
77	JOURNAL OF INVESTIGATIONAL ALLERGOLOGY AND CLINICAL IMMUNOLOGY	2,703	4.333	0.002080
78	CLINICAL AND EXPERIMENTAL IMMUNOLOGY	16,216	4.330	0.009230
79	ARCHIVUM IMMUNOLOGIAE ET THERAPIAE EXPERIMENTALIS	2,389	4.291	0.002010
79	Current Topics in Microbiology and Immunology	6,980	4.291	0.006670
81	Current Opinion in HIV and AIDS	3,006	4.283	0.007440
82	Journal of Asthma and Allergy	882	4.258	0.001710
83	Immunotherapy	3,372	4.196	0.005680
84	AIDS	20,317	4.177	0.029400
85	INFLAMMATION	7,257	4.092	0.007960
86	World Allergy Organization Journal	2,492	4.084	0.002600

8.2.2. Print Copy

Article

Impact of Key Nicotinic AChR Subunits on Post-Stroke Pneumococcal Pneumonia

Sandra Jagdmann¹, Claudia Dames^{1,2}, Daniel Berchtold², Katarzyna Winek²,
Luis Weitbrecht², Andreas Meisel^{2,3,4,5,*} and Christian Meisel^{1,6}

- ¹ Institute for Medical Immunology, Charité-Universitätsmedizin Berlin, Corporate Member of Freie Universität Berlin, Humboldt-Universität zu Berlin, Berlin Institute of Health, 13353 Berlin, Germany; Sandra.jagdmann@charite.de (S.J.); Claudia.dames@charite.de (C.D.); chr.meisel@charite.de (C.M.)
 - ² Department of Experimental Neurology, Charité-Universitätsmedizin Berlin, Corporate Member of Freie Universität Berlin, Humboldt-Universität zu Berlin, Berlin Institute of Health, 10117 Berlin, Germany; daniel.berchtold@charite.de (D.B.); Katarzyna.winek@alumni.charite.de or katarzyna.winek@mail.huji.ac.il (K.W.); Luis.weitbrecht@charite.de (L.W.)
 - ³ Center for Stroke Research Berlin, Charité-Universitätsmedizin Berlin, Corporate Member of Freie Universität Berlin, Humboldt-Universität zu Berlin, and Berlin Institute of Health, 10117 Berlin, Germany
 - ⁴ Neurocure Clinical Research Center, Charité-Universitätsmedizin Berlin, Corporate Member of Freie Universität Berlin, Humboldt-Universität zu Berlin, and Berlin Institute of Health, 10117 Berlin, Germany
 - ⁵ Department of Neurology, Charité-Universitätsmedizin Berlin, Corporate Member of Freie Universität Berlin, Humboldt-Universität zu Berlin, and Berlin Institute of Health, 10117 Berlin, Germany
 - ⁶ Labor Berlin, Charité-Universitätsmedizin Berlin Vivantes, 10117 Berlin, Germany
- * Correspondence: andreas.meisel@charite.de; Tel.: +49-(0)-3045-056-0026

Received: 30 April 2020; Accepted: 25 May 2020; Published: 28 May 2020



Abstract: Pneumonia is the most frequent severe medical complication after stroke. An overactivation of the cholinergic signaling after stroke contributes to immunosuppression and the development of spontaneous pneumonia caused by Gram-negative pathogens. The $\alpha 7$ nicotinic acetylcholine receptor ($\alpha 7$ nAChR) has already been identified as an important mediator of the anti-inflammatory pathway after stroke. However, whether the $\alpha 2$, $\alpha 5$ and $\alpha 9/10$ nAChR expressed in the lung also play a role in suppression of pulmonary innate immunity after stroke is unknown. In the present study, we investigate the impact of various nAChRs on aspiration-induced pneumonia after stroke. Therefore, $\alpha 2$, $\alpha 5$, $\alpha 7$ and $\alpha 9/10$ nAChR knockout (KO) mice and wild type (WT) littermates were infected with *Streptococcus pneumoniae* (*S. pneumoniae*) three days after middle cerebral artery occlusion (MCAo). One day after infection pathogen clearance, cellularity in lung and spleen, cytokine secretion in bronchoalveolar lavage (BAL) and alveolar-capillary barrier were investigated. Here, we found that deficiency of various nAChRs does not contribute to an enhanced clearance of a Gram-positive pathogen causing post-stroke pneumonia in mice. In conclusion, these findings suggest that a single nAChR is not sufficient to mediate the impaired pulmonary defense against *S. pneumoniae* after experimental stroke.

Keywords: MCAo; immunosuppression; nicotinic acetylcholine receptor; aspiration-induced pneumonia; *Streptococcus pneumoniae*

1. Introduction

Stroke is a leading cause of death worldwide. The outcome depends on the occurrence of complications. Up to 95% of stroke patients experience medical complications in the first three months after stroke. Among these, infection is one of the most frequent, severe complications [1–4]. Long-lasting immunosuppression due to overactivation of neurohumoral stress pathways, besides other factors

such as neurological deficits leading to dysphagia and aspiration, contribute to the high incidence of pneumonia in stroke patients [5–7]. We have previously shown in an experimental mouse model, that excessive cholinergic signaling induced by stroke results in impaired innate immune responses in the lung [8]. In this cholinergic anti-inflammatory pathway, acetylcholine (ACh) released by vagal efferents and by non-neuronal cells was shown to impair antibacterial responses in the lung via the $\alpha 7$ nAChR expressed on alveolar epithelial cells (AECs) and macrophages (M Φ), contributing to an increased susceptibility to spontaneous Gram-negative bacterial pneumonia [8–12]. Nicotine as well as the $\alpha 7$ nAChR-specific agonist PNU282987 diminished LPS-induced IL-6 secretion in AECs isolated from WT but not $\alpha 7$ nAChR KO mice in a dose-dependent manner. In contrast, nicotine and PNU282987 dose-dependently reduced LPS-induced IL-6 secretion in M Φ from WT as well as $\alpha 7$ nAChR KO mice. Thus, nicotine suppressed the TLR-induced pro-inflammatory cytokine secretion in the absence of $\alpha 7$ nAChR, suggesting that suppression of pulmonary immune responses after stroke by the cholinergic anti-inflammatory pathway may in part be independent from the $\alpha 7$ nAChR [8]. nAChRs are homomeric or heteromeric combinations of $\alpha 2$ -10 and $\beta 3$ -4 subunits. Beyond the $\alpha 7$ nAChR subunit, mRNA expression of $\alpha 2$ nAChR, $\alpha 5$ nAChR, $\alpha 6$ nAChR, $\alpha 9$ nAChR and $\alpha 10$ nAChR was detected in immune cells including mononuclear leukocytes, dendritic cells (DCs), M Φ and T-cells supporting our hypothesis that not only $\alpha 7$ nAChRs are involved in the regulation of immune response after stroke [12–14].

Clinical studies have shown that impaired swallowing, aspiration and stroke-induced immunosuppression contribute to the increased incidence of bacterial pneumonia after stroke [7,15]. Microbiological analysis identified especially Gram-negative bacteria such as *Pseudomonas aeruginosa*, *Klebsiella pneumoniae*, *Enterobacter*, *Escherichia coli* and *Acinetobacter* in blood and lung of patients. However, also Gram-positive bacteria such as *S. pneumoniae*, the leading cause of community-acquired pneumonia, are relevant pathogens causing post-stroke pneumonia [16–18]. We have previously shown in an experimental mouse model, that nasal infection with 200 colony-forming units (CFU) of *S. pneumoniae* resulted in severe pulmonary infection after stroke, whereas sham operated mice were able to clear bacteria [19]. β -adrenoreceptor blockade by propranolol treatment significantly reduced bacterial burden in the lung suggesting sympathetic hyperactivity contributes to impaired pulmonary defense after experimental stroke [19–21].

In the present study, we aimed to investigate the role of various nAChRs expressed in the lung in the impaired antibacterial responses after stroke in an aspiration-induced model of post-stroke pneumococcal pneumonia.

2. Materials and Methods

2.1. Animals and Housing

Experiments were executed in accordance with the European directive on the protection of animals used for scientific purposes and further applicable legislation, and approved on 31 March 2016 by the relevant authority, Landesamt für Gesundheit und Soziales (LAGeSo), Berlin, Germany (project identification code: G0244/15). Male $\alpha 2$ nAChR KO (MMRRC_030508-UCD B6.129 \times 1-Chrna2^{tm1 Jbou}/Mmucd; University of California Davis Mutant Mouse Regional Resource Center (MMRRC)) [22], $\alpha 5$ nAChR KO (MMRRC_000421-UNC B6.129S7-Chrna5^{tm1 Mdb}/MmNc; University of North Carolina MMRRC) [23], $\alpha 7$ nAChR KO (JAX #003232B6.129 S7-Chrna7^{tm1 Bay}/J; The Jackson Laboratory, Bar Harbor) [24], $\alpha 9/10$ nAChR KO (JAX #005696 CBACaJ; 129 S-Chrna9^{tm1 Bedv}/J; The Jackson Laboratory, Bar Harbor and MMRRC_030509-UCD 129 S4-Chrna10^{tm1 Bedv}/Mmcd; University of California Davis MMRRC) [25,26] mice and corresponding WT littermates were used for infection experiments. Standard-genotyping using STR-marker and C57BL/6 substrain-specific mutation analysis confirmed that $\alpha 2$ nAChR KO, $\alpha 5$ nAChR KO and $\alpha 7$ nAChR KO strains carry an autosomal C57BL/6JCr1 background (GVG genetic monitoring). $\alpha 9/10$ nAChR KO strain was backcrossed for 8 generations to C57BL/6JCr1. Since all mouse strains carry the same genetic

background, mixed WT littermates from all strains were used as control groups (WT MCAo and WT naïve). C57BL/6J mice (The Jackson Laboratory, Bar Harbor, ME, USA) were used for nAChR expression analysis in lung and brain. All animals were housed with identical conditions in cages with chip bedding, mouse tunnel and mouse igloo on a 12 h light/dark cycle with ad libitum access to standard food and water. Experiments were performed with 12–20 weeks old mice.

2.2. Experimental Model of Stroke

The surgical procedure of MCAo was performed according to the standard operating procedures of the Department of Experimental Neurology, Charité-Universitätsmedizin Berlin [27]. Under general isoflurane anesthesia, a silicon-coated filament (7019PK5Re, Doccol Corp. Redlands, CA, USA) was introduced into the left common carotid artery and advanced to the origin of the middle cerebral artery (MCA) for 60 min. Infarct volume and success of MCAo was verified by hematoxylin staining from fresh-frozen brains. Animals without infarcts were excluded from the study.

2.3. Antibiotic Treatment

Spontaneously developing infection after MCAo was prevented by intraperitoneal (i.p.) injection of marbofloxacin (5 g/kg BW, Vétoquinol GmbH, Ravensburg, Germany) one day before and on the day of MCAo.

2.4. Bronchoscopy-Guided Application of *S. Pneumoniae* Three Days after MCAo

S. pneumoniae (D39 capsular type 2 *S. pneumoniae*, Rockefeller University, New York, NY, USA) was grown as described elsewhere [19] and diluted in PBS to 2000 CFU/50 µL. In previous experiments, an optimal dose of bacterial load of 200 CFU for intranasal infection in 129S6SvEv mice was established [19]. Since the C57BL/6J mouse strain used in this study is less susceptible to bacterial infection including *S. pneumoniae* D39 as compared to 129S6SvEv mice [28,29], we established 2000 CFU for infection in previous experiments when developing a miniaturized bronchoscopy protocol in mice [30]. Therefore, we used 2000 CFU for all experiments in this study. The same batch of bacteria from Rockefeller University was used for all experiments.

Under anesthesia with midazolam (5.0 mg/kg BW, Roche Pharma AG, Grenzach-Whylen, Germany) and medetomidin (0.5 mg/kg BW, Orion Corporation, Espoo, Finland) the bronchoscope (Polydiagnost, Pfaffenhofen, Germany) was inserted under visual control into the trachea and advanced to the bifurcation. Subsequently, 50 µL of defined pneumococcal suspension was applied in the main bronchi. Afterward, anesthesia was antagonized subcutaneous (s.c.) with flumazenil (0.5 mg/kg BW, Inresa, Freiburg, Germany) and atipamezol (5 mg/kg BW, Orion Corporation, Espoo, Finland) injection [30].

2.5. Microbiological Investigation

Bronchoalveolar lavage (BAL) was performed as described elsewhere [31]. Lungs were removed and homogenized in 500 µL PBS. BAL fluid, blood and lung tissue homogenate were serially diluted, plated on Columbia-Agar plates (BD Bioscience, Heidelberg, Germany), incubated at 37 °C for 18 h and bacterial colonies were counted to calculate the CFUs per ml tissue/liquid.

2.6. Flow Cytometry

Isolation of lung cells and splenocytes was performed as described elsewhere [8]. Cell phenotyping was performed on LSRII flow cytometer using FACS Diva software (BD Bioscience, Heidelberg, Germany) and Flowjo software 9.6.6 (Tree Star Inc, San Carlos, CA, USA) with the following anti-mouse monoclonal antibodies: CD45 Peridinin-Chlorophyll-protein (PerCP), CD11b Allophycocyanin-cyanine dye 7 (APC-Cy7), NK1.1 phycoerythrin (PE), CD19 Fluorescein (FITC), CD3 APC, CD4 Alexa Fluor 700 (A700), CD8 Pacific-Blue (PB), Gr1PE, CD11bPE-Cy7, F480 APC, Siglec F APC-Cy7, CD11 c PB (Biolegend, San Diego, CA, USA).

2.7. Analysis of Cytokines in BAL and Albumin in BAL and Plasma

Macrophage inflammatory protein-1 α (MIP-1 α), IL-10, keratinocyte chemoattractant (KC) and tumor necrosis factor α (TNF α) concentration in BAL were measured by using a commercially available Milliplex Map Kit (Merk Millipore, Darmstadt, Germany). Albumin level in BAL and plasma were quantified by an enzyme-linked immunosorbent assay (ELISA) (Bethyl Laboratories Inc., Montgomery, AL, USA).

2.8. Quantitative Reverse Transcriptase Polymerase Chain Reaction (qRT-PCR)

RNA from naïve lung and brain was extracted in Trizol according to the manufacturer's protocol (Roth, Karlsruhe, Germany). All samples were subsequently incubated with DNase (Promega, Fichtburg, MA, USA) followed by purification with Phenol-Chloroform. cDNA synthesis was performed using ProtoScript[®] II Reverse Transcriptase (New England Biolabs, Ipswich, UK) and the expression of nAChRs was quantified using a LightCycler 480 (Roche, Mannheim, Germany) and the LightCycler-FastStart-DNA-Master-SYBR-Green-I-Kit (Roche, Mannheim, Germany) according to the manufacturer's guidelines. β -actin was used as "housekeeping gene" for normalization. The following primers were used: mChrnaalpha2 (F: TGGATGGGCTGCAGAGAGACAGG, R: GGTCCTCGGCATGGGTGTGC), mChrnaalpha5 (F: ATCAACATCCACCACCGCTC, R: CTTCAACAACCTCGCGGACG), mChrnaalpha7 (F: TCCGTGCCCTTGATAGCACA, R: TCTCCCGGCCTTTCATGCG), mChrnaalpha9 (F: CGGACGCGGTGCTGAACGTC, R: AGACTCGTCATCGGCCTTGTTGT), mChrnaalpha10 (F: ACCCTCTGGCTGTGGTAGCG, R: GCACTTGGTTCGGTTCATCCATA). The amplification of Chrna 2, Chrna 7, Chrna 9, Chrna 10 and β -actin was performed at 95 °C (5 s), 66 °C (10 s) and 72 °C (15 s) for 45 cycles. Chrna 5 was amplified with the following conditions: 95 °C (5 s), 60 °C (10 s) and 72 °C (15 s) for 45 cycles. Melting curve analysis was performed to exclude the measurement of non-specific products. PCR products were sequenced to verify primer specificity.

2.9. Statistics

Statistical analysis was performed using Prism 6.0 Software (GraphPad, San Diego, CA, USA). Nonparametric one-way analysis of variance (ANOVA) with Dunn's multiple comparison test was used to compare the mean rank of each group with WT naïve group as a control group.

3. Results

3.1. α 2, α 5, α 9 and α 10 nAChR Subunits are Expressed in Lung and Brain of Naïve Mice

We previously demonstrated expression of α 7 nAChR in M Φ and AECs [8]. To investigate which additional nAChR subunits are expressed in lungs and brain, α 2, α 5, α 9 and α 10 nAChR mRNA expression in whole organ tissue isolated from naïve mice was quantified by qRT-PCR and compared to α 7 nAChR mRNA expression. All subunits were found to be expressed in both lung and brain, however with higher levels in brain compared to lung except for the α 10 subunit (Figure 1). These data suggest that other nicotinic receptors in addition to α 7 nAChR may be involved in cholinergic suppression of pulmonary immune response after stroke.

3.2. Role of Various nAChRs in an Aspiration-Induced Post-Stroke Pneumococcal Pneumonia

To investigate the impact of various nAChRs on the clearance of aspiration-induced pneumococcal pneumonia after experimental stroke, a pneumococcal suspension was applied at the tracheal bifurcation from α 2, α 5, α 7, α 9/10 KO mice and WT littermates three days after MCAo. Infected naïve WT mice served as controls. Bacterial burden in the lung, BAL and blood was determined one day after infection. Whereas naïve WT mice were able to clear bacteria, MCAo treated mice showed increased bacterial burden in lung and BAL one day after infection (Figure 2A,B), although the effect in BAL

was not significant compared to naïve WT mice. In contrast to naïve WT mice and stroked $\alpha 7$ KO mice, several MCAo-treated $\alpha 2$, $\alpha 5$, $\alpha 9/10$ KO mice and WT littermates suffered from bacteremia after bacterial challenge, whereby $\alpha 9/10$ KO mice exhibited significantly increased bacterial burden in blood compared to naïve WT mice (Figure 2C). However, bacterial burden in lung, BAL and blood was not significantly different between all nAChR KO and WT MCAo groups using WT MCAo mice as the reference group (Figure 2A,C). The infarct size was determined by histological staining and did not differ significantly between WT mice and nAChR KO mice (Figure 2D).

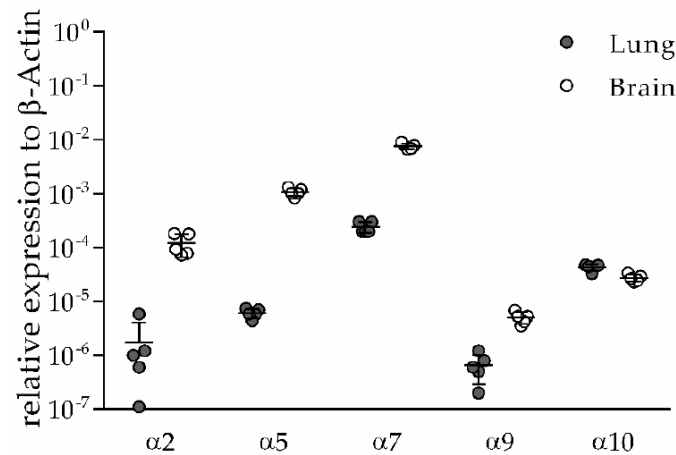


Figure 1. Expression of nAChR subunits in lung and brain tissue. $\alpha 2$, $\alpha 5$, $\alpha 7$, $\alpha 9$ and $\alpha 10$ nAChR subunits are expressed in lung and brain tissue of naïve wild type (WT) mice suggesting a possible role in anti-inflammatory cholinergic signaling after stroke. RNA was isolated from lung and brain tissue, and expression levels were determined by qRT-PCR. Target gene expression was normalized to β -actin as the housekeeping gene. Values are given as mean \pm SD ($n = 5$).

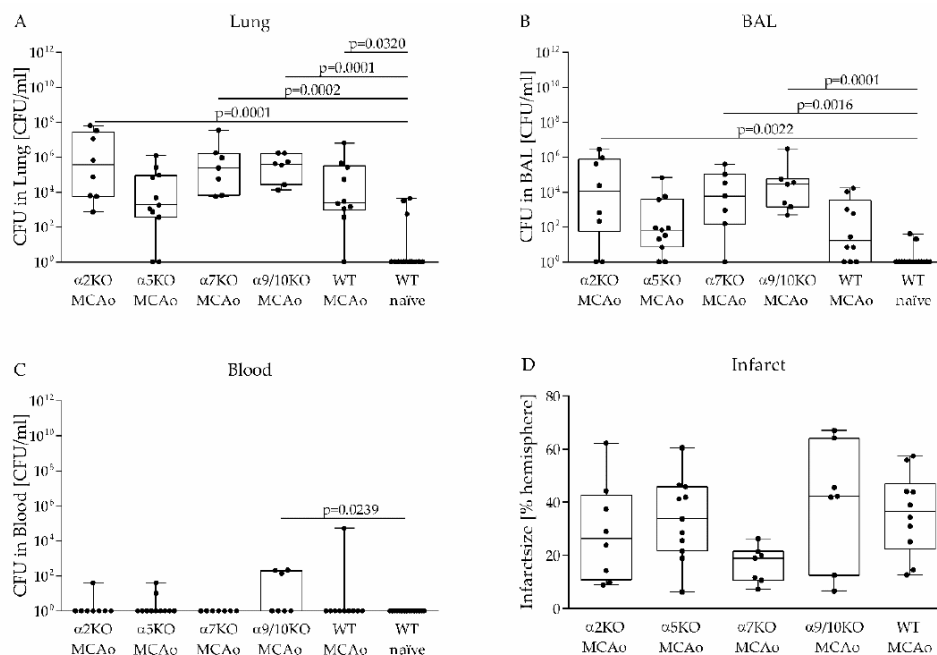


Figure 2. The susceptibility to aspiration-induced pneumococcal pneumonia after experimental stroke is not altered in nAChR knockout (KO) mice. (A–C) Untreated WT mice (naïve) or WT and nAChR KO

mice subjected to MCAo surgery were infected with *S. pneumoniae* three days after MCAo. Microbiological analysis of lung, bronchoalveolar lavage (BAL) and blood was performed one day after infection. Deficiency of $\alpha 2$, $\alpha 5$, $\alpha 7$ and $\alpha 9/10$ nAChRs had no effect on bacterial burden in lung, BAL and blood after experimental stroke. (D) nAChRs does not have an impact on infarct size assessed four days after MCAo by histological staining. Data from 6 independent experiments are shown ($n = 7$ – 15 per group) as box plots compared to WT naïve mice as a reference group for bacterial analysis and compared to WT MCAo mice as the reference group for infarct analysis using the Kruskal–Wallis test followed by Dunn’s test for multiple comparisons.

3.3. $\alpha 2$, $\alpha 5$, $\alpha 7$, $\alpha 9/10$ nAChRs Have No Effect on Immune Cell Recruitment after Stroke

To investigate the underlying mechanisms of impaired clearance of induced pneumococcal lung infection after stroke and the impact of nAChRs on immune cell recruitment, cellularity in the lung and spleen was determined by flow cytometry one day after infection, which was induced on day three after stroke onset. The number of pulmonary interstitial macrophages (IM) was significantly reduced in $\alpha 7$, $\alpha 9/10$ KO mice and WT littermates and non-significantly reduced in $\alpha 2$ and $\alpha 5$ KO mice compared to naïve WT mice one day after infection. In contrast, MCAo surgery had no effect on the number of neutrophils and lymphocytes in the lung (Figure 3A,C,E). Investigation of cellularity in the spleen revealed a significant decrease in the number of macrophages in $\alpha 9/10$ KO and WT MCAo mice, neutrophils in $\alpha 5$ KO and WT MCAo mice and lymphocytes in $\alpha 5$ KO and $\alpha 9/10$ KO mice compared to infected naïve WT mice (Figure 3B,D,F). The Kruskal–Wallis test using WT MCAo mice as the reference group showed that cell counts of leukocytes in lung and spleen were similar in $\alpha 2$ KO, $\alpha 5$ KO, $\alpha 7$ KO, $\alpha 9/10$ KO and MCAo treated WT mice one day after infection.

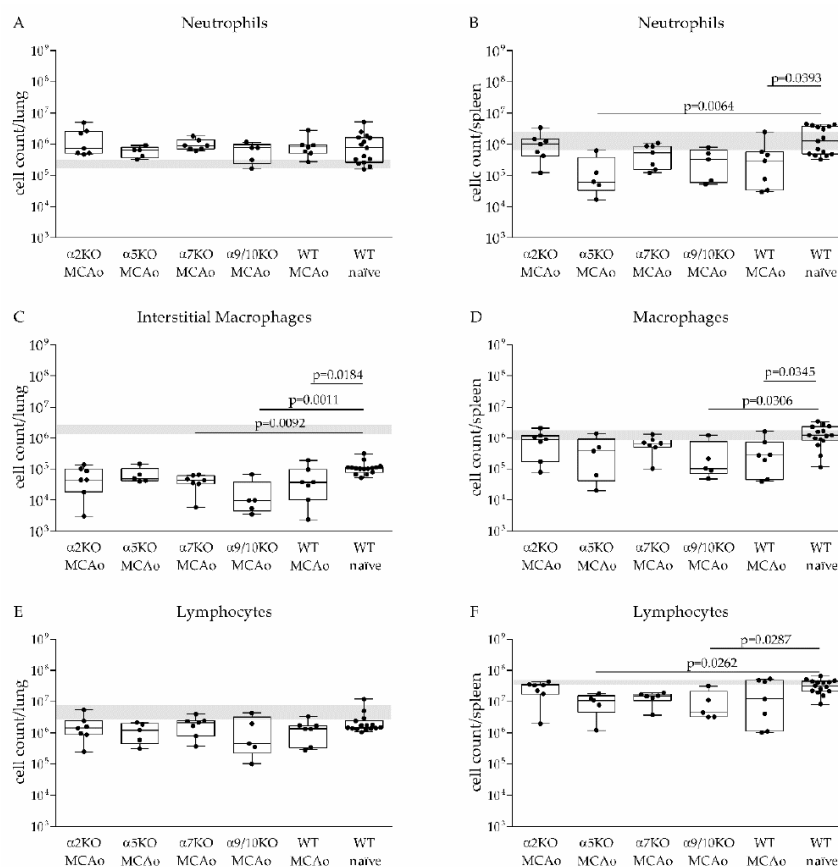


Figure 3. Impact of *S. pneumoniae* infection on cellularity in the lung and spleen of WT and nAChR KO mice. Lung and spleen cells were isolated and quantified by flow cytometry one day after infection with

S. pneumoniae. WT mice without MCAo surgery show significantly increased numbers of interstitial macrophages (IMs) (CD45/Gr1–/SiglecF–/CD11 b^{high}/F480) in the lung (C) and increased number of neutrophils (CD45+/CD11 b^{high}/Gr1^{high}), macrophages (CD45+/Gr1–/CD11 b+/CD11c–) and lymphocytes (B cells: CD45+/CD11 b–/CD19+; T cells: CD45+/CD11 b–/CD3+; NK cells: CD45+/NK1.1+/CD3–; NKT cells: CD45+/NK1.1+/CD3+) in the spleen (B,D,F) compared to MCAo mice. No differences between MCAo mice and naïve WT mice in the number of pulmonary lymphocytes and neutrophils were found (A,E). Cellularity of the lung and spleen does not differ between WT MCAo mice and nAChR KO MCAo mice. The grey area represents numbers of leukocyte subsets in healthy mice (median with IQR). Data from 6 independent experiments are shown ($n = 5–15$ per group) as box plots compared to naïve WT mice as a reference group using the Kruskal–Wallis test followed by Dunn’s test for multiple comparison.

3.4. Effect of $\alpha 2$, $\alpha 5$, $\alpha 7$, $\alpha 9/10$ nAChRs on Alveolar-Capillary Barrier and Cytokine Secretion in BAL after Stroke

To investigate the inflammatory response during pneumococcal pneumonia after stroke, MIP-1 α , IL-10, KC and TNF α concentrations in BAL were measured one day after infection. Cytokine levels tended to be lower in naïve WT mice compared to MCAo mice. MIP-1 α , KC, IL-10 and TNF α concentrations were only increased in some mice and did not differ significantly between groups. (Figure 4A–D). Regression analysis between cytokine concentrations and CFU in BAL showed positive correlation between MIP-1 α , KC and TNF α level and bacterial burden in BAL (KC: $r = 0.5186$, $p = 0.0004$; MIP-1 α : $r = 0.3391$, $p = 0.028$; TNF α : $r = 0.4492$, $p = 0.0028$) (Figure 4E).

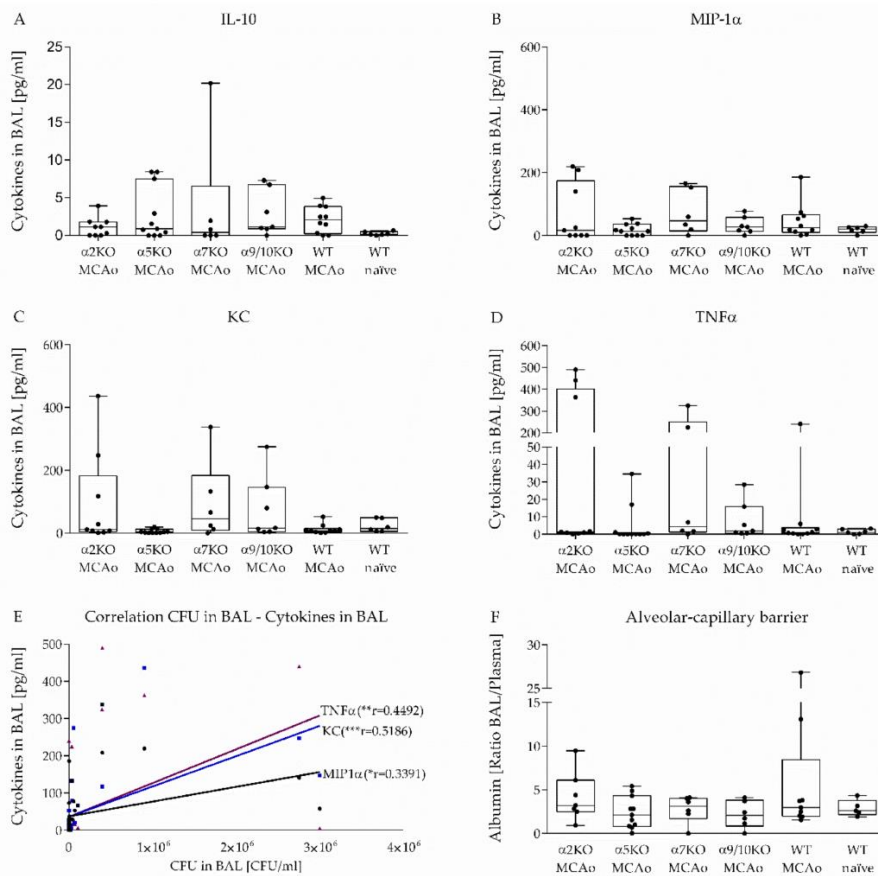


Figure 4. nAChR deficiency has no impact on the alveolar-capillary barrier or cytokine response in lung during *S. pneumoniae* infection after experimental stroke. MIP-1 α , IL-10, KC and TNF α concentrations

in BAL were measured one day after infection as described in Material and Methods. MIP-1 α , IL-10, KC and TNF α level did not differ between groups (A–D). Positive correlation between MIP-1 α , KC and TNF α concentrations and bacterial burden in BAL was found (Pearson Correlation, two tailed) (E). To investigate the effect of α 2, α 5, α 7 and α 9/10 nAChRs on the permeability of the alveolar-capillary barrier after MCAo, albumin concentrations in BAL and plasma were measured and the ratio of BAL albumin and plasma albumin was calculated. Albumin ratio is increased in several mice but does not differ between nAChR KO mice and WT mice (F). Data from 6 independent experiments are shown ($n = 5$ –11 per group) as box plots compared to naïve WT mice as a reference group using the Kruskal–Wallis test followed by Dunn’s test for multiple comparison.

To investigate changes in permeability of the alveolar-capillary barrier in the model of aspiration-induced post-stroke pneumonia, we measured albumin concentrations in BAL and plasma one day after infection. Since the plasma albumin concentrations fluctuate, the ratio of BAL albumin and plasma albumin was calculated. It has been shown that albumin ratio in healthy mice is up to three [32]. Here, we found that albumin ratio one day after pneumococcal infection was only increased in some mice and did not differ significantly between the study groups (Figure 4F).

4. Discussion

The main finding of the present study is that the depletion of single α nAChR subunits has no effect on the course of an aspiration-induced pneumococcal pneumonia after stroke. Experimental stroke results in severe pneumococcal pneumonia after induced aspiration of *S. pneumoniae* three days after stroke onset, which was harmless for naïve mice. α 2 KO, α 5 KO, α 7 KO, α 9/10 KO mice do not show significant differences in the clearance of pathogens, recruitment of immune cells in the lung or pro-inflammatory cytokine secretion compared to WT littermates following stroke.

Pneumonia is the most frequent complication of acute stroke and increases acute and long-term mortality. Besides old age, diabetes mellitus and dysphagia, immunosuppression is recognized as an important contributor for the development of spontaneous infection after stroke. Findings in animals and patients have shown that this impaired peripheral cellular immune response after central nervous system (CNS) injury is a result of activation of the hypothalamic-pituitary-adrenal (HPA) axis, the sympathetic nervous system (SNS) and the cholinergic signaling [5,6,33–37].

Overactivation of the cholinergic signaling in response to infection or inflammation-induced tissue damage is also called ‘the cholinergic anti-inflammatory pathway’ and is described as a protective mechanism that controls the inflammatory response [11]. Peripheral inflammation is sensed by vagal afferent fibers, which leads to an activation of vagal efferent fibers resulting in ACh release in the reticuloendothelial system and interacts with various muscarinic receptors (mAChRs) and nAChRs [10,11]. ACh is not only synthesized as a classical neurotransmitter by parasympathetic nerve fibers but also by non-neuronal cells including airway epithelia cells [38]. This excessive ACh release by non-neuronal and neuronal cells following nervus vagus activation suppresses via nAChRs endotoxin-inducible pro-inflammatory cytokine production, such as TNF α , IL-1 β , IL-6 and IL-18 [39].

Until now, five mAChRs subtypes (M1–M5) were found expressed by neuronal and non-neuronal cells including epithelial cells, fibroblasts, smooth muscle cells, macrophages, lymphocytes, mast cells and neutrophils. Non-neuronal mAChRs were shown to mediate inflammation and tissue remodeling in the airways [40]. In the CNS, mAChRs have been associated with the cholinergic anti-inflammatory pathway. An anti-inflammatory and anti-oxidant effect in the hippocampus of rats was demonstrated by stimulation of mAChRs with the agonist oxotremorine [41]. Furthermore, adrenocorticotropin treatment of rats diminished hemorrhagic shock by activation of the cholinergic anti-inflammatory pathway via mAChRs in the CNS [42]. Stimulation of the central localized M1 and M2 receptors resulted in a decrease of TNF α level in blood in an endotoxemia model. Interestingly, a blockade of peripheral mAChRs did not enhance TNF α secretion [43]. These data indicate that stimulation of the mAChRs in the CNS elicits—through cholinergic and potentially other neurotransmitter systems—an anti-inflammatory response in the periphery, whereas anti-inflammatory cholinergic

effects in the periphery do not appear to be mediated by mAChRs. Thus, the immunomodulatory effects of cholinergic signaling via mAChRs differ considerably from nAChRs such as $\alpha 7$, which directly exert anti-inflammatory responses in the periphery. Nonetheless, whether central mAChRs play a role in mediating stroke-induced immunosuppression remains to be elucidated.

nAChRs are composed of different combinations of α ($\alpha 2$ – $\alpha 10$) and β subunits ($\beta 2$ – $\beta 4$) and found both in the nervous system and in non-neuronal cells. Structural analysis has shown that $\alpha 10$ subunits form functional channels, when they are co-expressed with $\alpha 9$ and that $\alpha 9$ and $\alpha 7$ subunits are able to form homomeric receptors [44]. So far, especially the $\alpha 7$ nAChR was identified as an important mediator of the cholinergic anti-inflammatory pathway. Previous studies have reported that electrical stimulation of the vagus nerve inhibits the macrophage TNF α release from WT mice but not from $\alpha 7$ nAChR KO mice [9]. Furthermore, it was shown that stimulation of nAChRs with nicotine is associated with decreased neutrophils migration by inhibition of adhesion molecule expression both on the endothelial surface and neutrophils, whereas deficiency of $\alpha 7$ leads to a faster recruitment of neutrophils and decreased bacterial burden after i.p. infection with *Escherichia coli* [45,46]. In addition, $\alpha 7$ nAChR has been demonstrated to play an important role in the development of spontaneous infection after experimental stroke. Depletion of the $\alpha 7$ nAChR by using KO mice reduced bacterial burden in BAL significantly compared to WT littermates [8]. However, the role of nAChRs including the $\alpha 7$ nAChR in pulmonary infections caused by Gram-positive bacteria such as *S. pneumoniae* after stroke had not been investigated, so far.

Expression analysis has shown that $\alpha 5$, $\alpha 7$, $\alpha 9$ and $\alpha 10$ are the most frequently expressed subunits in non-neuronal cells including immune cells [12,13,44]. Besides the anti-inflammatory effect of ACh on macrophages, a cholinergic immunosuppressive effect on human DCs was observed. mRNAs encoding the $\alpha 2$, $\alpha 5$, $\alpha 6$, $\alpha 7$, $\alpha 10$ nAChRs and $\beta 2$ were found in DC isolated from C57BL/6 J mice suggesting that these subunits mediate anti-inflammatory signaling of DC [47,48]. While the $\alpha 7$ and $\alpha 9$ subunits form either homomeric or, in case of $\alpha 9$ together with the $\alpha 10$ subunit, heteromeric nAChR receptors, respectively, the $\alpha 2$ and $\alpha 5$ subunit co-assembles with other alpha ($\alpha 3$ – 5) and beta subunits ($\beta 2$, $\beta 4$) to different heteromeric receptors [44]. Findings that the $\alpha 3\beta 2$ and $\alpha 3\beta 4$ receptors can also be functional without the $\alpha 5$ subunit suggested that depletion of $\alpha 5$ has no impact on physiological processes and diseases [49]. Nevertheless, $\alpha 5$ KO mice showed reduced hyperalgesia and allodynic responses to carrageenan and complete Freund's adjuvant (CFA) injections and reduced sensitivity to nicotine-induced seizures and hypolocomotion [23,50,51]. Furthermore, it was shown that the $\alpha 5$ subunit influences the affinity and sensitivity of agonists and antagonists. A 50-fold increased acetylcholine sensitivity was detected if the $\alpha 5$ subunit incorporated with $\alpha 3\beta 2$ [49,52]. Depletion of the $\alpha 2$ subunit resulted in major changes in immune-adipose communication including compromised adaptation to chronic cold challenge, dysregulation of whole-body metabolism and exacerbates diet-induced obesity [53]. In this study, we found expression of $\alpha 2$, $\alpha 5$, $\alpha 7$, $\alpha 9$ and $\alpha 10$ subunits in lungs of naïve mice and suspected that depletion of these subunits may modify the immunomodulatory effects of cholinergic signaling after stroke.

In our experimental stroke model, we have previously shown that signs of immunosuppression in blood, spleen and thymus started as early as 12 h after MCAo with a maximum at day three. Already after five to seven days, lymphocyte numbers and pro-inflammatory cytokines in blood started to recover. Correspondingly, spontaneous bacterial infections in mice were observed between days three and five after experimental stroke [54]. This is in accordance with the clinical observation that the risk to develop infections in stroke patients is highest within two to five days after stroke onset [55]. Therefore, in a translational approach we choose to infect MCAo mice before day five, in the phase of maximum immunosuppression. This time window has been used in aspiration-induced post-stroke pneumonia models using a low number of *S. pneumoniae* capable of inducing severe pneumonia with high bacterial burden in lung of MCAo but not sham animals [19]. Moreover, bacterial burden in lung was lower at day two compared to day one after inoculation [56]. Since naïve mice require usually 24 h

to clear induced infection, we used this time point to assess immune parameters and bacterial burden after inoculation of *S. pneumoniae*.

In the present study, we have demonstrated that induced aspiration with *S. pneumoniae* by applying a bacterial suspension at the tracheal bifurcation leads to severe pneumonia after experimental stroke but remains harmless in naïve mice. Microbiological analysis demonstrated significantly lower bacterial burden in WT naïve mice compared to stroked animals (Figure 2A). Analysis of the lung showed that out of 15 WT naïve mice, 12 mice were able to completely clear inoculated bacteria within 24 h compared to only 3 out of 43 stroked mice (Figure 2A). Microbiological analysis of BAL obtained from the same animals showed similar results (Figure 2B). Moreover, all naïve mice remained symptomless in contrast to the MCAo mice suggesting near complete bacterial clearance. This finding corroborates previous findings that stroke impairs the antibacterial defense [7,8,19–21,34,54]. *S. pneumoniae* infection in healthy mice leads to neutrophil recruitment in BAL starting 12 h after infection. A reduction of neutrophil numbers was observed 60 h after infection due to cell death [57,58]. Investigation of the lung showed up to 10^6 neutrophils/mL 24 h after infection, whereas 10^4 neutrophils/mL were reported in the lung of uninfected mice [59]. In the present study, we could also observe increased numbers of neutrophils in the lung (up to 10^6 neutrophils/lung) of naïve WT mice and MCAo mice. We found no differences between stroke and naïve mice in terms of neutrophil numbers in the lung at day one after infection. One explanation could be a faster kinetic of neutrophil recruitment in naïve animals with already decreasing numbers of neutrophils in the lung one day after bacterial inoculation due to clearance of bacteria. Therefore, a diminished neutrophil recruitment after MCAo would not have been detected with our experimental design. Nevertheless, since we also not observed differences in lung neutrophil counts between WT and nAChR KO mice after stroke, the nAChR subunit status does not seem to have a major impact on neutrophil recruitment into the lung due to *S. pneumoniae* infection after stroke.

Stroke has been demonstrated to induce a long-lasting lymphopenia in blood and spleen starting very early after stroke onset, which is a hallmark of stroke-induced immune depression [54]. In addition, investigations of the lung immunity after stroke have shown a significant reduction of CD4+, CD8+ and B cells 24 h and 72 h after MCAo [60]. Here, we did not observe a significant difference in lung lymphocyte counts between naïve WT and MCAo mice. Investigation of the spleen showed a significant reduction of lymphocyte numbers only in MCAo treated $\alpha 5$ and $\alpha 9/10$ nAChR KO mice compared to naïve WT mice, whereas MCAo treated $\alpha 2$, $\alpha 7$ nAChR KO mice and WT littermates showed no differences compared to naïve WT mice. Notably, we found that infected WT naïve mice also showed diminished lymphocyte counts in the lung compared to normal lymphocyte numbers in untreated WT mice. Clinical data from patients with pneumococcal infections have shown that the acute phase of infection was associated with a diminished number of lymphocytes in blood. Further analysis demonstrated increased apoptosis among lymphocytes [61]. This is in line with experimental data showing increased lymphocyte apoptosis in a mouse model of pneumococcal pneumonia [62]. In addition, *S. pneumoniae* D39 strain has been shown to mediate activation-dependent death in human lymphocytes [63]. Nevertheless, it was reported that the number of CD4+ cells reached normal levels in blood one week after infections suggesting trafficking of CD4+ cells instead of inflow of de novo-generated cells after apoptosis-induced lymphopenia. Therefore, it was assumed that the reduced number of lymphocytes in blood is also caused by migration of lymphocytes to the site of inflammation [61]. This was supported by experiment findings in mice showing that pneumococcal infection increased the number of lymphocytes in BAL compared to uninfected mice [64]. These data suggest that in the present study naïve WT mice developed lymphopenia in spleen and lung due to pneumococcal infection, and consequently, the number of lymphocytes differs only marginally between MCAo mice and naïve WT mice.

Besides alveolar macrophages, a smaller subset of interstitial macrophages (IMs) is found in the lung. While generally IMs are believed to have homeostatic and immunomodulatory functions, these cells may also play an important role in host pathogen defense. Experiments in mice have shown

that pulmonary infection induces accumulation of IMs in the lung. In addition, depletion of IMs results in increased bacterial burden after infection suggesting that these cells are essential for controlling pathogens in the lung [65]. Here, we observed a diminished number of IMs in MCAo mice compared to naïve WT mice. These data suggest that the decreased number of IMs in the lung in MCAo mice may contribute to impaired clearance of *S. pneumoniae*.

It is well known that several pneumococcal factors such as opaque variants might disrupt epithelial barriers resulting in a transition of bacteria from the mucosal surface to the bloodstream [66]. Findings in animals and patients have demonstrated that alveolar-capillary barrier disruption leads to increased albumin concentrations in BAL and is associated with neutrophil recruitment into the lung [67–69]. Experiments in mice have shown that infection with a lethal dose of *S. pneumoniae* D39 leads to increased albumin level in BAL due to the disruption of the alveolar barrier [70,71]. In healthy mice, the BAL/plasma albumin ratio is 1–3 [32]. Here, we found an increased albumin ratio in several mice, but no differences between groups of various nAChR KO mice, WT littermates and naïve WT mice. Possibly the low impact of pneumococcal infection on the permeability of the alveolar-capillary barrier can be explained by the use of a low infection dose in our model compared to the lethal infection dose in the acute pneumococcal pneumonia mouse model. Neutrophils have been demonstrated to mediate increased epithelial permeability in the lung during pulmonary infection [71,72]. Since nAChR depletion has no effect on neutrophil recruitment into the lung during pneumococcal infection, nAChRs also do not influence the alveolar-capillary barrier 24 h after infection.

In addition, we have investigated the level of pro-inflammatory cytokines in BAL fluid. WT mice without MCAo surgery were able to clear the induced infection within 24 h and did not show elevated levels of pro-inflammatory cytokines in BAL fluid. In contrast, persistent bacterial infection in MCAo mice leads to continuous cytokine secretion, which correlated with bacterial burden in BAL fluid. Experiments in mice have shown that MIP-1 α , KC and TNF α level in BAL fluid dramatically increase in the acute phase of pneumococcal pneumonia. [57,59]. In the present study, we could observe that only several MCAo mice were able to induce the pro-inflammatory cytokine response in BAL during the acute phase of pneumococcal infection after stroke. Previous studies have shown that TNF α , KC and MIP-1 α secretion is regulated by the cholinergic anti-inflammatory pathway [39,73,74]. These data indicate that stroke impairs pro-inflammatory cytokine secretion during pneumococcal infection contributing to impaired pathogen clearance.

Nevertheless, we found no significant differences between nAChR KO mice and WT mice concerning bacterial burden, cellularity of the lung and spleen, permeability of the alveolar-capillary barrier and cytokine secretion in BAL fluid. These results suggest that various nAChRs including the $\alpha 7$ nAChR do not play a role in increased susceptibility to pneumococcal lung infection after stroke. The apparent discrepancy between earlier studies [8,9,45,46] and the current study concerning the anti-inflammatory effect mediated by the $\alpha 7$ nAChR may be caused by the usage of different types of bacteria in these models. So far, the protective effect of $\alpha 7$ nAChR was solely detected in conjunction with Gram-negative infections. In a mouse model of spontaneous infections after stroke, it was shown that >95% of bacteria cultures from peripheral blood and lung were *E. coli* and depletion of $\alpha 7$ nAChR resulted in diminished bacterial burden in BAL [8,54]. Experiments in mice have shown that the $\alpha 7$ nAChR also mediates impaired immunity in an induced infection with Gram-negative *Pseudomonas aeruginosa* after stroke. $\alpha 7$ nAChR depletion attenuated the effect of stroke on lung injury due to *P. aeruginosa* infection. In contrast, blockade of β -adrenergic receptors by propranolol increased lung injury [75]. Interestingly, propranolol treatment of MCAo mice prevented pulmonary infection with Gram-positive bacteria, such as *S. pneumoniae* [19] and *Listeria monocytogenes* [76]. Many studies investigated the cholinergic anti-inflammatory pathway in the context of uncontrolled inflammatory host response such as sepsis. Findings in animals have demonstrated that stimulation of the cholinergic anti-inflammatory pathway reduced inflammation and mortality in sepsis-induced lung injury due to pulmonary *E. coli* infection and enhanced survival in oral *Salmonella typhimurium* infection [77,78]. Interestingly, nonselective stimulation of nAChRs had no effect on lung inflammation in induced

pneumococcal pneumonia with bacteremia [79]. These data suggest that cholinergic activation due to CNS injury may preferentially impair immunity against Gram-negative bacteria. However, further comparative studies including infection models with Gram-negative bacteria and other Gram-positive bacterial strains after stroke are required to further elucidate the immunomodulatory role in cholinergic signaling during infections with different types of bacteria.

5. Conclusions

In summary, our findings show that stroke results in impaired pulmonary immunity against *S. pneumoniae* resulting in reduced bacterial clearance and prolonged infection. Blocking of cholinergic signaling by depletion of various nAChRs subunits does not enhance antibacterial immune response suggesting that cholinergic pathways, at least not mediated by $\alpha 2$ nAChR, $\alpha 5$ nAChR, $\alpha 7$ nAChR, $\alpha 9/10$ nAChR subunits, does not play a role in impaired immunity against *S. pneumoniae* after stroke. In this respect, it would be interesting to study the impact of non- $\alpha 7$ nAChRs on spontaneous infections or induced-aspiration infections with Gram-negative bacteria, such as *Pseudomonas aeruginosa*, *Klebsiella pneumoniae*, *Enterobacter*, *Escherichia Coli* after stroke.

Author Contributions: Conceptualization, C.M., A.M. and C.D.; methodology, S.J., C.D., D.B. and K.W.; formal analysis, S.J.; investigation, S.J.; writing—original draft preparation, S.J.; writing—review and editing, C.M., A.M., S.J. and C.D.; visualization, D.B., L.W., C.D., K.W., A.M. and C.M.; supervision, C.M. and A.M.; project administration, C.M. and A.M.; funding acquisition, C.M. and A.M. All authors have read and agreed to the published version of the manuscript.

Funding: This research was funded by the German Research Foundation (SFB-TR84), Einstein Foundation and Leducq Foundation.

Acknowledgments: We thank Sabine Kolodziej, Claudia Muselmann-Genschow and Susanne Metzkwow for excellent technical assistance, Désirée Kunkel for support with flow cytometry. We acknowledge support from the German Research Foundation (DFG) and the Open Access Publication Funds of Charité-Universitätsmedizin Berlin.

Conflicts of Interest: The authors have declared that no conflict of interest exists.

References

1. Davenport, R.J.; Dennis, M.S.; Wellwood, I.; Warlow, C.P. Complications after acute stroke. *Stroke* **1996**, *27*, 415–420. [[CrossRef](#)] [[PubMed](#)]
2. Johnston, K.C.; Li, J.Y.; Lyden, P.D.; Hanson, S.K.; Feasby, T.E.; Adams, R.J.; Faught, R.E., Jr.; Haley, E.C., Jr. Medical and neurological complications of ischemic stroke: Experience from the RANTTAS trial. RANTTAS Investigators. *Stroke* **1998**, *29*, 447–453. [[CrossRef](#)] [[PubMed](#)]
3. Langhorne, P.; Stott, D.J.; Robertson, L.; MacDonald, J.; Jones, L.; McAlpine, C.; Dick, F.; Taylor, G.S.; Murray, G. Medical complications after stroke: A multicenter study. *Stroke* **2000**, *31*, 1223–1229. [[CrossRef](#)] [[PubMed](#)]
4. Weimar, C.; Roth, M.P.; Zillesen, G.; Glahn, J.; Wimmer, M.L.; Busse, O.; Haberl, R.L.; Diener, H.C.; German Stroke Data Bank Collaborators O. Complications following acute ischemic stroke. *Eur. Neurol.* **2002**, *48*, 133–140. [[CrossRef](#)]
5. Meisel, C.; Schwab, J.M.; Prass, K.; Meisel, A.; Dirnagl, U. Central nervous system injury-induced immune deficiency syndrome. *Nat. Rev. Neurosci.* **2005**, *6*, 775–786. [[CrossRef](#)]
6. Sellars, C.; Bowie, L.; Bagg, J.; Sweeney, M.P.; Miller, H.; Tilston, J.; Langhorne, P.; Stott David, J. Risk Factors for Chest Infection in Acute Stroke. *Stroke* **2007**, *38*, 2284–2291. [[CrossRef](#)]
7. Hoffmann, S.; Harms, H.; Ulm, L.; Nabavi, D.G.; Mackert, B.-M.; Schmehl, I.; Jungehulsing, G.J.; Montaner, J.; Bustamante, A.; Hermans, M.; et al. Stroke-induced immunodepression and dysphagia independently predict stroke-associated pneumonia—The PREDICT study. *J. Cereb. Blood Flow Metab.* **2017**, *37*, 3671–3682. [[CrossRef](#)]
8. Engel, O.; Akyuz, L.; da Costa Goncalves, A.C.; Winek, K.; Dames, C.; Thielke, M.; Herold, S.; Bottcher, C.; Priller, J.; Volk, H.D.; et al. Cholinergic Pathway Suppresses Pulmonary Innate Immunity Facilitating Pneumonia after Stroke. *Stroke* **2015**, *46*, 3232–3240. [[CrossRef](#)]

9. Wang, H.; Yu, M.; Ochani, M.; Amella, C.A.; Tanovic, M.; Susarla, S.; Li, J.H.; Wang, H.; Yang, H.; Ulloa, L.; et al. Nicotinic acetylcholine receptor $\alpha 7$ subunit is an essential regulator of inflammation. *Nature* **2003**, *421*, 384–388. [[CrossRef](#)]
10. Pavlov, V.A.; Wang, H.; Czura, C.J.; Friedman, S.G.; Tracey, K.J. The cholinergic anti-inflammatory pathway: A missing link in neuroimmunomodulation. *Mol. Med.* **2003**, *9*, 125–134. [[CrossRef](#)]
11. Tracey, K.J. The inflammatory reflex. *Nature* **2002**, *420*, 853–859. [[CrossRef](#)] [[PubMed](#)]
12. Fujii, T.; Mashimo, M.; Moriwaki, Y.; Misawa, H.; Ono, S.; Horiguchi, K.; Kawashima, K. Physiological functions of the cholinergic system in immune cells. *J. Pharmacol. Sci.* **2017**, *134*, 1–21. [[CrossRef](#)] [[PubMed](#)]
13. Qian, J.; Galitovskiy, V.; Chernyavsky, A.I.; Marchenko, S.; Grando, S.A. Plasticity of the murine spleen T-cell cholinergic receptors and their role in in vitro differentiation of naïve CD4 T cells toward the Th1, Th2 and Th17 lineages. *Genes Immun.* **2011**, *12*, 222–230. [[CrossRef](#)] [[PubMed](#)]
14. Papke, R.L.; Lindstrom, J.M. Nicotinic acetylcholine receptors: Conventional and unconventional ligands and signaling. *Neuropharmacology* **2020**, *168*, 108021. [[CrossRef](#)] [[PubMed](#)]
15. Perry, L.; Love, C.P. Screening for dysphagia and aspiration in acute stroke: A systematic review. *Dysphagia* **2001**, *16*, 7–18. [[CrossRef](#)]
16. Kollef, M.H.; Shorr, A.; Tabak, Y.P.; Gupta, V.; Liu, L.Z.; Johannes, R.S. Epidemiology and outcomes of health-care-associated pneumonia: Results from a large US database of culture-positive pneumonia. *Chest* **2005**, *128*, 3854–3862. [[CrossRef](#)]
17. Trouillet, J.L.; Chastre, J.; Vuagnat, A.; Joly-Guillou, M.L.; Combaux, D.; Dombret, M.C.; Gibert, C. Ventilator-associated pneumonia caused by potentially drug-resistant bacteria. *Am. J. Respir. Crit. Care Med.* **1998**, *157*, 531–539. [[CrossRef](#)]
18. Kishore Amit, K.; Vail, A.; Jeans Adam, R.; Chamorro, A.; Di Napoli, M.; Kalra, L.; Langhorne, P.; Roffe, C.; Westendorp, W.; Nederkoorn Paul, J.; et al. Microbiological Etiologies of Pneumonia Complicating Stroke. *Stroke* **2018**, *49*, 1602–1609. [[CrossRef](#)]
19. Prass, K.; Braun Johann, S.; Dirnagl, U.; Meisel, C.; Meisel, A. Stroke Propagates Bacterial Aspiration to Pneumonia in a Model of Cerebral Ischemia. *Stroke* **2006**, *37*, 2607–2612. [[CrossRef](#)]
20. McCulloch, L.; Smith, C.J.; McColl, B.W. Adrenergic-mediated loss of splenic marginal zone B cells contributes to infection susceptibility after stroke. *Nat. Commun.* **2017**, *8*, 15051. [[CrossRef](#)]
21. Wong, C.H.; Jenne, C.N.; Lee, W.Y.; Léger, C.; Kubes, P. Functional innervation of hepatic iNKT cells is immunosuppressive following stroke. *Science* **2011**, *334*, 101–105. [[CrossRef](#)] [[PubMed](#)]
22. Lotfipour, S.; Byun, J.S.; Leach, P.; Fowler, C.D.; Murphy, N.P.; Kenny, P.J.; Gould, T.J.; Boulter, J. Targeted deletion of the mouse $\alpha 2$ nicotinic acetylcholine receptor subunit gene (Chrna2) potentiates nicotine-modulated behaviors. *J. Neurosci.* **2013**, *33*, 7728–7741. [[CrossRef](#)]
23. Salas, R.; Orr-Urtreger, A.; Broide, R.S.; Beaudet, A.; Paylor, R.; De Biasi, M. The Nicotinic Acetylcholine Receptor Subunit $\alpha 5$ Mediates Short-Term Effects of Nicotine in Vivo. *Mol. Pharmacol.* **2003**, *63*, 1059. [[CrossRef](#)]
24. Orr-Urtreger, A.; Göldner, F.M.; Saeki, M.; Lorenzo, I.; Goldberg, L.; De Biasi, M.; Dani, J.A.; Patrick, J.W.; Beaudet, A.L. Mice Deficient in the $\alpha 7$ Neuronal Nicotinic Acetylcholine Receptor Lack α -Bungarotoxin Binding Sites and Hippocampal Fast Nicotinic Currents. *J. Neurosci.* **1997**, *17*, 9165. [[CrossRef](#)] [[PubMed](#)]
25. Vetter, D.E.; Katz, E.; Maison, S.F.; Taranda, J.; Turcan, S.; Ballesterio, J.; Liberman, M.C.; Elgoyhen, A.B.; Boulter, J. The $\alpha 10$ nicotinic acetylcholine receptor subunit is required for normal synaptic function and integrity of the olivocochlear system. *Proc. Natl. Acad. Sci. USA* **2007**, *104*, 20594. [[CrossRef](#)] [[PubMed](#)]
26. Vetter, D.E.; Liberman, M.C.; Mann, J.; Barhanin, J.; Boulter, J.; Brown, M.C.; Saffiote-Kolman, J.; Heinemann, S.F.; Elgoyhen, A.B. Role of $\alpha 9$ Nicotinic ACh Receptor Subunits in the Development and Function of Cochlear Efferent Innervation. *Neuron* **1999**, *23*, 93–103. [[CrossRef](#)]
27. Engel, O.; Kolodziej, S.; Dirnagl, U.; Prinz, V. Modeling stroke in mice-middle cerebral artery occlusion with the filament model. *J. Vis. Exp.* **2011**. [[CrossRef](#)]
28. Jeong, D.-G.; Jeong, E.-S.; Seo, J.-H.; Heo, S.-H.; Choi, Y.-K. Difference in Resistance to Streptococcus pneumoniae Infection in Mice. *Lab. Anim. Res.* **2011**, *27*, 91–98. [[CrossRef](#)]
29. Schulte-Herbrüggen, O.; Klehmet, J.; Quarcoo, D.; Meisel, C.; Meisel, A. Mouse strains differ in their susceptibility to poststroke infections. *Neuroimmunomodulation* **2006**, *13*, 13–18. [[CrossRef](#)]

30. Dames, C.; Akyüz, L.; Reppe, K.; Tabeling, C.; Dietert, K.; Kershaw, O.; Gruber, A.D.; Meisel, C.; Meisel, A.; Witzenrath, M.; et al. Miniaturized bronchoscopy enables unilateral investigation, application, and sampling in mice. *Am. J. Respir. Cell Mol. Biol.* **2014**, *51*, 730–737. [[CrossRef](#)]
31. Sun, F.; Xiao, G.; Qu, Z. Murine Bronchoalveolar Lavage. *Bio-protocol* **2017**, *7*, e2287. [[CrossRef](#)] [[PubMed](#)]
32. Müller-Redetzky, H.C.; Felten, M.; Hellwig, K.; Wienhold, S.-M.; Naujoks, J.; Opitz, B.; Kershaw, O.; Gruber, A.D.; Suttorp, N.; Witzenrath, M. Increasing the inspiratory time and I:E ratio during mechanical ventilation aggravates ventilator-induced lung injury in mice. *Crit. Care* **2015**, *19*, 23. [[CrossRef](#)] [[PubMed](#)]
33. Huang, Y.-Y.; Li, X.; Li, X.; Sheng, Y.-Y.; Zhuang, P.-W.; Zhang, Y.-J. Neuroimmune crosstalk in central nervous system injury-induced infection and pharmacological intervention. *Brain Res. Bull.* **2019**, *153*, 232–238. [[CrossRef](#)] [[PubMed](#)]
34. Shi, K.; Wood, K.; Shi, F.-D.; Wang, X.; Liu, Q. Stroke-induced immunosuppression and poststroke infection. *Stroke Vasc. Neurol.* **2018**, *3*, 34. [[CrossRef](#)]
35. El Husseini, N.; Laskowitz, D.T. The role of neuroendocrine pathways in prognosis after stroke. *Expert Rev. Neur.* **2014**, *14*, 217–232. [[CrossRef](#)]
36. Dirnagl, U.; Klehmet, J.; Braun Johann, S.; Harms, H.; Meisel, C.; Ziemssen, T.; Prass, K.; Meisel, A. Stroke-Induced Immunodepression. *Stroke* **2007**, *38*, 770–773. [[CrossRef](#)]
37. Chamorro, Á.; Meisel, A.; Planas, A.M.; Urra, X.; van de Beek, D.; Veltkamp, R. The immunology of acute stroke. *Nat. Rev. Neurol.* **2012**, *8*, 401. [[CrossRef](#)]
38. Kummer, W.; Lips, K.S.; Pfeil, U. The epithelial cholinergic system of the airways. *Histochem. Cell Biol.* **2008**, *130*, 219. [[CrossRef](#)]
39. Borovikova, L.V.; Ivanova, S.; Zhang, M.; Yang, H.; Botchkina, G.I.; Watkins, L.R.; Wang, H.; Abumrad, N.; Eaton, J.W.; Tracey, K.J. Vagus nerve stimulation attenuates the systemic inflammatory response to endotoxin. *Nature* **2000**, *405*, 458–462. [[CrossRef](#)]
40. Koarai, A.; Ichinose, M. Possible involvement of acetylcholine-mediated inflammation in airway diseases. *Allergol. Int.* **2018**, *67*, 460–466. [[CrossRef](#)]
41. Frinchi, M.; Nuzzo, D.; Scaduto, P.; Di Carlo, M.; Massenti, M.F.; Belluardo, N.; Mudò, G. Anti-inflammatory and antioxidant effects of muscarinic acetylcholine receptor (mAChR) activation in the rat hippocampus. *Sci. Rep.* **2019**, *9*, 14233. [[CrossRef](#)] [[PubMed](#)]
42. Guarini, S.; Cainazzo, M.M.; Giuliani, D.; Mioni, C.; Altavilla, D.; Marini, H.; Bigiani, A.; Ghiaroni, V.; Passaniti, M.; Leone, S.; et al. Adrenocorticotropin reverses hemorrhagic shock in anesthetized rats through the rapid activation of a vagal anti-inflammatory pathway. *Cardiovasc. Res.* **2004**, *63*, 357–365. [[CrossRef](#)] [[PubMed](#)]
43. Pavlov, V.A.; Ochani, M.; Gallowitsch-Puerta, M.; Ochani, K.; Huston, J.M.; Czura, C.J.; Al-Abed, Y.; Tracey, K.J. Central muscarinic cholinergic regulation of the systemic inflammatory response during endotoxemia. *Proc. Natl. Acad. Sci. USA* **2006**, *103*, 5219–5223. [[CrossRef](#)] [[PubMed](#)]
44. Zoli, M.; Pucci, S.; Vilella, A.; Gotti, C. Neuronal and Extraneuronal Nicotinic Acetylcholine Receptors. *Curr. Neuropharmacol.* **2018**, *16*, 338–349. [[CrossRef](#)] [[PubMed](#)]
45. Giebelen, I.A.J.; Le Moine, A.; van den Pangaart, P.S.; Sadis, C.; Goldman, M.; Florquin, S.; van der Poll, T. Deficiency of $\alpha 7$ Cholinergic Receptors Facilitates Bacterial Clearance in Escherichia coli Peritonitis. *J. Infect. Dis.* **2008**, *198*, 750–757. [[CrossRef](#)]
46. Speer, P.; Zhang, Y.; Gu, Y.; Lucas, M.J.; Wang, Y. Effects of nicotine on intercellular adhesion molecule expression in endothelial cells and integrin expression in neutrophils in vitro. *Am. J. Obstet. Gynecol.* **2002**, *186*, 551–556. [[CrossRef](#)]
47. Kawashima, K.; Yoshikawa, K.; Fujii, Y.X.; Moriwaki, Y.; Misawa, H. Expression and function of genes encoding cholinergic components in murine immune cells. *Life Sci.* **2007**, *80*, 2314–2319. [[CrossRef](#)]
48. Nouri-Shirazi, M.; Guinet, E. Evidence for the immunosuppressive role of nicotine on human dendritic cell functions. *Immunology* **2003**, *109*, 365–373. [[CrossRef](#)]
49. Wang, F.; Gerzanich, V.; Wells, G.B.; Anand, R.; Peng, X.; Keyser, K.; Lindstrom, J. Assembly of human neuronal nicotinic receptor $\alpha 5$ subunits with $\alpha 3$, $\beta 2$, and $\beta 4$ subunits. *J. Biol. Chem.* **1996**, *271*, 17656–17665. [[CrossRef](#)]
50. Kedmi, M.; Beaudet, A.L.; Orr-Urtreger, A. Mice lacking neuronal nicotinic acetylcholine receptor $\beta 4$ -subunit and mice lacking both $\alpha 5$ - and $\beta 4$ -subunits are highly resistant to nicotine-induced seizures. *Physiol. Genom.* **2004**, *17*, 221–229. [[CrossRef](#)]

51. Bagdas, D.; AlSharari, S.D.; Freitas, K.; Tracy, M.; Damaj, M.I. The role of alpha5 nicotinic acetylcholine receptors in mouse models of chronic inflammatory and neuropathic pain. *Biochem. Pharmacol.* **2015**, *97*, 590–600. [[CrossRef](#)] [[PubMed](#)]
52. Wang, N.; Orr-Urtreger, A.; Chapman, J.; Rabinowitz, R.; Nachman, R.; Korczyn, A.D. Autonomic function in mice lacking alpha5 neuronal nicotinic acetylcholine receptor subunit. *J. Physiol.* **2002**, *542*, 347–354. [[CrossRef](#)] [[PubMed](#)]
53. Jun, H.; Yu, H.; Gong, J.; Jiang, J.; Qiao, X.; Perkey, E.; Kim, D.-i.; Emont, M.P.; Zestos, A.G.; Cho, J.-S.; et al. An immune-beige adipocyte communication via nicotinic acetylcholine receptor signaling. *Nat. Med.* **2018**, *24*, 814–822. [[CrossRef](#)] [[PubMed](#)]
54. Prass, K.; Meisel, C.; Höflich, C.; Braun, J.; Halle, E.; Wolf, T.; Ruscher, K.; Victorov, I.V.; Priller, J.; Dirnagl, U.; et al. Stroke-induced Immunodeficiency Promotes Spontaneous Bacterial Infections and Is Mediated by Sympathetic Activation Reversal by Poststroke T Helper Cell Type 1–like Immunostimulation. *J. Exp. Med.* **2003**, *198*, 725. [[CrossRef](#)] [[PubMed](#)]
55. Kishore, A.K.; Jeans, A.R.; Garau, J.; Bustamante, A.; Kalra, L.; Langhorne, P.; Chamorro, A.; Urra, X.; Katan, M.; Napoli, M.D.; et al. Antibiotic treatment for pneumonia complicating stroke: Recommendations from the pneumonia in stroke consensus (PISCES) group. *Eur. Stroke J.* **2019**, *4*, 318–328. [[CrossRef](#)] [[PubMed](#)]
56. Mracsko, E.; Stegemann-Koniszewski, S.; Na, S.Y.; Dalpke, A.; Bruder, D.; Lasitschka, F.; Veltkamp, R. A Mouse Model of Post-Stroke Pneumonia Induced by Intra-Tracheal Inoculation with *Streptococcus pneumoniae*. *Cerebrovasc. Dis.* **2017**, *43*, 99–109. [[CrossRef](#)] [[PubMed](#)]
57. Fillion, I.; Ouellet, N.; Simard, M.; Bergeron, Y.; Sato, S.; Bergeron, M.G. Role of chemokines and formyl peptides in pneumococcal pneumonia-induced monocyte/macrophage recruitment. *J. Immunol.* **2001**, *166*, 7353–7361. [[CrossRef](#)]
58. Haste, L.; Hulland, K.; Bolton, S.; Yesilkaya, H.; McKechnie, K.; Andrew, P.W. Development and Characterization of a Long-Term Murine Model of *Streptococcus pneumoniae* Infection of the Lower Airways. *Infect. Immun.* **2014**, *82*, 3289. [[CrossRef](#)]
59. Peñaloza, H.F.; Nieto, P.A.; Muñoz-Durango, N.; Salazar-Echegarai, F.J.; Torres, J.; Parga, M.J.; Alvarez-Lobos, M.; Riedel, C.A.; Kalergis, A.M.; Bueno, S.M. Interleukin-10 plays a key role in the modulation of neutrophils recruitment and lung inflammation during infection by *Streptococcus pneumoniae*. *Immunology* **2015**, *146*, 100–112. [[CrossRef](#)]
60. Farris, B.Y.; Monaghan, K.L.; Zheng, W.; Amend, C.D.; Hu, H.; Ammer, A.G.; Coad, J.E.; Ren, X.; Wan, E.C.K. Ischemic stroke alters immune cell niche and chemokine profile in mice independent of spontaneous bacterial infection. *Immun. Inflamm. Dis.* **2019**, *7*, 326–341. [[CrossRef](#)]
61. Kemp, K.; Bruunsgaard, H.; Skinhøj, P.; Klarlund Pedersen, B. Pneumococcal infections in humans are associated with increased apoptosis and trafficking of type 1 cytokine-producing T cells. *Infect. Immun.* **2002**, *70*, 5019–5025. [[CrossRef](#)] [[PubMed](#)]
62. Schreiber, T.; Swanson, P.E.; Chang, K.C.; Davis, C.C.; Dunne, W.M.; Karl, I.E.; Reinhart, K.; Hotchkiss, R.S. Both gram-negative and gram-positive experimental pneumonia induce profound lymphocyte but not respiratory epithelial cell apoptosis. *Shock* **2006**, *26*. [[CrossRef](#)] [[PubMed](#)]
63. Grayson, K.M.; Blevins, L.K.; Oliver, M.B.; Ornelles, D.A.; Swords, W.E.; Alexander-Miller, M.A. Activation-dependent modulation of *Streptococcus pneumoniae*-mediated death in human lymphocytes. *Pathog. Dis.* **2017**, *75*. [[CrossRef](#)] [[PubMed](#)]
64. McKenzie, C.W.; Klonoski, J.M.; Maier, T.; Trujillo, G.; Vitiello, P.F.; Huber, V.C.; Lee, L. Enhanced response to pulmonary *Streptococcus pneumoniae* infection is associated with primary ciliary dyskinesia in mice lacking *Pcdp1* and *Spf2*. *Cilia* **2013**, *2*, 18. [[CrossRef](#)] [[PubMed](#)]
65. Huang, L.; Nazarova, E.V.; Tan, S.; Liu, Y.; Russell, D.G. Growth of *Mycobacterium tuberculosis* in vivo segregates with host macrophage metabolism and ontogeny. *J. Exp. Med.* **2018**, *215*, 1135–1152. [[CrossRef](#)] [[PubMed](#)]
66. Kadioglu, A.; Weiser, J.N.; Paton, J.C.; Andrew, P.W. The role of *Streptococcus pneumoniae* virulence factors in host respiratory colonization and disease. *Nat. Rev. Microbiol.* **2008**, *6*, 288. [[CrossRef](#)]
67. Chignard, M.; Balloy, V. Neutrophil recruitment and increased permeability during acute lung injury induced by lipopolysaccharide. *Am. J. Physiol. Lung Cell. Mol. Physiol.* **2000**, *279*, L1083–L1090. [[CrossRef](#)]

68. O'Grady, N.P.; Preas, H.L.; Pugin, J.; Fiuza, C.; Tropea, M.; Reda, D.; Banks, S.M.; Suffredini, A.F. Local Inflammatory Responses following Bronchial Endotoxin Instillation in Humans. *Am. J. Respir. Crit. Care Med.* **2001**, *163*, 1591–1598. [[CrossRef](#)]
69. Speyer, C.L.; Neff, T.A.; Warner, R.L.; Guo, R.-F.; Sarma, J.V.; Riedemann, N.C.; Murphy, M.E.; Murphy, H.S.; Ward, P.A. Regulatory effects of iNOS on acute lung inflammatory responses in mice. *Am. J. Pathol.* **2003**, *163*, 2319–2328. [[CrossRef](#)]
70. Williams, A.E.; José, R.J.; Brown, J.S.; Chambers, R.C. Enhanced inflammation in aged mice following infection with *Streptococcus pneumoniae* is associated with decreased IL-10 and augmented chemokine production. *Am. J. Physiol. Lung Cell. Mol. Physiol.* **2015**, *308*, L539–L549. [[CrossRef](#)]
71. José, R.J.; Williams, A.E.; Mercer, P.F.; Sulikowski, M.G.; Brown, J.S.; Chambers, R.C. Regulation of neutrophilic inflammation by proteinase-activated receptor 1 during bacterial pulmonary infection. *J. Immunol.* **2015**, *194*, 6024–6034. [[CrossRef](#)] [[PubMed](#)]
72. Kantrow, S.P.; Shen, Z.; Jagneaux, T.; Zhang, P.; Nelson, S. Neutrophil-mediated lung permeability and host defense proteins. *Am. J. Physiol. Lung Cell. Mol. Physiol.* **2009**, *297*, L738–L745. [[CrossRef](#)] [[PubMed](#)]
73. Li, S.; Zhou, B.; Liu, B.; Zhou, Y.; Zhang, H.; Li, T.; Zuo, X. Activation of the cholinergic anti-inflammatory system by nicotine attenuates arthritis via suppression of macrophage migration. *Mol. Med. Rep.* **2016**, *14*, 5057–5064. [[CrossRef](#)] [[PubMed](#)]
74. Sadis, C.; Teske, G.; Stokman, G.; Kubjak, C.; Claessen, N.; Moore, F.; Loi, P.; Diallo, B.; Barvais, L.; Goldman, M.; et al. Nicotine protects kidney from renal ischemia/reperfusion injury through the cholinergic anti-inflammatory pathway. *PLoS ONE* **2007**, *2*, e469. [[CrossRef](#)] [[PubMed](#)]
75. Lafargue, M.; Xu, L.; Carlès, M.; Serve, E.; Anjum, N.; Iles, K.E.; Xiong, X.; Giffard, R.; Pittet, J.-F. Stroke-induced activation of the $\alpha 7$ nicotinic receptor increases *Pseudomonas aeruginosa* lung injury. *FASEB J.* **2012**, *26*, 2919–2929. [[CrossRef](#)] [[PubMed](#)]
76. Liu, Q.; Jin, W.-N.; Liu, Y.; Shi, K.; Sun, H.; Zhang, F.; Zhang, C.; Gonzales, R.J.; Sheth, K.N.; La Cava, A.; et al. Brain Ischemia Suppresses Immunity in the Periphery and Brain via Different Neurogenic Innervations. *Immunity* **2017**, *46*, 474–487. [[CrossRef](#)]
77. Fernandez-Cabezudo, M.J.; Lorke, D.E.; Azimullah, S.; Mechkarska, M.; Hasan, M.Y.; Petroianu, G.A.; al-Ramadi, B.K. Cholinergic stimulation of the immune system protects against lethal infection by *Salmonella enterica* serovar Typhimurium. *Immunology* **2010**, *130*, 388–398. [[CrossRef](#)]
78. Su, X.; Matthay, M.A.; Malik, A.B. Requisite role of the cholinergic $\alpha 7$ nicotinic acetylcholine receptor pathway in suppressing Gram-negative sepsis-induced acute lung inflammatory injury. *J. Immunol.* **2010**, *184*, 401–410. [[CrossRef](#)]
79. Giebelen, I.A.J.; Leendertse, M.; Florquin, S.; van der Poll, T. Stimulation of acetylcholine receptors impairs host defence during pneumococcal pneumonia. *Eur. Respir. J.* **2009**, *33*, 375. [[CrossRef](#)]



© 2020 by the authors. Licensee MDPI, Basel, Switzerland. This article is an open access article distributed under the terms and conditions of the Creative Commons Attribution (CC BY) license (<http://creativecommons.org/licenses/by/4.0/>).

8.3. Publication 3

8.3.1. Excerpt From the ISI Journal Summary List

Journal Data Filtered By: **Selected JCR Year: 2020** Selected Editions: SCIE,SSCI

Selected Categories: **“MATERIALS SCIENCE, MULTIDISCIPLINARY”**

Selected Category Scheme: WoS

Gesamtanzahl: 333 Journale

Rank	Full Journal Title	Total Cites	Journal Impact Factor	Eigenfactor Score
1	Nature Reviews Materials	19,887	66.308	0.056770
2	Nature Energy	28,166	60.858	0.080070
3	NATURE MATERIALS	112,429	43.841	0.130050
4	Joule	17,275	41.248	0.046240
5	PROGRESS IN MATERIALS SCIENCE	21,332	39.580	0.018870
6	Nature Nanotechnology	75,845	39.213	0.106790
7	MATERIALS SCIENCE & ENGINEERING R-REPORTS	8,652	36.214	0.004770
8	Materials Today	20,082	31.041	0.022450
9	ADVANCED MATERIALS	320,972	30.849	0.431450
10	Advanced Energy Materials	93,801	29.368	0.169490
11	InfoMat	1,460	25.405	0.001930
12	ACS Energy Letters	30,194	23.101	0.072680
13	Nano Today	10,434	20.722	0.011020
14	INTERNATIONAL MATERIALS REVIEWS	7,219	19.559	0.004410
15	ADVANCED FUNCTIONAL MATERIALS	151,020	18.808	0.206450
16	Nano Energy	74,385	17.881	0.124640
17	Energy Storage Materials	17,077	17.789	0.028130
18	Advanced Science	27,067	16.806	0.054300
19	Nano-Micro Letters	5,972	16.419	0.007680
20	Annual Review of Materials Research	9,204	16.286	0.005300

A Primeval Mechanism of Tolerance to Desiccation Based on Glycolic Acid Saves Neurons in Mammals from Ischemia by Reducing Intracellular Calcium-Mediated Excitotoxicity

Alexandra Chovsepian, Daniel Berchtold, Katarzyna Winek, Uta Mamrak, Inés Ramírez Álvarez, Yanina Dening, Dominika Golubczyk, Luis Weitbrecht, Claudia Dames, Marine Aillery, Celia Fernandez-Sanz, Zdzislaw Gajewski, Marianne Dieterich, Mirosław Janowski, Peter Falkai, Piotr Walczak, Nikolaus Plesnila, Andreas Meisel, and Francisco Pan-Montojo*

Stroke is the second leading cause of death and disability worldwide. Current treatments, such as pharmacological thrombolysis or mechanical thrombectomy, reopen occluded arteries but do not protect against ischemia-induced damage that occurs before reperfusion or neuronal damage induced by ischemia/reperfusion. It has been shown that disrupting the conversion of glyoxal to glycolic acid (GA) results in a decreased tolerance to anhydrobiosis in *Caenorhabditis elegans* dauer larva and that GA itself can rescue this phenotype. During the process of desiccation/rehydration, a metabolic stop/start similar to the one observed during ischemia/reperfusion occurs. In this study, the protective effect of GA is tested in different ischemia models, i.e., in commonly used stroke models in mice and swine. The results show that GA, given during reperfusion, strongly protects against ischemic damage and improves functional outcome. Evidence that GA exerts its effect by counteracting the glutamate-dependent increase in intracellular calcium during excitotoxicity is provided. These results suggest that GA treatment has the potential to reduce mortality and disability in stroke patients.

1. Introduction

Stroke is the second leading cause of death and disability worldwide and is responsible for ≈5.5 million deaths and 116.4 million disability-adjusted life years globally.^[1] Ischemic stroke comprises 87% of all stroke cases^[2] and is caused by a thrombotic or embolic vessel occlusion, which results in focal cerebral ischemia. It takes only minutes for the affected area of the brain to become irreversibly damaged, often resulting in long-term neurological deficits (such deficits occur in 50% to 60% of stroke patients^[3]). Blood flow to the tissue surrounding the necrotic infarct core is reduced, but this tissue, which is referred to as the penumbra, is salvageable because of collateral perfusion.^[4] The penumbra is thus the main target of current treatment strategies.^[5]

A. Chovsepian, Y. Dening, P. Falkai, F. Pan-Montojo
Department of Psychiatry and Psychotherapy
Ludwig-Maximilian University Hospital
Nussbaumstrasse, 7, 80336 Munich, Germany
E-mail: Francisco.Pan-Montojo@med.uni-muenchen.de

 The ORCID identification number(s) for the author(s) of this article can be found under <https://doi.org/10.1002/advs.202103265>

[+] Present address: Present address: Edmond and Lily Safra Center for Brain Sciences, Hebrew University of Jerusalem, Jerusalem 9190401, Israel

[++] Present address: Present address: Seppic, Île-de-France, La Garenne-Colombes 92250, France

[+++] Present address: Present address: Center for Translational Medicine, Department of Medicine, Thomas Jefferson University, Philadelphia, PA 19107, USA

© 2021 The Authors. Advanced Science published by Wiley-VCH GmbH. This is an open access article under the terms of the Creative Commons Attribution License, which permits use, distribution and reproduction in any medium, provided the original work is properly cited.

DOI: 10.1002/advs.202103265

D. Berchtold, K. Winek^[+], L. Weitbrecht, C. Dames, M. Aillery^[++], A. Meisel
Department of Neurology
NeuroCure Clinical Research Center
Center for Stroke Research
Charité University Medicine
Charitéplatz 1, 10117 Berlin, Germany

U. Mamrak, N. Plesnila
Laboratory of Experimental Stroke Research
Institute for Stroke and Dementia Research (ISD)
University of Munich Medical Center
Feodor-Lynen-Strasse 17, 81377 Munich, Germany

I. Ramírez Álvarez, Y. Dening, C. Fernandez-Sanz^[+++], M. Dieterich, F. Pan-Montojo
Department of Neurology
Ludwig-Maximilian University Hospital
Marchioninstrasse, 15, 81377 Munich, Germany

I. Ramírez Álvarez, C. Fernandez-Sanz^[+++], M. Dieterich, N. Plesnila, F. Pan-Montojo
Munich Cluster for Systems Neurology (SyNergy)
Ludwig-Maximilian University Munich
81377 Munich, Germany

Several treatments have been tested after stroke, including *N*-methyl-D-aspartate (NMDA) and NMDA antagonists,^[6] free radical scavengers,^[7,8] and immunomodulators (tumor necrosis factor alpha,^[9] interleukin-10^[10]). However, no treatment has been successful in the preclinical or clinical phase apart from the free radical scavenger edaravone, which received clinical approval in Japan.^[11] Hence, identifying novel neuroprotective compounds is essential for improving treatment options in ischemic stroke.

The inherent ability of *Caenorhabditis elegans* to tolerate extreme desiccation in the dauer larva stage, a special diapause stage that occurs in unfavorable environmental conditions, may have interesting implications in stroke. The strategies that enable the *C. elegans* dauer larva to survive desiccation have been extensively studied.^[12–15] Desiccation and rehydration represent a form of metabolic stress (metabolic stop/start)^[16] and mirror the metabolic halt and reactivation that occur during ischemia–reperfusion damage due to restriction of blood flow, oxygen, and nutrients,^[17,18] followed by an abrupt reinitiation of metabolic activity during rehydration/reperfusion. Research has been shown that *djr-1.1*, *djr-1.2*, and *glod-4* are strongly upregulated in dauer larva during preparation for desiccation and that these genes are crucial for desiccation tolerance.^[14,15,19] *djr-1.1* and *djr-1.2* are orthologs of the Parkinson's disease-associated glyoxalase DJ-1 (locus PARK 7), which is known to convert the reactive aldehydes glyoxal and methylglyoxal to glycolic acid (GA) and D-lactic acid (DL), respectively.^[20,21] A previous study^[19] showed that mutant worms without any glyoxalase activity (i.e., that lacked *djr* and *glod-4* genes) were less likely to survive desiccation. Moreover, mitochondria of *djr-1.1*; *djr-1.2* double mutant larvae and DJ-1-knockdown HeLa cells showed defects in their network structure and membrane potential. These phenotypes were rescued by GA and DL, demonstrating that the aforementioned deficits are not just a result of the accumulation of toxic aldehydes but are also caused by the absence of the DJ-1 glyoxalase activity products GA and DL themselves.^[19]

On the basis of these findings and the similarity between desiccation–rehydration and ischemia–reperfusion,^[16–18] we hypothesized that GA and DL might protect against damage caused by ischemic stroke. Therefore, we tested these substances in vitro by oxygen–glucose deprivation (OGD) and in vivo by global cerebral ischemia (GCI) and middle cerebral artery occlusion (MCAO) in mice and in an endovascular stroke model in swine. Overall, our results showed that GA treatment exerts powerful protection against ischemia and improves functional outcome.

D. Golubczyk
Ti-com LLC
Trylinskiego 2, Olsztyn 10-683, Poland
Z. Gajewski

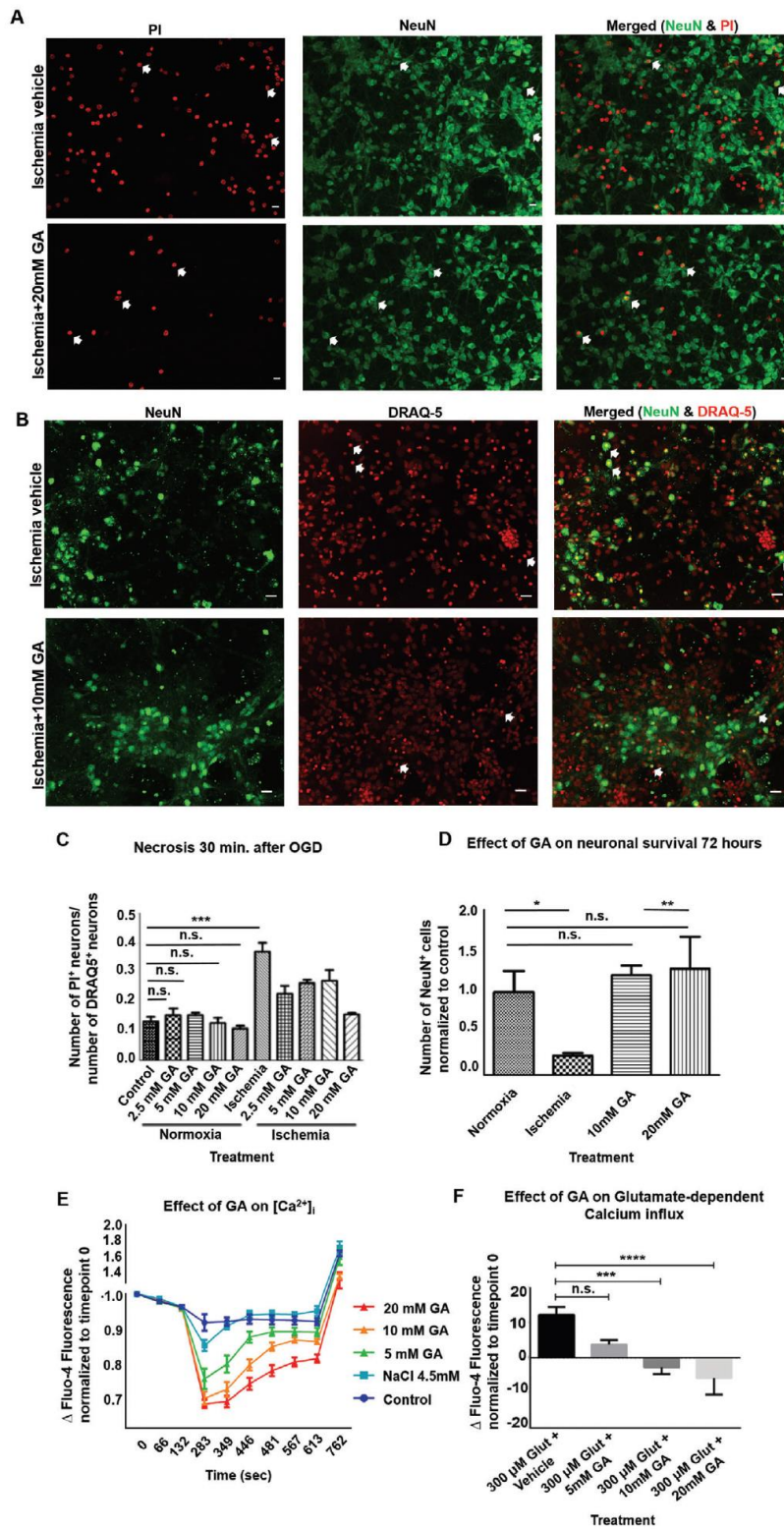
Center for Translational Medicine
Warsaw University of Life Sciences
Warsaw 02-787, Poland

M. Janowski, P. Walczak
Program in Image Guided Neurointerventions
Department of Diagnostic Radiology and Nuclear Medicine
University of Maryland
Baltimore, MD 21201, USA

2. Results

2.1. GA Protects from Ischemia-Induced Neuronal Death and Reduces Glutamate-Dependent [Ca²⁺] Influx in Cortical Neurons In Vitro

The current standard of care for treating acute stroke is to restore blood flow to the ischemic region, known as reperfusion. However, this procedure can also cause damage, an effect known as “ischemia–reperfusion injury.”^[22] Oxygen–glucose deprivation is a well-established in vitro model mimicking ischemia/reperfusion (IR) injury, leading to apoptotic and excitotoxicity-induced necrotic and apoptotic cell death.^[23] Therefore, we used this model to determine the neuroprotective properties of GA during ischemia–reperfusion damage by testing the effects of GA in different concentrations added to the culture media immediately after mimicking 1 h of ischemia. Briefly, on day in vitro (DIV) 7, normoxic medium was replaced by either normoxic medium (normal medium) or ischemic medium (phosphate-buffered saline (PBS), pH 6.4, bubble in N₂) and neurons were placed for 1 h in either the incubator again (normoxia) or an anoxic environment consisting of an N₂-filled gas chamber; both the incubator and chamber were held at 37 °C. To mimic reperfusion, the anoxic buffer was washed out and replaced by normal medium supplemented with water as vehicle or GA at final concentrations of 2.5 × 10^{−3}, 5 × 10^{−3}, 10 × 10^{−3}, or 20 × 10^{−3} M. For the normoxic group, neurons were kept at 5% CO₂ for 1 h, and then the medium was replaced again with normal medium. To differentiate between necrosis and apoptosis, we used two different approaches. Necrosis just after the ischemic insult was assessed as the ratio of necrotic propidium iodide positive (PI⁺) cells to the total number of neuronal nuclei positive (NeuN)⁺ cells 30 min after OGD compared to normoxic neurons treated with the same concentrations of GA. We observed a significant increase in the number of PI⁺ nuclei in the neuronal cultures that underwent OGD compared with the number in the normoxic cultures (OGD, 0.368 ± 0.059; normoxic, 0.132 ± 0.030; *p* < 0.001; one-way analysis of variance (ANOVA) followed by Tukey's multiple comparisons test; Figure 1A,C). Upon OGD, treatment with GA during reperfusion decreased necrotic nuclei/total nuclei ratio compared to vehicle treatment; the highest effect was observed with the 20 × 10^{−3} M concentration (OGD + 20 × 10^{−3} M GA: 0.156 ± 0.008, *p* < 0.001). In the normoxia group, the various concentrations of GA had no effect compared with the normoxia vehicle, even at the highest concentrations (normoxia + 20 × 10^{−3} M GA: 0.108 ± 0.021, *p* > 0.05). We then evaluated the number of NeuN⁺ neurons at 72 h after OGD to evaluate the total cell death (i.e., combined cell death from necrosis that occurs at early stages after OGD and apoptosis that takes place at later stages). As shown in Figure 1, OGD resulted in the loss of 76% of NeuN⁺ cells when compared with normoxia (OGD, 255.3 ± 35.32; normoxia, 1092 NeuN⁺ cells in 10 fields per well ± 284.0; *p* < 0.05; unpaired *t*-test; Figure 1B,D). Treatment with 10 × 10^{−3} and 20 × 10^{−3} M GA immediately after OGD exerted a clear protection, increased the number of surviving neurons to levels comparable to those found with normoxia (OGD + 10 × 10^{−3} M GA, 1230 ± 154.8, *p* = 0.693; OGD + 20 × 10^{−3} M GA, 1404 ± 422.5, *p* = 0.573). We found no significant difference in neuronal survival between treatment with



10×10^{-3} and 20×10^{-3} M GA ($p = 0.718$). These results show that treatment with 10×10^{-3} or 20×10^{-3} M GA during reperfusion rescued neurons from ischemia-induced cell death after OGD. Excitotoxicity is a major mechanism underlying neuronal death in stroke and is caused by the abnormally high calcium influx into cells via NMDA receptors (also known as glutamate-dependent excitotoxicity).^[24] We previously described that GA reduces intracellular calcium in HeLa cells.^[25] Therefore, we decided to investigate whether it also reduces intracellular calcium in cortical neurons in vitro, even in the presence of glutamate. To that end, we tested the effect of GA on primary cortical neuronal cultures from mouse embryos loaded with Fluo-4-AM, an intracellular calcium indicator. With the help of a plate reader, intracellular calcium concentrations inside mouse cortical neurons ($[Ca^{2+}]_i$) were recorded at different time points before and after the addition of GA and ionomycin (Figure 1E). We found that increasing concentrations of GA (5×10^{-3} , 10×10^{-3} , and 20×10^{-3} M) significantly reduced the intracellular calcium compared with vehicle (PBS) and the osmolarity control 4.5×10^{-3} M NaCl (two-way ANOVA, all $p < 0.0001$), with 20×10^{-3} M GA showing the strongest effect. Addition of ionomycin just before the measurement at 762 s strongly increased the influx of calcium into the cells, but 20×10^{-3} and 10×10^{-3} M of GA were able to keep the calcium levels lower than control and 4.5×10^{-3} M NaCl-treated neurons (one-way ANOVA_{762 s}, $p = 0.0011$). We then tested whether GA reduced the calcium influx even in the presence of a high concentration of glutamate (300×10^{-6} M), which mimicked excitotoxicity. Indeed, our results show that the higher concentrations of GA (10×10^{-3} and 20×10^{-3} M) significantly decreased $[Ca^{2+}]_i$ in cortical neurons in the presence of glutamate (one-way ANOVA, $p < 0.0001$) (Figure 1F). Taken together, these data indicate that GA can mitigate the deleterious intracellular calcium increases that are associated with ischemia/reperfusion damage.

2.2. Unilateral Intra-Arterial (i.a.) Administration of GA during Reperfusion Protects against Neuronal Death in the Ipsilateral CA1 Region of the Hippocampus during GCI in Mice

On the basis of these results, we decided to evaluate the effect of GA in a well-established in vivo model of GCI. GCI occurs in case of a pronounced drop in the oxygen or blood supply to the brain (e.g., due to myocardial infarction, heart arrhythmias, sudden and prolonged decrease in blood pressure, insufficient oxygen or blood supply in protracted or complicated labor, and strangulation by the umbilical cord), which leads to anoxic/hypoxic brain damage. In adult patients, 5 min of anoxia are sufficient to cause significant neuronal metabolic impairment, leading to permanent brain damage and, in some cases, coma or even death.^[26]

For these experiments, we used the previously described mouse model of GCI^[27,28] to test the effect of PBS (vehicle) or GA injected into the left carotid artery during reperfusion (Figure 2A–C). In short, a catheter was placed in the left common carotid artery and then both common carotid arteries were occluded with atraumatic clips. After 7.5 min, the clips were removed (reperfusion) and 50 μ L of 120×10^{-3} M GA ($n = 7$ mice) or PBS (0.01 M, $n = 9$) was injected into the left common carotid artery. Sham-operated mice ($n = 16$) underwent the same surgical procedure without carotid clipping. GCI resulted in neuronal death in the hippocampal cornu ammonis 1 (CA1) region of both hemispheres in the vehicle group (sham vs vehicle, right side, mean difference = 32.78, $p < 0.001$; sham vs vehicle, left side, mean difference = 27.67, $p < 0.01$; one-way ANOVA followed by Dunnett's multiple comparisons test; Figure 2D). Interestingly, the injection of GA into the left carotid artery during reperfusion resulted in a significant increase in neuronal survival in the left CA1 compared with the contralateral (right) CA1, where a substantial loss of neurons was observed when compared with sham animals (sham vs GA, right side, mean difference = 45.71,

Figure 1. Glycolic acid reduces necrosis and apoptosis in the oxygen–glucose deprivation model by reducing intracellular calcium. A) Representative fluorescence microscopy images of neurons stained with propidium iodide (PI, left panel, red) during reperfusion to evaluate necrosis and imaged 30 min after reperfusion. The middle panel shows the same neuronal population stained for neuronal nuclei (NeuN, green) to label all neuronal bodies, and the right panel shows both stainings together. White arrows indicate examples of necrotic (PI^+ , $NeuN^+$) neurons. Upper panel: Neurons that underwent ischemia and were treated with vehicle containing reperfusion medium (ischemia + vehicle). Lower panel: Neurons that underwent ischemia and were treated with reperfusion medium containing 20×10^{-3} M glycolic acid [GA; (ischemia+ 20×10^{-3} M GA)]. B) Representative fluorescence microscopy images of neurons stained for NeuN (left panel, green) and DRAQ5 nuclear labeling (middle panel, red) 72 h after oxygen–glucose deprivation (OGD) and reperfusion. The right panel shows the merge of the two stainings. White arrows show examples of pyknotic nuclei that are identified by overaccumulation of DRAQ5 and their small size. Upper panel: ischemia + vehicle. Lower panel: ischemia + 10×10^{-3} M GA. The figure shows that neuron morphology was severely damaged in the vehicle group, which had affected or absent neurites, but was more conserved in the GA-treated group. Three biological replicates ($n = 3$) were used, consisting of 5 technical replicates each (mean of 5 wells per condition per plate). Scale bars: 20 μ m. C) GA at all tested concentrations significantly reduced the levels of necrosis at 30 min after OGD, as measured by the ratio of PI^+ (necrotic) neurons to $NeuN^+$ (non-necrotic) neurons. The strongest effect was achieved by 20×10^{-3} M GA (one-way analysis of variance [ANOVA] followed by Tukey's multiple comparison's test, $p < 0.0001$). D) GA treatment during reperfusion protected cortical neurons against 60 min ischemia-induced cell death, up to 72 h after the insult. Numbers are normalized to normoxia (control); an unpaired *t*-test was performed. Data are presented as mean \pm SEM; n.s.: nonsignificant, * $p < 0.05$, ** $p < 0.01$, *** $p < 0.001$, and **** $p < 0.0001$. E) The graph shows the effect of 5×10^{-3} , 10×10^{-3} , and 20×10^{-3} M GA on intracellular calcium levels (here, expressed as Δ Fluo-4-fluorescence normalized to timepoint 0) before and after addition of 2×10^{-6} M ionomycin in mouse cortical neurons loaded with 5×10^{-6} M Fluo-4-AM. Two-way ANOVA followed by Sidak's multiple comparisons test: control versus 5×10^{-3} M GA, $p < 0.001$; control versus 10×10^{-3} M GA, $p < 0.0001$; control versus 20×10^{-3} M GA, $p < 0.0001$; control versus 4.5×10^{-3} M NaCl, n.s.; 4.5×10^{-3} M NaCl versus 5×10^{-3} M GA, $p < 0.0001$; 4.5×10^{-3} M NaCl versus 10×10^{-3} M GA, $p < 0.0001$; 4.5×10^{-3} M NaCl versus 20×10^{-3} M GA, $p < 0.0001$; 5×10^{-3} M GA versus 10×10^{-3} M GA, $p < 0.0001$; 5×10^{-3} M GA versus 20×10^{-3} M GA, $p < 0.0001$; and 10×10^{-3} M GA versus 20×10^{-3} M GA, $p = 0.0018$. F) The graph shows the effect of GA on glutamate-dependent calcium influx, measured as Δ Fluo-4-fluorescence normalized to the timepoint pretreatment. One-way ANOVA followed by Tukey's multiple comparisons test: vehicle versus 5×10^{-3} M GA, n.s.; vehicle versus 10×10^{-3} M GA, $p < 0.001$; vehicle versus 20×10^{-3} M GA, $p < 0.0001$; 5×10^{-3} M GA versus 10×10^{-3} M GA, n.s.; 5×10^{-3} M GA versus 20×10^{-3} M GA, $p < 0.05$; and 10×10^{-3} M GA versus 20×10^{-3} M GA, n.s. GA, glycolic acid; Glut, glutamate; PI, propidium iodide; NeuN, total neuronal nuclei.

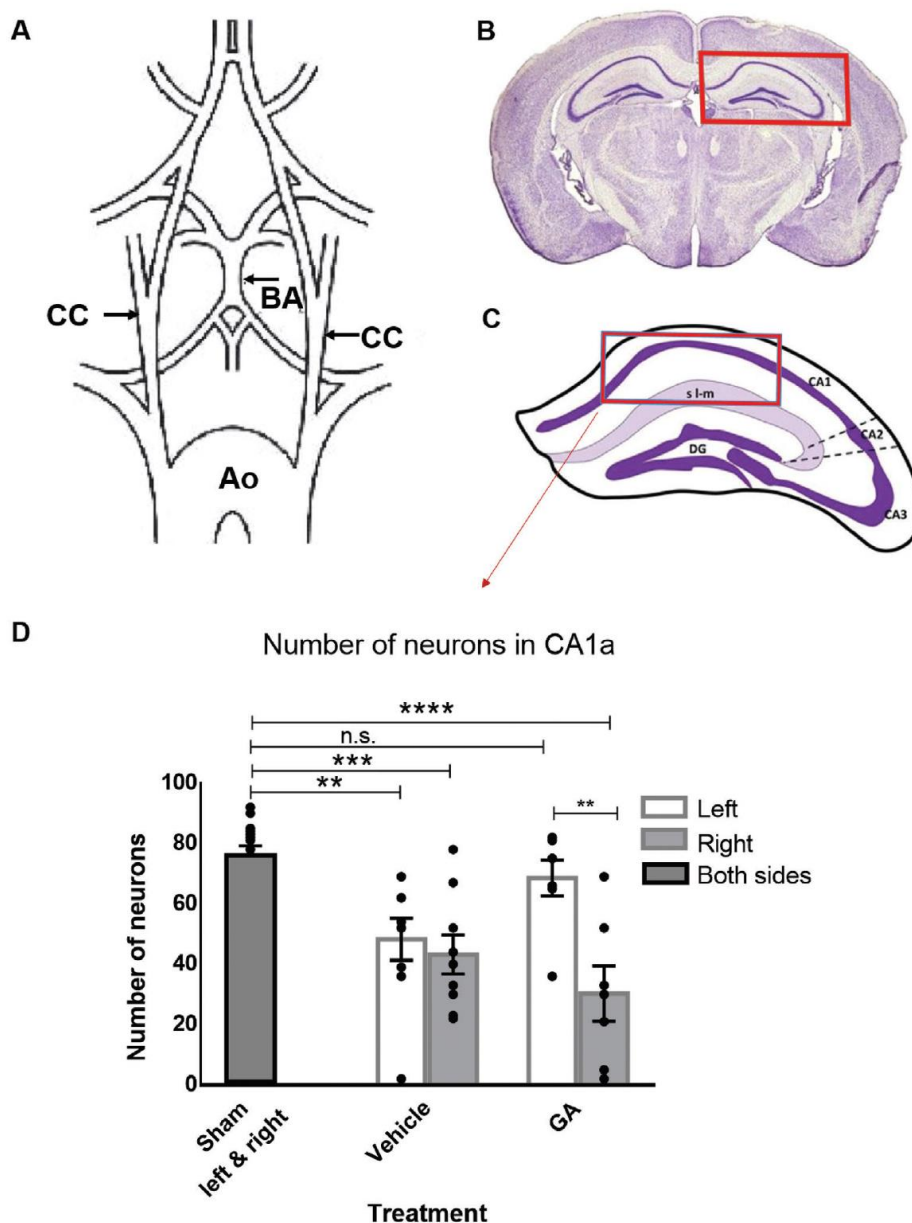


Figure 2. Glycolic acid increases neuronal survival in the hippocampus of a global cerebral ischemia mouse model. A) Schematic illustration of the arterial brain supply indicating (arrows) the positions of transient clipping (for 7.5 min) to induce of global cerebral ischemia (GCI). B) GCI model affects the hippocampus, shown in the red rectangle. C) Neurons were quantified inside the area indicated by the red rectangle (cornu ammonis 1 [CA1] area). D) Number of neurons quantified after administration of 50 μ L glycolic acid (GA) or phosphate-buffered serum (PBS) immediately after ischemia at the moment of reperfusion through a catheter placed in the left carotid artery. The number of surviving neurons in the left CA1 was significantly lower in PBS-treated animals than in sham animals, but no significant difference was observed for the GA-treated group. In contrast, the right CA1, i.e., contralateral to the injection site, showed significant neuronal death in both PBS- and GA-treated animals, underscoring that the neuroprotective effect of GA is local. One-way analysis of variance followed by Dunnett's multiple comparisons test, $**p < 0.01$, $***p < 0.001$, and $****p < 0.0001$. Data shown as mean \pm SEM; $n_{\text{sham}} = 16$, $n_{\text{veh}} = 9$, and $n_{\text{GA}} = 7$. Ao, aorta; BA, basilar artery; CA1a, cornu ammonis 1a; CC, common carotid artery.

$p < 0.0001$). Remarkably, the number of surviving neurons in the left CA1 (ipsilateral to the GA injection) was not different from the sham group (sham vs GA, left side, mean difference = 7.429, $p > 0.05$).

2.3. Intraperitoneal GA Treatment during Reperfusion Improves Histopathological and Functional Outcome in the MCAO Mouse Model

To further confirm the observed neuroprotective effects of GA in another relevant *in vivo* model, we tested the effects of GA in the MCAO mouse model, the most commonly used model in stroke studies.^[29] The MCAO procedure involves the insertion of a silicon monofilament into the common carotid artery; the monofilament is then advanced until it reaches the origin of the middle cerebral artery (MCA), where it occludes the artery and is left in place for 60 min. After 60 min of MCA occlusion, the monofilament is retracted, and the internal carotid artery is permanently ligated. The sham operation ($n = 6$) uses the identical procedure, but the monofilament is removed as soon as it reaches the origin of the MCA. GA ($\approx 100 \mu\text{L}$, 60 mg kg^{-1} ; $n = 18$) or vehicle (NaCl, $\approx 100 \mu\text{L}$, 0.9%; $n = 16$) was administered by intraperitoneal (i.p.) injection at the end of the operation, immediately after closure of the skin wound. Our experimental timeline is described in detail in Figure 3A. Briefly, MCAO or sham operation was performed on day 0. The next day, the early infarct size was measured by magnetic resonance imaging (MRI). On day 8, mice underwent the first motor function evaluation (pole test). Gait was then assessed on day 10 with the catwalk test, and laterality (preference for nonaffected side), on day 12 with the corner test. On day 13, the late infarct size was measured by MRI, and on day 14, the brain was fixed for further analysis.

As illustrated in Figure S1A in the Supporting Information, the number of surviving mice at the endpoint (14 days after MCAO) was higher in the GA-treated group than in the vehicle-treated group, although the difference was not statistically significant (94.44% vs 76.47%, respectively; Mantel–Cox test, Chi square = 3.411, $p = 0.181$); all sham-operated mice survived until the endpoint. Death occurred only in mice with large infarcts (>18% of the hemispheric volume; Figure 3B-i). Therefore, we conducted a separate survival analysis in the subgroup with such large infarcts. In this analysis, a Mantel–Cox test showed that GA significantly increased mouse survival. More specifically, 66% of the vehicle-treated mice were euthanized by day 5 because they fulfilled humane endpoint criteria, whereas only 14.2% of the GA-treated mice fulfilled the humane endpoint criteria by that time (Chi square = 6.215, $p = 0.044$; Figure 3B-ii). Moreover, upon daily careful health monitoring, we observed that GA treatment had no effect on ischemia-induced weight loss compared with vehicle and showed only a nonsignificant tendency to improve the general health score (evaluation as previously described;^[30] Figure S1B,C, Supporting Information). The body surface temperature was not influenced by ischemia or treatment (Figure S1D, Supporting Information).

According to our MRI observations, on day 1 after MCAO GA did not significantly alter the total lesion size compared with the vehicle (see Figure S2 in the Supporting Information). However, GA treatment had a strong effect on the evolution of the lesion

size. As shown in Figure 3C,D, the infarct size was significantly smaller at day 13 after MCAO than at day 1 (paired *t*-test, $p = 0.0004$). In contrast, no significant reduction in infarct size was observed in the vehicle group (Figure 3E; paired *t*-test, $p = 0.091$). This finding shows that GA significantly improved the late outcome after ischemia.

Regarding the assessment of motor function, the pole and catwalk tests did not detect any significant differences between sham- and MCAO-operated mice, regardless of treatment (Figures S3 and S4, and Table S1, Supporting Information). However, GA had a positive effect on performance in the corner test. As shown in Figure 3F, the laterality index (LI) of the corner test was significantly higher after MCAO without treatment than after sham (0.48 ± 0.242 vs -0.065 ± 0.172 , respectively; $p = 0.006$; one-way ANOVA followed by Bonferroni's multiple comparisons test). In contrast, LI in the GA-treated group was not significantly different from the sham-operated group (0.26 ± 0.451 , $p = 0.104$) (see videos in the Supporting Information). Thus, GA treatment reduced the ischemia-induced sensorimotor asymmetry to levels similar to those in the sham group. Subsequently, we examined the relationship between infarct size and performance in the corner test. In principle, large infarcts are expected to lead to greater impairments and higher LI values. We found a tendency toward a positive correlation between infarct size and impairment in the corner test in the vehicle-treated group (Pearson's $r = 0.508$, $p = 0.075$; Figure 3G) but not in the GA-treated group (Pearson's $r = -0.032$, $p = 0.902$). This finding again suggests that GA improved the functional outcome, especially in animals with larger ischemic lesions.

After the aforementioned *in vivo* tests, we performed a histological analysis of the brains collected at the endpoint of the experiment on day 14 after MCAO. We used Neurotrace (a Nissl-based fluorescence staining) to differentiate between healthy and infarcted tissue and NeuN immunostaining to identify and count surviving neurons in infarcted tissue. Nissl substance redistributes within the cell body in injured or regenerating neurons and thereby acts as a marker for the physiological state of the neuron. However, although it identifies damaged areas, it cannot differentiate between the part of the penumbra that survived and is regenerating and the part that has died within the next days after stroke in a patched manner due to apoptosis and did not liquefy and detach. Additionally, during slicing of the brain for histological processing, in some brains with large infarcts we noticed that part of the tissue within the ischemic area had a different, more fragile quality than the surrounding infarct. This part of the tissue tended to detach during histological processing (Figure S5, Supporting Information). We hypothesized that this area may have corresponded to the ischemic core and was undergoing liquefactive necrosis.^[5,31,32] In this case, one would assume that i) contrary to being an artifact, the volume of missing tissue would show a direct correlation with the ischemic volume measured by MRI and ii) tissue undergoing necrotic liquefaction would have a higher water content than the surrounding ischemic tissue and a higher signal in the T2-weighted MRI scan. Indeed, the volume of missing tissue as measured by stereology was significantly correlated with the infarct volume as measured by MRI on day 13 after MCAO (Figure S6A,B, Supporting Information) in both the vehicle-treated group (Pearson's $r_{\text{veh}} = 0.598$, $p < 0.01$) and the GA-treated group (Pearson's $r_{\text{GA}} = 0.517$,

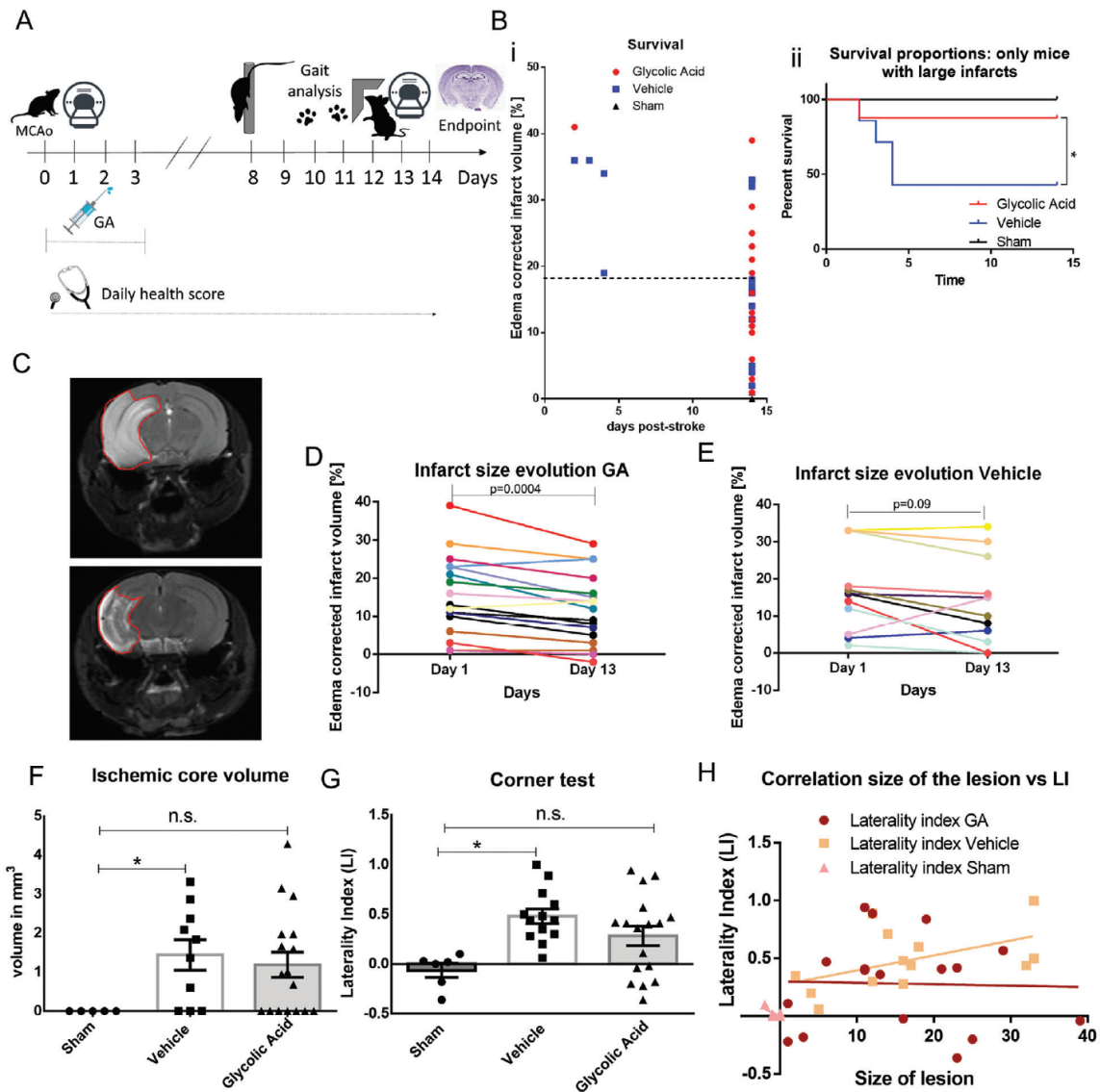


Figure 3. Glycolic acid improves histological and functional outcomes after middle cerebral artery occlusion. A) Experimental design: day 0, middle cerebral artery occlusion (MCAO) or sham operation; day 1, measurement of early infarct size by magnetic resonance imaging (MRI); day 8, motor assessment with the pole test; day 10, gait analysis with the catwalk test; day 12, assessment of laterality (preference for nonaffected side) with the corner test; day 13, measurement of late infarct size by magnetic resonance imaging (MRI); and day 14, brain fixation for further analysis. B-i) Survival until poststroke day 14. Euthanasia because of fulfilment of humane endpoint criteria was necessary only in mice with infarcts larger than 18% of hemispheric volume. ii) In mice with larger infarcts (>18% of the hemispheric volume), by day 5, 66% of the vehicle group reached the endpoint but only 14.2% of the GA group did (Mantel–Cox survival test: Chi square = 6.215, $p = 0.0447$; $n_{GA} = 18$, $n_{veh} = 16$, and $n_{sham} = 6$). C) Example MRI image showing the evolution of an MCAO-induced infarct in a GA-treated mouse. Upper panel: Day 1 after ischemia. Lower panel: Day 13 after ischemia. D) Evolution of MCAO-induced infarct in GA-treated mice: significant reduction of the infarct size on day 13 versus day 1 (paired t -test, $p = 0.0004$, $n_{GA} = 17$). E) Evolution of MCAO-induced infarct in vehicle-treated mice: no significant reduction of the infarct size on day 13 versus day 1 (paired t -test, $p = 0.091$, $n_{veh} = 10$). F) Stereological quantification: Although the vehicle group had a significantly higher ischemic core volume than the sham mice ($p = 0.0243$), the difference between GA and sham was not significant ($p = 0.0638$, unpaired t -test; $n_{GA} = 17$, $n_{veh} = 10$, and $n_{sham} = 5$). G) Corner test assessed the preference for the side not affected by ischemia over the affected side, with a higher laterality index (LI) indicating higher impairment of the ischemia-affected side. The LI was significantly higher in the vehicle-treated group than in sham mice ($p = 0.0064$). In contrast, the LI of the GA-treated group was not significantly different from the sham mice ($p = 0.1042$) and the difference between GA-treated and vehicle-treated mice was also not significant ($p = 0.3433$, one-way ANOVA followed by Bonferroni's multiple comparisons test; $n_{GA} = 17$, $n_{veh} = 13$, and $n_{sham} = 6$). H) The functional outcome after MCAO (LI index) was not correlated with the infarct size in GA-treated mice (Pearson's $r = -0.03202$, $p = 0.9$), but the correlation was almost significant in vehicle-treated mice (Pearson's $r = 0.5086$, $p = 0.07$; $n_{GA} = 17$, $n_{veh} = 13$, and $n_{sham} = 6$). GA, glycolic acid; LI, laterality index; MCAO, middle cerebral artery occlusion.

$p < 0.01$). The correlation was significant even when treatment groups were pooled (Pearson's $r = 0.548$, $p = 0.01$). In addition, we performed a detailed assessment of the corresponding MRI images (on day 13) of brains with missing tissue and found that the area that detached during histological processing had a significantly higher contrast in the T2-weighted MRI scan (i.e., a higher water content) than the surrounding nondetached ischemic area and the contralateral nonaffected hemisphere (one-way ANOVA, mean difference_{detached vs ischemic} = $35\,093 \pm 6284$, $p < 0.01$; mean difference_{detached vs contralateral side} = $50\,576 \pm 8623$, $p < 0.01$; Figure S6A-iii, Supporting Information). Taken together, these results support our hypothesis that the missing tissue can be considered as the ischemic core.

Stereological analysis (Stereo Investigator, MBF) provided an estimate of cell density inside the Neurotrace⁺ area and the volume of the infarct (Figure S5, Supporting Information). We observed only a small, nonsignificant reduction in the number of neurons inside the Neurotrace⁺ area, and GA did not change the size of the total Neurotrace⁺ area (Figure S6A,D, Supporting Information). Although we found a significant difference in the volume of missing tissue (ischemic core) between vehicle and sham (sham, 0.00 ± 0.00 ; vehicle, 1.444 ± 0.393 ; $p = 0.024$), we did not find a significant difference between GA and sham (GA, 1.189 ± 0.323 ; $p = 0.063$) (Figure 3H).

Last, we tested the effect of GA on the MCAO-associated increase in numbers of astrocytes and microglia in the brain. We used immunohistochemistry to stain for ionized calcium-binding adaptor molecule 1 (IBA1), a well-established marker for microglia and macrophages,^[33] and glial fibrillary acidic protein (GFAP), a well-established marker for astrocytes^[34] (Figure 4A-i-iii). We measured the fluorescence intensity of these markers in the ischemic area, the nonischemic area of the affected hemisphere (ipsilateral), and the nonaffected (contralateral) hemisphere (Figure 4A-iv). As shown in Figure 4B-i,C-i, when the brains were pooled independently of their infarct volume as measured by MRI we observed no significant changes in the signal intensity of microglia or astrocytes inside the ischemic area between sham, vehicle- or GA-treated mice (one-way ANOVA with Tukey's multiple comparisons test; sham vs vehicle, $p = 0.148$; sham vs GA, $p = 0.066$). When we examined mice with large infarcts separately (infarct volume >18% of the hemispheric volume), the signal intensity of microglia and astrocytes in the ischemic area were significantly higher in the vehicle group than in the sham group (IBA1, mean difference = -11.31 , $p < 0.05$; GFAP, mean difference = -13.00 , $p < 0.05$). Furthermore, the numbers of microglia and astrocytes in the ischemic area in GA-treated mice were not significantly different from sham (IBA1, mean difference = -4.35 , $p > 0.05$; GFAP, mean difference = -4.354 , $p > 0.05$), as shown in Figure 4B-ii,C-ii. In the ipsilateral, nonischemic tissue, we found no significant differences in the IBA1 and GFAP fluorescence signal between groups (one-way ANOVA with Tukey's multiple comparisons test; IBA1, $F = 3.198$, $p = 0.103$; GFAP, $F = 0.416$, $p = 0.674$). In the hemisphere contralateral to the MCAO side, we found a trend for a higher IBA1 signal in the vehicle group compared with the sham group that was close to reaching statistical significance (mean difference = -4.531 , $p = 0.055$), whereas the levels in the GA group were similar to sham (mean difference = 0.495 , $p = 0.842$). The contralateral GFAP signal did not seem to

be significantly affected by MCAO or treatment ($F = 1.259$, $p = 0.341$).

To reduce the time between reperfusion and GA treatment, we performed a second batch of experiments with 30 additional animals. In these experiments, the operations were performed by a different experimenter and, to reduce the time window between reperfusion and treatment, GA was administered via intraperitoneal injection immediately after monofilament removal before suturing the wound. In this set of experiments, no significant difference was observed between groups in any of the parameters analyzed (infarct size, survival, functional tests, general health; see Figures S8–S10 in the Supporting Information), so we could not perform any comparisons between GA and vehicle to test for neuroprotection.

2.4. Glycolic Acid Protects the Penumbra and Part of the Core when Administered Intra-Arterially after Reperfusion in Swine

On the basis of the above results and the differences observed between i.p. and i.a. administration, we hypothesized that i.a. administration of GA at the site of ischemia should lead to better protection against stroke than i.p. administration. Moreover, rodent brains lack the complexity of those of larger mammals such as swine, monkeys, and humans, limiting the translational potential of the results obtained in mice.^[35,36] To address both concerns, we tested GA in a novel endovascular model of stroke in swine that was recently established by Golubczyk and colleagues and allows for intra-arterial application of drugs upon pharmacologically induced reperfusion.^[37] As shown in the experimental design (Figure 5A), after baseline MRI scans ischemia was induced by i.a. injection of 200 U mL^{-1} thrombin. The MRI sequences used were as follows: T2w for anatomical reference, T1 and T1+contrast, perfusion-weighted imaging (PWI), susceptibility weighted imaging (SWI) to detect thrombus, and diffusion-weighted imaging (DWI), as well as mean transit time (MTT) and apparent diffusion coefficient (ADC) 2 h after thrombin injection to visualize the infarct core and penumbra (mismatch). After the MRI evaluation of the presence and size of the lesion, 20 mg of tissue plasminogen activator (tPA, 1 mg mL^{-1}) was injected into the ascending pharyngeal artery to dissolve the clots, and reperfusion was confirmed by MRI. Once reopening of the occluded vessels was confirmed ($\approx 5\text{--}10\text{ min}$ after tPA injection), an 8 mL bolus of GA or vehicle (NaCl) was administered by i.a. injection directly into the reperfused brain territory. The next day, GA (60 mg kg^{-1}) or control (NaCl) was injected intravenously. Behavioral testing (Neurological Evaluation Grading Scale)^[38] was performed before stroke as a baseline and on day 1, day 2, day 3, day 7, day 14, day 21, and day 28 after stroke to assess functional outcome after ischemia. T2 MRI was repeated on day 7 and day 28 to evaluate the infarct size at different stages (see Figure 5A). Animals were euthanized on day 30 after stroke.

Our results showed that, before reperfusion, the infarct size after 2 h of ischemia was not significantly different between groups (see Figure S11 in the Supporting Information). Remarkably, GA treatment had a strong protective effect on both the penumbra and the ischemic core: Whereas the mean ratio of T2 lesion volume on day 7 to ADC lesion volume on day 0 was 1.24 ± 0.24 in the control group, indicating an expansion of the ischemic

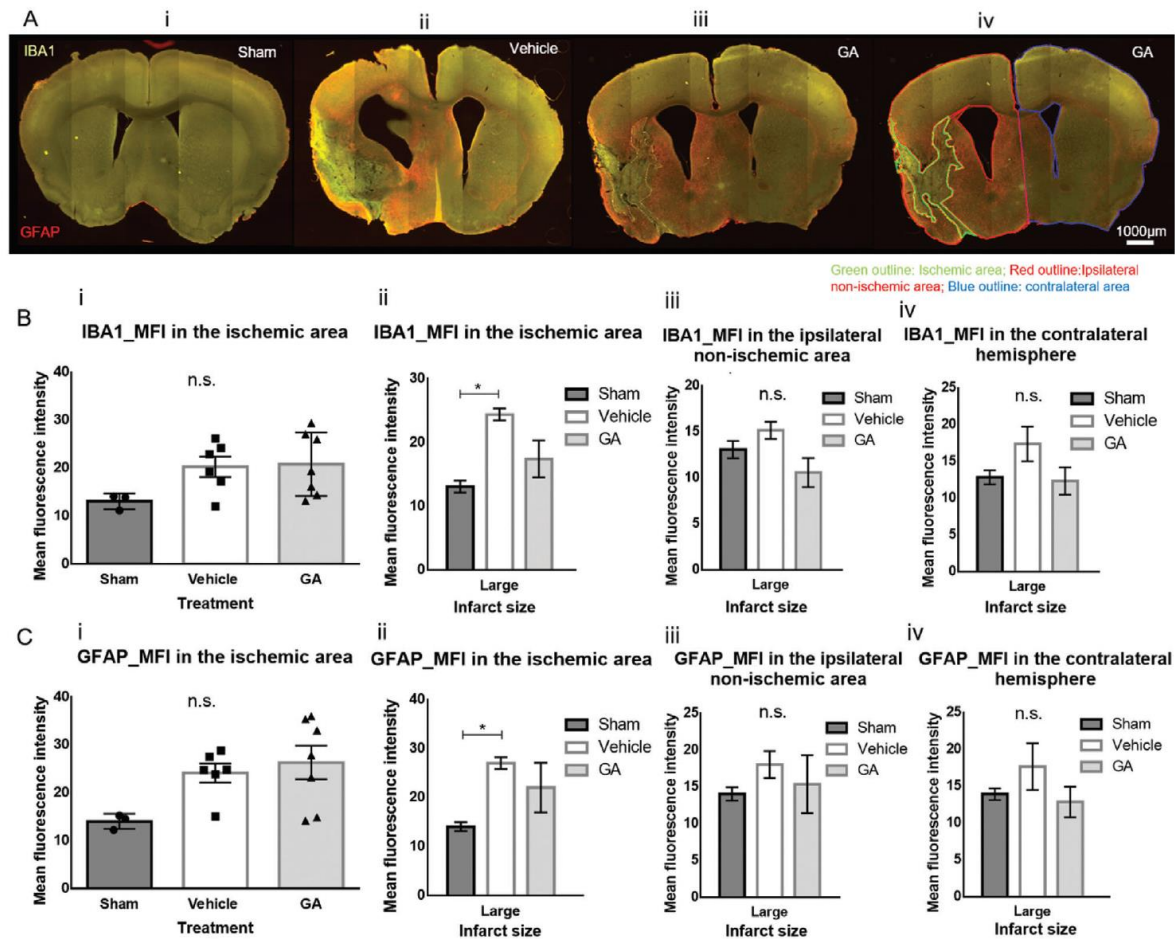


Figure 4. Glycolic acid mitigates the increase in the number of astrocytes and microglia in large infarcts after middle cerebral artery occlusion. A) Fluorescence microscopy images showing the staining for microglia (ionized calcium-binding adaptor molecule 1 [IBA1], green) and astrocytes (glial fibrillary acidic protein [GFAP], red) in i) a sham brain section, ii) a vehicle-treated brain section, and iii) a glycolic acid (GA)-treated brain section with large infarcts. iv) The same brain section as in (iii) indicating the outlines of the different areas in which mean fluorescence intensity (MFI) was measured. B-i) MFI of IBA1 staining in the ischemic area showing no significant differences between groups ($p = 0.1482$). ii) When large infarcts (>18% of hemispheric volume) were analyzed separately, the MFI of IBA1 inside the infarct area was significantly higher in the vehicle group than in sham mice (mean difference = -11.31 , $p < 0.05$), but GA did not differ from sham (mean difference = -4.354 , $p > 0.05$). iii) The MFI of IBA1 in the affected (ipsilateral) hemisphere outside the ischemic area was not significantly affected by MCAO ($p = 0.1032$). iv) A trend for higher IBA1 MFI in the contralateral hemisphere was observed in the vehicle group compared with the sham mice and almost reached statistical significance ($p = 0.0555$). C-i) MFI of GFAP staining in the ischemic area showing no significant differences between groups ($p = 0.0665$). ii) When large infarcts (>18% of hemispheric volume) were analyzed separately, the MFI of GFAP inside the infarct area was significantly higher in the vehicle group than in the sham mice (mean difference = -13.00 , $p < 0.05$), but GA did not differ from sham (mean difference = -4.354 , $p > 0.05$). The MFI of GFAP in the affected (ipsilateral) hemisphere iii) outside the ischemic area or iv) in the contralateral hemisphere was not significantly affected by MCAO ($p = 0.6747$ and $p = 0.3412$, respectively). For all aforementioned comparisons, one-way ANOVA followed by Tukey's multiple comparisons test was performed. Data are shown as mean \pm SEM; $n_{\text{sham}} = 3$, $n_{\text{veh}} = 6$, and $n_{\text{GA}} = 7$; scale bar: $\approx 1000 \mu\text{m}$. GA, glycolic acid; GFAP, glial fibrillary acidic protein; IBA1, ionized calcium-binding adaptor molecule 1; MFI, mean fluorescence intensity.

lesion into the penumbra, it was 0.69 ± 0.13 in the GA-treated group (control vs GA, $p = 0.0016$), suggesting that GA treatment not only completely protected the penumbra but also reduced the size of the ischemic core (Figure 5C,D). The MRI performed on day 28 after stroke showed a reduction of the lesion size in the control group (T2 Day 28 to ADC Day 0 ratio, 0.82 ± 0.19) and a greater decrease in the GA-treated group (T2 Day 28 to ADC Day 0 ratio, 0.43 ± 0.18 ; control vs GA, $p = 0.0119$). We also found a

nonsignificant positive effect of GA treatment on survival compared with controls (100% of GA-treated vs 80% vehicle-treated mice survived, as shown in Figure 5B).

The score of the neurological evaluation showed no statistically significant difference in behavioral outcome between the experimental and control group at any time point. In absolute values, the difference between the means was highest at day 2, when the score of the neurological evaluation in the GA-treated group was

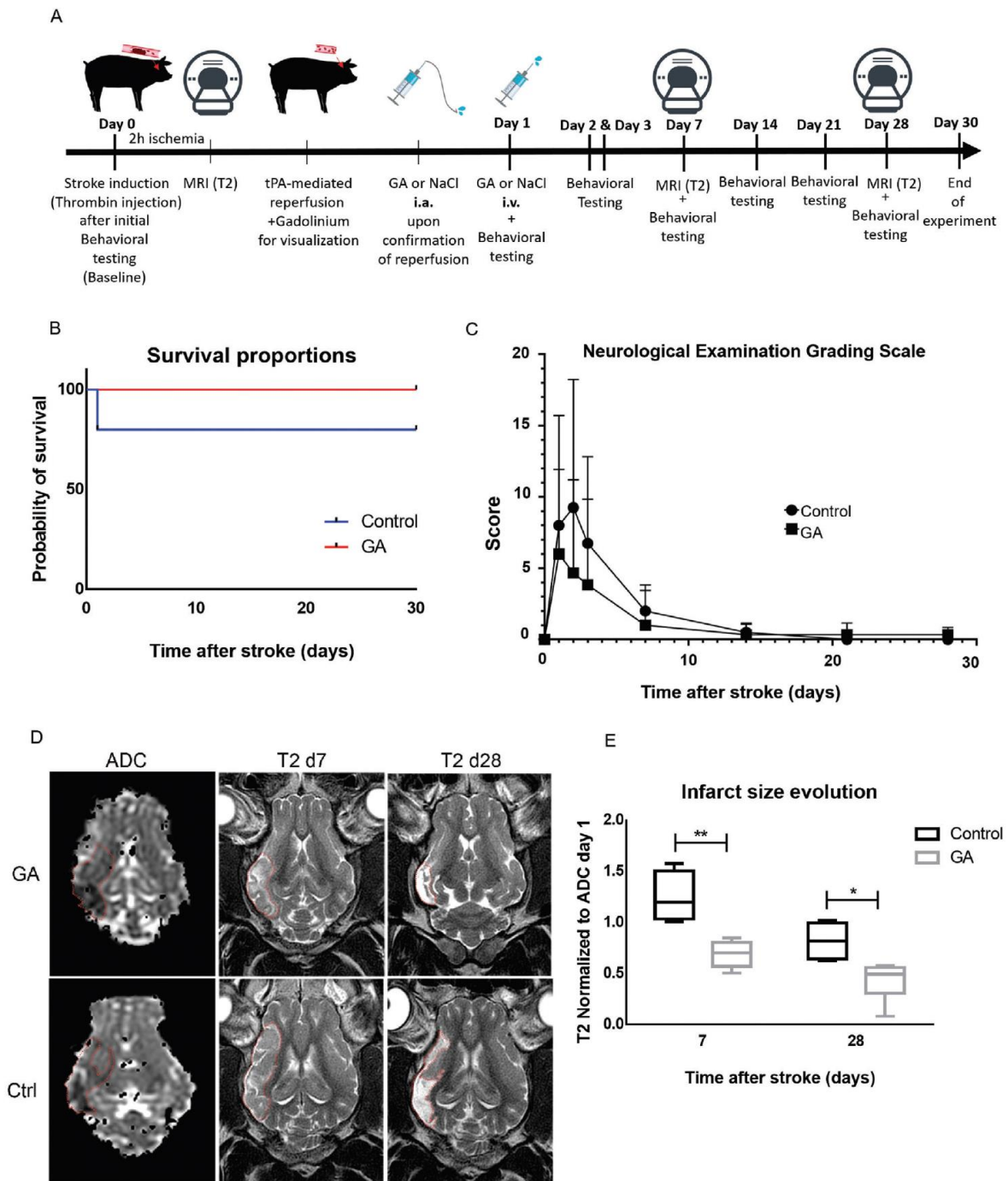


Figure 5. Effect of intra-arterial administration of glycolic acid on the endovascular model of stroke in swine. A) Experimental design: day 0, behavioral testing to establish baseline function followed by induction of stroke, apparent diffusion coefficient (ADC) magnetic resonance imaging (MRI) 2 h later to assess early infarct size, i.a. tissue plasminogen activator (tPA) injection for reperfusion, and i.a. glycolic acid (GA) or NaCl administration; day 1, GA or NaCl intravenous injection 24 h after stroke; day 1, day 2, day 3, day 7, day 14, day 21, and day 28 after stroke, behavioral testing to evaluate functional outcome; day 7 and day 28 after stroke, T2 MRI to evaluate infarct size evolution; and day 30 after stroke, transcardial perfusion. B) Graph showing the survival proportions in the GA-treated versus control group. Survival was 100% after GA treatment but only 80% in the control group. C) Scoring of functional outcomes with the Neurological Examination Grading Scale, assessed on day 1, day 2, day 3, day 7, day 14, day 21, and day 28 after stroke.

almost half of that in the control group. This lack of statistical significance could be attributed to the high variability of outcomes between animals. However, the effect size was large ($g = 0.61$) according to Cohen's rule of thumb, indicating that the findings may still be of practical significance. Notably, all animals had almost recovered by day 14, according to a selected battery of behavioral tests, despite the persisting brain damage seen in the MRI, indicating a relatively low sensitivity of the neurological evaluation scale.

3. Discussion

The protective role of GA has been studied in only one study in one neurological disease (Parkinson's disease).^[19] The study revealed that GA increased the viability of dopaminergic neurons exposed to a neurotoxin in vitro and that the increase in viability was mediated through support of mitochondrial activity.^[19] The current study is the first to investigate the neuroprotective effects of GA in stroke models both in vitro and in vivo. Important indications that GA may improve stroke outcomes were obtained from previous research: GA was found to protect mitochondrial function, and the genes responsible for the endogenous production of GA (i.e., *djr1.1*, *djr1.2*, and *glod-4*, which encode glyoxalases) were found to be upregulated in *C. elegans* dauer larva (an evolutionary survival strategy of that enables the larva to survive desiccation/rehydration). *C. elegans* L1 larvae enter dauer, a diapause larval stage, in metabolically unfavorable environmental conditions.^[14,15,19] Diapause allows invertebrates and nonmammalian vertebrates to survive for extended periods under adverse environmental conditions,^[39] whereas in mammals, it leads to delayed implantation.^[40] Broad comparisons of transcriptomic profiles among diapausing stages of distantly related invertebrates suggest that physiologically similar dormancy responses are achieved convergently by diverse regulatory strategies^[41] or, conversely, that diapause may be phylogenetically conserved, at least among mammals, given the common regulatory factors in different mammalian orders.^[42] Higher organisms, including humans, produce small amounts of GA in their cells through glyoxalases.^[21] However, such organisms appear to have lost the ability to dramatically increase the expression of those genes responsible for the production of GA during metabolic stress.^[43] Supporting this hypothesis, several studies have shown a neuroprotective effect of upregulating DJ-1 in certain neurological diseases.^[44–46] Although DJ-1 may appear to be a therapeutic target, gene-targeting treatments upregulating DJ-1 would need to be performed at least 24 h before an ischemic insult; clearly, such an approach cannot be applied in clinical care, as it would be required that the time-point of the ischemic insult is known in advance. In addition, it is unclear whether large enough amounts of glyoxal and methylglyoxal, the substrates of DJ-1 and glyoxalase domain-containing protein 4 (GLOD-4), are produced during is-

chemia and reperfusion to obtain the high amounts of GA and DL needed to allow them to exert their protective effect. Therefore, we hypothesized that artificially increasing GA levels in the brain would protect tissue from damage in the hypoxic state and metabolic halt induced by an ischemic stroke.

In order to test our hypothesis, we investigated the effects of GA in in vitro (OGD) and in vivo models of ischemia/reperfusion (GCI and MCAO). Our in vitro experiments showed that treatment with GA during reperfusion (i.e., during the change from ischemic to normal medium) resulted in strong protection against OGD-induced necrotic and apoptotic neuronal death. To differentiate between both types of cell death, we measured PI and NeuN 30 min after reperfusion to quantify necrotic cells and stained against NeuN and DRAQ5 to measure total neuronal loss 72 h after OGD to quantify apoptosis. PI is widely used to detect necrosis.^[47–50] The difference in the total amount of neurons 72 h after OGD allows one to discriminate between necrotic and apoptotic death.

Glutamate-mediated excitotoxicity has been shown to play a role in stroke and ischemia–reperfusion damage through increases in $[Ca^{2+}]_i$, which has a negative impact on cellular function and can activate apoptosis. In a recent study, we showed that GA reduces $[Ca^{2+}]_i$ in HeLa cells and sperm cells and enhances mitochondrial energy production.^[25] Therefore, we tested whether it also had such an effect on $[Ca^{2+}]_i$ in cortical neurons in the absence and presence of glutamate. Indeed, our results showed that increasing concentrations of GA reduced $[Ca^{2+}]_i$ in a concentration-dependent manner in both the absence and presence of 300×10^{-6} M glutamate, suggesting that the reduction of $[Ca^{2+}]_i$ could be one of the underlying mechanisms of action for the protective effect of GA in stroke.

We confirmed these strong neuroprotective properties of GA in 2 mouse models and an endovascular swine model of stroke. In general, postischemia treatment by i.a. administration of GA into the left carotid (GCI mice) or ipsilateral ascending pharyngeal artery (swine) immediately after reperfusion had a strong, positive effect on neuronal survival; the effect was not as strong after i.p. administration of GA in MCAO mice. In addition, groups treated with GA exhibited a significant reduction in infarct volume (MCAO and swine model) and complete rescue of neurons in brain areas with anoxic/hypoxic damage (GCI model). These effects were correlated with a better, if not significant, functional outcome and, in the case of the MCAO model, a nonsignificant reduction of the inflammatory reaction.

In the GCI mouse model, the method used to induce ischemia caused bilateral damage, but GA was applied only to the left carotid artery. In this way, the side ipsilateral to the intra-arterial GA injection was considered as the “treated side.” In contrast, the opposite hemisphere was regarded as the “control side” in each animal. The lack of effect on the contralateral side indicates that choosing an injection site of high proximity as close as possible

The lower score in the GA group compared with the control group was not statistically significant. $n_{\text{control}} = 5$ and $n_{\text{GA}} = 6$. D) Representative image showing the ADC signal on day 0 (left column) and the T2 signal on day 7 (middle column) and day 28 (right column) for a GA-treated (upper row) and control (lower row). E) Quantification of the infarct size. T2 signal on day 7 and day 28 after stroke normalized to ADC on day 0: GA-treated animals exhibited a significantly higher reduction in the infarct size compared with control on both day 7 and day 28 after stroke (day 7: control, 1.24 ± 0.24 ; GA, 0.69 ± 0.13 , $p = 0.0016$; day 28: control, 0.82 ± 0.19 ; GA, 0.43 ± 0.18 , $p = 0.0119$, unpaired *t*-test). ADC, apparent diffusion coefficient; GA, glycolic acid; MRI, magnetic resonance imaging.

to the damaged brain tissue can lead to better results because of faster distribution and increased accumulation of GA. This finding is in accordance with previous studies, which showed that the i.a. application route is more efficient than other methods in yielding high concentrations of the administered substance within a region of interest.^[51–53] Research has also shown that the permeability of the blood-brain barrier increases after a stroke^[54] and that i.a. injection of hyperosmotic solutions (such as the high concentrations of GA in our study) increases the permeability of the blood-brain barrier 30- to 50-fold for a short but essential time window (≈ 6 min).^[51] Thus, we hypothesized that ipsilateral intracarotid administration of GA may also positively influence the histological and functional outcome in focal stroke.

To examine that hypothesis, we aimed to administer GA intra-arterially in a mouse model of focal stroke. We selected the most commonly used and reliable animal model of stroke, the MCAO mouse model. However, because of technical difficulties, intracarotid application was not feasible in the available setting. Therefore, we decided to test the effects of i.p. GA on the outcome of focal ischemia. In agreement with previous findings in this model, MCAO led to infarcts that included large parts of the ipsilateral cortex and striatum, as observed by MRI (Figure 3C). Independent of the treatment, the infarct size showed a relatively high variability (Figure S3, Supporting Information), ranging from 2% to 40% of the ipsilateral hemisphere volume, although the mean was $\approx 15\%$, which is similar to previous reports.^[55] Large variations in ischemic volumes are not uncommon in this animal model and are generally attributed to the cerebral vasculature of C57Bl6 mice. Up to 40% variability is considered acceptable, as determined by a published protocol of standard operating procedures.^[56] This variability is due to interindividual anatomical differences in the Circle of Willis, i.e., the presence or absence of the ipsilateral posterior communicating artery (PcomA).^[57,58] To avoid this high interindividual variability, we used MRI to compare the intraindividual infarct volume reduction between day 1 and day 13 after ischemia with a paired *t*-test and found that GA but not vehicle significantly improved the evolution of infarct volume in this period (Figure 3D,E). Thus, GA treatment resulted in a better long-term anatomical outcome. GA treatment also positively affected MCAO-induced mortality and functional outcome and did not show any signs of toxicity. Furthermore, when considering only infarcts with volumes greater than 18% of the hemispheric volume, GA reduced mortality compared with vehicle treatment.

Regarding functional outcome, the corner test detected a positive effect of GA treatment on sensorimotor function after MCAO. Our results showed that vehicle-treated mice displayed significantly lower performance than sham-operated mice and that i.p. administration of GA reduced sensorimotor asymmetry to levels that were not significantly different from sham (Figure 3F). The corner test has consistently and reliably detected the influence of various substances on functional outcome after MCAO in previous studies^[59–61] and was the only functional test used in the present study that was sensitive enough to detect differences between sham- and vehicle-treated mice. Interestingly, the improvement in performance achieved by GA was independent of the infarct volume, suggesting that GA either increased the number of surviving neurons inside this area or supported neuronal plasticity. The quantification of surviving neu-

rons within the ischemic area did not show any significant differences between any of the groups. There are two possible hypotheses that may explain this surprising result: i) the Neurotrace⁺ area corresponds to the penumbra and ii) NeuN protein is expressed not only by neurons but also by astrocytes^[62,63] (astrocytes are known to be increased after stroke in the infarct and peri-infarct area^[64–66]). Supporting the first hypothesis, at the MRI on day 14, we found a significant positive correlation between ischemic volume and both the volume of missing tissue and the increased T2 signal in the areas of missing tissue compared with adjacent areas. This finding suggests that these areas had a higher water content because unrelated artifacts would not have shown any correlation with any of these parameters, and it may reflect an underlying liquefactive transformation on day 14 after stroke, as previously described.^[31,32] This missing tissue should not be mistaken for an enlargement of the lateral ventricles. In this study, we observed missing tissue even in regions posterior to the end of the lateral ventricles (approximately at the bregma between -3.7 and -3.15 mm). In this region, the pyramidal cell layer and the CA1 region of the hippocampus were completely missing (example in Figure S5D in the Supporting Information). If this were the case, the remaining Neurotrace⁺ tissue around this area would correspond to the penumbra. In the penumbra, the neuronal loss is patchy, as described previously,^[67,68] and therefore it is difficult to detect a significant reduction in cell density. Although GA did not alter the cell density in the infarct site, it reduced the ischemic core volume (measured as the missing volume) compared with the vehicle (the GA group was not significantly different from sham) and thus contributed to the improved functional outcome observed after stroke. Nevertheless, the hypothesis that this lack of difference is due to the presence of NeuN⁺ astrocytes or that the functional improvement is related to an increase in neuronal plasticity cannot be excluded and should be further investigated.

Because ischemia induces a robust immune response in the human and mouse brain, including an increase in numbers of astrocytes and microglia,^[62] we also tested whether GA affected the immune reaction in this model. When we evaluated the fluorescence marker levels of astrocytes and microglia between vehicle- and GA-treated groups independently of the infarct volume, we detected no significant difference. However, as indicated by functional and survival data, when analyzed independently, larger infarcts were associated with a significantly higher GFAP and Iba1 signal in the vehicle group but not in the GA group compared with sham. We did not observe this difference in smaller infarcts, where GFAP and Iba1 signals were increased in the both the vehicle- and GA-treated mice.

A possible explanation for the differences in the results between small and large infarct volumes may be the regions affected in each case. In brains with smaller infarct volumes, the main affected area was the striatum, which is the primary target of MCA supply and is known to have very low collateral density.^[69–71] The striatum is consistently infarcted even in mild strokes (30 min MCAO),^[29,72] whereas in severe MCAO (lasting 120 min), the necrotic area expands over the striatum to a significant fraction of the surrounding cortex, where a penumbra area is observed because of better collateral perfusion.^[73,74] Moreover, after MCAO the striatum displays certain metabolic changes that are typical of the infarct core rather than the penumbral area.^[71]

Comparing the GCI and MCAO models, the latter did not show significant differences between GA and vehicle groups, despite the apparent improvement in the infarct core and corner test performance for the GA group, which was not significantly different to sham. We believe that this is due to the route of administration in the MCAO model that delays the timing and reduces the concentration of GA achieved in the brain after reperfusion. Moreover, the other functional tests implemented in this model (pole test, catwalk test) were not sensitive enough to detect any significant differences between sham and MCAO independently of the treatment, so the lack of significant differences between the GA and vehicle groups was not unexpected.

Finally, rodent models lack the complexity of brains in larger mammals such as monkeys, swine, or humans, which have lobes, gyri, and sulci and much longer and more numerous axons. These differences may limit the potential of translating results from the mouse model into clinical practice. Therefore, we decided to test the effects of GA in an endovascular model of ischemic stroke in swine that was recently developed by Golubczyk et al.^[37] In this animal model, i.a. administration of GA during reperfusion after the pharmacological lysis of a clot showed remarkable results: GA treatment was able not only to completely salvage the penumbra but also to reduce the damage in the ischemic core. This reduction was associated with a nonsignificant improvement in functional outcome. However, in our study the functional data were difficult to interpret because large infarcts caused the pigs to lie on the ground, and they subsequently either recovered and stood up or, as in the case of one vehicle-treated animal, died. The fact that even swine with large infarcts could completely recover within a few days might reflect a lack of sensitivity of the functional tests performed. The lack of statistical significance could also be attributed to the high variability of outcomes between animals and the low number of animals used. In our experimental setup, the use of each animal as its own control (by MRI evaluation of damage before and after GA administration) was highly advantageous and relevant to the clinical setting. However, this approach was not possible for the functional tests, which reduced the number of animals in each group although it should be closer to a typical clinical study. As an example, a group size of at least 35 was necessary to show significant differences in neurological outcome with the same neurological score,^[38] but a study with such a large sample size would be impossible to perform in our setting. Despite the lack of statistical significance in our results on functional outcome, we believe that the behavioral results add value to the study. In absolute numbers, on day 2 the behavioral deficit in the control group was nearly twice that in the GA-treated group and the effect size ($g = 0.61$) was large according to Cohen's rule of thumb, indicating that the results may still have a practical significance. In any case, this endovascular model of ischemic stroke in swine, an animal in which the anatomical brain complexity is comparable to that in humans, almost completely mimics the ischemia time and current protocols used in stroke units. In the clinical setting, to protect the brain from the negative consequences of reperfusion, GA could be administered intra-arterially immediately after mechanical thrombectomy or localized pharmacological thrombolysis by using the same catheter that is normally used to perform these procedures. It is known that the mean time between patient arrival and thrombectomy/thrombolysis is 2.5 h,^[8] which is a rel-

atively small deviation from the administration protocol used in the swine model (2 h of ischemia + ≈ 15 min until reperfusion was observed). Thus, we believe that GA treatment is particularly valuable in the current era of mechanical thrombectomy and local lysis, and we hypothesize that it can facilitate broadening indications for these two procedures; however, this hypothesis can be tested only in clinical settings. To sum up, we believe that the results obtained in this model are representative of the results that can be expected in stroke patients.

The underlying molecular mechanism by which GA exerts its neuroprotective effects is currently being investigated in an ongoing study by our group. Previous research has suggested that GA can act as a calcium chelator.^[75] We recently published data suggesting that GA reduces $[Ca^{2+}]_i$, which is increased during stroke-induced excitotoxicity and preserves normal mitochondrial function, which is impaired after stroke.^[25] Our *in vitro* data obtained from cortical neurons suggest that the reduction of $[Ca^{2+}]_i$ is the critical neuroprotective factor in this case, and we hypothesize that this is the case because—as shown in the aforementioned study—increases in energy production were observed with GA concentrations as low as 2.5×10^{-3} M. Nevertheless, this concentration was not as effective as higher concentrations in preventing neuronal death. Regulation of $[Ca^{2+}]_i$ is a common feature among species that undergo desiccation at any developmental stage. The most extreme form of vertebrate diapause occurs in annual killifish, a polyphyletic assemblage of freshwater fish within the Aplocheilidae family (order Cyprinodontiformes), which are able to complete their life cycle in ephemeral habitats within a year.^[76–80] When their pond dries up, adult killifish die, leaving their fertilized eggs buried in the substrate, and developing embryos survive until the following wet season by entering diapause.^[81] Interestingly, in this species many of the genes that are upregulated only during desiccation in the diapause stage are linked to the regulation of calcium.^[82]

4. Conclusion

Taken together, our results suggest that GA treatment has a solid neuroprotective effect when administered at high concentrations, especially intra-arterially, immediately after the ischemic insult. This effect is mediated by the reduction of $[Ca^{2+}]_i$ during excitotoxicity. However, our results in mice have certain limitations, for example i) all experiments were performed on young male mice, so the effect in female mice and/or different age groups still needs to be studied, ii) mouse strains (C57BL/6N vs C57BL/6J), ischemia duration, analysis time points, and treatment administration routes differed between the two *in vivo* models, and this can create a discrepancy in their sensitivity, iii) although both models mimicked the mechanical thrombectomy that occurs in the clinical setting, neither of them mimicked the pharmacological thrombolysis that is achieved clinically with recombinant tissue plasminogen activator (rTPA), which could interact with GA.^[37,83,84] A swine model of stroke overcame these limitations by allowing thrombolysis with TPA and the *i.a.* delivery of GA. The results in this model not only further validated the results in the mouse models but even exceeded the expected outcome as GA ultimately protected the penumbra and even reduced the ischemic core. These results challenge the current knowledge that the fate of the ischemic core, as measured by DWI-sequences

in MRI, is already determined and could have important implications in the clinical setting as a potential treatment for stroke patients.

5. Experimental Section

In Vitro Hypoxia—OGD Procedure: To simulate IR in vitro, primary cortical neurons from E15.5 mice embryos were prepared and plated in 2 × 96-well plates (one for normoxia and one for evaluation of necrosis with DRAQ5 and PI 30 min after OGD or, alternatively, one for normoxia and one for evaluation of survival with NeuN 72 h after OGD). Plates were coated with poly-L-lysine (PLL), 10 µg per well in 100 µL H₂O, and neurons were plated at a concentration of 1 × 10⁶ cells mL⁻¹ in Neurobasal A (#1088022) media containing 5% B27 (#17504044), Pen-Strep (#10378016), and L-glutamine (#25030024) (all from Thermo Fischer Scientific, MA, USA), as previously described.^[85] On DIV 7, neurons were placed within the anoxic atmosphere and incubated in an N₂-filled gas chamber for 1 h with glucose-free acidic anoxic buffer (previously deoxygenated in an autoclave and bubbled with N₂ for 20 min) containing (in mmol L⁻¹): 140 NaCl, 3.6 KCl, 1.2 MgSO₄, 1 CaCl₂, and 20 HEPES at pH 6.4 and supplemented with 4 µmol L⁻¹ resazurin, 100 µmol L⁻¹ ascorbic acid, 0.5 mmol L⁻¹ dithionite, and 100 U mL⁻¹ superoxide dismutase. To mimic reperfusion, the anoxic buffer was washed out and replaced with Neurobasal A media as above but without phenol red and without antioxidants (pH 7.4) and supplemented with GA (stock solution 3.92 M diluted in water, pH adjusted to 7 with NaOH, final concentration 10 × 10⁻³ and 20 × 10⁻³ M, Sigma-Aldrich, Germany) or vehicle (ddH₂O). For the normoxic group, media was replaced with Neurobasal A media without phenol red and without antioxidants, and neurons were kept at 5% CO₂ and 37 °C. The reperfusion media in the plates used to evaluate necrosis included PI (81845, end concentration 5 × 10⁻⁶ M, Sigma-Aldrich, Germany), and these plates were fixed with 2% paraformaldehyde (PFA) 30 min after the OGD/normoxia. Plates used to evaluate apoptosis after 72 h were kept at 5% CO₂ and 37 °C for 1 h, after which more medium was added to the well to achieve a concentration of 5 × 10⁻³ M GA and the plates were left in the incubator for 72 h until fixation. This approach ensured that neurons were subjected to the same OGD conditions.

In Vitro Hypoxia—Cell Immunofluorescence and Quantification: To evaluate necrosis, cells were fixed as mentioned above 30 min after OGD/normoxia and imaged with an Opera High-Content Screening System (20× Air, PI: Ex: 561, Em: 600/40, PerkinElmer, MA, USA). Cells were then incubated at room temperature (RT) with blocking solution (5% donkey serum, 0.05% Triton X-100, and PBS) for 1 h. Primary antibody (NeuN Polyclonal, ab104224, Abcam, MA, USA) was added in block solution (1:1000 dilution) and incubated for 1 h at RT and then overnight at 4 °C. The next day, cells were washed three times (for 10 min per wash) with PBS and then incubated with the secondary antibody solution (AlexaFluor 555 a31570, Thermo Fisher Scientific, MA, USA; 1:500 in blocking buffer) for 2 h at RT and protected from light. After three washings with PBS, the cells were ready for observation. Microscopy images were obtained with an Opera High-Content Screening System (20× Air, Ex: 488 nm, Em: 568, PerkinElmer, MA USA). The same 10 fields per well were imaged after addition of PI and after staining with NeuN, and the numbers of NeuN⁺ and PI⁺ neurons were quantified with Image J software (National Institutes of Health, Bethesda, MD) in a semiautomated manner.

To quantify the surviving neurons, at 72 h after OGD/normoxia cells were fixed with 2% PFA for 35 min at RT or overnight at 4 °C. Cells were then incubated at RT with blocking solution (5% donkey serum, 0.05% Triton X-100, and PBS) for 1 h. Primary antibody (NeuN Polyclonal, ab104224, Abcam, USA) was added in blocking solution (1:1000 dilution) and incubated for 1 h at RT and then overnight at 4 °C. The next day, cells were washed three times (for 10 min per wash) with PBS and then incubated with the secondary antibody solution (AlexaFluor 555 a31570 Thermo Fisher Scientific, MA, USA; 1:500 in blocking buffer) for 2 h at RT and protected from light. After three washings with PBS, the neurons were incubated with DRAQ5 (62251, 1:10 000, Thermo Fischer Scientific, MA, USA) diluted in PBS for 5 min at RT, followed by aspiration and 3× PBS

rinsing. Microscopy images were obtained with an Opera High-Content Screening System (20× Air, NeuN: Ex: 488 nm, Em: 568, DRAQ5: Ex: 640, Em: 690/50 nm PerkinElmer, MA, USA). Ten fields per well were imaged, and the number of NeuN⁺ neurons was quantified with Image J software (National Institutes of Health, BethesdaMD, USA) in a semiautomated manner.

In Vitro Intracellular Calcium Measurements on Cortical Neurons: Primary cortical neurons from E15.5 C57Bl6 mouse embryos were prepared and plated in 96-well plates as previously described. At DIV 7, neurons were incubated for 20 min at 37 °C with 50 µL per well of 2.5 × 10⁻⁶ M FLUO-4-AM (#F14201; Thermo Fischer Scientific, MA, USA) diluted in HBSS. After incubation, FLUO-4-AM was replaced by HBSS (H6648, Sigma-Aldrich, Germany) for 5 min at 37 °C. HBSS was then replaced by 50 µL per well of fresh medium A (Neurobasal A media [#1088022]) containing 2% B27 (#17504044), 0.4% Pen-Strep (#10378016) and 1% L-glutamine (#25030024), all from Thermo Fischer Scientific, MA, USA. The cells were left to stabilize in medium A for 10 min before starting the measurements. Fluorescence measurements were performed in a FLUOstar Optima (BMG Labtech, Germany) plate reader with the 485 nm excitation filter and the 520 nm emission filter. A baseline was recorded for 3 min, after which the fluorometer was paused and 5 µL of either PBS (vehicle), 4.5 × 10⁻³ M NaCl (as osmolality control), or 5 × 10⁻³, 10 × 10⁻³, and 20 × 10⁻³ M of GA diluted in PBS were added to each well. The measurement continued for the next 6 min and was followed by another pause for the addition of ionomycin (#I3909; Sigma-Aldrich, Germany) at a concentration of 2 × 10⁻⁶ M. The measurement was allowed to continue for a total of 25 cycles (762 s).

For the experiments with glutamate, the baseline was recorded up to the addition of 300 × 10⁻⁶ M glutamate (#G8415; Sigma-Aldrich, Germany) after 230 s of measurements and the posterior addition of GA at time-point 296 s. After that, the measurements continued for a total of 25 cycles without adding ionomycin.

GCI Mouse Model—Animals and Housing: A total of 32 six- to eight-week-old male C57BL/6N mice (Charles River Laboratories, Sulzfeld, Germany) were used in this part of the study. All experimental procedures were performed in accordance with German guidelines on animal welfare and were approved by the local regulatory committee (Regierung von Oberbayern, Munich, Germany). The mice were housed at the Institute of Stroke and Dementia Research animal husbandry area, where they were kept under a 12 h light/dark cycle (lights on from 6:00 to 18:00) in an enriched environment with ad libitum access to food and water.

GCI Mouse Model—Surgery: GCI was induced as previously described.^[27,28] Briefly, 32 C57BL/6N six- to eight-week-old male mice with a bodyweight of 20 to 24 g (Charles River Laboratories, Sulzfeld, Germany) were anesthetized with a combination of buprenorphine (0.1 mg kg⁻¹, Essex Pharma, Germany) and 2% isoflurane (Halocarbon Laboratories, Peachtree Corners, GA, USA) in 50% O₂/50% N₂. Body temperature was tightly controlled with a feedback-controlled heating pad (FHC, Bowdoinham, ME, USA). Regional cerebral blood flow (rCBF) was continuously monitored over the right hemisphere with a laser Doppler perfusion monitor (Periflux 4001 Master, Perimed, Sweden). The neck was opened, and both common carotid arteries were exposed. A catheter was placed in the left common carotid artery, and then both common carotid arteries were occluded with atraumatic clips. After 7.5 min, the clips were removed and 50 µL of GA (3.92 M stock solution in water, with a pH adjusted to 7 with NaOH; end concentration in PBS, 120 × 10⁻³ M; n = 7 mice) or PBS (0.01 M, n = 9) were injected into the left common carotid artery. Thereafter, the catheter was removed, the incision was sutured, and the animals received 100 µL of carprofen (1 mg mL⁻¹) s.c. for postoperative analgesia. Sham-operated mice (n = 16) underwent the same surgical procedure without carotid clipping. Animals were randomly and blindly allocated to the respective treatment group shortly before injection of GA or PBS.

GCI Mouse Model—Histology: One week after GCI, mice were reanesthetized and transcardially perfused with 4% PFA. Brains were extracted, dehydrated, embedded in paraffin, cut into 4 µm thick coronal sections and stained with cresyl violet for neuronal cell counting. Intact neurons in the hippocampal CA1a, CA1b, CA2, and CA3 subregions were counted

with Image J (National Institutes of Health, Bethesda, MD) by an investigator blinded to the treatment of the mice. For this analysis, sections were assessed per mouse.

MCAO Mouse Model—Animals and Housing: A total of 40 C57BL/6J 12-week-old male mice (Janvier Labs, Le Genest-Saint-Isle, France) were used in this study. All experimental procedures were performed according to the ARRIVE guidelines, European Community Council Directives 86/609/EEC, and German national laws and were approved by the local authority (Landesamt für Gesundheit und Soziales, Berlin, Germany). The mice were housed at the Charité animal facility, where they were kept under a 12 h light/dark cycle (lights on from 6:00 to 18:00) in an enriched environment with ad libitum access to food and water.

MCAO Mouse Model—Surgery: Transient (60 min) MCAO was performed according to a standard protocol.^[86] This process creates a brain infarction in the MCA area. The resulting infarct includes broad damage in the striatum and ipsilateral cerebral cortex and the presence of a relatively small penumbral area in the cortex.^[74] A total of 34 mice underwent MCAO surgery (18 treated with GA and 16 with the vehicle), and 6 mice received sham surgery and GA treatment. Animals were randomly allocated to the two treatment MCAO groups or the sham group. Anesthesia was induced with 2.5% isoflurane (Forene, Abbott, Wiesbaden, Germany) in a 1:2 oxygen/nitrous oxide mixture and maintained at 1.0% to 1.5% throughout the operation. A silicon rubber-coated monofilament (no. 701956PK5Re Doccol Corporation, Sharon, MA, USA) of 0.19 ± 0.01 mm in diameter was inserted into the common carotid artery and advanced until it reached the origin of the MCA, where it remained for 60 min while the mouse was allowed to recover from anesthesia inside a heated cage that maintained body temperature at 37 °C. At the end of the 60 min of MCA occlusion, the mouse was reanesthetized, the monofilament was gently retracted, and the internal carotid artery was permanently ligated. Exactly the same procedure was used in the sham operation, but the monofilament was removed as soon as it reached the origin of the MCA. GA or NaCl i.p. injection was performed at the end of the operation, immediately after closure of the skin wound. Bupivacaine gel (1%) was topically applied to the wound for postsurgical pain prevention, and the mouse received 500 μ L of saline subcutaneously for rehydration. After the operation, mice were placed in a heated cage for 1 h before being returned to their home cages. In the recovery phase after the operation, food and pellets soaked in water were provided on the cage floor.

The second batch of MCAO operations was performed to test whether administering GA sooner after MCAO would improve the efficacy of the treatment. This batch included 30 12-week-old male C57Bl/6J mice (14 treated with GA, 14 treated with vehicle, and 2 untreated [sham]). In this experiment, the i.p. injection was performed immediately after removal of the monofilament to minimize the delay introduced by wound suturing. Except for the timing of administration of GA or vehicle, the rest of the surgical and postoperation process remained unaltered.

MCAO Mouse Model—Substance Preparation for i.p. Administration: 100 μ L of GA or 0.9% NaCl (vehicle) solution were injected i.p. after the operation until day 3 after the MCAO/sham operation. For the GA solution, GA powder (Glycolic Acid, Sigma-Aldrich) was diluted in pure water to obtain a final concentration of 15.6 mg mL⁻¹ (60 mg kg⁻¹) for i.p. injection. The pH was adjusted to 7 with NaOH.

MCAO Mouse Model—Histology: Fourteen days after MCAO, mice were deeply anesthetized with ketamine/xylazine (150 and 15 mg kg⁻¹, respectively) and, upon complete loss of pedal reflexes, transcardially perfused with a 0.1 M PBS solution. Brains were carefully extracted and kept in 4% PFA in a 15 mL Falcon tube overnight at 4 °C. On the next day, for cryoprotection brains were incubated in 30% sucrose until they sank. Then, brains were frozen with the *n*-butanol procedure in which 10 mL of *n*-butanol were added in a 15 mL Falcon tube and cooled in liquid nitrogen to -50 °C. Once this temperature was reached, the brains were inserted into the Falcon tube, which was kept in liquid nitrogen for one minute to cool it to -80 °C. The brains were then ready for immediate storage at -80 °C. Deeply frozen brain tissue was mounted on the sliding microtome (Leica SM210R) with OCT Tissue-Tek (Sakura Finetek Europe B.V., NL) and kept frozen with the addition of dry ice for cutting. Sequential sections of 60 μ m

in thickness were acquired and transferred sequentially into 96-well plates filled with freezing medium (50% PBS, 25% glycerol, and 25% ethylene glycol) for further storage at -20 °C.

MCAO Mouse Model—Staining of Brain Sections: NeuroTrace staining was performed for the histological definition of lesion volume, and NeuN staining was performed for quantification of surviving neurons. On staining day 1, sections were washed with PBS (pH 7.4) three times for 10 min each and then incubated with blocking buffer (5% donkey serum, 0.1% TritonX-100 in PBS) for 1 h at RT. Subsequently, the primary antibody (rabbit anti-NeuN, ABN78, Sigma-Aldrich, Germany) was added in a 1:500 dilution and the sections were kept at 4 °C overnight. On staining day 2, after washing three times for 10 min each with 0.1% Triton-PBS, the sections were incubated with the secondary antibody solution containing 1% donkey serum, 1:500 Ab[†] (antirabbit Alexa 568, A-10042 Invitrogen, USA), 1:250 NeuroTrace 435 (N21479 Invitrogen, USA) and 0.1% Triton in PBS. After 2 h at RT, the sections were washed again with PBS three times for 10 min each, mounted on gelatin-covered glass slides and coverslipped for later observation. For the GFAP and Iba1 staining of brain sections, the same process was followed, but the primary antibodies were goat anti-GFAP (ab53554, Abcam USA) in 1:750 dilution and rabbit anti-Iba1 (019-19741, FUJIFILM Wako Pure Chemical Corporation USA) in 1:750 dilution. The secondary antibodies used were donkey antigoat Alexa 555 (A-21432 Invitrogen, USA) for the GFAP labeling and donkey antirabbit Alexa 488 (A-21206, Invitrogen, USA) for the Iba1 labeling.

MCAO Mouse Model—Functional Tests: Besides causing histological damage, MCAO is known to induce deficits in motor function, including motor coordination, balance, and muscle strength, with mice showing a preference for using the nonaffected limb.^[87] Therefore, different functional tests were performed to assess such deficits.

MCAO Mouse Model—Pole Test: The pole test is a method for simple motor function evaluation.^[88,89] After preoperative training, the mice performed the test on day 8 after MCAO. Animals were placed on top of a vertical pole, 10 mm in diameter and 55 cm long, and were observed as they turned around and descended the pole (snout first). The scoring began when the animal started the turning movement. The time taken to make a full 180° turn (time to turn) and latency to reach the ground (time to descend) were recorded. Mice had to descend successfully three times. Trials in which mice took longer than 5 s to turn or longer than 20 s to descend were excluded. Pausing was also an exclusion criterion.

MCAO Mouse Model—Gait Analysis: For gait analysis, the CatWalk (Noldus Information Technology) automated, computer-assisted system was used, which is often used to assess locomotion defects in stroke mouse models.^[90] The CatWalk apparatus comprises a long, elevated glass runway platform that is fluorescently illuminated from the inside; the light is reflected in the direction of the floor when pressure (weight) is applied on top. A camera is mounted underneath the glass platform to record the walking pattern. At the beginning of the experiment, the animals' home cage was placed at one end of the platform. Then, the mice were placed on the opposite end and allowed to walk across the platform voluntarily toward their home cage. Analysis was performed with CatWalk XT 10.5 Software, which visualizes the footprints and calculates statistics regarding their dimensions and the time and distance ratios between footfalls. For a trial to be considered successful, the speed should not vary by more than 60% and the run should be uninterrupted (i.e., the mouse should not stop on the runway). Unsuccessful trials were repeated until three successful trials were reached. Before baseline acquisition, mice were preoperatively trained for 3 days with the CatWalk system (3 runs per day). The test was then performed on day 10 after MCAO.

MCAO Mouse Model—Corner Test: The corner test, which was developed for measuring sensorimotor asymmetries after unilateral corticostriatal damage, was performed on day 12 after stroke.^[91] The testing arena was composed of two connected cardboard walls that form a corner of $\approx 30^\circ$. A small opening was left at the junction of the walls to motivate the mice to reach deep into the corner. At the beginning of the test, each animal was placed halfway from the corner and facing it. As the mice walk into the corner, their vibrissae were stimulated and, in response, they rear and turn to either side (left or right). Each session lasted 10 min, and the turns

in each direction were recorded. The LI was calculated with the following formula, as described previously by Balkaya and Endres, 2010^[92]

$$LI = \frac{TL - TD}{TD + TL} \quad (1)$$

where TL means turn left (stroke-affected side), and TD means turn right (nonaffected side).

MCAO Mouse Model—Infarct Volume Measurement by MRI: Ischemic lesion size was quantified by MRI (Bruker 7T PharmaScan 70/16) on day 1 and day 13 after MCAO. Analysis software (AnalyzeDirect, Overland Park, USA) was used to manually define the infarct size. After focal ischemia, cerebral edema is a commonly observed pathology that must be accounted for when measuring the infarct size. Lesion volumes were determined by computer-aided manual tracing of the lesions and corrected for the space-occupying effect of brain edema with the following equation^[93]

$$\%HLVe = \frac{2 \times LVe}{HVC + HVi} \times 100 \quad (2)$$

where %HLVe is the edema-corrected lesion volume as a percentage of the hemispheric volume, HVC and HVi represent the contralateral and ipsilateral hemispheric volumes, and LVe is the edema-corrected lesion volume.

MCAO Mouse Model—Stereological Evaluation: For the stereological analysis, a Zeiss Axiomager I (Zeiss, Göttingen, Germany) and StereoInvestigator Software 8.0 (MicroBrightField, Magdeburg, Germany) was used. To calculate the infarct volume and the number of surviving (NeuN-positive) neurons in the infarct area, a series of brain sections of 60 μm in thickness was used. Every 360 μm was sampled, starting from the first section with an obvious infarct (as defined by the Neurotrace 435 staining) and ending with the last one with an obvious infarct. Then, the optical fractionator workflow provided by the software was used to extrapolate the sampled subvolumes and thus estimate the volume of the entire cell population. A virtual space called an optical dissector was used, and counting rules were followed to prevent overestimating. In each brain section, the infarcted area that was still present (infarct volume) and the infarcted area that was missing because of cyst formation after necrosis (ischemic core volume) were separately outlined. Then, the neuronal density within the infarcted volume and the neuronal density on the intact contralateral (control) side were estimated and the ratio between the two densities were calculated.

MCAO Mouse Model—GFAP and Iba1 Fluorescence Signal Analysis: Three sections per brain were imaged with an Apotome.2 fluorescence microscope (Zeiss, DE), 4 \times objective, and mosaic function. The images were then analyzed in Image J (National Institutes of Health, Bethesda, MD). Briefly, after background removal, the ischemic area defined by a high Iba1 signal was outlined, and the mean fluorescence intensities of the Iba1 and GFAP signals in that area were measured. The rest of the hemisphere ipsilateral to ischemia (excluding the ischemic area and ventricles) was also outlined, and the mean fluorescence intensity of both markers was measured. Last, the contralateral hemisphere (ventricles excluded) was outlined, and the mean fluorescence intensity for both markers was measured.

Endovascular Model of Ischemic Stroke in Swine: Animal procedures were approved by the local Ethics Committee of the Warsaw University of Life Sciences in Warsaw, Poland (WAW2/046/2021). Eleven male juvenile (5-month-old) domestic pigs (mean weight, 35 kg) were included in the study. Endovascular procedures were performed in a dedicated large animal surgical suite located in the vicinity of the MRI scanner at the School of Life Sciences, Warsaw, Poland. Animals were randomly divided into two groups: GA treatment ($n = 6$) and placebo control ($n = 5$). To minimize stress, the animals were acclimated after arrival at the animal facility for at least 1 week.

X-Ray Guided Endovascular Procedure: Anesthesia was induced with atropine (0.05 mg kg⁻¹ i.m., Polfa, Poland), xylazine (3 mg kg⁻¹ i.m., Vetoquinol, Poland), and ketamine (6 mg kg⁻¹ i.m., Vetoquinol, Poland). Before intubation, animals received propofol (5 mg kg⁻¹ per hour i.v., B. Braun Melsungen AG, Germany), and after intubation, anesthesia was

continued with isoflurane (1% to 3%, Baxter, USA). During the entire procedure, vital parameters were monitored (blood pressure, respiratory rate, and heart rate). Analgesia was provided every 4 h with butorphanol (0.2 mg kg⁻¹ i.m., Zoetis, Poland). The endovascular procedure was performed under sterile conditions. The introducer (4F) was inserted percutaneously into the femoral artery. Then, the endovascular catheter (4F, 110 cm, Vertebral, Balton) was advanced to the right ascending pharyngeal artery (APA) over a hydrophilic guidewire (Balton) by using contrast agent (Iomeron, 400 mg J mL⁻¹ Medicovert) and a C-arm. Then, the catheter was secured in place, and the animal was transferred from the surgical suite to a 3T MRI scanner (GE Healthcare).

Magnetic Resonance Imaging, Infarct Induction, and Treatment Administration: The MRI protocol included the following: T2w (TE/TR = 98/4381) for anatomical reference, T1 and T1+contrast (TE/TR = 14/500), PWI, SWI (TE/TR = 33/42) to detect thrombus, and DWI to visualize the infarct core (with multi b value; TE/TR = 99/3979). Dynamic gradient-recalled echo sequences/echo planar imaging (GRE/EPI, TE/TR = 52/3200) were also used for real-time MRI assessment of intravenous perfusion and trans-catheter cerebral perfusion. After acquiring the baseline scans, intravenous sodium nitroprusside (5 mg mL⁻¹, Sigma-Aldrich) was administered to reduce blood pressure, with an initial bolus of 0.5 mL and continuous infusion at 10 mL per hour for 30 min. Thrombin (200 U mL⁻¹, Biomed, Poland) was mixed with Gadovist at a 1:20 volume ratio, and then a sodium nitroprusside 500 μL bolus of a mixture was immediately injected intra-arterially (400 mL per hour) with an infusion pump. After thrombin administration, SWI and DWI scans were performed to confirm blockage. Two hours after thrombin injection, tPA (20 mg at a concentration of 1 mg mL⁻¹ with an infusion speed of 400 mL per hour) was injected intra-arterially. Five minutes after tPA injection, the experimental and vehicle groups received GA or vehicle, respectively, intra-arterially. Then, the animals were removed from the scanner, and the catheter and introducer were removed. After recovery from anesthesia, animals were returned to the livestock housing, except for 2 animals that had to be transferred to the intensive care unit. The second dose of treatment (GA vs vehicle) was administered intravenously after 24 h. Follow-up MRI scans were performed 7 and 28 days after stroke induction.

Blood Sample Tests: Before surgery and during MRI follow-ups, blood samples were collected for morphology and gasometry. Morphology included white blood cell count (WBC), red blood cells (RBCs) and platelets (PLT), hemoglobin level (HGB), hematocrit (HCT), mean red blood cell volume (MCV), mean corpuscular hemoglobin (MCH), mean hemoglobin concentration (MCHC), red blood cell content, red blood cell distribution width (RDW), mean platelet volume (MPV), platelet distribution width (PDW), and plateletcrit (PCT). Blood gas analysis was aimed at assessing the acid-base balance. Blood pH, partial pressure of carbon dioxide (pCO₂), partial pressure of oxygen (pO₂), the concentration of bicarbonate (cHCO₃), oxygen saturation (SO₂), level of Na⁺, K⁺, Ca⁺⁺, Cl⁻, total carbon dioxide concentration (cTCO₂), anion gap (Agap and Agapk), hematocrit (Hct), hemoglobin (cHgb), glucose (Glu), lactate (Lac), and creatinine (Crea) were measured.

Postoperative Care: For 24 h after the procedure, animals were kept in solitary confinement to allow them to recover and enable to assess their condition before they were returned to the herd. Animals received antibiotic prophylaxis (Penicillin LA 24 000 U kg⁻¹) and analgesic therapy (butorphanol 0.4 mg kg⁻¹ and metamizole 30 mg kg⁻¹) administered intramuscularly. After the operation, the animals were in good general condition with easily detectable deficits. Two pigs (one from the control group and one from the GA group) required intensive care for 3 days after the procedure because of contralateral paralysis. In addition, one pig in the control group died 24 h after stroke induction.

Behavioral Assessment: Animals were subjected to neurological assessment with the Neurological Examination Grading Scale, as previously described.^[38] Testing was done on day 0 (before the procedure) and day 1, day 2, day 3, day 7, day 14, day 21, and day 28.

Euthanasia: After the last MRI follow-up scan at 28 days, animals received a lethal dose of sodium pentobarbital (Euthasol, Fatro, Poland). After obtaining access to the heart, transcardial perfusion was performed. Perfusion pressure was maintained at 120–140 mm Hg and included a

prewash with 5% sucrose and 4% PFA solution. The brains were extracted from the skull and placed in the PFA solution for postfixation.

Statistical Analysis: All data were analyzed with GraphPad Prism 6 (GraphPad Software, San Diego, USA). The statistical tests used for each analysis are explained in the figure legends. Generally, p values of less than 0.05 were considered statistically significant. Data were presented as mean \pm SEM. A total of 3 biological replicates ($n = 3$) consisting of 5 technical replicates each (mean of 5 wells per condition per plate) were used in the in vitro OGD model for evaluation of necrosis (ratio of PI+/NeuN+ neurons, 30 min after OGD; Figure 1C; one-way ANOVA followed by Tukey's multiple comparisons test) and apoptosis (number of NeuN+ neurons normalized to normoxia, 72 h after OGD; Figure 1D; unpaired t -test); a total of $n = 6$ was used for the calcium influx experiments (Δ Fluo-4 fluorescence normalized to timepoint 0; Figure 1E; two-way ANOVA followed by Sidak's multiple comparisons test); and a total of $n = 12$ was used for the glutamate-dependent calcium influx experiments (Δ Fluo-4 fluorescence normalized to the timepoint pretreatment; Figure 1F; one-way ANOVA followed by Tukey's multiple comparisons test).

In the in vivo GCI model, the group sizes were as follows: $n_{\text{sham}} = 16$, $n_{\text{vehicle}} = 9$, and $n_{\text{GA}} = 7$. The number of neurons stained with cresyl violet is presented (Figure 2C). One-way ANOVA followed by Dunnett's multiple comparisons test was performed.

In the in vivo MCAO model, the group sizes and statistical tests used were described for each graph. Survival graph: Figure 3B; $n_{\text{GA}} = 18$, $n_{\text{vehicle}} = 16$, and $n_{\text{sham}} = 6$; Mantel–Cox survival test, Chi square evaluation. Infarct size day 13 versus day 1 for GA group: Figure 3D, values represent the size of infarct; $n_{\text{GA}} = 17$; paired t -test. Infarct size day 13 versus day 1 for vehicle group: Figure 3E, values represent the size of infarct; $n_{\text{vehicle}} = 10$; paired t -test. Stereological quantification: Figure 3F, values represent the volume in mm^3 ; $n_{\text{GA}} = 17$, $n_{\text{vehicle}} = 10$, and $n_{\text{sham}} = 5$; unpaired t -test. Corner test: Figure 3G, values represent the laterality index; $n_{\text{GA}} = 17$, $n_{\text{vehicle}} = 13$, and $n_{\text{sham}} = 6$; one-way ANOVA followed by Bonferroni's multiple comparisons test. Correlation between LI and infarct size: Figure 3H, $n_{\text{GA}} = 17$, $n_{\text{veh}} = 13$, and $n_{\text{sham}} = 6$; Pearson's r evaluation. Microglia and astrocyte activation: Figure 4, values represent the mean fluorescence intensity; $n_{\text{sham}} = 3$, $n_{\text{veh}} = 6$, and $n_{\text{GA}} = 7$; one-way ANOVA followed by Tukey's multiple comparisons test. Endovascular model of stroke in swine: in Figure 5B, values represent probability of survival, $n_{\text{control}} = 5$ and $n_{\text{GA}} = 6$; in Figure 5C, values represent neurological score, $n_{\text{control}} = 4$ and $n_{\text{GA}} = 6$, and in Figure 5D, values represent the lesion volume in the T2 MRI sequence normalized to the lesion volume in the ADC sequence (ischemic core on day 0), $n_{\text{control}} = 4$ and $n_{\text{GA}} = 6$.

Supporting Information

Supporting Information is available from the Wiley Online Library or from the author.

Acknowledgements

This work was funded by the Deutsche Forschungsgemeinschaft (DFG, German Research Foundation) under Germany's Excellence Strategy within the framework of the Munich Cluster for Systems Neurology (EXC 2145 SyNergy - ID 390857198) and by the German Ministry for Economy and Energys with an EXIST-Forschungstransfer Grant (GLYMIPRO-FKZ03EFLBY173). The authors would like to thank Maria Sady from the DVM Center for Translational Medicine for her support with the paperwork and work with the pigs during the experimental procedures.

Conflict of Interest

F.P.-M. has a patent pending on the use of glycolic acid in ischemia. D.G., P.W., and M.J. are co-owners of Ti-com, which performed the swine experiments. All other authors declare no competing interests.

Author Contributions

A.C. and D.B. contributed equally to this work. F.P.-M. designed and coordinated the study. F.P.-M., I.R.Á., and C.F.-S. designed the OGD experiments. F.P.-M. and N.P. designed the GCI experiments. A.M., K.W., and F.P.-M. designed the MCAO experiments. M.J., P.W., Z.G., D.G., and F.P.-M. designed the swine experiments. I.R.Á. and Y.D. performed the OGD in vitro experiments, including imaging and analysis. N.P. coordinated the GCI experiments. U.M. performed the GCI operations and assessment of neuronal survival. A.M., D.B., and K.W. coordinated the MCAO experiments. D.B., K.W., and C.D. performed the MCAO operations and GA administration. L.W., M.A., and A.C. performed the assessment of infarct size by MRI and functional tests and analyzed them for the MCAO mouse model. A.C. and Y.D. performed the histological processing and analysis of the MCAO brain tissue. A.C. performed the stereological analysis of the MCAO brains. P.W., Z.G., and D.G. performed the endovascular swine model experiments. M.J., P.W., and D.G. analyzed the data from the swine model. F.P.-M., A.M., N.P., A.C., D.B., and U.M. wrote the manuscript. All other authors critically revised and corrected the manuscript.

Data Availability Statement

The data that support the findings of this study are available from the corresponding author upon reasonable request.

Keywords

glutamate-dependent excitotoxicity, ischemia–reperfusion damage, neuroprotection, Stroke

Received: July 28, 2021

Revised: November 2, 2021

Published online: December 14, 2021

- [1] GBD 2016 Stroke Collaborators, *Lancet Neurol.* **2019**, *18*, 439.
- [2] D. Mozaffarian, E. J. Benjamin, A. S. Go, D. K. Arnett, M. J. Blaha, M. Cushman, S. R. Das, S. de Ferranti, J.-P. Després, H. J. Fullerton, V. J. Howard, M. D. Huffman, C. R. Isasi, M. C. Jiménez, S. E. Judd, B. M. Kissela, J. H. Lichtman, L. D. Lisabeth, S. Liu, R. H. Mackey, D. J. Magid, D. K. McGuire, E. R. Mohler, C. S. Moy, P. Muntner, M. E. Mussolino, K. Nasir, R. W. Neumar, G. Nichol, L. Palaniappan, *Circulation* **2016**, <https://doi.org/10.1161/cir.0000000000000350>
- [3] J. D. Schaechter, *Prog. Neurobiol.* **2004**, *73*, 61.
- [4] R. Leigh, L. Knutsson, J. Zhou, P. C. van Zijl, *J. Cereb. Blood Flow Metab.* **2018**, *38*, 1500.
- [5] A. G. Chung, J. B. Frye, J. C. Zbesko, E. Constantopoulos, M. Hayes, A. G. Figueroa, D. A. Becktel, W. Antony Day, J. P. Konhilas, B. S. McKay, T.-V. V. Nguyen, K. P. Doyle, *eneuro* **2018**, <https://doi.org/10.1523/eneuro.0076-18.2018>
- [6] L. Hoyte, P. A. Barber, A. M. Buchan, M. D. Hill, *Curr. Mol. Med.* **2004**, *4*, 131.
- [7] A. Shuaib, K. R. Lees, P. Lyden, J. Grotta, A. Davalos, S. M. Davis, H.-C. Diener, T. Ashwood, W. W. Wasiewski, U. Emeribe, *New Eng. J. Med.* **2007**, *357*, 562.
- [8] Á. Chamorro, S. Amaro, M. Castellanos, T. Segura, J. Arenillas, J. Martí-Fàbregas, J. Gállego, J. Krupinski, M. Gomis, D. Cánovas, X. Carné, R. Deulofeu, L. S. Román, L. Oleaga, F. Torres, A. M. Planas, *Lancet Neurol.* **2014**, *13*, 453.
- [9] K. L. Lambertsen, B. H. Clausen, A. A. Babcock, R. Gregersen, C. Fenger, H. H. Nielsen, L. S. Haugaard, M. Wirenfeldt, M. Nielsen, F. Dagnaes-Hansen, H. Bluethmann, N. J. Faergeman, M. Meldgaard, T. Deierborg, B. Finsen, *J. Neurosci.* **2009**, *29*, 1319.

- [10] F. deBilbao, D. Arsenijevic, T. Moll, I. Garcia-Gabay, P. Vallet, W. Langhans, P. Giannakopoulos, *J. Neurochem.* **2009**, *110*, 12.
- [11] P. A. Lapchak, *Expert Opin. Pharmacother.* **2010**, *11*, 1753.
- [12] C. Erkut, S. Penkov, H. Khesbak, D. Vorkel, J.-M. Verbavatz, K. Fahmy, T. V. Kurzchalia, *Curr. Biol.* **2011**, *21*, 1331.
- [13] C. Erkut, S. Penkov, K. Fahmy, T. V. Kurzchalia, *Worm* **2012**, *1*, 61.
- [14] C. Erkut, A. Vasilj, S. Boland, B. Habermann, A. Shevchenko, T. V. Kurzchalia, *PLoS ONE* **2013**, *8*, e82473.
- [15] C. Erkut, V. R. Gade, S. Laxman, T. V. Kurzchalia, *eLife* **2016**, *5*, e13614.
- [16] C. Erkut, T. Kurzchalia, *Planta* **2015**, *242*, 389.
- [17] M. Gourdin, P. Dubois, *Artery Bypass*, IntechOpen, London **2013**.
- [18] J. Sullivan, *Bad Things Happen in Ischemia*, WSU Emergency Medicine Cerebral Resuscitation Laboratory, **2008**. <https://en-academic.com/dic.nsf/enwiki/2049350>
- [19] Y. Toyoda, C. Erkut, F. Pan-Montojo, S. Boland, M. P. Stewart, D. J. Müller, W. Wurst, A. A. Hyman, T. V. Kurzchalia, *Biol. Open* **2014**, *3*, 777.
- [20] P. J. Thornalley, *Biochem. Soc. Trans.* **2003**, *31*, 1343.
- [21] J.-Y. Lee, J. Song, K. Kwon, S. Jang, C. Kim, K. Baek, J. Kim, C. Park, *Hum. Mol. Genet.* **2012**, *21*, 3215.
- [22] L. Lin, X. Wang, Z. Yu, *Biochem. Pharmacol.* **2016**, *5*, 213.
- [23] M. P. Goldberg, D. W. Choi, *J. Neurosci.* **1993**, *13*, 3510.
- [24] T. W. Lai, S. Zhang, Y. T. Wang, *Prog. Neurobiol.* **2014**, *115*, 157.
- [25] S. Bour, Y. Dening, M. Balbach, I. Poser, I. Ramírez Álvarez, H. den Haan, C. Kluge, R. Naumann, R. Oertel, I. Alba-Alejandre, D. Accardi, C. G. Stief, M. Dieterich, P. Falkai, R. A. Böckmann, H. Pérez-Sánchez, A. Hyman, M. Trottmann, F. Pan-Montojo, *bioRxiv* **2021**, <https://doi.org/10.1101/2021.01.16.426934>.
- [26] J. I. Ramiro, A. Kumar, *Mo. Med.* **2015**, *112*, 136.
- [27] M. L. Smith, R. N. Auer, B. K. Siesjö, *Acta Neuropathol.* **1984**, *64*, 319.
- [28] T. H. Sanderson, R. Kumar, J. M. Sullivan, G. S. Krause, *J. Neurochem.* **2008**, *106*, 1248.
- [29] S. T. Carmichael, *NeuroRx* **2005**, *2*, 396.
- [30] S. Hetze, O. Engel, C. Römer, S. Mueller, U. Dirnagl, C. Meisel, A. Meisel, *J. Cereb. Blood Flow Metab.* **2013**, *33*, 846.
- [31] T.-V. V. Nguyen, J. B. Frye, J. C. Zbesko, K. Stepanovic, M. Hayes, A. Urzua, G. Serrano, T. G. Beach, K. P. Doyle, *Acta Neuropathol. Commun.* **2016**, <https://doi.org/10.1186/s40478-016-0371-y>
- [32] J. C. Zbesko, T.-V. V. Nguyen, T. Yang, J. B. Frye, O. Hussain, M. Hayes, A. Chung, W. A. Day, K. Stepanovic, M. Krumberger, J. Mona, F. M. Longo, K. P. Doyle, *Neurobiol. Dis.* **2018**, *112*, 63.
- [33] Y. Sasaki, K. Ohsawa, H. Kanazawa, S. Kohsaka, Y. Imai, *Biochem. Biophys. Res. Commun.* **2001**, *286*, 292.
- [34] M. Pekny, M. Pekna, *J. Pathol.* **2004**, *204*, 428.
- [35] S. L. Eaton, T. M. Wishart, *Mamm. Genome* **2017**, *28*, 324.
- [36] A. J. Sorby-Adams, R. Vink, R. J. Turner, *Am. J. Physiol.: Regul., Integr. Comp. Physiol.* **2018**, *315*, R165.
- [37] D. Golubczyk, L. Kalkowski, J. Kwiatkowska, M. Zawadzki, P. Holak, J. Glodek, K. Milewska, A. Pomianowski, M. Janowski, Z. Adamiak, P. Walczak, I. Malysz-Cymborska, *Scientific Reports* **2020**, <https://doi.org/10.1038/s41598-020-74411-3>
- [38] Y. Tanaka, H. Imai, K. Konno, T. Miyagishima, C. Kubota, S. Puentes, T. Aoki, H. Hata, K. Takata, Y. Yoshimoto, N. Saito, *Stroke* **2008**, *39*, 205.
- [39] H. G. Andrewartha, *Biol. Rev.* **1952**, *27*, 50.
- [40] M. B. Renfree, G. Shaw, *Annu. Rev. Physiol.* **2000**, *62*, 353.
- [41] G. J. Ragland, D. L. Denlinger, D. A. Hahn, *Proc. Natl. Acad. Sci. USA* **2010**, *107*, 14909.
- [42] G. E. Ptak, E. Tacconi, M. Czernik, P. Toschi, J. A. Modlinski, P. Loi, *PLoS ONE* **2012**, *7*, e33027.
- [43] M. D. Hoos, B. M. Richardson, M. W. Foster, A. Everhart, J. W. Thompson, M. A. Moseley, C. A. Colton, *J. Proteome Res.* **2013**, *12*, 4462.
- [44] N. Lev, Y. Barhum, I. Lotan, I. Steiner, D. Offen, *PLoS One* **2015**, *10*, e0117190.
- [45] T. Wang, N. Zhao, L. Peng, Y. Li, X. Huang, J. Zhu, Y. Chen, S. Yu, Y. Zhao, *Front. Cell and Dev. Biol.* **2020**, <https://doi.org/10.3389/fcell.2020.593890>
- [46] H. Ariga, K. Takahashi-Niki, I. Kato, H. Maita, T. Niki, S. M. M. Iguchi-Ariga, *Oxid. Med. Cell. Longevity* **2013**, *2013*, 1.
- [47] I. Vermes, C. Haanen, H. Steffens-Nakken, C. Reutelingsperger, *J. Immunol. Methods* **1995**, *184*, 39.
- [48] I. Vermes, C. Haanen, C. Reutelingsperger, *J. Immunol. Methods* **2000**, *243*, 167.
- [49] L. Faleiro, Y. Lazebnik, *J. Cell Biol.* **2000**, *151*, 951.
- [50] A. M. Rieger, K. L. Nelson, J. D. Konowalchuk, D. R. Barreda, *J. Visualized Exp.* **2011**, *50*, 2597.
- [51] J. Fenstermacher, J. Gazendam, *Cancer Treat. Rep.* **1981**, *65*, 27.
- [52] R. L. Dedrick, *J. Natl. Cancer Inst.* **1988**, *80*, 84.
- [53] S. Joshi, C. W. Emala, J. Pile-Spellman, *J. Neurosurg. Anesthesiol.* **2007**, *19*, 111.
- [54] S. Bernardo-Castro, J. A. Sousa, A. Brás, C. Cecília, B. Rodrigues, L. Almendra, C. Machado, G. Santo, F. Silva, L. Ferreira, I. Santana, J. Sargento-Freitas, *Front. Neurol.* **2020**, <https://doi.org/10.3389/fneur.2020.594672>
- [55] K. P. Doyle, N. Fathali, M. R. Siddiqui, M. S. Buckwalter, *J. Neurosci. Methods* **2012**, *207*, 31.
- [56] U. Dirnagl, Members of the MCAO-SOP Group, *Nat. Prec.* **2012**, <http://doi.org/10.1038/npre.2012.3492.3>.
- [57] F. C. Barone, D. J. Knudsen, A. H. Nelson, G. Z. Feuerstein, R. N. Willette, *J. Cereb. Blood Flow Metab.* **1993**, *13*, 683.
- [58] M. Fujii, H. Hara, W. Meng, J. P. Vonsattel, Z. Huang, M. A. Moskowitz, *Stroke* **1997**, *28*, 1805.
- [59] J. Hao, A. Mdzinarishvili, T. J. Abbruscato, J. Klein, W. J. Geldenhuys, C. J. Van der Schyf, U. Bickel, *Brain Res.* **2008**, *1196*, 113.
- [60] T. Abe, A. Kunz, M. Shimamura, P. Zhou, J. Anrather, C. Iadecola, *J. Cereb. Blood Flow Metab.* **2009**, *29*, 66.
- [61] J. Chen, C. Zhang, H. Jiang, Y. Li, L. Zhang, A. Robin, M. Katakowski, M. Lu, M. Chopp, *J. Cereb. Blood Flow Metab.* **2005**, *25*, 281.
- [62] P. J. Darlington, J. S. Goldman, Q. L. Cui, J. P. Antel, T. E. Kennedy, *J. Neurochem.* **2008**, *104*, 1201.
- [63] V. V. Gusel'nikova, D. E. Korzhevskiy, *Acta Nat.* **2015**, *7*, 42.
- [64] G. E. Barreto, X. Sun, L. Xu, R. G. Giffard, *PLoS One* **2011**, *6*, e27881.
- [65] N. Sims, W. Yew, *Neurochem. Int.* **2017**, *107*, 88.
- [66] M. Kudabayeva, A. Kisel, G. Chernysheva, V. Smol'yakova, M. Plotnikov, M. Khodanovich, *J. Phys.: Conf. Ser.* **2017**, *886*, 012009.
- [67] S. Ejaz, J. V. Emrich, S. J. Sawiak, D. J. Williamson, J.-C. Baron, *Stroke* **2015**, *46*, 1084.
- [68] J.-C. Baron, *Hum. Brain Mapp.* **2017**, *38*, 5822.
- [69] F. Block, M. Dihné, M. Loos, *Prog. Neurobiol.* **2005**, *75*, 342.
- [70] M. Bacigaluppi, G. Comi, D. M. Hermann, *Open Neurol. J.* **2010**, *4*, 34.
- [71] C. Kiewert, A. Mdzinarishvili, J. Hartmann, U. Bickel, J. Klein, *Brain Res.* **2010**, *1312*, 101.
- [72] D. M. Hermann, E. Kilic, R. Hata, K. A. Hossmann, G. Mies, *Neuroscience* **2001**, *104*, 947.
- [73] R. Hata, K. Maeda, D. Hermann, G. Mies, K. A. Hossmann, *J. Cereb. Blood Flow Metab.* **2000**, *20*, 306.
- [74] R. Hata, K. Maeda, D. Hermann, G. Mies, K. A. Hossmann, *J. Cereb. Blood Flow Metab.* **2000**, *20*, 937.
- [75] X. Wang, *Med. Hypotheses* **1999**, *53*, 380.
- [76] G. Myers, *Stanford Ichthyol. Bull.* **1942**, *2*, 89.
- [77] J. P. Wourms, *J. Exp. Zool.* **1972**, *182*, 143.
- [78] J. P. Wourms, *J. Exp. Zool.* **1972**, *182*, 169.
- [79] J. P. Wourms, *J. Exp. Zool.* **1972**, *182*, 389.
- [80] J. B. Wourms, *A naturally occurring vertebrate dispersion-reaggregation system subject to developmental arrest*, **1967**.
- [81] R. G. Simpson, J. E. Cross, R. L. Best, M. M. Ellsbury, A. F. Coseglia, *Environ. Entomol.* **1979**, *8*, 96.

- [82] A. W. Thompson, G. Ortí, *Mol. Biol. Evol.* **2016**, *33*, 2391.
- [83] J. Lundberg, K. Le Blanc, M. Söderman, T. Andersson, S. Holmin, *Neuroradiology* **2009**, *51*, 661.
- [84] J. Lundberg, E. Södersten, E. Sundström, K. Le Blanc, T. Andersson, O. Hermanson, S. Holmin, *Cell Transplant.* **2012**, *21*, 333.
- [85] C. Sciarretta, L. Minichiello, *Methods Molecular Biol.* **2010**, *633*, 221.
- [86] O. Engel, S. Kolodziej, U. Dirnagl, V. Prinz, *JoVE* **2011**, *47*, e2423.
- [87] M. Balkaya, J. M. Krober, A. Rex, M. Endres, *J. Cereb. Blood Flow Metab.* **2013**, *33*, 330.
- [88] V. Bouët, T. Freret, J. Toutain, D. Divoux, M. Boulouard, P. Schumann-Bard, *Exp. Neurol.* **2007**, *203*, 555.
- [89] V. Prinz, U. Laufs, K. Gertz, G. Kronenberg, M. Balkaya, C. Leithner, U. Lindauer, M. Endres, *Stroke* **2008**, *39*, 433.
- [90] E. Caballero-Garrido, J. C. Pena-Philippides, Z. Galochkina, E. Erhardt, T. Roitbak, *Behav. Brain Res.* **2017**, *331*, 282.
- [91] L. Zhang, T. Schallert, Z. G. Zhang, Q. Jiang, P. Arniego, Q. Li, M. Lu, M. Chopp, *J. Neurosci. Methods* **2002**, *117*, 207.
- [92] M. Balkaya, J. Krober, K. Gertz, S. Peruzzaro, M. Endres, *J. Neurosci. Methods* **2013**, *213*, 179.
- [93] T. Gerriets, E. Stolz, M. Walberer, C. Müller, A. Kluge, A. Bachmann, M. Fisher, M. Kaps, G. Bachmann, *Stroke* **2004**, *35*, 566.

9. Curriculum Vitae

Mein Lebenslauf wird aus datenschutzrechtlichen Gründen in der elektronischen Version meiner Dissertation nicht veröffentlicht.

My curriculum vitae will not be published in the electronic version of my dissertation for reasons of data protection.

Mein Lebenslauf wird aus datenschutzrechtlichen Gründen in der elektronischen Version meiner Dissertation nicht veröffentlicht.

My curriculum vitae will not be published in the electronic version of my dissertation for reasons of data protection.

12. List of Publications

Luis Weitbrecht and Daniel Berchtold, Tian Zhang, Sandra Jagdmann, Claudia Dames, Katarzyna Winek, Christian Meisel and Andreas Meisel. "CD4+ T Cells Promote Delayed B Cell Responses in the Ischemic Brain after Experimental Stroke." *Brain Behav Immun* 91 (2021): 601-14.

Impact factor 2020: 7.217

Sandra Jagdmann, Claudia Dames, Daniel Berchtold, Katarzyna Winek, Luis Weitbrecht, Andreas Meisel, and Christian Meisel. "Impact of Key Nicotinic Achr Subunits on Post-Stroke Pneumococcal Pneumonia." *Vaccines* 8, no. 2 (2020).

Impact factor 2020: 4.422

Alexandra Chovsepian, Daniel Berchtold, Katarzyna Winek, Uta Mamrak, Inés Ramirez Álvarez, Yanina Dening, Dominika Golubczyk, Luis Weitbrecht, Claudia Dames, Marine Aillery, Celia Fernandez-Sanz, Zdzislaw Gajewski, Marianne Dieterich, Mirosław Janowski, Peter Falkai, Piotr Walczak, Nikolaus Plesnila, Andreas Meisel, and Francisco Pan-Montojo. "A Primeval Mechanism of Tolerance to Desiccation Based on Glycolic Acid Saves Neurons from Ischemia in Mammals by Reducing Intracellular Calcium-Mediated Excitotoxicity." *Advanced Science* (2022): 9, 2103265. <https://doi.org/10.1002/advs.202103265>.

Impact factor 2020: 16.8

Daniel Berchtold, Luis Weitbrecht, Christian Meisel, and Andreas Meisel. "Friend or Foe? – B Cells in Stroke." *Neuroforum* 25, no. 3 (2019): 173-83.

Impact factor: NA, Cite Score 0.9

Acknowledgements

First and foremost, I would like to thank my supervisor and doctoral mentor Univ.-Prof. Andreas Meisel for giving me the opportunity to study this intriguing topic in his lab and providing me with all the scientific advice, resources and encouragement necessary to complete this dissertation. Particularly, I want to thank him for giving me the chance to discuss my research with various experts which led to fruitful collaborations.

Additionally, I want to express my gratitude to Dr. med. Christian Meisel for contributing to vivid discussions in countless lab meetings with his profound immunological knowledge.

I also want to thank Dr. Katarzyna Winek for the warm introduction to the lab and the extraordinary effort she put into teaching me all the methods required for my studies.

Many thanks to all the current and former members of the AG Meisel, fellow PhD students and technical assistants. Without you, the hours I spent in the lab and office would have been only half as fun and much less productive. Daniel Berchtold, Dr. Katarzyna Winek, Dr. Andreas Pelz, Dr. Claudia Dames, Sandra Jagdmann, Dr. Celeste Sassi, Claudia Muselmann-Genschow, I would like to thank you for the great times inside and outside of the Charité, the collegial support and fruitful discussions.

My deepest and most sincere gratitude goes to my family and friends for their endless encouragement and emotional support. Particularly I want to thank my parents Birgit Degeler-Weitbrecht and Florian Weitbrecht, my siblings Moritz and Sophia, my dearest friends and all the others who bring joy to my life each day.